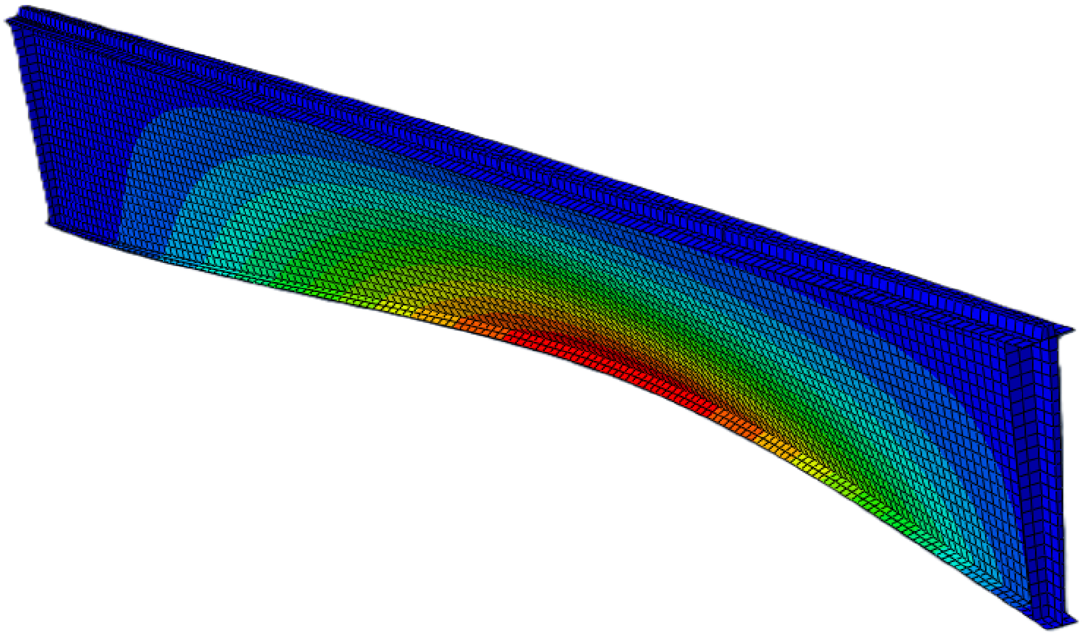

Effect of Bottom Flange Bracing on Crane Runway Girders

A Parametric Study on Ultimate Capacity Using Finite Element Analysis

Master's thesis in Structural Engineering and Building Technology

Andreas Karlsson
Kajsa Tengberg

DEPARTMENT OF STRUCTURAL ENGINEERING AND BUILDING TECHNOLOGY
CHALMERS UNIVERSITY OF TECHNOLOGY
Gothenburg, Sweden 2026
www.chalmers.se

Master's thesis 2026

Effect of Bottom Flange Bracing on Crane Runway Girders

A Parametric Study on Ultimate Capacity Using Finite Element Analysis

ANDREAS KARLSSON, KAJSA TENGBERG

CHALMERS
UNIVERSITY OF TECHNOLOGY

Department of Architecture and Civil Engineering
Division of Structural Engineering
Chalmers University of Technology
Gothenburg, Sweden 2026

Effect of Bottom Flange Bracing on Crane Runway Girders
A Parametric Study on Ultimate Capacity Using Finite Element Analysis
ANDREAS KARLSSON, KAJSA TENGBERG

Supervisor: Lars Holm, Afry, Mohammad SadeghKhani, Afry
Examiner: Mohammad al-Emrani, Architecture and civil engineering

Master's Thesis 2026
Department of Architecture and Civil Engineering
Division of Structural Engineering
Chalmers University of Technology
SE-412 96 Gothenburg
Telephone +46 31 772 1000

Cover: Finite element model of a crane runway girder constructed in Abaqus, showing the lateral deformation of the bottom flange.

Typeset in LaTeX
Printed by Chalmers Reproservice
Gothenburg, Sweden 2026

Effect of Bottom Flange Bracing on Crane Runway Girders
A Parametric Study on Ultimate Capacity Using Finite Element Analysis
Master's Thesis in the Master's Programme Structural Engineering and Building Technology

ANDREAS KARLSSON, KAJSA TENGBERG

Department of Architecture and Civil Engineering
Division of Structural Engineering
Chalmers University of Technology

Abstract

Crane runway girders in heavy industry carry large vertical and horizontal loads, placing significant demands on structural stability. While bracing of the top flange to prevent lateral-torsional buckling is well established, guidance on bottom flange bracing is inconsistent: the American Institute of Steel Construction (AISC) has reduced its previous requirement to a recommendation and Eurocode provides no explicit guidance on the matter. This study investigates the effect of bottom flange bracing on crane runway girders through a parametric finite element study in Abaqus, comparing the ultimate load capacity, quantified by the load proportionality factor (LPF), and lateral displacement of the bottom flange between girders braced at both flanges and girders with top flange bracing only. A range of web heights, bottom flange widths, and geometric imperfection amplitudes were considered. The model was verified against analytical hand calculations based on Eurocode, and the results were compared to AISC provisions for web sidesway buckling.

The results show no significant capacity gain between the configurations, with a maximum ΔLPF gain of approximately 5-6%. The largest improvements are observed for intermediate web heights, and bottom flange widths, where bottom flange restraint allows for a more even stress distribution over the web. For larger geometric imperfection amplitudes, bracing the bottom flange can reduce capacity due to a self-straightening behavior that restraint prevents. The AISC comparison shows a consistent pattern, where narrower bottom flanges and lower web heights are more susceptible. Based on these findings, no strong case is found for introducing mandatory bottom flange bracing requirements in Eurocode for the geometries and load cases investigated. Rather than mandatory bracing requirements, a more appropriate approach may be to control the bottom flange behavior through serviceability deflection limits, though further investigation is needed into how the lateral deflection of the bottom flange can be analytically determined, as this is dependent on cross sectional geometry.

Keywords: crane runway girder, bottom flange bracing, finite element analysis, parametric study

Inverkan av stagning av underfläns på kranbanebalkar
En parametrisk studie av ultimat lastkapacitet med finita elementanalys
Examensarbete inom masterprogrammet Konstruktionsteknik och Byggnadsteknologi

ANDREAS KARLSSON, KAJSA TENGBERG

Instutitionen för Arkitektur och Samhällsbyggnadsteknik
Avdelningen för Konstruktionsteknik
Chalmers Tekniska Högskola

Sammanfattning

Kranbanebalkar i tunga industrier utsätts för stora vertikala och horisontella laster, vilket ställer höga krav på strukturell stabilitet. Medan stagning av överfläns för att förhindra vippning är väl etablerad i standarderna, är riktlinjerna för stagning av underflänsen inkonsekvent: American Institute of Steel Construction (AISC) har omklassificierat dess tidigare krav till en rekommendation och Eurokod har inga riktlinjer. Denna studie undersöker effekten av stagning av underfläns på kranbanebalkar genom en parametrisk finita element studie i ABAQUS, där den ultimata lastkapaciteten, uttagen genom lastpropotionalitetsfaktorn (LPF), och underflänsens laterala förskjutning jämförs mellan balkar stagade i båda flänsar och balkar med endast stagning av överflänsen. Varierande höjder på livet, bredder av udnerflänsar och olika geometriska imperfektionsamplituder studeras. Modellen verifieras mot analytiska handberäkningar baserade på Eurocode och resultaten jämfördes med de rekommendationer från AISC för sidoknäckning av liv.

Resultaten visar ingen betydande kapacitetsökning mellan de olika stagningskonfigurationerna, med en maximal ΔLPF-ökning på cirka 5-6%. Effekten är störst för de livhöjderna i mitten av intervallet för livhöjder och med smalare underflänsbredder, där stagning av underfläns möjliggör en mer distribuerad spänningingsfördelning över livet. För större geometriska imperfektionsamplituder kan stagning av underflänsen minska kapaciteten, vilket förklaras av att balken vill räta ut sig själv under last som stagningen förhindrar. Jämförelsen med AISC:s rekommendationer visar ett konsekvent mönster, där smalare underflänsar och lägre livhöjder är mindre stabila. Snarare än obligatoriska stagningskrav kan underflänsbeteendet kontrolleras genom deformationsgränser i bruksgränstillstånd, men hur den laterala deformationen av underflänsens bestäms analytiskt kräver vidare undersökning, då detta beror på tvärsnittets geometri.

Nyckelord: kranbanebalkar, stagning av underfläns, finita element analys, parametrisk studie

Acknowledgements

This master's thesis was carried out in collaboration between AFRY AB and the Division of Structural Engineering at Chalmers University of Technology. We would like to thank AFRY as a company and the industry division for being welcoming and providing us with the opportunity to experience the day-to-day work of structural engineering in industry. A special thanks to the entire team at the industry division for creating a great working environment throughout the project. We would like to give particular thanks to our supervisors Lars Holm and Mohammad SadeghKhani for guiding us through this work and helping us understand the complex behaviour of large crane girder systems. Finally, we would like to thank our supervisor and examiner Mohammad Al-Emrani for his extensive knowledge of steel structures and for his valuable guidance in the development of the finite element model.

Andreas Karlsson, Kajsa Tengberg, Gothenburg, June 2026

Use of AI tools

AI tools were used to assist in the development and optimization of the Python script that was used for the finite element model in Abaqus, to automate the large number of model configurations required for the parametric study. It was also used in the development of the MATLAB-script for the bracing system design and to help structure the Excel post-processing for extracting, and organizing results from the parametric study. Finally, AI tools were used to check grammar and improve the language throughout the report. All the work processed with AI has been carefully reviewed and verified by the authors.

List of Acronyms

Below is the list of acronyms that have been used throughout this thesis listed in alphabetical order:

AISC	American Institute of Steel Construction
AISE	Association for Iron and Steel Engineers
AIST	Association for Iron and Steel Technology
BC	Boundary condition
CAE	Computer-Aided Engineering
CG	Centre of gravity
DOF	Degree of freedom
FEM	Finite Element Method
HC	Hoisting Class
LPF	Load Proportionality Factor
LRFD	Load and Resistance Factor Design
LTB	Lateral-Torsional buckling
SC	Shear centre
SLS	Serviceability limit state
ULS	Ultimate limit state

Nomenclature

Below is the nomenclature of indices, sets, parameters, and variables that have been used throughout this thesis.

Roman Upper Case Letters

A_w	Web area
C_r	Coefficient in the web sidesway buckling formula, dependent on the ratio of required moment to yield moment
E	Modulus of elasticity
F	Form factor for I-beams (used in shear deflection calculation)
F_d	Design value of any load component
F_k	Characteristic value of any load component
G	Shear modulus
G_b	Bridge weight
G_c	Trolley weight
$H_{m,d}$	Design transverse force from long travel
$H_{m,k}$	Characteristic transverse force from long travel
I_T	St Venant torsional constant
I_w	Warping constant
I_y	Moment of inertia around the strong axis y-y for a mono symmetric I-beam
I_z	Moment of inertia around the weak axis z-z for a mono symmetric I-beam
$I_{z,bf}$	Moment of inertia of the bottom flange around the weak axis z-z
$I_{z,tf}$	Moment of inertia of the top flange around the weak axis z-z
$K_{a,k}$	Characteristic transverse force from cross travel
$K_{r,d}$	Design longitudinal horizontal force
$K_{r,k}$	Characteristic longitudinal horizontal force

L	Beam length
L_b	The largest laterally unbraced length along either flange at the point of load
L_{cr}	Critical buckling length
$L_{vertical}$	Length of vertical bar
LPF_{top}	Load proportionality factor with only the top flange restrained
LPF_{both}	Load proportionality factor with both flanges restrained
$M_{b,Rd}$	Design buckling resistance moment
M_{cr}	Elastic critical moment for lateral-torsional buckling
M_{Ed}	Design bending moment
$M_{Ed,brace}$	Bending moment in the bracing truss
M_{el}	Elastic moment resistance
$M_{f.Rd}$	Moment capacity of flanges
M_{pl}	Plastic moment resistance
M_r	Required flexural strength
M_y	Yield moment
$N_{Ed,brace}$	Compressive force in the top chord of the bracing truss
P_{cr}	Critical buckling load
$P_{vertical}$	Disrcete nodal force transferred by the vertical member
$P_{wheel,d}$	Maximum design wheel load
Q_h	Crane capacity
R_n	Nominal strength
R_{perm}	Ratio of permanent loads
R_{var}	Ratio of variable loads
S	Guiding force at end wheel from skewing
S_f	First moment of area of the beam flanges
S_x	Elastic section modulus about the strong axis (AISC notation)
T_{Ed}	Design value of the torsional moment
$T_{t,Ed}$	Design value of the St Venant torsional moment
$T_{w,Ed}$	Design value of the warping moment
V_{Ed}	Design shear force
$V_{b.Rd}$	Design shear capacity
$V_{bf.Rd}$	Shear contribution from flanges
$V_{bw.Rd}$	Shear contribution from web
W_y	Section modulus

W_{pl}	Plastic section modulus
W_{el}	Elastic section modulus
W_{eff}	Effective elastic section modulus
Y_i	Skewing force at each wheel i

Roman Lower Case Letters

b_{bf}	Bottom flange width
b_f	Flange width
b_{tf}	Top flange width
c	Length between two plastic hinges
e_0	Initial bow imperfection
f_y	Yield strength
g	Acceleration due to gravity
h	Clear distance between flanges for built-up members
h_{mid}	Height between the midpoint of the flanges
h_{tot}	Total height of the cross section
h_w	Web height
k_{stiff}	Equivalent spring stiffness
k_w	Effective length factor related to the restrain against warping at the boundaries
k_z	Effective length factor related to the restrain against lateral bending at the boundaries
l	Span between runway beams (bridge length)
m_{brace}	Number of restrained members
$q_{d,brace}$	Equivalent line load on bracing system
t_{bf}	Thickness of the bottom flange
t_{tf}	Thickness of the top flange
t_w	Thickness of the web
u_i	Translation in global i-direction
ur_i	Rotation about i-axis
v_h	Hoisting speed
w	Distributed load
z_{bot}	Centre of gravity for the cross section measured from the bottom

z_{top}	Centre of gravity for the cross section measured from the top

Greek Letters

α	Imperfection factor for minor axis flexural buckling
α_m	Reduction factor for multiple restrained members
α_s	Load factor for LRFD
β_2, β_3	Dynamic factor coefficients
$\beta_{LT,1}$	Equivalent geometric imperfection for structural members for LTB
$\beta_{LT,2}$	Reference relative bow imperfection for LTB
γ_{Ff}	Partial factor for fatigue loading
γ_{Mf}	Partial factor for fatigue strength
γ_{M1}	Partial factor
Δ	Difference or change in a quantity
δ_{avg}	Average deflection of the four nodes in that specific bay
δ_q	In-plane deflection of the bracing system
ϵ	Material parameter of steel
η	Global imperfection factor
λ_1	First positive eigenvalue
μ	Friction factor
ν	Poisson's ratio
π	Mathematical constant ≈ 3.14159
σ_1	Principal stress in tension
σ_2	Principal stress in compression
τ	Shear stress
χ	Reduction factor
χ_{LT}	Reduction factor for lateral-torsional buckling
χ_w	Reduction factor for shear buckling
ϕ	Safety factor
ϕ'	First derivative of angle of rotation
ϕ'''	Third derivative of angle of rotation
φ_i	Dynamic factor applied to loads

Indices

i	Index, context dependent (e.g. wheel number for Y_i, dynamic factor number for φ_i, or global direction for u_i)

Contents

List of Figures

List of Tables

1
Introduction

In this chapter, an introduction of the thesis will be given by presenting the purpose in terms of a brief background description, and the aim of this master's thesis. Relevant limitations and simplifications are also taken into account. The chapter ends with an overview of how the work will be achieved and a brief outline of the report structure.

1.1 Background

Crane runway girders are vital components in industrial structures, ensuring safe and reliable crane operations. They are subjected to multiple different loads, large vertical forces from the self weight of the crane and the object being lifted, as well as lateral loads from the crab moving from side to side and horizontal loads from the lifting system moving along the runway. These large and complex loads in combination with the very large cross section these crane girders require, can lead to multiple different failure modes. Failure of these components can lead to significant financial losses and safety risks. The design of these mega crane girders requires some type of back-up bracing system against lateral torsional buckling (LTB) and improve its stiffness against horizontal loads.

American design practice has historically included explicit requirements for bottom flange bracing in long-span crane runway girders, which in more recent editions have been revised to recommendations for certain cross-sections. Eurocode does not provide equivalent guidance on bottom flange bracing, leaving a gap in the design provisions for this failure mode. For very deep and slender girders, the bottom flange may experience lateral displacement even when the top flange is fully braced, potentially reducing capacity and leading to instability. This raises the question of whether bottom flange behaviour needs to be considered in Eurocode and whether dedicated bracing remains necessary for large crane girders.

This study builds on the earlier work of (Nyman, 2025), who conducted a comparative study of lateral-torsional buckling in crane runway girders across three design standards: the current Eurocode, the upcoming Eurocode and the American standard (AISC 360-16). The study identified differences in how the critical moment is calculated between the standards, with particular focus on differences in moment factors, reduction factors and interaction formulas between the standards. The present study extends this work by numerically investigating the effect of bottom flange bracing on the ultimate load capacity and lateral deformation behavior of crane runway girders through a parametric finite element study.

1.2 Aim and objective

The aim of this thesis is to investigate the structural behaviour of the bottom flange in large crane runway girders. It examines which parameters govern the behavior and capacity of these girders, with a specific focus on how bottom flange deformation influences overall performance in both stiffened and unstiffened configurations. The stiffening systems considered are built-up truss arrangements, which is commonly used for mega crane girders. The investigation compares scenarios where only the top flange is braced against those where both flanges have bracing.

By varying key parameters, such as cross sectional geometry, imperfection amplitudes and bracing configuration, the thesis evaluates how bottom flange behavior affects global stability and load-carrying capacity. The results are then used to assess whether bottom flange bracing should be considered a necessary design measure for large-scale crane runway girders.

1.3 Limitations

This thesis does not cover fatigue design of the crane girder. Residual stresses from welding are not explicitly modelled. Instead, they are accounted for through increased geometric imperfection amplitudes in accordance with standard practice. The connections are modelled as rigid, both at the rail-to-beam interface and at the supports. In reality, bearing pads introduce some flexibility at these locations. The bracing is modelled as continuous along the length to simulate varying stiffness, meaning the discrete nature of bracing connections is not considered. The cross sections investigated are limited to symmetric and mono-symmetric I-beams, which represent the most common profiles used for crane runway girders.

1.4 Method

The project began with a literature study focused on the instability behavior of steel structures, with particular emphasis on previous research concerning lateral–torsional buckling and other relevant buckling modes of crane girders with slender webs and the stiffness requirements for backup bracing. Additional theoretical material on torsion, distortional behavior, and the influence of the bottom flange on global stability was reviewed. Recommendations from American design practice were also considered, as these include guidance on bottom flange stabilization which is not present in Eurocode.

Following the literature and standards study, an analytical buckling analysis of the crane girder was performed to investigate its global instability behavior and to estimate the required stiffness of the backup bracing system. These calculations were carried out in Mathcad Prime for a base case geometry selected from a previously designed girder. The bracing system was modelled in Matlab using the CALFEM library.

The analytical model served as a reference for validating the numerical analysis for a finite element model developed in Abaqus using the finite element method (FEM), to simulate the behavior of the crane runway girder. A nonlinear analysis was performed for each girder configuration, considering variations in bracing position, web heights, bottom flange width, and geometric imperfection amplitude. The influence of initial geometric imperfections was also assessed to better reflect realistic structural conditions and ensure that the simulations capture expected physical deviations. The resulting load proportionality factors (LPF) and the lateral displacement were then extracted to evaluate the effect of bracing the bottom flange.

1.5 Outline of Report

Chapter 1 introduces the thesis by presenting the background to bottom flange bracing in large crane runway girders and the gap between American and Eurocode design practice. The formulation of the problem, the aim, the limitations, and the method are also presented.

Chapter 2 presents the theoretical foundation of the thesis. It covers the structural behaviour of I-girders, including cross sectional properties and stability phenomenons such as lateral-torsional and local buckling, along with the boundary conditions relevant to the FEM. Design provisions from Eurocode and American standards regarding crane girders and bracing systems are also reviewed. Finally, the software tools used for calculations and finite element modelling are introduced.

Chapter 3 presents the crane loads acting on the runway girder and how they are transformed into ULS and SLS design loads. The base case geometry is introduced, followed by the vertical and horizontal wheel loads. The design of the top flange bracing system and the support boundary conditions of the girder are also described.

Chapter 4 describes how the finite element model is built and verified in Abaqus. It covers the modelling assumptions, boundary conditions, material properties, mesh, and load application. The parametric study setup is then presented, including the geometry variations, imperfection magnitudes, and the analysis procedure used to obtain the results.

Chapter 5 presents the results obtained from the nonlinear finite element analyses. The influence of web height, bottom flange width, and imperfection amplitude on the ultimate load capacity is examined for both the critical moment and shear load cases and localised bottom flange imperfection types.

Chapter 6 discusses the results from the parametric study, explaining the physical behaviour observed for varying web heights, load cases, and imperfection amplitudes. The influence of bottom flange displacement on ultimate capacity is also examined, followed by a discussion of the study's limitations.

Chapter 7 states the conclusions of the research and recommendations for future studies are being presented.

2
Theory

This chapter establishes the theoretical foundation for the thesis, detailing the analytical principles upon which the subsequent calculations and finite element (FE) simulations are based. It provides the necessary theoretical background for defining the input parameters of the FE-model, such as material behavior and cross sectional properties to accurately reflect the physical crane girder system.

2.1 Beam properties

In this section we will define the notation and properties of a cross section that will be used to calculate various capacities of a beam. Fig. 2.1 shows the notation of the different parts in a cross section, for symmetric sections both flanges have the same width and thickness, and for mono-symmetric sections they can both have different width and thicknesses.

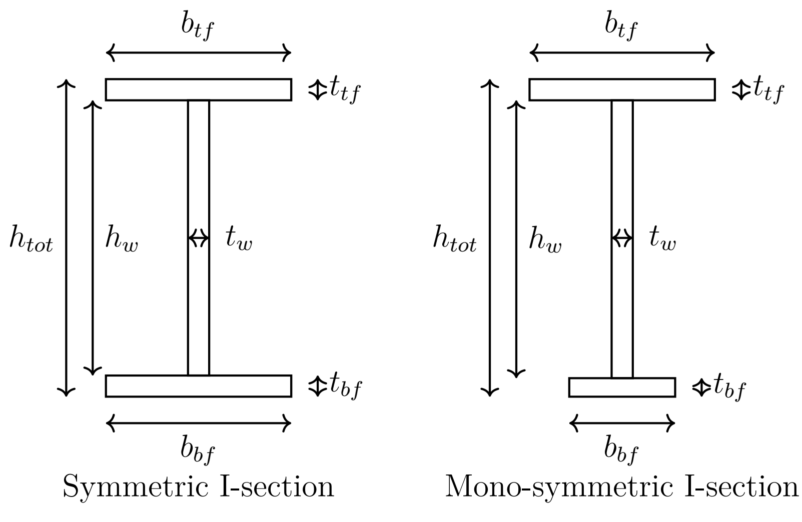

Figure 2.1: Cross section notation for symmetric and asymmetric I-girders.

where: h_{tot} is the total height of the cross section [mm]
h_w is the height of the web [mm]
t_w is the thickness of the web [mm]
b_{tf} is the width of the top flange [mm]
t_{tf} is the thickness of the top flange [mm]
b_{bf} is the width of the bottom flange [mm]
t_{bf} is the thickness of the bottom flange [mm]

2.1.1 Centre of gravity

The centre of gravity (CG) is the point through which the resultant weight of an object acts and about which it would balance if supported. For a symmetric I-section, the CG lies at the midpoint of the height, whereas for a monosymmetric cross section it shifts toward the flange with the larger area. Determining the CG is essential for evaluating the bending capacity of a cross section, since sectional properties such as the second moments of area are defined relative to this point.

$$z_{\text{top}} = \frac{t_{tf}b_{tf}\frac{t_{tf}}{2} + t_w h_w(t_{tf} + \frac{h_w}{2}) + t_{bf}b_{bf}(t_{tf} + h_w + \frac{t_{bf}}{2})}{t_{tf}b_{tf} + t_w h_w + t_{bf}b_{bf}} \tag{2.1}$$

where: z_{top} is the centre of gravity for the cross section (measured from the top of the cross section) [mm]

2.1.2 Axis of bending

In the Eurocode convention, the axis parallel to the flanges is denoted as the y-axis, and bending about this axis corresponds to strong-axis bending for I-sections. The axis perpendicular to the flanges is denoted as the z-axis and represents the weak axis. These axes are also commonly referred to as the major and minor axes, respectively, and they define the notation used for sectional forces and moments throughout this work. Accordingly, M_y denotes the bending moment about the major (y) axis. The definition of the coordinate system is illustrated in Fig. 2.2.

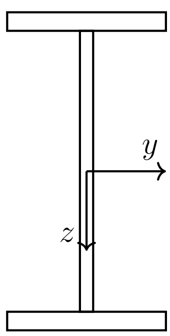

Figure 2.2: Coordinate system for an I-section.

2.1.3 Moment of inertia and constants of a cross section

The second moment of area, also known as the moment of inertia, is a geometric property that characterizes the resistance of a cross section to bending (The Efficient Engineer, 2024). As noted previously, an I-section has two principal bending axes: a strong axis and a weak axis. This distinction is reflected in the sectional properties I_y and I_z, which represent the second moments of area about the strong and weak axes, respectively. The bending stiffness of a cross section depends on how its area is distributed relative to the CG. Sections with more material located farther from the centroid generally have higher stiffness, which is why I-sections are efficient for resisting bending about their strong axis. In addition to the second moments of area, other sectional properties must be defined, including the torsional constant and the warping constant. These parameters describe the resistance of a cross section to torsion and its tendency to deform through warping (Al-Emrani and Åkesson, 2013).

$$I_y = \frac{t_w h_w^3}{12} + \frac{b_{tf} t_{tf}^3}{12} + b_{tf} t_{tf} (z - \frac{t_{tf}}{2})^2 + \frac{b_{bf} t_{bf}^3}{12} + b_{bf} t_{bf} (z - (t_{tf} + h_w + \frac{t_{bf}}{2}))^2 \quad (2.2)$$

$$I_z = \frac{h_w t_w^3}{12} + \frac{t_{tf} b_{tf}^3}{12} + \frac{t_{bf} b_{bf}^3}{12} \quad (2.3)$$

$$I_T \approx \sum_{i=1}^{n} \frac{t_i^3 h_i}{3} \quad (2.4)$$

$$I_w = \frac{I_{z.bf} \cdot I_{z.tf} (\frac{t_{tf}}{2} + h_w + \frac{t_{bf}}{2})}{I_{z.tf} + I_{z.bf}} \quad (2.5)$$

where:
- I_y is the moment of inertia around the strong axis y-y for a mono symmetric I-beam [mm^4]
- I_z is the moment of inertia around the weak axis z-z for a mono symmetric I-beam [mm^4]
- I_T is the St Venant torsional constant [mm^4]
- I_w is the warping constant [mm^6]
- $I_{z,tf}$ is the moment of inertia of the top flange around the axis z-z [mm^4]
- $I_{z,bf}$ is the moment of inertia of the bottom flange around the axis z-z [mm^4]

2.1.4 Shear centre

The shear centre (SC) is the point where if a load is applied the resulting shear force will only impact the beam in bending without any twisting or torsion (Hughes A F et al., 2011). In doubly-symmetric cross sections, the SC and the CG coincide at the geometric centroid. However, in mono-symmetric sections, while both points shift toward the larger flange, they do not coincide. The SC's position is governed by the relative flexural stiffness of the flanges, causing it to shift further than the CG, which is governed by the distribution of the cross sectional area.

$$SC = \frac{t_{bf} b_{bf}^3 h_{tot}}{t_{tf} b_{tf}^3 + t_{bf} b_{bf}^3} \tag{2.6}$$

where: SC is the shear centre (measured from the top) [mm]

2.2 Degrees of freedom

In finite element analysis the behavior of a structural system is described through a set of degrees of freedom (DOF) which is assigned to nodes in the model. They represents the movements and directions a node may undergo in the structural model. In this three dimensional space there are in total six DOF: three translational and three rotational. See Fig. 2.3 below.

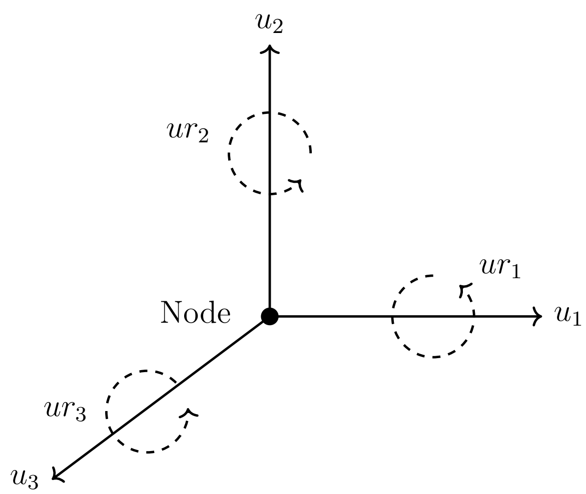

Figure 2.3: Solid arrows represent translational degrees of freedom (u_1, u_2, u_3) and dashed circular arrows represent rotational degrees of freedom (ur_1, ur_2, ur_3).

The translational DOF correspond to displacements in the global coordinate system, while the rotational represent the independent rotations around the same axis. The notation is defined as:

- u_1 - translation in the global x-direction
- u_2 - translation in the global y-direction
- u_3 - translation in the global z-direction
- ur_1 - rotation about the x-axis
- ur_2 - rotation about the y-axis
- ur_3 - rotation about the z-axis

Boundary conditions and constraints are introduced in the model by restricting selected degrees of freedom at specific nodes or reference points. By controlling these movements, the structural behavior of supports, restraints and connections can be represented within the model.

2.3 Stability and Buckling Behavior

This section presents the different instability phenomena the I-girder is subjected to, such as global, local and interacting buckling behaviours, including the influence of cross-sectional geometry and restraint conditions on buckling resistance.

2.3.1 Global buckling

Global buckling refers to elastic instability modes involving deformation of the entire member. Flexural buckling is where buckling only occurs in one plane (Fig.2.4) and torsional buckling appears as twisting of the cross section due to presence of compression in the member (Fig.2.5) (Hughes A F et al., 2011). Torsional buckling is further discussed in Chapter 2.3.2.

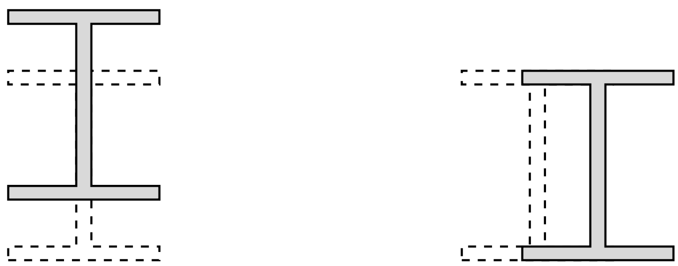

Translation over z-axis. Translation over y-axis.

Figure 2.4: Flexural buckling of an I-beam in the principle axis.

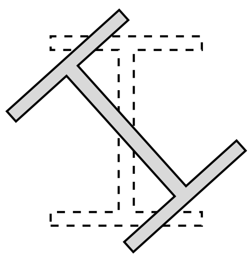

Figure 2.5: Torsional buckling.

2.3.2 Torsion

When transverse loads act with an eccentricity relative to the SC, a torsional moment is induced about the longitudinal axis of the beam (Hughes A F et al., 2011). This

torsional loading is resisted through two mechanisms. St Venant torsion represents the uniform torsional response governed by shear stresses in the cross section.
When a twisting moment acts on a beam, the flanges will be subjected to tension and compression in opposite to each other. The tension and compression will cause the flanges to deform out of their initial planes (Al-Emrani and Åkesson, 2013). This deformation is called warping and is shown in Fig 2.6. Warping torsion arises when axial warping deformations of the cross section are partially or fully restrained, leading to additional normal and shear stresses. The total torsional effect is therefore a combination of these two contributions.

$$T_{Ed} = T_{t,Ed} + T_{w,Ed} \tag{2.7}$$

where: T_{Ed} is the design value of the torsional moment [N·mm]
$T_{t,Ed}$ is the design value of the St Venant torsional moment [N·mm]
$T_{w,Ed}$ is the design value of the warping moment [N·mm]

$$T_{t,Ed} = GI_T\phi' \tag{2.8}$$

$$T_{w,Ed} = -EI_w\phi''' \tag{2.9}$$

where: G is the shear modulus [Pa]
E is the modulus of elasticity [Pa]
ϕ' is the first derivative of angle of rotation [1/mm]
ϕ''' is the third derivative of angle of rotation [1/mm^3]

The shear modulus is calculated as followed:

$$G = \frac{E}{2(1+\nu)} \tag{2.10}$$

where: ν Poisson's ratio [-]

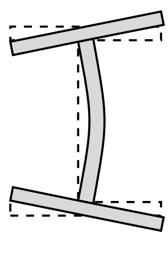

Figure 2.6: Warping of an I-section under torsion. The flanges rotate in opposite directions while the web displaces laterally.

2.3.3 Lateral torsional buckling

For an unrestrained and slender beam subjected to pure moment about its major axis, the upper flange will be subjected to compression and may become laterally unstable (Al-Emrani and Åkesson, 2013). In the absence of sufficient lateral restraint, bending about the major axis is accompanied by lateral deflection and twisting of the cross section, leading to lateral-torsional buckling (LTB) before the full material resistance is reached (Fig.2.7). The compression flange tends to buckle laterally, while its connection to the tension flange through the web causes a coupled torsional deformation of the member.

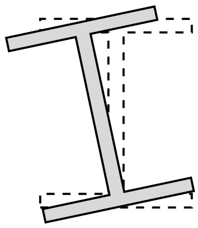

Figure 2.7: Schematic of an I-section undergoing lateral deformation.

2.3.4 Local buckling

Local buckling, also known as plate buckling, may occur in slender plate elements subjected to compression, such as the compression flange and the compressed zone of the web in a beam, shown in Fig. 2.8. Due to their slenderness, these plate members may experience out-of-plane deformation before the material reaches its yield stress, leading to a reduction in the effective cross sectional resistance (Al-Emrani and Åkesson, 2013). The susceptibility to local buckling is governed by the plate slenderness, which depends on the ratio between the effective loaded width and plate thickness. In slender beams, local buckling may occur independently of the global behavior of the member.

Cross sections subjected to bending are grouped into Classes 1 to 4 based on their susceptibility to local buckling, as illustrated in Fig. 2.9. Class 1 and 2 sections can utilize their full plastic moment resistance M_{pl}, with Class 1 additionally allowing plastic hinge formation for plastic analysis. Class 3 sections are limited to the elastic moment resistance M_{el}, as local buckling prevents full plastification. For Class 4 sections, local buckling occurs before the elastic resistance is reached, and the cross section resistance is determined by reducing slender plate elements to their effective widths, discarding the buckled portions from the calculation.

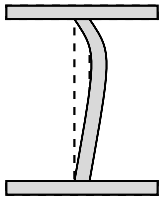

Figure 2.8: Web plate buckling of an I-section. The web bows laterally while the flanges remain horizontal.

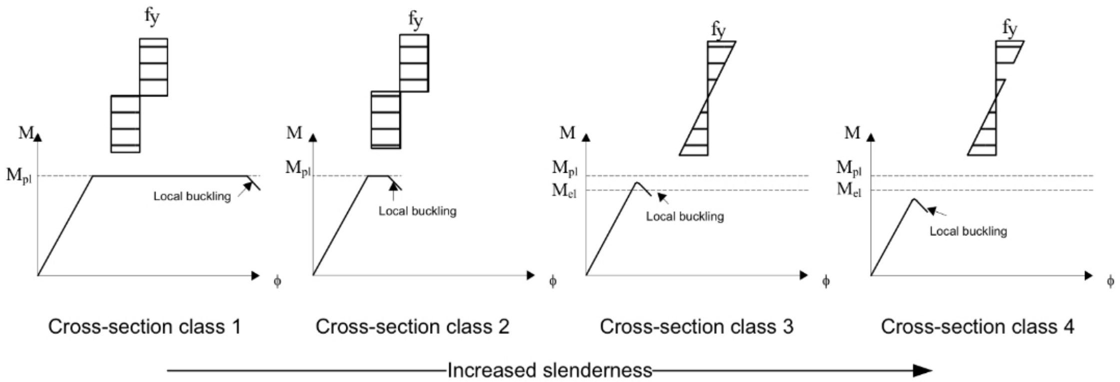

Figure 2.9: Risk for local buckling (Al-Emrani and Åkesson, 2013).

2.3.5 Shear buckling

Shear stresses (τ) are present in beams subjected to bending, and the resistance to these stresses is primarily provided by the web (Al-Emrani and Åkesson, 2013). For slender webs, this capacity is often limited by buckling rather than material yielding. Under the assumption of pure shear loading typical in the outer panels of a girder, the internal state of stress can be resolved into principal stresses using Mohr's circle.

$$\tau = \frac{V_{Ed}\ S_f}{I_y\ t_w} \tag{2.11}$$

$$\tau = \sigma_1 = -\sigma_2 \tag{2.12}$$

where:
- τ is the shear stress in the web [Pa]
- V_{Ed} is the design value of the shear force [N]
- S_f is the first moment of area of the beam flanges [mm^3]
- σ_1 is the principal stress in tension [Pa]
- σ_2 is the principal stress in compression [Pa]

As illustrated in Fig. 2.10, these principal stresses act at a 45° angle to the longitudinal axis of the web. The stress σ_1 represents a diagonal tensile stress, while σ_2 represents a diagonal compressive stress. Before shear buckling occurs, the web acts as a continuous plate resisting these forces. However, because slender plates are highly susceptible to instability under compression, the diagonal compressive component (σ_2) can trigger elastic buckling at loads well below the plastic shear capacity. This transition can be visualized through a truss analogy as shown in Fig. 2.11, here the web's internal resistance is modelled as a system of compressive and tensile struts:

- Tensile Struts (σ_1): Provide a stabilizing effect, pulling the web straight.
- Compressive Struts (σ_2): Act as the primary driver of instability, causing the web to bow out-of-plane when the critical buckling stress is exceeded.

Consequently, the ultimate shear resistance is governed by the geometric properties of the web and the spacing of transverse stiffeners, which increase resistance by dividing the girder into smaller, more stable panels.

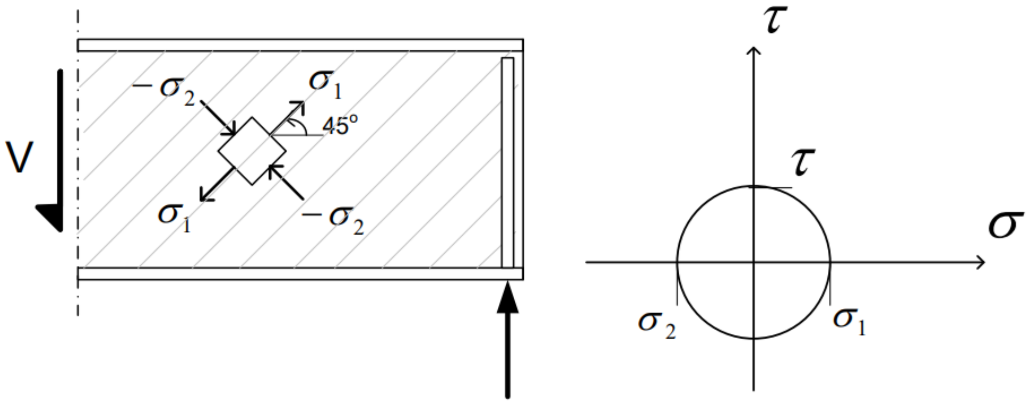

Figure 2.10: State of stress in a web panel. The stress element and Mohr's circle illustrate the principal tensile (σ_1) and compressive (σ_2) stresses. (Al-Emrani and Åkesson, 2013).

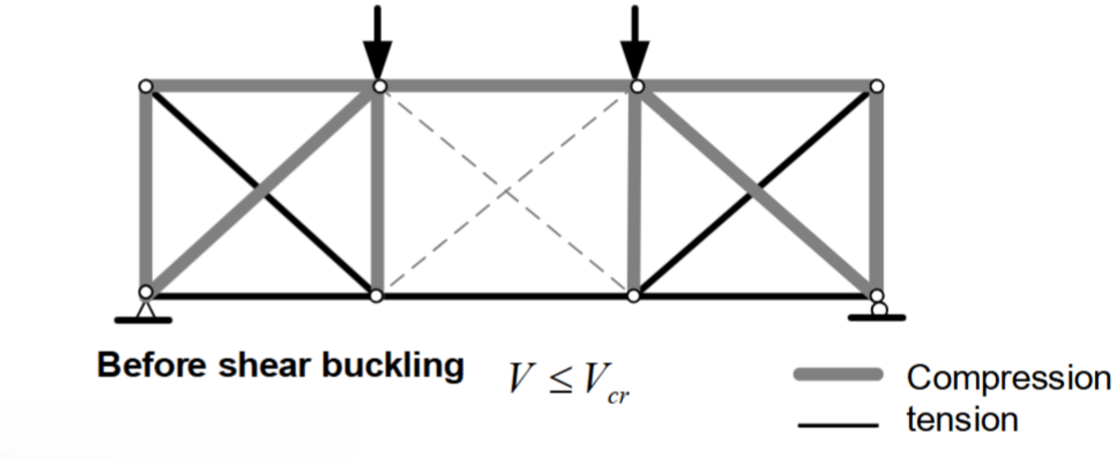

Figure 2.11: Truss analogy of a plate girder web showing the internal distribution of diagonal tensile and compressive struts before shear buckling (Al-Emrani and Åkesson, 2013).

2.3.6 Web sidesway buckling

Web sidesway buckling is an instability phenomenon that may occur in girders when subjected to a concentrated load, which causes the web to bend laterally out of its own plane, causing lateral displacement of the tension flange (Summers et al., 1982). The phenomenon is strongly influenced by the web geometry and the restraint conditions of the flanges. Web sidesway buckling is most likely to occur when the top flange is restrained against rotation while the bottom flange remains unrestrained. Under load application on the top flange, a compressive stress field develops in the web, causing the web to behave similarly to a slender column between the flanges. As the web bends sideways, the tension flange is forced to sway laterally, resulting in distortion of the cross section. This behaviour is illustrated in Fig. 2.12.

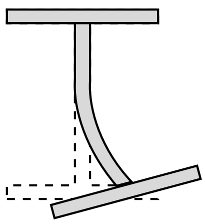

Figure 2.12: Schematic of web sidesway buckling induced by lateral buckling of the tension flange.

Web sidesway buckling may lead to significant out-of-plane deformation of the bottom flange together with a reduction in the overall stability of the girder. This behaviour is further discussed in Chapter 2.6, since web sidesway buckling is considered a relevant limit state in American design standards, while equivalent requirements are not found in Eurocode.

2.3.7 Eigenvalues and mode shapes

The behavior of a system can be described through an eigenvalue problem, where the elastic stiffness is related to the geometric stiffness (Modares et al., 2004). The solution to this problem gives a set of eigenvalues and corresponding eigenvectors. The eigenvalues represent scaling factors of the applied load on the structure, while the eigenvectors describe the correlated deformation patterns which are commonly referred to as mode shapes.

For buckling, each eigenvalue corresponds to a critical load level at which the structure may become unstable (ANSYS, 2024). The lowest positive eigenvalue is important, since it defines the critical buckling load of the system. The associated mode shape represents the expected deformation pattern of instability. Higher eigenvalues correspond to additional, less critical buckling modes. These concepts form the basis for evaluating the stability behavior of the crane girder in this study.

2.4 Structure of a crane girder system

The double girder overhead crane system is a structural framework that allows a crane to move longitudinally along a building while carrying heavy loads. To maximize the resistance of the runway beams, stiffeners or bracing systems are commonly used to prevent global and local buckling, resist vertical loads, and limit twisting from the horizontal loads induced by trolley and crane movement.

The key components of the system are the runway beams, the wheel blocks, the crane bridge, and the trolley. The runway girder system consists of two parallel crane runway girders with crane rails mounted on top, running along the length of the building. Due to the long spans and high wheel loads associated with heavy cranes, web stiffeners are often provided along the girders to enhance their stability. The crane bridge spans transversely between the two runway girders and consists of two girders connected by end wheel blocks that run along the rails. On top of the crane bridge, the trolley moves laterally across the bridge, carrying the hoist and hook that lift the load. See Fig. 2.13 for an illustration of the crane system with its key components.

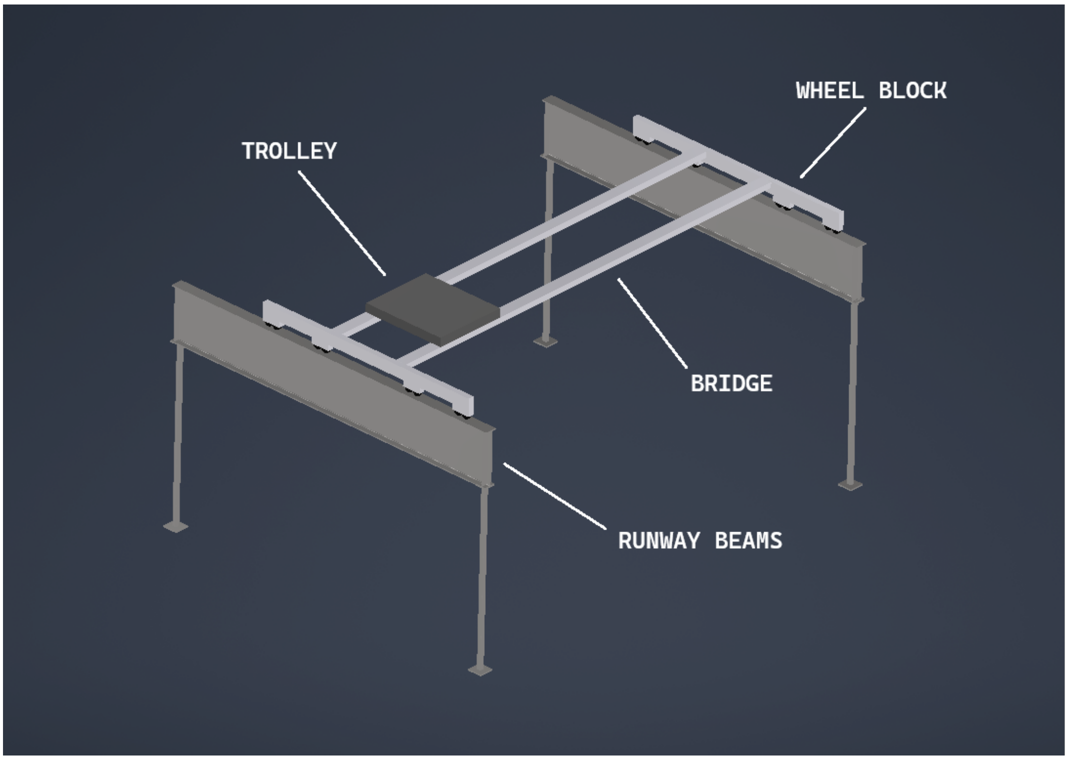

Figure 2.13: Schematic overhead crane runway system.

2.4.1 Design of bracing system

The stabilizing system for the compression flange is typically designed as a built-up truss, with its configuration depending on the loading conditions, span length and cross-sectional dimensions. The first step is to determine the equivalent force that the truss must resist, as given by Eq. 2.13 and illustrated in Fig. 2.14.

$$q_{d,brace} = \sum N_{Ed} \; 8 \; \frac{e_0 + \delta_d}{L^2} \tag{2.13}$$

$$N_{Ed} = \frac{M_{Ed}}{h_{mid}} \tag{2.14}$$

where:

- N_{Ed} is the design value of the axial force from the bending moment [N]
- M_{Ed} is the design value of the maximum moment in the beam [N·mm]
- e_0 is the initial bow imperfection [mm]
- δ_q is the inplane deflection of the bracing system [mm]
- h_{mid} is the height between the midpoints of the flanges [mm]

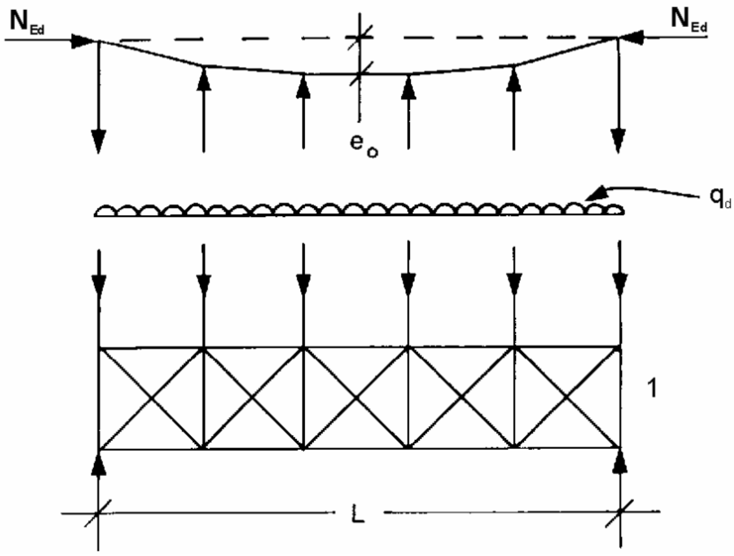

Figure 2.14: Force on the stabilizing system (SIS, 2008a).

To prevent lateral–torsional buckling, the compression flange must be restrained (see Fig 2.16a). The governing parameter is the critical buckling length of the compressive flange, which is denoted L_{cr} and in practice corresponds to the spacing between lateral restraints (see Fig 2.15a and 2.15b). When the top flange is adequately restrained, lateral–torsional buckling is suppressed and the beam capacity increases. However, for longer spans and higher loads, the bottom flange may still experience lateral displacement even when the top flange is fully restrained. In such cases, bracing of the bottom flange is also introduced, extending the system to stabilize both flanges as shown in Fig 2.16b. Whether this additional restraint is necessary and under what conditions it improves the structural performance is the central question investigated in this thesis.

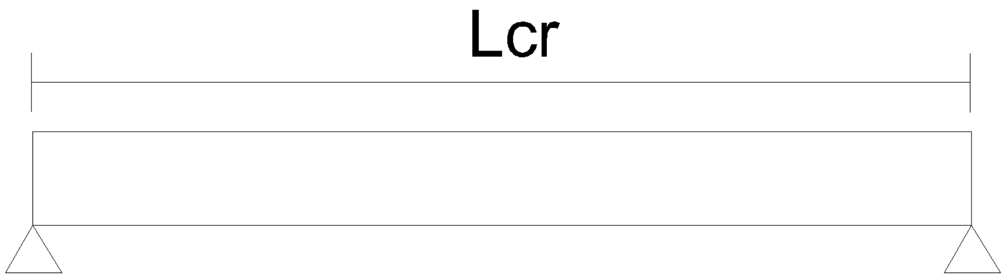

(a) L_{cr} with no intermediate restraints

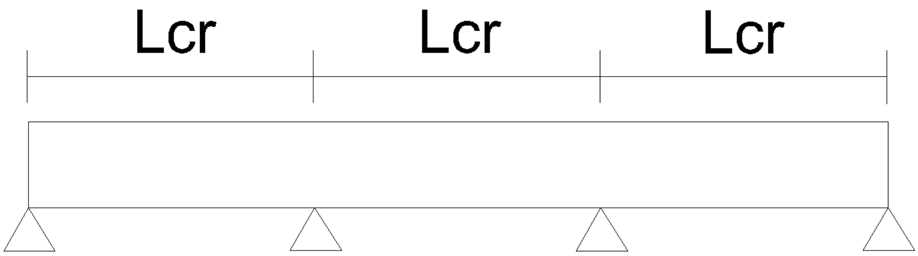

(b) L_{cr} with intermediate lateral restraints

Figure 2.15: Effect of intermediate lateral restraints on the critical buckling length L_{cr}.

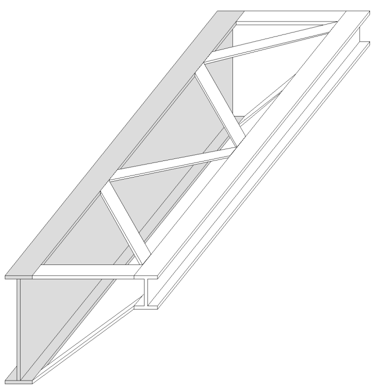

(a) Top flange restrained

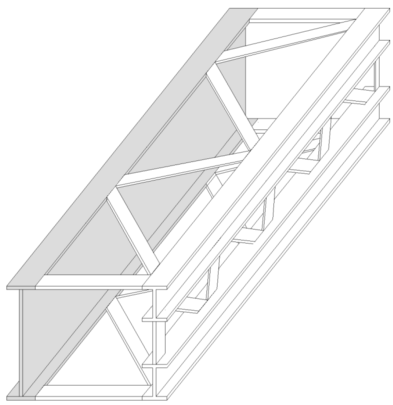

(b) Top and bottom flange restrained

Figure 2.16: Conceptual illustration of lateral restraint configurations for I-girders, with the main crane girder shown in grey and the bracing system in white.

2.5 Design standards

This section provides an overview of relevant design standards for crane girders. The focus is on the provisions from Eurocode that govern load combinations, dynamic factors and stability requirements.

2.5.1 Boverket EKS

In addition to European design standards such as Eurocode, buildings in Sweden must also comply with Boverkets konstruktionsregler (EKS), which is the Swedish national regulation issued by Boverket. EKS supplements Eurocode by providing nationally determined parameters and additional requirements applicable to Swedish conditions. This includes partial safety factors according to Table 2.1 for the design of load-bearing members and the load-bearing capacity of geotechnical structures. The partial factors are also dependent on the reliability class that is required for the system according to Table 2.2.

Table 2.1: Design values of actions.

Persistent and transient	Permanent actions		Leading variable action	Accompanying variable actions
	Unfavorable	Favorable		
6.10a	γ_d 1.35 $G_{kj.sup}$ γ_d 1.35 P_k	1.00 $G_{kj.inf}$ 1.00 P_k	-	-
6.10b	γ_d 0.89 1.35 $G_{kj.sup}$ γ_d 1.35 P_k	1.00 $G_{kj.inf}$ 1.00 P_k	When the action is unfavorable: γ_d 1.5 $Q_{k,1}$ When the action is favourable: 0	When the action is unfavorable: γ_d 1.5 ψ_i $Q_{k,i}$ When the action is favourable: 0

Table 2.2: Values of γ_d depending on reliability class.

Reliability class	γ_d [-]
1	0.83
2	0.91
3	1

2.5.2 Load combinations according to Eurocode

To obtain relevant load combinations without being overly conservative by considering all loads acting simultaneously, Eurocode have different groups for different ultimate limit state cases (SIS, 2010). These load groups specify which dynamic factors should be applied to each load and which loads should be considered simultaneously, as shown in Fig. 2.17. For ULS cases 1 and 2, dynamic factors are applied to both the hoist load and self-weight to capture the maximum vertical loading and the acceleration of the crane bridge is also included. ULS case 3 considers crane bridge acceleration without the hoist load. ULS case 4 is similar to cases 1 and 2 but with different dynamic factors applied. For ULS case 5, φ_4 is applied to both self-weight and hoist load, however crane bridge acceleration is not considered, instead the skewing of the crane bridge is included. ULS case 6 considers the braking or acceleration of the crab or hoist block. In-service wind is included in load groups 1-5 and 8 according to Annex A and load groups 7-10 cover special cases such as test loads and accidental loads. Each load group therefore represents a physical scenario, ensuring that only loads which can realistically occur simultaneously are combined.

		Symbol	Section	Groups of loads									
				Ultimate Limit State							Test load	Accidental	
				1	2	3	4	5	6	7	8	9	10
1	Self-weight of crane	Q_c	2.6	φ_1	φ_1	1	φ_4	φ_4	φ_4	1	φ_1	1	1
2	Hoist load	Q_h	2.6	φ_2	φ_3	-	φ_4	φ_4	φ_4	$\eta^{1)}$	-	1	1
3	Acceleration of crane bridge	H_L, H_T	2.7	φ_5	φ_5	φ_5	φ_5	-	-	-	φ_5	-	-
4	Skewing of crane bridge	H_S	2.7	-	-	-	-	1	-	-	-	-	-
5	Acceleration or braking of crab or hoist block	H_{T3}	2.7	-	-	-	-	-	1	-	-	-	-
6	In-service wind	F_W^*	Annex A	1	1	1	1	1	-	-	1	-	-
7	Test load	Q_T	2.10	-	-	-	-	-	-	-	φ_6	-	-
8	Buffer force	H_B	2.11	-	-	-	-	-	-	-	-	φ_7	-
9	Tilting force	H_{TA}	2.11	-	-	-	-	-	-	-	-	-	1

NOTE: For out of service wind, see Annex A.

[1] η is the proportion of the hoist load that remains when the payload is removed, but is not included in the self-weight of the crane.

Figure 2.17: Loading groups and dynamic factors that shall be used together (SIS, 2010).

2.5.3 Dynamic factors according to Eurocode

Since the loads applied to a crane structure are variable and dynamic, certain dynamic factors are introduced to account for these effects. Eurocode defines seven dynamic factors φ_1-φ_7, each accounting for a specific dynamic phenomenon associated with crane operations, where the first five are related to normal operating conditions and the remaining two cover test loads and accidental loads. The dynamic factors and their corresponding effects are summarised in Tab. 2.3.

Table 2.3: Dynamic factors φ_i (SIS, 2010).

Dynamic factors	Effects to be considered	To be applied to
φ_1	excitation of the crane structure due to lifting the hoist load off the ground	self-weight of the crane
φ_2 or φ_3	dynamic effects of transferring the hoist load from the ground to the crane dynamic effects of sudden release of the payload if for example grabs or magnets are used	hoist load
φ_4	dynamic effects induced when the crane is traveling on rail tracks or runways	self-weight of the crane and hoist load
φ_5	dynamic effects caused by drive forces	drive force
φ_6	dynamic effects of a test load moved by the drives in the way the crane is used	test load
φ_7	dynamic elastic effects of impact on buffers	buffer loads

How the values of the dynamic factors are calculated according to Eurocode are presented in Tab. 2.4, and the values for calculating φ_2 are found in Tab. 2.5. φ_1 accounts for the vibrational pulse when lifting the hoist load off the ground and takes values between 0.9 and 1.1 reflecting the upper and lower bounds of this effect. φ_2 depends on the hoisting class of the crane and the steady hoisting speed, where higher hoisting classes correspond to larger dynamic effects. φ_3 depends on the proportion of the load that is released and the release method, where rapid release devices such as magnets result in larger dynamic effects than slower release devices such as grabs. φ_4 accounts for dynamic effects when the crane travels on rail tracks and is equal to 1.0 provided that the rail tolerances specified in EN 1993-6 are observed. φ_5 depends on the specific drive system of the crane, its values are presented in Tab. 2.6. φ_6 accounts for the dynamic effects of a test load moved by the drives and φ_7 accounts for the dynamic elastic effects of impact on buffers.

Table 2.4: Dynamic factors φ_i for vertical loads (SIS, 2010).

Dynamic factors	Values of dynamic factors
φ_1	$0.9 < \varphi_1 < 1.1$ The two values 1.1 and 0.9 reflect the upper and lower values of the vibrational pulses
φ_2	$\varphi_2 = \varphi_{2,\min} + \beta_2 v_h$ v_h - steady hoisting speed in m/s $\varphi_{2.min}$ and β_2 see Tab. 2.5
φ_3	$\varphi_3 = 1 - \frac{\Delta m}{m}(1 + \beta_3)$ where Δm released or dropeed part of the hoisting mass m total hoisting mass $\beta_3 = 0.5$ for cranes equipped with grabs or similar slow release devices $\beta_3 = 1$ for cranes equipped with magnets or similar rapid-release devices
φ_4	$\varphi_4 = 1.0$ Provided that the tolerances for rail tracks as specified in EN 1993-6 are observed

Table 2.5: Values of β_2 and $\varphi_{2,min}$ depending on hoisting class (SIS, 2010).

Hoisting class of appliance	β_2	$\varphi_{2,\min}$
HC1	0.17	1.05
HC2	0.34	1.1
HC3	0.51	1.15
HC4	0.68	1.2

Table 2.6: Dynamic factor φ_5 (SIS, 2010).

Values of the dynamic factor φ_5	Specific use
$\varphi_5 = 1$	for centrifugal forces
$1.0 \leq \varphi_5 \leq 1.5$	for systems where forces change smoothly
$1.5 \leq \varphi_5 \leq 2.0$	for cases where sudden changes can occur
$\varphi_5 = 3.0$	for drives with considerable backlash

2.5.4 Imperfection Modelling in Finite Element Analyses According to Eurocode

Imperfections in beams are a natural occurrence, as no beam is perfectly straight. When modelling structural behaviour, these imperfections must be accounted for to avoid favourable results. Eurocode provides guidance on this in the part on design assisted by finite element analysis (SIS, 2025b), where equivalent geometric imperfections are introduced to capture the combined effects of residual stresses and geometric imperfections. For beams subjected to LTB, the equivalent geometric imperfection is given by Eq. 2.15.

$$e_0 = \alpha \cdot L \cdot \beta_{LT,1} \qquad \text{but} \qquad e_0 \geq \frac{L}{1000} \tag{2.15}$$

where: α is the imperfection factor for minor axis flexural buckling [-]

$\beta_{LT,1}$ is the equivalent geometric imperfections for structural members for LTB ,shown in Fig 2.18 [-]

Table 5.5 — Equivalent geometric imperfections for structural members for lateral torsional buckling

Shape	β_{LT}	Illustration
bow	combination of 1/150 (half-sine wave) and 1/215 (full sine wave)	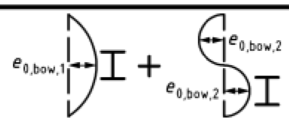
buckling shape	1/150	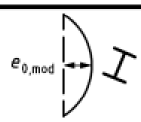

Figure 2.18: Values of $\beta_{LT,1}$ (SIS, 2025b).

Further guidance specific to crane runway beams is given in SS-EN 1993-6 (SIS, 2025a), which refers to SS-EN 1993-1-1 (SIS, 2008a) for global analysis. For plastic analysis of crane runway beams, the equivalent initial bow imperfection $e_{0,LT}$ is given by Eq. 2.16, where the LTB factor β_{LT} is taken from a more detailed table that differentiates between rolled and welded cross sections, the height to width ratio, and whether elastic or plastic cross section verification is used, resulting in a range of values for β_{LT} , as shown in Fig. 2.19.

$$e_{0,LT} = \beta_{LT,2} \cdot \frac{L}{\varepsilon} \tag{2.16}$$

where: ε is a material parameter [-]

$\beta_{LT,2}$ is the reference relative bow imperfection for LTB, shown in Fig. 2.19 [-]

Table 7.2 — Reference relative bow imperfection β_{LT} for lateral torsional buckling

Cross-section	Condition	Elastic cross-section verification	Plastic cross-section verification
rolled	$h/b \le 2{,}0$	1/250	1/200
	$h/b > 2{,}0$	1/200	1/150
welded	$h/b \le 2{,}0$	1/200	1/150
	$h/b > 2{,}0$	1/150	1/100

Figure 2.19: Values of $\beta_{LT,2}$ (SIS, 2022).

The equations above describe imperfections governing the global behaviour of the beam. Local imperfections of the web, which may reduce capacity against shear buckling or other local failure modes, require separate treatment. For practical manufacturing tolerances such as plate curvature and squareness at bearings, SS-EN 1090-2:2018 defines the requirements across different execution classes (SIS, 2024). The plate curvature limits are shown in Figure 2.20.

No	Criterion	Parameter	Essential tolerances Permitted deviation Δ	Functional tolerances Permitted deviation Δ	
			Class 1 and 2	Class 1	Class 2
7	Plate curvature: 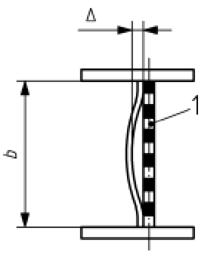	Deviation Δ over plate height b:	$\Delta = \pm b/200$ if $b/t \le 80$ $\Delta = \pm b^2/(16\,000\,t)$ if $80 < b/t \le 200$ $\Delta = \pm b/80$ if $b/t > 200$ but $\lvert\Delta\rvert \ge t$ (t = plate thickness)	$\Delta = \pm b/100$ but $\lvert\Delta\rvert \ge 5$ mm	$\Delta = \pm b/150$ but $\lvert\Delta\rvert \ge 3$ mm

Figure 2.20: Plate curvature imperfection limits (SIS, 2024).

2.6 American guidance for bottom flange bracing

American design practice has in history included explicit provisions regarding bottom flange bracing of crane runway girders. Earlier editions of AISE Technical Report No. 13 specified that crane girders exceeding certain span limits should be provided with bottom flange bracing connected to an adjacent girder or stiffening truss (AISE, 2003). The bracing system was required to resist a force corresponding to 2.5% of the axial force in the bottom flange at midspan.

Recent AIST publications mentions the importance of bottom flange stability, although in the form of recommendations rather than mandatory requirements. In the 2021 guidance bottom flange stiffening is recommended for spans longer than

50 ft (15.24 m) regardless of building class (AIST, 2021). The purpose of the backup bracing system is to increase torsional stiffness and restrain distortion caused by the combined effects of vertical loads, lateral wheel loads and torsional actions. Instead of the earlier 2.5% axial-force criterion, the recommended design force for the bottom flange bracing is at least 25% of the force used for the top-flange bracing system.

In additions to the AIST recommendations, the American Institute of Steel Construction (AISC) address a limit state for web sidesway buckling in Section J10.4 (AISC, 2022). This provision applies to members where a concentrated compressive force is applied to the compression flange, and the tension flange is free to move laterally at the point of load application, see section 2.3.6.

When the compression flange is restrained against rotation, the limit state ratio is $(h/t_w)/(L_b/b_f)$ and if that does not exceeds 2.3, web sidesway buckling may occur and the nominal strength R_n shall be determined as:

$$R_n = \frac{C_r t_w^3 t_f}{h^2}\left[1 + 0.4\left(\frac{h/t_w}{L_b/b_f}\right)^3\right] \tag{2.17}$$

where:	α_s	1.0 (LRFD)	
	C_r	$= 960{,}000$ ksi (6.6×10^6 MPa)	when $\alpha_s M_r < M_y$
	C_r	$= 480{,}000$ ksi (3.3×10^6 MPa)	when $\alpha_s M_r \geq M_y$
	L_b	is the largest laterally unbraced length along either flange at the point of load [mm]	
	h	is the clear distance between flanges for built-up members [mm]	
	t_f	is the flange thickness [mm]	
	t_w	is the web thickness [mm]	
	b_f	is the flange width [mm]	
	M_r	is the required flexural strength [N·mm]	
	M_y	is the yield moment $= F_y S_x$ [N·mm]	
	R_n	is the nominal strength [N]	

If the ratio $(h/t_w)/(L_b/b_f)$ exceeds 2.3, the limit state of web sidesway buckling does not apply. The required strength is the nominal strength multiplied with the safety factor $\phi = 0.85$. And this needs to be larger than $P_{wheel,d}$ as shown in Eq. 2.18.
When the ratio is below 2.3, the available strength is given by the nominal strength R_n multiplied by the resistance factor $\phi = 0.85$, which must exceed the maximum design wheel load $P_{wheel,d}$ as shown in Eq. 2.18.

$$\phi R_n \geq P_{\mathrm{wheel,d}} \tag{2.18}$$

where:	$P_{wheel,d}$	is the maximum design wheel load [N]
	ϕ	is a safety factor $= 0.85$ [-]

2.7 Softwares used

In this section softwares used in the thesis are presented, this includes softwares for calculations and finite element modelling.

2.7.1 Abaqus CAE

Abaqus Computer-Aided Engineering is a finite element analysis software that lets users perform advanced simulations based on defined model parameters such as geometry, material properties, boundary conditions and analysis type. It supports a wide range of analysis, from linear simulations to nonlinear studies that may include effects such as material plasticity, geometric nonlinearity and initial imperfections. It has a wide range of different results that can be extracted, such as stresses, strains and displacements which can be visualized and evaluated through its interactive graphical interface.

2.7.2 MathCAD Prime

PTC MathCAD Prime is an engineering mathematics software designed to make the formulation, solution, documentation and presentation of technical calculations. Its built-in unit handling system automatically tracks and verifies dimensional consistency, reducing the risk of unit-related errors and improving reliability in engineering workflows. In addition, its integrated programming capabilities enable the implementation of conditional logic, iterative procedures and verification routines, providing flexibility for analyses that depend on multiple parameters or criteria.

2.7.3 MATLAB

MATLAB is a matrix-based programming language, used for modelling, simulations and numerical analysis in engineering and scientific research. It offers multiple numerical capabilities, visualization tools and specialized toolboxes for optimization and simulation.

The CALFEM toolbox implemented in MATLAB, is commonly used for finite element modelling in structural engineering. It enables the formulation of structural models using element formulations and stiffness matrices and provides a transparent implementation of the finite element method. CALFEM is particularly suitable for analysing structural systems, such as trusses and for evaluating their response under applied loads.

3

Design Basis and Analytical Calculations

This chapter presents the crane loads acting on the runway girder and describes how they are transformed into design loads for structural analysis. The design of the physical bracing system and the support conditions of the girder are also described.

3.1 Base case geometry

The finite element model is based on a crane runway girder from project drawings provided by the supervisors. The cross sectional dimensions and span length of this girder serve as the base case throughout the verification and parametric study, and are summarised in Table 3.1 with a visual representation shown in Fig. 3.1.

Table 3.1: Base case geometry of the crane runway girder.

Parameter	Value [mm]
Length of crane beam L	24000
h_w	3420
t_w	30
b_{tf}	800
t_{tf}	100
b_{bf}	700
t_{bf}	80

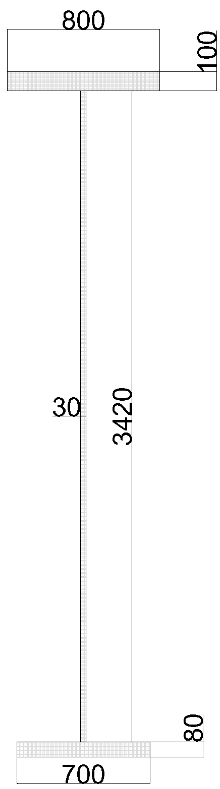

Figure 3.1: Visual representation of the cross section.

3.1.1 Crane rail

The crane moves along a rail mounted on top of the runway girder, specified according to European Standard DIN 536 with sizes ranging from A45 to A150. For large crane runways, A150 is the most common choice and is therefore used throughout the calculations and simulations in this work, as shown in Fig. 3.2.

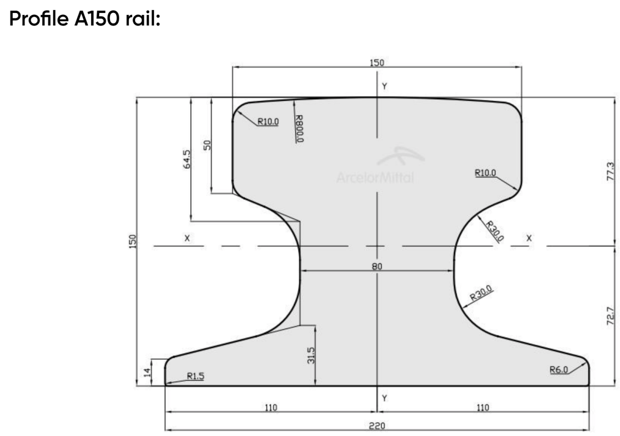

Figure 3.2: Profile of rail type A150 (ArcelorMittal, 2024).

3.2 Crane specifications

The loads governing the design are taken from crane manufacturer specifications for one specific crane type, with the key parameters summarised in Table 3.2. The wheel arrangement and spacing are shown in Fig. 3.3, which determines the point load positions acting along the length of the crane girder.

Table 3.2: Crane specification.

Explanation	Symbol	Value
Capacity of crane [kg]	Q_h	465000
Trolley weight [kg]	G_c	205000
Bridge weight [kg]	G_b	565000
Span between crane beams [mm]	l	31000
Crane lifting speed [m/s]	v_h	0.1

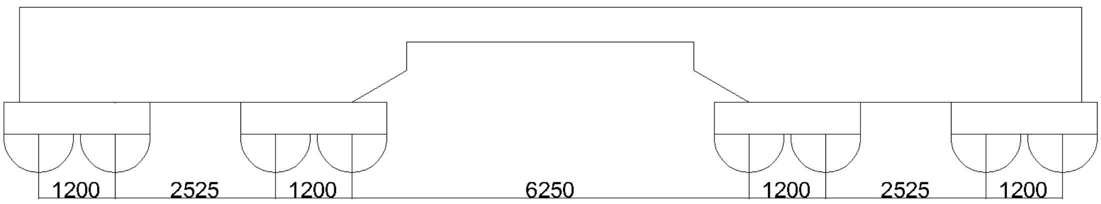

Figure 3.3: Wheel arrangement and spacing in the wheel block, based on crane document drawings.

3.3 Vertical loads

The vertical loads acting on the crane system consist of permanent actions from the self-weight of the bridge and trolley, alongside variable actions from the crane's rated capacity. While SS-EN 1991-3 (SIS, 2010) provides a theoretical framework for calculating these as resultant point loads, this analysis utilizes the comprehensive wheel load data provided by the manufacturer in Table 3.3.

The data is presented for two load cases corresponding to the trolley positioned at each end of the bridge, referred to as side 1 and side 2. Side 2 produces the larger total vertical wheel loads and therefore governs the vertical load case, while side 1 is associated with different horizontal load distributions which are presented in Section 3.4. These characteristic loads are subsequently amplified by the EKS load combination factors in Table 2.1 and the specific dynamic factors in Table 2.3. For this analysis, ULS load case 1 is considered, with the trolley positioned on side 2, which corresponds to the maximum vertical load scenario on the crane beam.

Table 3.3: Vertical Loads, $P_{wheel.k}$ [kg]

TROLLEY ON SIDE 1					TROLLEY ON SIDE 2				
W8	90678		**W16**	34622	**W8**	28941		**W16**	92468
W7	90678		**W15**	34622	**W7**	28941		**W15**	92468
W6	95471		**W14**	37818	**W6**	31612		**W14**	101004
W5	95471		**W13**	37818	**W5**	31612		**W13**	101004
W4	94798		**W12**	38377	**W4**	33397		**W12**	100451
W3	94798		**W11**	38377	**W3**	33397		**W11**	100451
W2	86787		**W10**	36450	**W2**	31720		**W10**	95407
W1	86787		**W9**	36450	**W1**	31720		**W9**	95407

3.4 Horizontal loads

The horizontal actions acting on the crane system are categorized into longitudinal and transversal forces, as summarized in Table 3.4. For this analysis, the specific load magnitudes provided by the crane manufacturer are used directly. These values reflect the actual mechanical specifications of the unit and allow for a more direct design process compared to general code-based estimations. However, the physical origins and categories of these forces remain defined by standard crane design theory in SS-EN 1991-3 (SIS, 2010), as detailed below. An overview of how these forces are applied in the system is shown in Fig. 3.4.

Table 3.4: Maximum Lateral Loads, $K_{r,k}$, $H_{m,k}$, $K_{a,k}$ [kg]

Side	**Wheel**	**Longitudinal Long Travel ($K_{r.k}$)**	**Transversal Long Travel ($H_{m.k}$)**	**Transversal Cross Travel ($K_{a.k}$)**
SIDE 1			H_{m1}	
	W1	0	6602	3844
	W2	11735	6602	3844
	W3	0	0	3844
	W4	0	0	3844
	W5	0	0	3844
	W6	0	0	3844
	W7	11735	-6602	3844
	W8	0	-6602	3844
SIDE 2			H_{m2}	
	W9	0	17977	0
	W10	11735	17977	0
	W11	0	0	0
	W12	0	0	0
	W13	0	0	0
	W14	0	0	0
	W15	11735	-17977	0
	W16	0	-17977	0

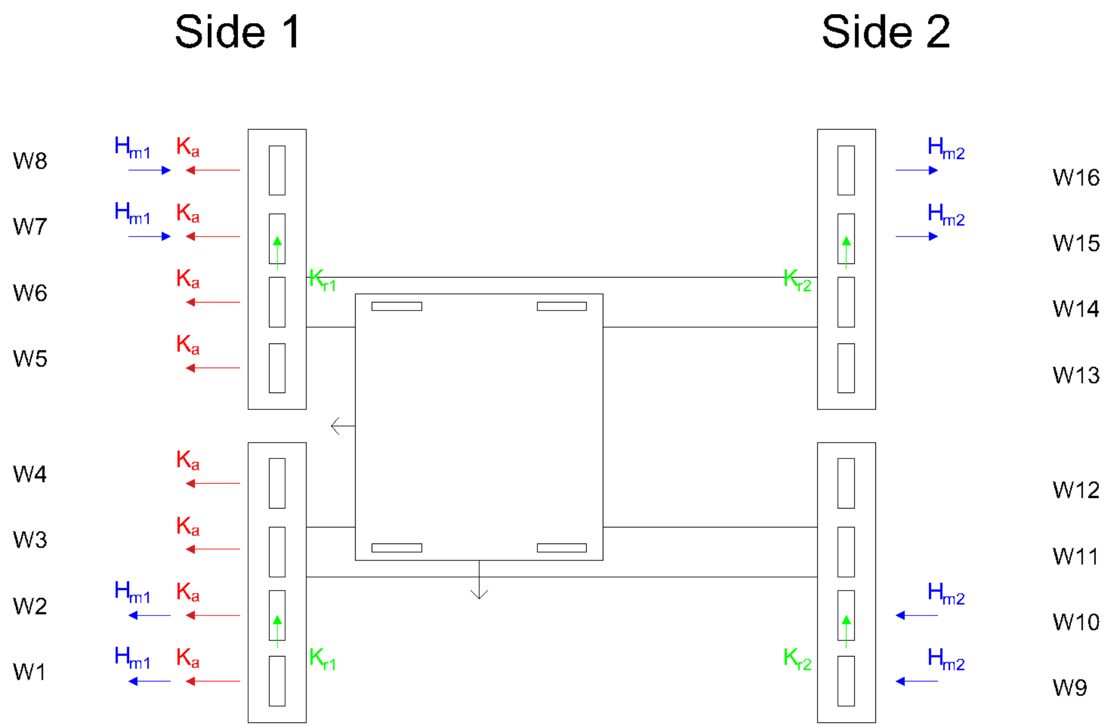

Figure 3.4: Identification and orientation of horizontal design forces K_a, K_r, H_{m1}, and H_{m2} across all wheel positions, based on crane document drawings.

3.4.1 Longitudinal forces (K_r)

Longitudinal forces denoted as K_r arise from the acceleration and deceleration of the crane bridge along the runway beams. In accordance with standard friction theory, these forces are a function of the drive force and the interaction between the steel wheels and the rail (typically using a friction factor of $\mu = 0.2$ (SIS, 2010)). The manufacturer's data accounts for the specific four-wheel drive configuration of this crane, ensuring the longitudinal thrust is correctly distributed across the rail system.

3.4.2 Transverse forces from long travel (H_{m1}, H_{m2})

Transversal forces during long travel, denoted as H_{m1} and H_{m2}, represent horizontal forces acting on the runway beams when the crane travels along the rails. These forces arise from the lateral interaction between the crane wheels and the rail during operation, for example due to slight misalignment of the crane bridge. The forces act perpendicular to the beam axis and are applied at the wheel positions. In the load data, they are represented as equal and opposite actions on the primary and secondary beams, forming a horizontal force system between the runway beams.

3.4.3 Transverse forces from cross travel (K_a)

Transversal forces K_a result from the acceleration or deceleration of the trolley as it moves across the bridge. While the Eurocode typically offers a general estimate of 10% of the combined hoist and crab weight for this action (SIS, 2010), the values provided in Table 3.4 are specific to the braking and acceleration curves of this particular trolley unit. These forces act transversally to the runway and are distributed among the wheels of the end carriages.

3.4.4 Skewing forces (S, Y_i)

Skewing forces arise when the crane bridge becomes slightly misaligned relative to the runway beams during travel. This misalignment causes the crane to rotate about a vertical axis, leading to lateral contact forces between the wheel flanges and rail. These forces act as a guidance forces that keep the crane aligned on the rails. According to SS-EN 1991-3 (SIS, 2010), such misalignment gives rise to horizontal forces acting on the runway beams.

As illustrated in Fig. 3.5, the forces are not uniformly distributed but are concentrated in the extreme wheels of each end carriage, where the largest forces occur. The distribution of forces at each wheel is represented by Y_i, while the resultant guidance force is denoted as S.

Table 3.5: Skewing Forces, S, $Y_{i,k}$ [kg]

Side	Wheel	Skewing Force (S)	Lateral Skewing Force ($Y_{i,k}$)
SIDE 1			
	W1	63438	16523
	W2	0	14925
	W3	0	11561
	W4	0	9963
	W5	0	1637
	W6	0	39
	W7	0	-3325
	W8	0	-4924
SIDE 2			
	W9	63438	6068
	W10	0	5481
	W11	0	4246
	W12	0	3659
	W13	0	601
	W14	0	14
	W15	0	-1221
	W16	0	-1808

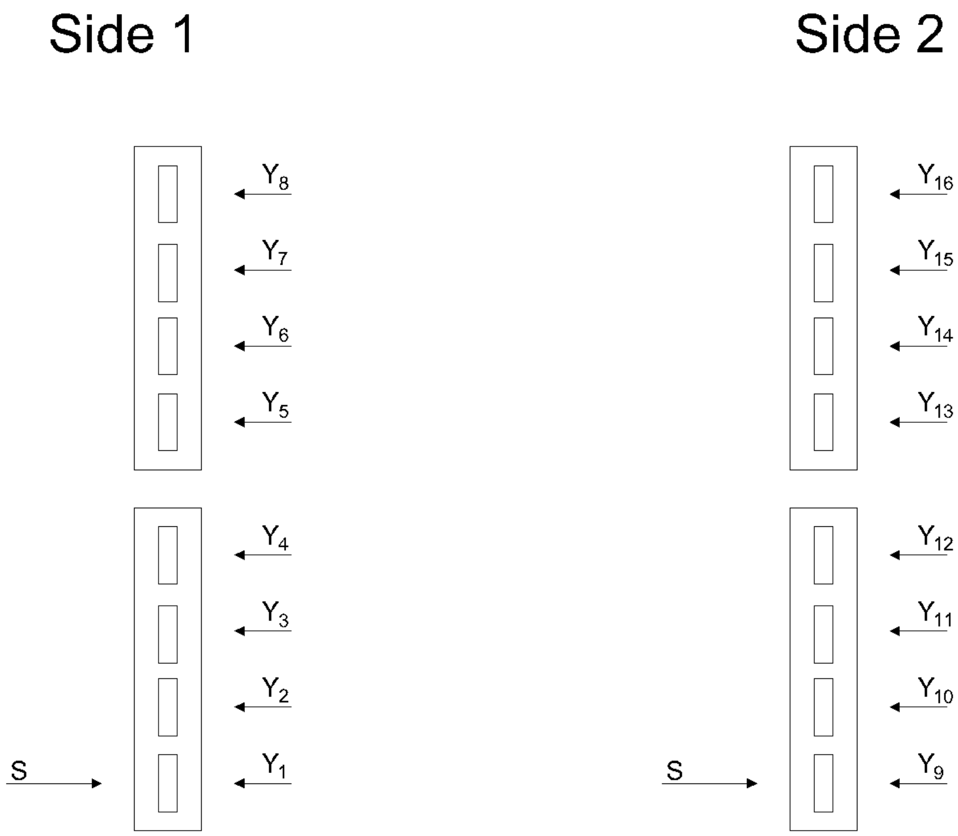

Figure 3.5: Distribution of lateral wheel forces due to skewing of the crane bridge, based on crane document drawings.

3.5 Design loads

The design loads are determined at ULS for the structural analysis, with the exception of the in-plane deflection calculation for the bracing system which uses SLS-loads.

3.5.1 ULS loads

The characteristic wheel loads are given directly in the project specifications and are presented in Table 3.3. To apply the correct partial factors, the total load must be separated into permanent and variable components. Since this split is not explicitly given, a ratio is derived from the known crane capacity, trolley weight and bridge weight, as shown in Eq. 3.1.

$$R_{perm} = \frac{G_c + G_b}{G_c + G_b + Q_h} \tag{3.1}$$

where: R_{perm} represents the permanent load fraction [-]

$R_{var} = 1 - R_{perm}$ represents the variable load fraction [-]

These ratios are applied to each characteristic load component to estimate its permanent and variable contributions, to which the partial factors φ_i are then applied respectively depending on what ULS case is chosen. Using reliability class 3 with $\gamma_d = 1.0$ according to Boverket, the design value for each load component is given by Eq. 3.2, which applies to the vertical wheel loads, the transverse horizontal loads, the skewing loads and the longitudinal loads.
In practice, all load combinations are evaluated to account for cases where a favorable permanent load in one direction may produce a worse loading condition overall. Here, expression 6.10b is used throughout as it produces the largest design loads for the crane actions considered.

$$F_{d.ULS} = \varphi_i \cdot 1.35 \cdot \gamma_d \cdot R_{perm} \cdot g \cdot F_k + \varphi_i \cdot 1.5 \cdot \gamma_d \cdot R_{var} \cdot g \cdot F_k \tag{3.2}$$

where: F_k is the characteristic value of any load component [N]
F_d is the corresponding design value [N]
g is the acceleration due to gravity, $g = 9.81$ [m/s^2]

3.5.2 SLS loads

In addition to the ULS design loads, the SLS loads are used to estimate the in-plane deflection δ_q of the girder, which is required as input for the equivalent load method in the design of the bracing system, as described in Section 2.4.1. For the SLS no partial factors are applied and the load reduces to the characteristic value converted to Newtons, given by Eq. 3.3:

$$F_{d.SLS} = g \cdot F_k \tag{3.3}$$

3.5.3 Load case used in FEM-analysis

Of the load combinations presented in Section 2.5.2, ULS 1 is selected for the analysis, as it produces the largest vertical wheel loads and is considered the most critical case based on guidance from our supervisors. This combination applies the dynamic factor φ_1 to the self-weight and φ_2 to the hoist load. A conservative upper value of $\varphi_1 = 1.1$ is used, while $\varphi_2 = 1.268$ is determined from hoisting class 4 and the lifting speed given in Table 3.2. The acceleration of the crane bridge gives rise to both longitudinal and transverse horizontal forces, which are included with the dynamic factor $\varphi_5 = 1.5$, corresponding to forces changing smoothly, chosen in accordance with guidance from the supervisors.

Applying these dynamic factors to the characteristic loads using Eq. 3.2, the design loads for all eight wheels are obtained and presented in Table 3.6. The loads correspond to the governing side 2, which produces the larger vertical wheel loads compared to side 1. For ULS 1, no skewing loads are present, and the transverse horizontal load $H_{m,d}$ and longitudinal load $K_{r,d}$ are only non-zero for the wheels where crane bridge acceleration is active.

While side 1 produces larger lateral forces, side 2 governs the compressive force in the top flange due to its larger vertical wheel loads. When evaluating which side governs the design of the bracing system, both sides produce similar results, meaning either could be used. To improve clarity and consistency throughout the report, side 2 is used for both the bracing system design and the finite element model verification, resulting in a single governing load case across all analyses.

Table 3.6: Design loads for the load combination ULS 1, side 2.

Wheel	$P_{wheel,d}$ [kN]	$H_{m,d}$ [kN]	$K_{r,d}$ [kN]
1	1489	371.931	0
2	1489	371.931	242.788
3	1626	0	0
4	1626	0	0
5	1618	0	0
6	1618	0	0
7	1536	-371.931	242.788
8	1536	-371.931	0

3.6 Design of the bracing system

The stabilizing system is designed to provide lateral restraint to the top flange in compression, thereby preventing lateral-torsional buckling. The design process was implemented through a MATLAB-based optimization script following the equivalent load method, using SLS loads from side 2. This script allows for a parametric approach, where the height of the vertical bars and the desired bay length are specified as input, and the script then adjusts the bay length to ensure an even number of bays along the full span of the beam.

3.6.1 Determination of equivalent loads

The equivalent line load $q_{d,brace}$ is derived from the unbraced beam's response to the crane and normative loads, as described in Section 2.4.1. It incorporates the design axial force N_{Ed}, the initial bow imperfection e_0 and the in-plane deflection δ_q under SLS loads, taken conservatively as the deflection of the unrestrained beam (Eq. 3.4). In this study, only a single restrained member is considered ($m_{brace} = 1$), resulting in an adjustment factor $\alpha_m = 1.0$, representing the most conservative case, see Eq. 3.5.

$$e_0 = \frac{\alpha_m \cdot L}{500} \tag{3.4}$$

$$\alpha_m = \sqrt{0.5\left(1 + \frac{1}{m_{brace}}\right)} \tag{3.5}$$

where: α_m is a reduction factor for multiple restrained members [-]

m_{brace} is the number of restrained members [-]

The key parameters and the resulting equivalent line load are summarised in Table 3.7, with the full calculation presented in Appendix B.

Table 3.7: Key parameters for the equivalent line load calculation.

Parameter	Symbol	Value
Initial deflection	e_0	48 [mm]
In-plane deflection	δ_q	58.056 [mm]
Design axial force	N_{Ed}	1241 [kN]
Equivalent line load	$q_{d,brace}$	18.276 [N/mm]

3.6.2 Computational Design and Component Sizing

With the equivalent load $q_{d,brace}$ determined as described in Section 2.4.1, the truss configuration was defined, consisting of an I-beam top chord and round bar verticals and diagonals, with the top flange of the primary girder acting as the bottom chord. The truss was modelled using the CALFEM library in MATLAB, which utilizes the finite element method to assemble global stiffness matrices from beam and bar elements, automating node numbering and element connectivity to calculate member forces and displacements.

The stability of these members was verified by calculating the critical buckling load P_{cr} using Eq. 3.6. To ensure that local member failure does not govern the global design, a safety factor of 1.5 was applied to the capacity of the bars. In the automated design check, the buckling length L_{cr} was adjusted according to the member type: for verticals and diagonals, L_{cr} corresponds to their respective lengths, while for the top chord, L_{cr} is defined as the distance between vertical members.
The top chord was designed as a secondary I-beam. The global bending moment of the truss $M_{Ed,brace}$ is first determined from the equivalent line load according to Eq. 3.7, from which the compressive chord force $N_{Ed,brace}$ is derived using Eq. 3.8. The top chord dimensions were verified against this compressive force. The full results and codes are presented in Appendix C.1.

$$P_{cr} = \frac{\pi^2 EI}{L_{cr}^2} \tag{3.6}$$

$$M_{Ed,brace} = \frac{q_{d,brace} \cdot L^2}{8} \tag{3.7}$$

$$N_{Ed,brace} = \frac{M_{Ed,brace}}{L_{vertical}} \tag{3.8}$$

where: P_{cr} is the critical buckling load of the member [N]

L_{cr} is the buckling length of the member being analysed [mm]

$M_{Ed,brace}$ is the bending moment in the truss from the equivalent line load [N·mm]

$q_{d,brace}$ is the equivalent line load on the bracing system [N/mm]

$N_{Ed,brace}$ is the compressive force in the top chord [N]

$L_{vertical}$ is the effective depth of the truss (length of the vertical bar) [mm]

3.7 Boundary conditions

The boundary conditions are modelled based on engineering drawings provided by the project supervisors. The beam rests on a rubber pad on top of the supporting column, secured by two bolts on each side of the web. The bolts are installed in elongated holes, permitting a limited degree of longitudinal movement. This configuration is modelled as one pinned and one roller support, as shown in Fig. 3.6. The pinned support restrains all translations while the roller support allows movement in the longitudinal direction. The two-bolt arrangement on each side of the web provides rotational restraint about the longitudinal axis at both supports. Rotation about the vertical axis is left free, as the elongated bolt holes permit longitudinal movement and reduce the rotational fixity in that direction. Rotation about the bending axis remains free to allow the beam to deflect under load. Additionally, a stabilizing connection at the top flange prevents lateral translation at the support, as illustrated in Fig. 3.7, providing stability against lateral tipping of the cross section.

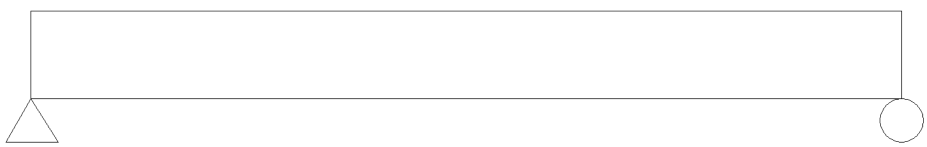

Figure 3.6: Schematic illustration of the simply supported beam with pinned and roller support

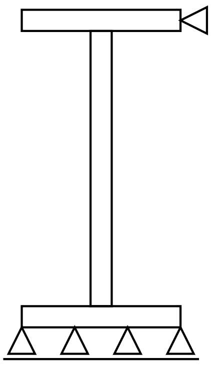

Figure 3.7: Cross sectional view showing vertical support conditions at the bottom flange and lateral restraint at the top flange

3.8 Control of sidesway buckling

The web sidesway buckling check follows the procedure described in Section 2.6. The first step is to evaluate the ratio in Eq. 3.9, which determines whether the limit state is applicable. Here h is the web height, L_b is the largest laterally unbraced length along either flange - taken as the full span of 24 m for the unbraced bottom flange - and b_f is the width of the flange under consideration, in this case the bottom flange.

$$\text{Ratio} = \frac{h/t_w}{L_b/b_f} \qquad \text{Ratio} \geq 2.3 \tag{3.9}$$

For the base case geometry, the ratio is 3.325, which exceeds 2.3, meaning the limit state for web sidesway buckling does not govern and no further check is required for this configuration. However, since the parametric study varies the web height and bottom flange width, the ratio will fall below 2.3 for some combinations, and the full check must then be applied. The procedure for those cases is therefore outlined here and the results are presented in Section 6.5. When the ratio is below 2.3, the elastic sectional modulus S_x is calculated according to Eq. 3.10 and multiplied by the yield strength f_y to obtain the yield moment M_y. Comparing M_y to the required moment M_r with $\alpha_s = 1.0$ determines the value of C_r, which for this cross section is $6.6 \cdot 10^6$ MPa.

$$S_x = \min\left(\frac{I_y}{z_{\text{top}}}, \frac{I_y}{z_{\text{bot}}}\right) \tag{3.10}$$

where: S_{x} is the elastic sectional modulus (AISC notation) [mm^3]

z_{bot} is the distance from the centre of gravity to the bottom of the cross section [mm]

With C_r established, Eq. 2.17 gives the nominal strength R_n, which is then multiplied by ϕ to obtain the available strength. This is compared against the maximum design wheel load of 1626 kN from Table 3.6 using Eq. 2.18 to determine whether the cross section satisfies the sidesway buckling limit state. See Appendix B for full calculations.

4
Finite Element Model

This chapter describes how the finite element model of the crane runway girder is constructed and verified. The modelling assumptions, boundary conditions, material properties, and mesh are defined, followed by a description of the parametric study setup and the analysis procedure used to obtain the results.

4.1 Modelling approach

The finite element model is implemented as a Python script running within Abaqus, where all key geometric and structural variables are defined at the beginning of the script, allowing the girder configuration to be modified efficiently by changing the input parameters. The most critical wheel load positions are determined using MATLAB based on an influence line search, and subsequently implemented in the model. The base case geometry is defined in Section 3.1 and serves as the reference throughout the verification and parametric study.

4.1.1 Boundary conditions

The boundary conditions are applied directly to nodes in the shell model at the support locations, reflecting the physical support configuration described in Section 3.7. The beam axis is aligned with the x-axis, the vertical direction along the y-axis and the lateral direction with z-axis.

The left support is modelled as a pinned support applied to the bottom flange, where all translational DOF are restrained, see Fig. 4.1. The right support is modelled as a roller support, where vertical and lateral translations are restrained while longitudinal displacements are allowed, see Fig. 4.2. At both supports, rotation about the longitudinal axis is restrained, while the rotations about the remaining axes are left free.

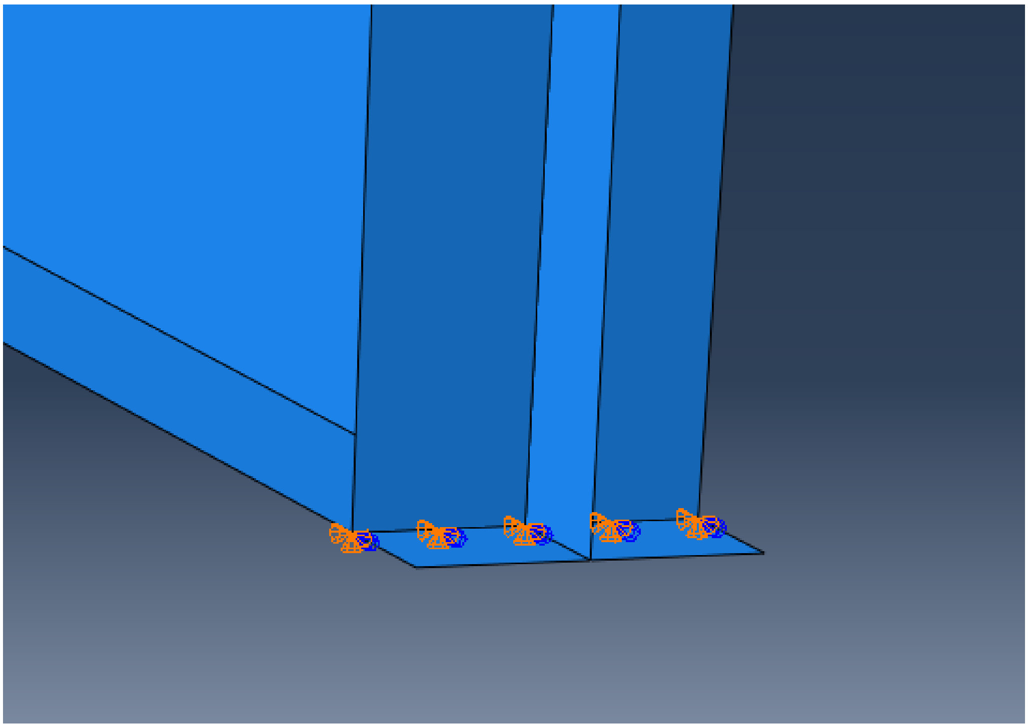

Figure 4.1: Left support modelled as a pinned support, orange arrows represents the restrained translational DOF and blue arrows the restrained rotational DOF.

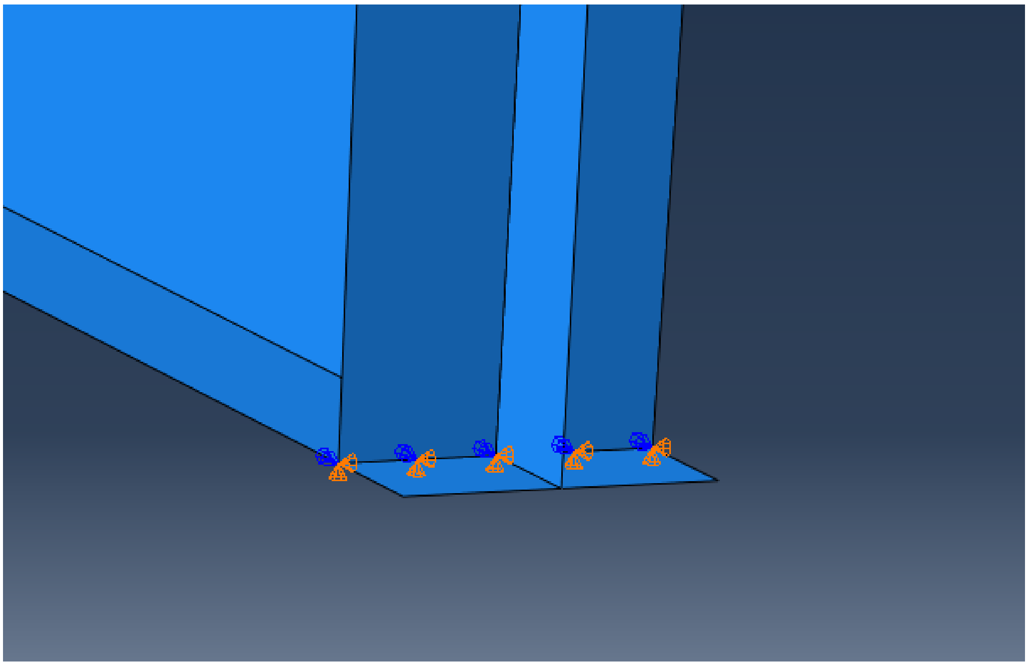

Figure 4.2: Right support modelled a roller support, orange arrows represents the restrained translational DOF and blue arrows the restrained rotational DOF.

To represent the stabilizing effect of the support connection, an additional lateral restraint is applied at the top of the web at both supports by restraining the displacement in the global z-direction. This prevents lateral movement at the support and improves the lateral stability of the girder cross section, see Fig. 4.3

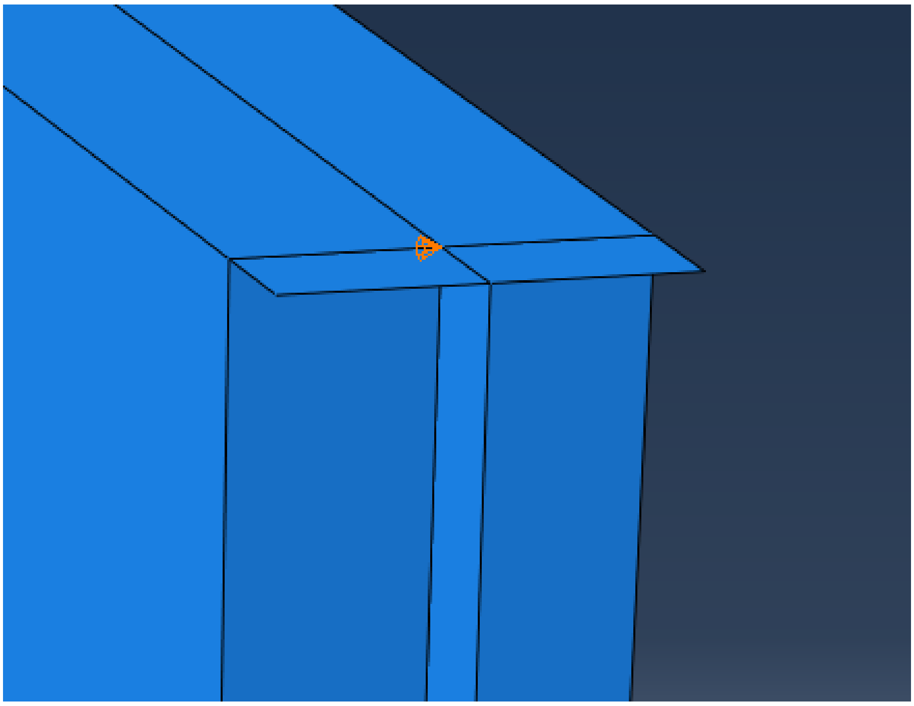

Figure 4.3: BC at top of the web, restraining lateral movement.

4.1.2 Restraint modelling

Lateral bracing of the girder was represented using discrete spring restraints applied at regular intervals along the span length. These springs simulated the stabilizing effect of bracing systems commonly used in large crane runway girders, such as built-up truss arrangements connected to the girder flanges.

Each spring was connected between a flange node and the ground and provided restraint in the lateral direction. The spacing between the spring locations was defined as a parameter in the model. The stiffness of the springs was also adjustable, enabling different levels of lateral restraint to be represented. Two principal configurations were investigated:

- Top flange bracing only, shown in Fig. 4.4.
- Top and bottom flange bracing, shown in Fig. 4.5.

This modelling approach allowed the influence of bottom flange restraint on the global behaviour and stability of the girder to be examined, which was central to the objective of this study.

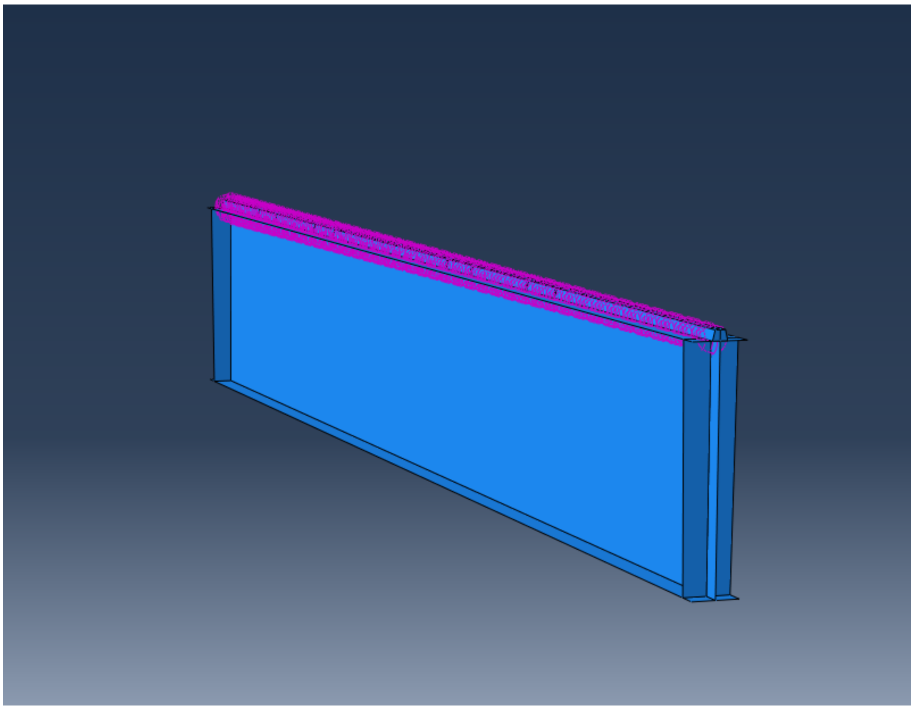

Figure 4.4: Spring restraints applied at the centreline of the top flange, with stiffness varying along the beam length.

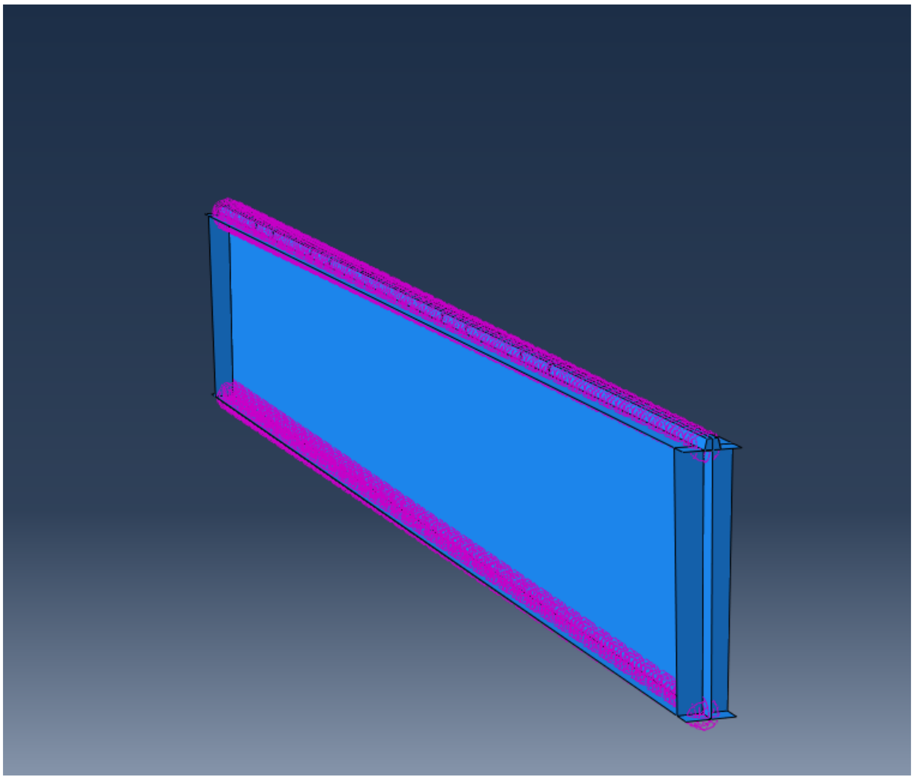

Figure 4.5: Spring restraints applied at the centreline of the top flange and bottom flange, with stiffness varying along the beam length.

4.1.3 Simplification of stiffness distribution

Once the physical truss was sized using the MATLAB script described in Section 3.6, it was translated into an equivalent discrete spring system for implementation in Abaqus. This simplified the complex truss geometry while retaining its mechanical influence on the beam.

The stiffness of a truss varies parabolically along the span, reaching its maximum at the supports and its minimum at midspan, as shown in Fig. 4.6. This continuous variation was discretized into zones of constant stiffness corresponding to each truss bay, as shown in Fig. 4.7. The equivalent spring stiffness for each bay was determined from the relationship between the internal force in the vertical members and the resulting nodal displacements, given by Eq. 4.1. This simplification maintains the global behaviour of the bracing system while reducing the complexity of the Abaqus input.

$$k_{stiff} = \frac{P_{vertical}}{\delta_{avg}} \tag{4.1}$$

where: k_{stiff} is the equivalent spring stiffness [N/mm]

$P_{vertical}$ is the discrete nodal force transferred by the vertical member, calculated by integrating the line load $q_{d,brace}$ over the tributary width of the respective bay [N]

δ_{avg} is the average deflection of the four nodes defining that specific bay [mm]

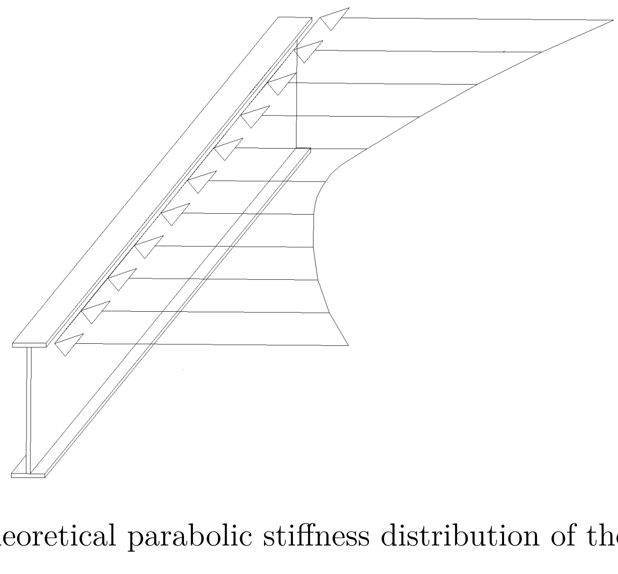

Figure 4.6: Theoretical parabolic stiffness distribution of the bracing system.

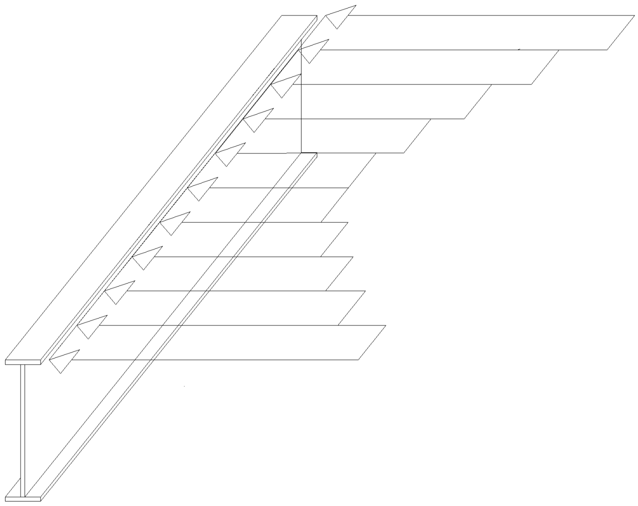

Figure 4.7: Discretized "step-wise" stiffness distribution used for Abaqus modeling.

4.1.4 Modelling of the rail

The rail described in Section 3.1.1 has a complex geometry that is difficult to reproduce exactly in Abaqus. Therefore, a simplified trapezoidal cross section was adopted, with a base width of 220 mm and a top width of 150 mm, approximating the outer profile of the real rail while avoiding the curved transitions of the actual shape, as shown in Fig. 4.8.

The rail is modelled as rigidly connected to the top flange along its full length, which introduces some additional stiffness to the girder. Including the rail raises the point of load application above the top flange, increasing the eccentricity of the horizontal loads and producing a more realistic torsional effect on the cross section. The rail geometry also allows the wheel loads to be distributed over a larger contact area through the distributing coupling constraint, reducing stress concentrations compared to applying the loads directly to the flange.

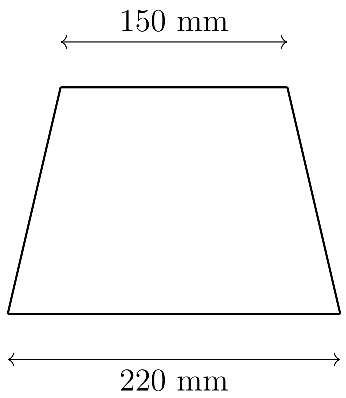

Figure 4.8: Simplified trapezoidal rail cross section used in the finite element model.

4.1.5 Load application

The crane runway girder is subjected to crane wheel forces and the self-weight of the structure. The self-weight is included through a gravity load applied in the global vertical direction, defined using the material density, ensuring that the weight of all structural components is automatically accounted for in the analysis.

The crane wheel loads are applied as concentrated forces at reference points, each distributed over a patch surface on the rail through a distributing coupling constraint. This approach simulates the contact area between the wheel and the rail, while also avoiding stress concentrations that would arise from applying large forces to a single node. Each patch has a length of 50 mm along the beam axis which is an assumption to reduce stress concentrations the point loads would produce and still try and simulate the contact area between the wheel and rail.

To replicate the eccentric loading condition specified in Eurocode, the vertical load is applied at an eccentricity of $b_r/4 = 37.5$ mm from the rail centreline, where b_r is the rail width, and distributed over half the width of the rail top surface. The distributing coupling constraint applied over the patch surface is shown in Fig. 4.9, and the resulting load arrows at the reference points are shown in Fig. 4.10. The transverse horizontal loads are applied in the same direction as the torsional moment from the eccentric vertical load, producing the maximum combined torsional effect on the cross-section.

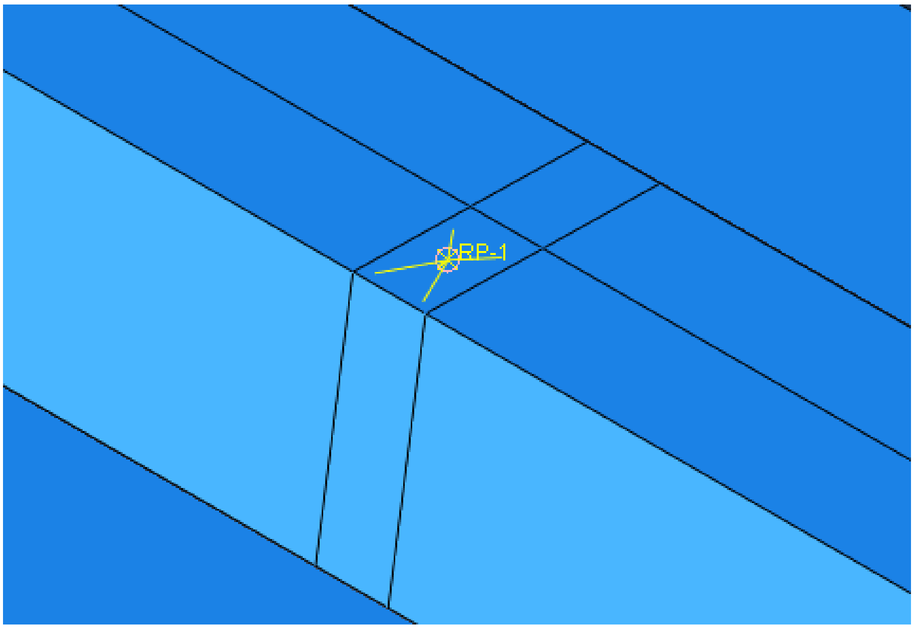

Figure 4.9: Distributing coupling constraint applied over the eccentric load patch on one side of the rail centreline, shown for wheel position W1.

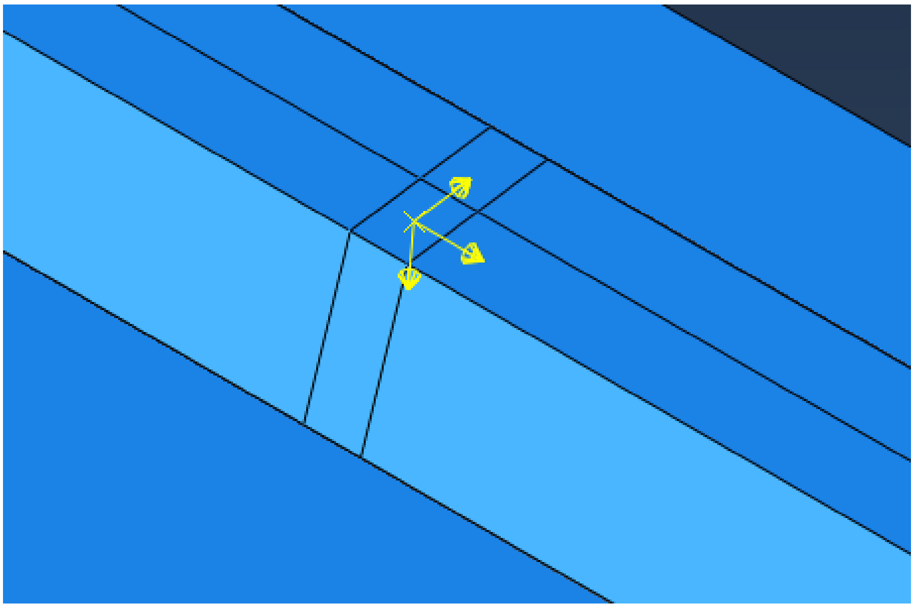

Figure 4.10: Vertical and horizontal forces applied at the reference points for wheel positions W2.

The wheel positions along the span are determined by an influence line search, placing the loads at the positions that produce either the maximum bending moment or maximum shear force at the critical section. Two load cases are therefore investigated — the moment case shown in Fig. 4.11 and the shear case shown in Fig. 4.12.

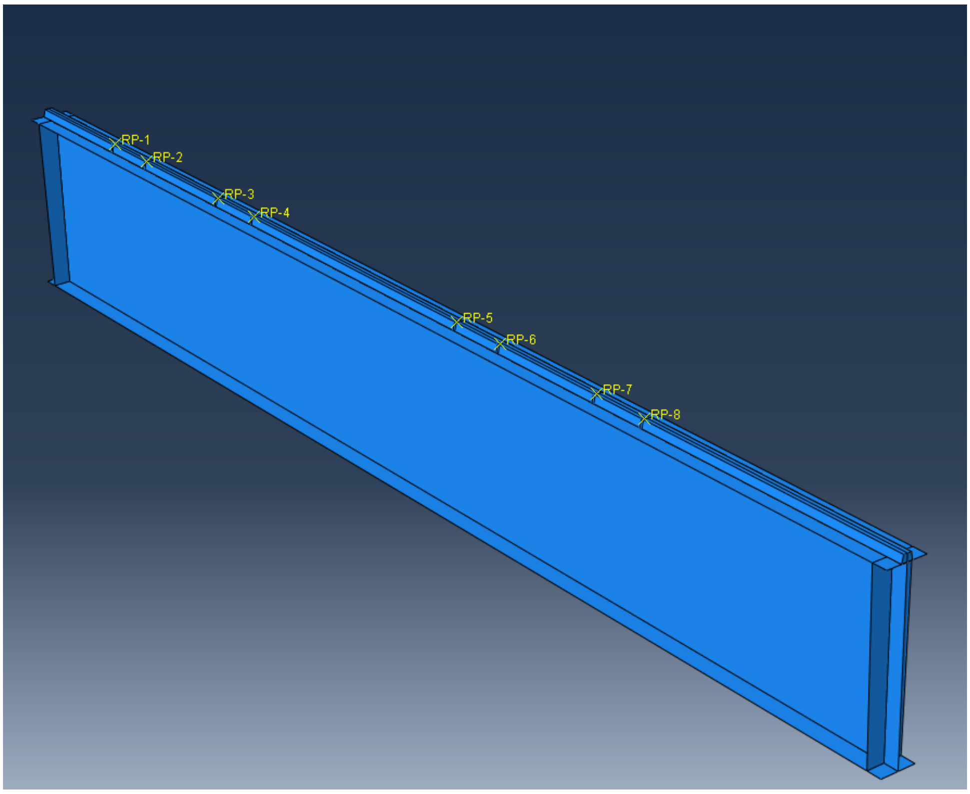

Figure 4.11: Wheel positions for the maximum bending moment load case, with the wheel block positioned near midspan.

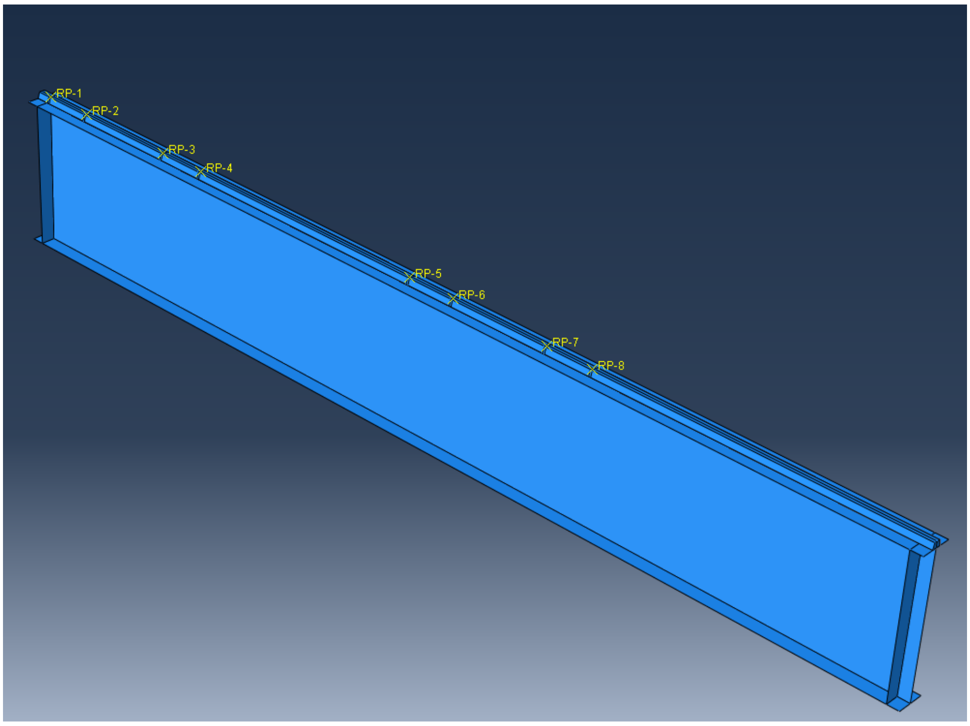

Figure 4.12: Wheel positions for the maximum shear force load case, with the wheel block positioned close to the support.

4.1.6 Material

The material model requires both elastic and plastic properties to support the linear elastic verification as well as the nonlinear analysis. The elastic behaviour is defined by the modulus of elasticity E and Poisson's ratio ν. The modulus of elasticity describes the stiffness of the material in the linear range, while Poisson's ratio defines the lateral contraction of the material under longitudinal loading. The values used are given in Table 4.1.

Table 4.1: Elastic material properties used in the finite element model.

Property	Value
Modulus of elasticity E [MPa]	207615
Poisson's ratio ν [-]	0.3

The plastic behaviour is defined using a true stress–true plastic strain relationship for carbon steel, provided as course material by the Division of Structural Engineering, Chalmers University of Technology (Al-Emrani, 2025). Abaqus requires the plastic material behaviour to be defined in terms of true stress and true plastic strain, rather than nominal engineering values. True stress accounts for the actual cross sectional area as the material deforms, while true plastic strain excludes the elastic component of the total strain. The stress–strain relationship used is presented in Table 4.2.

Table 4.2: True stress–plastic strain relationship used in the nonlinear analysis.

True stress [MPa]	True plastic strain [-]
370.6	0.000
382.9	0.018
429.6	0.025
458.7	0.032
543.3	0.065
637.9	0.163

It should be noted that SS-EN 1993-1-1 specifies reduced yield strengths for thicker plates, giving $f_y = 345$ MPa for the web ($t_w = 30$ mm) and $f_y = 315$ MPa for the flanges ($t_f = 80$–100 mm). Since the available nonlinear material data corresponds to a nominal yield strength of 355 MPa, this value is used consistently throughout all analyses. As the same material model is applied to all cases, this simplification is not expected to influence the relative comparisons between bracing configurations.

4.1.7 Mesh

The crane runway girder is discretized using continuum shell elements, in order to represent the behavior of the thin components in the model. Shell elements are well suited for modelling thin-walled structures where the thickness is small compared to the other geometric dimensions. They are suitable for complex situations since they can handle rotations and large deformations.

A global mesh size is defined for the model in order to ensure consistent discretization along the entire beam. The mesh is generated after the final geometry partitions have been created to present the wheel load patches. This ensures that the surfaces for load distribution is accurately represented and that the loads are applied to well-defined element regions. An illustration of the model with a mesh size of 150 mm is shown in Fig 4.13.

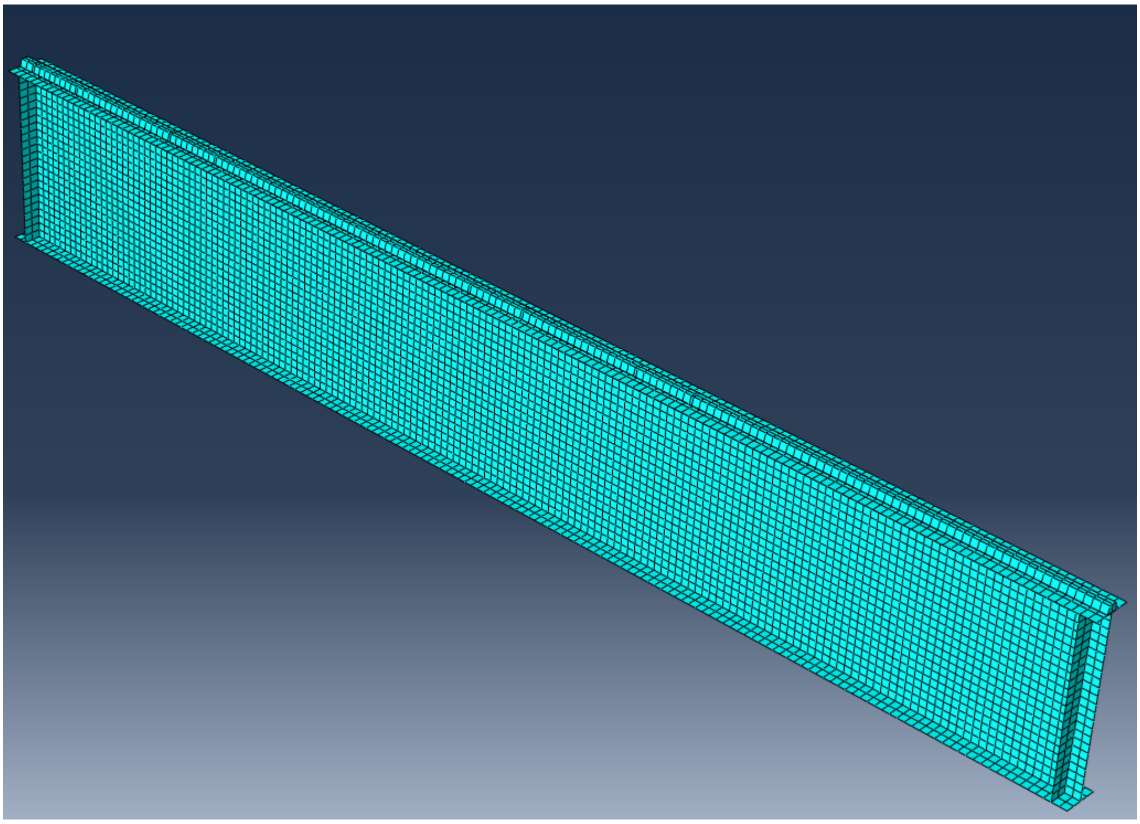

Figure 4.13: Visualization of mesh size 150 mm using shell elements.

4.1.8 Convergence study

Prior to the parametric study, a mesh convergence analysis was performed to identify a mesh size that accurately captures the structural behaviour of the girder without excessive computational cost. The midspan stress at the bottom flange and the vertical deflection were monitored as convergence indicators, as these quantities are most relevant to the subsequent analysis.

Mesh sizes ranging from 50 mm to 400 mm were evaluated, and the results are summarised in Table 4.3. As expected, both the stress and deflection converge monotonically towards a stable value with decreasing mesh size. Between the 150 mm and 50 mm meshes the difference is less than 0.03% for both quantities, indicating that the solution is effectively converged at 150 mm.

Refining the mesh from 150 mm to 50 mm increases the total number of elements from 5612 to 56104 - approximately a 10-fold increase, for a negligible improvement in accuracy. A global mesh size of 150 mm was therefore selected for all subsequent analyses, providing a good balance between numerical accuracy and computational efficiency.

Table 4.3: Mesh convergence study results

Mesh size [mm]	Number of elements	Stress [MPa]	Deflection [mm]	Deflection diff. vs 50 mm [%]
400	978	149.421	-26.623	0.20
350	1172	149.349	-26.615	0.17
300	1538	149.293	-26.606	0.14
250	2034	149.239	-26.595	0.10
200	3628	149.156	-26.582	0.05
150	**5612**	**149.128**	**-26.578**	**0.03**
100	14114	149.091	-26.572	0.01
50	56104	149.074	-26.569	-

4.1.9 Verification of model

The finite element model was verified by comparing the results of a linear elastic analysis against hand calculations, using the loads from side 2. To isolate the bending behaviour and minimize torsional effects, a simplified load case was used in which only the vertical loads were applied only over the centreline, with no lateral eccentricity. The wheels were placed at the critical bending moment positions along the span, determined by the influence line search. The rail was initially excluded from the model to verify the bare girder response directly, without the stiffening effect of the rail or its coupling to the cross section. Once the bare girder results were confirmed, the rail was reintroduced and the comparison was repeated to ensure that neither the rail nor the coupling constraint introduced any unintended additional stiffness into the system.

The reaction forces were first compared to confirm that the loads were correctly applied, showing agreement within 1.57%. The vertical deflection and longitudinal stresses were then extracted and compared to hand calculations based on classical beam theory. The results are summarised in Table 4.4. The stresses showed consistent agreement of approximately 9% for both the bare girder and with-rail cases. The deflections initially differed by approximately 15% and 17.3% respectively, which is more significant and warranted further investigation.

For beams with a span-to-depth ratio of 3 or more, the contribution of shear deformation to the total deflection is not negligible (Roark et al., 2012). In this case, with a span of 24 m and a total girder height of approximately 3.6 m, the ratio is 6.7, indicating that shear deformation should be accounted for. The additional deflection due to shear is given by Eq. 4.2.

$$y_s = \frac{F \cdot w \cdot L^2}{8 \cdot A_w \cdot G} \tag{4.2}$$

where: F is a form factor equal to 1.0 for I-beams [-]

w is the distributed load [N/mm]

A_w is the web area [mm^2]

Since this formula is derived for a uniformly distributed load, the equivalent distributed load was estimated by matching the maximum moment from the eight concentrated wheel loads, and dividing by the web area and shear modulus. This yields an additional shear deflection of 5.32 mm. When added to the previously calculated deflections, the discrepancy reduces to −3.37% for the bare girder case and −0.57% for the case with rail, as shown in Table 4.4. The hand calculations now predict a marginally larger deflection than ABAQUS, which is a physically consistent result. The close agreement across all quantities gives confidence that the model is correctly implemented, and the finite element model is considered sufficiently verified to proceed with the parametric study.

Table 4.4: Comparison of hand calculations and finite element results for model verification.

Parameter	Hand Calculations	Abaqus	Difference [%]
Without rail			
Reaction force [MN]	13.194	12.99	-1.566
Stress [MPa]	168.691	151.877	9.967
Deflection without shear addition [mm]	24.575	28.916	15.01
Deflection with shear addition [mm]	29.891	28.916	-3.374
With rail			
Stress [MPa]	163.829	149.128	8.973
Deflection without shear addition [mm]	21.975	26.578	17.319
Deflection with shear addition [mm]	26.728	26.578	-0.565

4.1.10 Verification of spring system

The spring restraints are intended to provide sufficient lateral stiffness to eliminate the risk of lateral-torsional buckling, while still permitting some longitudinal movement along the beam. To preserve symmetry in the model, the springs were attached at the centreline of the top flange rather than at the flange edge, as shown in Fig. 4.4. The spring stiffness varies along the beam length, with the largest values at the supports and the smallest at midspan, reflecting the step-wise approximation of the parabolic stiffness distribution of the physical truss system, as described in

Section 4.1.3.

To verify that the spring system functions as intended, a linear perturbation buckling analysis was performed with and without the spring restraints. For the unrestrained beam, the first critical buckling mode has an eigenvalue of $\lambda_1 = 0.956$, corresponding to lateral-torsional buckling as shown in Fig. 4.14. The top flange displaces laterally out of plane, which is precisely the failure mode the bracing system is designed to prevent.With the spring restraints applied, the first eigenvalue increases to $\lambda_1 = 1.784$, an increase of 87% compared to the unrestrained case.

As shown in Fig. 4.15, LTB is effectively suppressed and the critical mode shifts to shear buckling of the web. The top flange remains laterally stable, confirming that the spring system is correctly implemented and functioning as intended. Having established that the mesh is sufficiently converged, the global bending behaviour is correctly represented and the lateral restraint system functions as intended, the finite element model is considered validated. The following section, Section 4.2, describes the analysis procedure used in the parametric study.

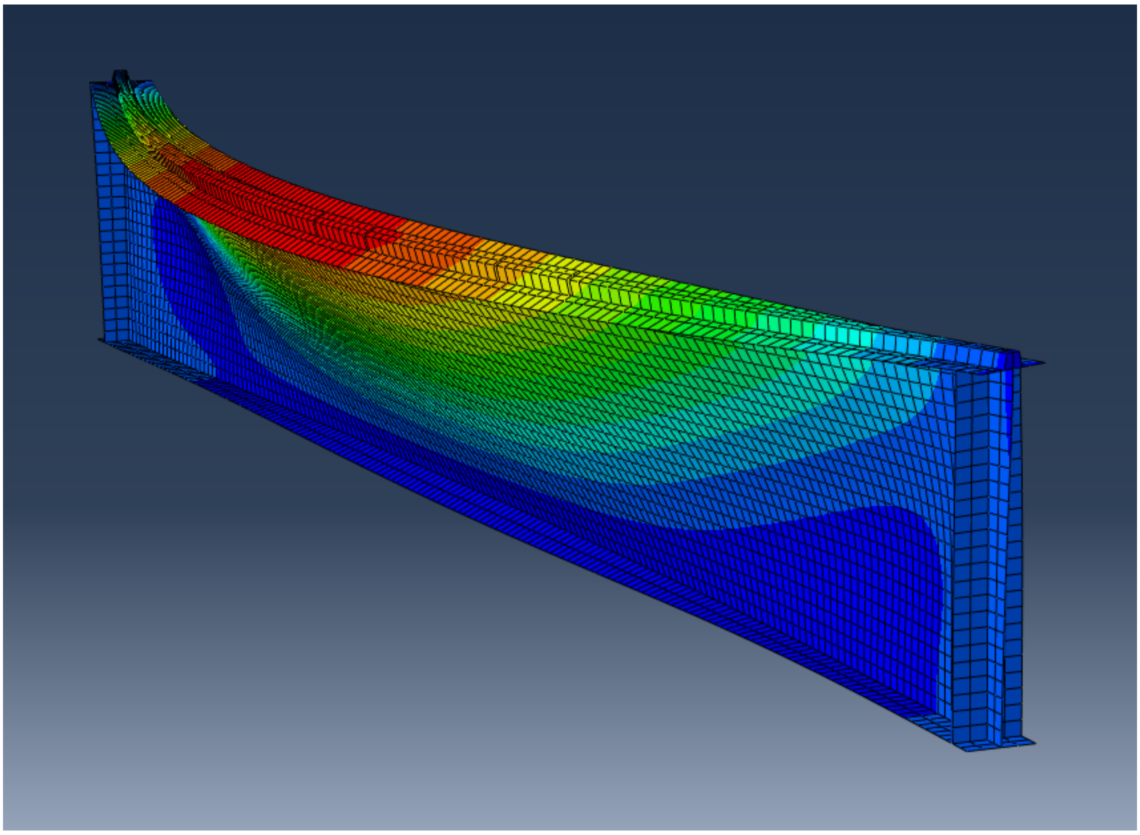

Figure 4.14: First buckling mode of the unrestrained girder ($\lambda_1 = 0.956$), showing lateral-torsional buckling.

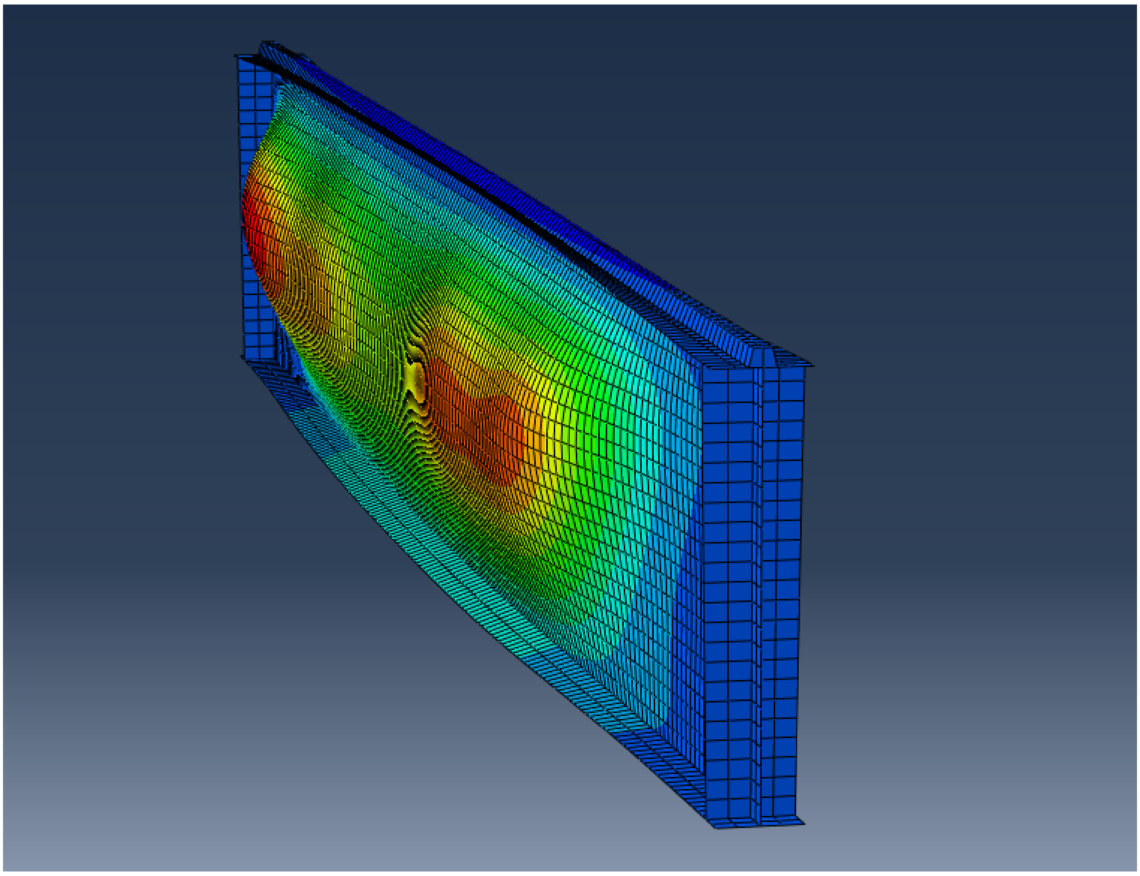

Figure 4.15: First buckling mode of the restrained girder ($\lambda_1 = 1.784$), showing web shear buckling with the top flange laterally restrained.

4.2 Parametric study

To investigate whether certain geometries present a greater risk of failure when the bottom flange is unrestrained, a parametric study is conducted varying the web height and bottom flange width. The parameters and their ranges are discussed in the following subsections.

4.2.1 Geometry

The web height is varied in increments of 500 mm, ranging from 2500 mm to 5000 mm, covering a range of slender but practically relevant girder geometries. Note that these are the web heights as modelled in Abaqus, measured between the mid-planes of the flanges, and the nominal web height of 3420 mm therefore becomes 3510 mm in the finite element model, accounting for half the flange thickness on each side ($3420 + 100/2 + 80/2 = 3510$ mm).

Since the lateral displacement of the bottom flange is the primary quantity of interest, a narrower bottom flange is expected to be more susceptible to lateral movement and therefore represents a more critical case. The bottom flange width is therefore varied from 700 mm, corresponding to the original design, down to 200 mm in increments of 100 mm. Below 200 mm, the localized yield on the support became excessive due to the insufficient contact area between the flange and the supporting column, and therefore no further reductions were considered. All geometric parameters investigated are summarised in Table 4.5.

Table 4.5: Geometry varied in the parametric study.

Parameter	Values [mm]
Web height h_w	2500, 3000, 3510, 4000, 4500, 5000
Bottom flange width b_{bf}	200, 300, 400, 500, 600, 700

4.2.2 Imperfection amplitudes

To determine appropriate imperfection amplitudes for the nonlinear analysis, the equivalent geometric imperfection is evaluated using the two approaches described in Section 2.5.4: the general LTB formulation shown in Eq. 2.15, and the crane-runway-specific formulation in Eq. 2.16. For the general LTB equation, the buckling shape mode gives $\beta_{LT} = 1/150$ according to Fig. 2.18.
The result depends on the imperfection factor α for minor axis flexural buckling, and produces values ranging from approximately 24 mm to 122 mm depending on the buckling curve used.

For the crane runway beam equation, the girder is a welded cross section with $h/b > 2.0$, and plastic cross section verification is used. From Fig. 2.19, this gives $\beta_{LT} = 1/100$, which is the most conservative value in the table. The material parameter ε is defined as:

$$\varepsilon = \sqrt{\frac{235}{f_y}} = \sqrt{\frac{235}{355}} = 0.814 \tag{4.3}$$

where $f_y = 355$ MPa corresponds to steel grade S355, consistent with the material model described in Section 4.1.6. The equivalent geometric imperfection then evaluates to:

$$e_0 = \beta_{LT} \cdot \frac{L}{\varepsilon} = \frac{1}{100} \cdot \frac{24000}{0.814} \approx 295 \text{ mm} \tag{4.4}$$

The two formulations produce notably different amplitudes — on the order of 100 mm from the general LTB equation and approximately 295 mm from the crane runway beam equation. To capture the full sensitivity of the structural response to imperfection amplitude, five values are investigated in the parametric study:

$$e_0 \in \{0,\ 50,\ 100,\ 200,\ 300\} \text{ mm} \tag{4.5}$$

The value $e_0 = 0$ represents a geometrically perfect beam and serves as a reference case. The value $e_0 = 100$ mm falls within the range produced by the general LTB formulation, while $e_0 = 300$ mm represents a rounded upper bound consistent with the crane runway beam formulation. The intermediate values allow the transition in structural behaviour between these two limits to be examined.

In addition to the global bottom bow imperfection, buckling mode imperfections are considered to assess their influence on shear buckling capacity. The plate curvature tolerances, shown in Fig. 2.20 and summarised in Table 4.6, provide the basis for these amplitudes. For the web geometry considered in this study, the essential tolerances range from 13 mm to 52 mm depending on web height, while the functional Class 1 tolerances range from 30 mm to 50 mm. Based on these values, three imperfection amplitudes are investigated for the local web buckling modes:

$$e_0 \in \{0,\ 25,\ 50\}\ \text{mm} \tag{4.6}$$

where $e_0 = 0$ again serves as the perfect reference case, and $e_0 = 50$ mm represents the upper bound of the functional tolerance range.

Table 4.6: Plate curvature tolerances according for web thickness $t_w = 30$ mm.

h_w [mm]	b/t [-]	Essential tolerance [mm]	Functional tolerance Class 1 [mm]
5000	166.7	52.1	50
4500	150.0	42.2	45
4000	133.3	33.3	40
3500	116.7	25.5	35
3000	100.0	18.8	30
2500	83.3	13.0	30

4.2.3 Eigenvalue buckling analysis

A linear perturbation buckling analysis solves the eigenvalue problem to find the critical load multipliers and their associated buckling mode shapes, which represent the most likely deformation patterns of the structure at the onset of buckling. While this analysis was also used in Section 4.1.10 to verify the spring system, here it serves a different purpose, to determine the geometric imperfection shape for the subsequent nonlinear analysis. The applied loads correspond to the crane wheel and normative loads, and the resulting eigenvalue represents the factor by which these loads would need to be scaled to cause buckling.

Initially, 40 eigenvalues were requested to investigate whether any higher-order modes exhibited bottom flange buckling behaviour. As no modes with clear web sidesway buckling or were significant deformation of the bottom flange were observed, the first positive eigenvalue and its associated mode shape were selected as the geometric imperfection input for the nonlinear analysis. Negative eigenvalues correspond to a reversal of the applied loads and are therefore not physically relevant for this study.

4.2.4 Geometric imperfection linear analysis

In addition to using the buckling mode shape from the eigenvalue analysis, a second imperfection approach is considered based on a linear static analysis. By applying a unit reference load of 1 N, the deformed shape of the beam under that load is obtained, which is then scaled by the imperfection amplitude in the nonlinear step. This allows different imperfection geometries to be studied independently of the buckling mode. For the considered imperfection case, the reference load is applied as a point load at the bottom of the web at mid-span, producing a deformed shape in which primarily the bottom flange is distorted.

4.2.5 Nonlinear analysis

With the imperfection geometry established from one of the two approaches described in Sections 4.2.3 and 4.2.4 the eigenvalue mode shape or localised bottom flange distortion, the ultimate load-carrying capacity of the crane girder is determined using a geometrically and materially nonlinear analysis. Unlike a standard static analysis, where the load is incremented in fixed steps, the Riks method increments along the load-displacement curve simultaneously, allowing the solution to follow the structural response past the peak load and into the post-buckling regime.

For each imperfection geometry, the amplitudes applied are those derived and justified in Section 4.2.2.

A maximum of 300 load increments was specified to ensure that the peak load was always captured. The ultimate load was defined as the load corresponding to the maximum load proportionality factor (LPF), which represents the scalar multiplier on the reference load at which the structure can no longer sustain additional loading.

4.2.6 Post-processing

The results of the nonlinear analysis are extracted to assess the ultimate behaviour of the crane girder. The von Mises stress distribution at the ultimate load is examined to identify the location and extent of yielding, providing insight into the governing failure mode for each geometry. Stresses along the beam length are also extracted to identify the maximum compression and tension regions.

The lateral and vertical deformations of the bottom flange are recorded to quantify the influence of the bracing configuration on the deformation behaviour at ultimate load. The maximum load proportionality factor (LPF) is extracted for each case, representing the scalar multiplier on the reference load at which the structure reaches its ultimate capacity. To quantify the effect of bottom flange restraint, the percentage gain in ultimate load capacity is defined as:

$$\Delta LPF = \frac{LPF_{both} - LPF_{top}}{LPF_{top}} \cdot 100 \quad [\%] \tag{4.7}$$

where LPF_{both} is the load proportionality factor with both flanges restrained and

LPF_{top} is the load proportionality factor with only the top flange restrained. A positive value of ΔLPF indicates that the addition of bottom flange restraint increases the ultimate load capacity of the girder.

5
Results

This chapter presents the results obtained from the nonlinear analyses performed in Abaqus. The geometric parameters and imperfection amplitudes investigated are summarised in Section 4.2. The results are organised by parameter, examining how web height, bottom flange width, and imperfection amplitude influence the ultimate load capacity and governing failure mode of the crane girder.

5.1 Buckling mode imperfection results

This section investigates how different buckling mode imperfection amplitudes influence the behaviour of the crane girder. The imperfection shape is derived from the first buckling eigenmode, dominated by web distortion, and scaled to the amplitudes discussed in Section 4.2.2. As described in Section 4.2.6, the LPF gain is used to quantify the improvement in buckling resistance when bottom flange bracing is added. Tables 5.1–5.6 summarise these gains for the moment and shear cases across all studied girder heights and bottom flange widths.

The influence of imperfections for the critical moment wheel positions is illustrated in Tables 5.1–5.3. The largest maximum ΔLPF is 4.16%, for an imperfection amplitude of $e_0 = 0$ mm, with $h_w = 3000$ mm and $b_{bf} = 500$ mm. In general, the results show that increasing imperfection amplitude decreases the LPF gain, which is further discussed in Section 6.4. For all imperfection amplitudes, the highest LPF gain can be seen for the heights $h_w = 3000$ mm and $h_w = 3510$ mm, with intermediate bottom flange widths. Additionally, cases marked with a red flag did not converge and have been estimated by linear interpolation from neighbouring values, and should be interpreted with caution.

Table 5.1: ΔLPF comparison for buckling mode imperfection amplitude $e_0 = 0$ mm with critical moment wheel positions.

ΔLPF% | e_0 = 0 mm | Web Buckling Imperfection | Moment						
hw \ bf	700	600	500	400	300	200
2500	2.92%	0.26%	1.67%	0.15%	-0.07%	-0.19%
3000	2.66%	3.55%	4.16%	4.12%	3.18%	-1.20%
3510	1.85%	2.35%	2.92%	3.54%	4.14%	3.75%
4000	1.07%	1.34%	1.63%	1.92%	2.16%	2.10%
4500	0.55%	0.66%	0.78%	0.89%	1.00%	0.90%
5000	0.19%	0.23%	0.26%	0.30%	0.35%	0.28%

Table 5.2: ΔLPF comparison for buckling mode imperfection amplitude $e_0 = 25$ mm with critical moment wheel positions.

ΔLPF% | e_0 = 25 mm | Web Buckling Imperfection | Moment						
hw \ bf	700	600	500	400	300	200
2500	2.12%	2.45%	1.88%	0.26%	-0.72%	-2.30%
3000	1.95%	2.40%	2.59%	2.06%	1.00%	-1.37%
3510	0.87%	1.02%	1.13%	1.17%	0.85%	0.32%
4000	0.62%	0.64%	0.69%	0.63%	0.40%	-0.28%
4500	0.34%	0.27%	0.25%	0.19%	0.07%	-0.26%
5000	0.10%	0.03%	-0.02%	-0.08%	-0.19%	-0.37%

Table 5.3: ΔLPF comparison for buckling mode imperfection amplitude $e_0 = 50$ mm with critical moment wheel positions.

ΔLPF% | e_0 = 50 mm | Web Buckling Imperfection | Moment						
hw \ bf	700	600	500	400	300	200
2500	1.86%	2.24%	1.96%	0.52%	-1.69%	-4.09%
3000	1.45%	1.56%	1.56%	1.08%	-0.45%	-3.25%
3510	0.33%	0.30%	0.15%	-0.26%	-1.23%	-2.52%
4000	0.29%	0.17%	0.10%	-0.13%	-0.67%	-1.73%
4500	0.20%	-0.02%	-0.16%	-0.33%	-0.68%	-1.18%
5000	0.00%	-0.16%	-0.30%	-0.44%	-0.67%	-0.93%

For the critical shear wheel positions, the results are shown in Tables 5.4–5.6. Compared to moment buckling, the influence of imperfections is smaller, and the LPF gain remains relatively stable across most configurations. The highest ΔLPF gain is

5.88% and for e_0=25 mm, with $h_w = 3000$ mm and $b_{bf} = 400$ mm. The highest gains appear again for the mid-range slenderness levels for all imperfection amplitudes, but decreases when for higher amplitudes except for the maximum ΔLPF observed.

Table 5.4: ΔLPF comparison for buckling mode imperfection amplitude $e_0 = 0$ mm with critical shear wheel positions.

ΔLPF% | e_0 = 0 mm | Web Buckling Imperfection | Shear						
hw \ bf	700	600	500	400	300	200
2500	-4.50%	0.40%	0.22%	-1.96%	0.01%	-0.83%
3000	2.68%	4.20%	4.03%	1.67%	1.72%	1.82%
3510	1.54%	1.94%	2.38%	2.84%	3.79%	2.25%
4000	0.95%	1.18%	1.42%	1.64%	1.90%	2.04%
4500	0.61%	0.76%	2.18%	1.03%	1.13%	1.63%
5000	0.27%	0.32%	0.39%	0.45%	0.51%	1.62%

Table 5.5: ΔLPF comparison for buckling mode imperfection amplitude $e_0 = 25$ mm with critical shear wheel positions.

ΔLPF% | e_0 = 25 mm | Web Buckling Imperfection | Shear						
hw \ bf	700	600	500	400	300	200
2500	-1.57%	1.54%	1.19%	-1.37%	-0.63%	-0.14%
3000	1.27%	2.49%	4.42%	5.88%	1.24%	-2.41%
3510	1.39%	1.67%	1.97%	2.25%	0.69%	1.52%
4000	0.83%	1.01%	1.20%	1.29%	0.41%	1.38%
4500	0.49%	0.57%	0.64%	0.60%	0.22%	1.17%
5000	0.18%	0.20%	0.21%	0.17%	-0.04%	1.36%

Table 5.6: ΔLPF comparison for buckling mode imperfection amplitude $e_0 = 50$ mm with critical shear wheel positions.

ΔLPF% | e_0 = 50 mm | Web Buckling Imperfection | Shear						
hw \ bf	700	600	500	400	300	200
2500	2.45%	0.86%	0.98%	-1.34%	-1.24%	-0.18%
3000	0.73%	1.72%	2.69%	4.05%	0.33%	-0.95%
3510	1.21%	1.38%	1.55%	1.64%	-1.35%	0.26%
4000	0.70%	0.81%	0.87%	0.82%	-0.69%	0.51%
4500	0.36%	0.40%	0.41%	0.26%	-0.47%	0.72%
5000	0.12%	0.12%	0.09%	-0.03%	-0.47%	1.15%

5.2 Geometric bottom flange imperfection results

The results for the geometric bottom flange imperfection at the critical moment wheel position are presented in Tables 5.7–5.11. Five imperfection amplitudes were investigated as defined in Section 4.2.2. The largest ΔLPF gain is observed for a web height of $h_w = 3000$ mm and a bottom flange width of $b_{bf} = 500$ mm, with a maximum gain of 4.16%. As the imperfection amplitude increases, the ΔLPF decreases consistently across all geometries, to the point where the largest imperfection amplitude of $e_0 = 300$ mm produces negative values for most configurations, indicating that bottom flange bracing has a negative impact on the load carrying capacity at large imperfection amplitudes.

Table 5.7: ΔLPF comparison for geometric bottom flange mode imperfection amplitude $e_0 = 0$ mm with critical moment wheel positions.

ΔLPF% | e_0 = 0 mm | Bot Flange Imperfection | Moment						
hw \ bf	**700**	**600**	**500**	**400**	**300**	**200**
2500	2.92%	2.74%	1.68%	0.15%	-0.07%	-0.19%
3000	2.66%	3.55%	4.16%	4.12%	3.18%	0.91%
3510	1.85%	2.35%	2.92%	3.54%	4.14%	3.75%
4000	1.07%	1.34%	1.63%	1.92%	2.16%	2.10%
4500	0.55%	0.66%	0.78%	0.89%	1.00%	0.90%
5000	0.19%	0.23%	0.26%	0.30%	0.35%	0.28%

Table 5.8: ΔLPF comparison for geometric bottom flange mode imperfection amplitude $e_0 = 50$ mm with critical moment wheel positions.

ΔLPF% | e_0 = 50 mm | Bot Flange Imperfection | Moment						
hw \ bf	**700**	**600**	**500**	**400**	**300**	**200**
2500	1.61%	0.82%	0.70%	0.24%	0.24%	0.38%
3000	1.57%	2.10%	2.53%	2.64%	2.25%	0.69%
3510	1.34%	1.67%	2.01%	2.35%	2.75%	2.46%
4000	0.77%	0.95%	1.13%	1.31%	1.46%	1.37%
4500	0.36%	0.43%	0.54%	0.58%	0.64%	0.55%
5000	0.13%	0.16%	0.18%	0.18%	0.21%	0.17%

Table 5.9: ΔLPF comparison for geometric bottom flange mode imperfection amplitude $e_0 = 100$ mm with critical moment wheel positions.

ΔLPF% | e_0 = 100 mm | Bot Flange Imperfection | Moment						
hw \ bf	700	600	500	400	300	200
2500	0.21%	0.40%	0.32%	0.27%	0.50%	0.91%
3000	0.60%	0.74%	0.85%	0.97%	0.97%	0.34%
3510	0.76%	0.91%	1.04%	1.12%	1.28%	1.10%
4000	0.46%	0.55%	0.63%	0.68%	0.74%	0.62%
4500	0.21%	0.25%	0.27%	0.28%	0.30%	0.24%
5000	0.07%	0.07%	0.07%	0.06%	0.07%	0.05%

Table 5.10: ΔLPF comparison for geometric bottom flange mode imperfection amplitude $e_0 = 200$ mm with critical moment wheel positions.

ΔLPF% | e_0 = 200 mm | Bot Flange Imperfection | Moment						
hw \ bf	700	600	500	400	300	200
2500	-2.41%	-2.26%	-0.95%	-0.03%	0.85%	1.90%
3000	-1.21%	-1.78%	-2.34%	-2.38%	-2.17%	-0.70%
3510	-0.45%	-0.66%	-0.94%	-1.35%	-1.64%	-1.77%
4000	-0.17%	-0.27%	-0.42%	-0.64%	-0.81%	-1.07%
4500	-0.11%	-0.18%	-0.27%	-0.39%	-0.44%	-0.45%
5000	-0.10%	-0.15%	-0.21%	-0.29%	-0.35%	-0.23%

Table 5.11: ΔLPF comparison for geometric bottom flange mode imperfection amplitude $e_0 = 300$ mm with critical moment wheel positions.

ΔLPF% | e_0 = 300 mm | Bot Flange Imperfection | Moment						
hw \ bf	700	600	500	400	300	200
2500	-4.64%	-5.12%	-4.25%	-1.67%	0.53%	2.71%
3000	1.98%	-4.03%	-5.00%	-5.34%	-5.68%	-3.03%
3510	-1.53%	-2.07%	-2.86%	-3.78%	-4.37%	-4.23%
4000	-0.83%	-1.15%	-1.59%	-2.12%	-2.58%	-2.83%
4500	-0.49%	-0.69%	-0.95%	-1.21%	-1.45%	-1.39%
5000	-0.30%	-0.41%	-0.57%	-0.77%	-0.95%	-0.77%

The shear wheel position results, presented in Tables 5.12–5.16, show the same overall trend. The maximum gain of 4.20% is observed for $h_w = 3000$ mm and $b_{bf} = 600$ mm, slightly higher than the moment case. Results for $b_{bf} = 200$ mm are disregarded as localised yielding over the support governs the response in all shear cases, making the results unreliable.

Table 5.12: ΔLPF comparison for geometric bottom flange mode imperfection amplitude $e_0 = 0$ mm with critical shear wheel positions.

ΔLPF% | e_0 = 0 mm | Bot Flange Imperfection | Shear						
hw \ bf	700	600	500	400	300	200
2500	0.12%	0.40%	0.22%	-0.20%	0.01%	0.12%
3000	2.68%	4.20%	4.03%	1.67%	1.05%	1.82%
3510	1.54%	1.94%	2.38%	2.84%	3.79%	2.25%
4000	0.95%	1.18%	1.42%	1.64%	1.90%	2.04%
4500	0.61%	0.76%	0.91%	1.03%	1.13%	1.63%
5000	0.27%	0.32%	0.39%	0.45%	0.51%	1.62%

Table 5.13: ΔLPF comparison for geometric bottom flange mode imperfection amplitude $e_0 = 50$ mm with critical shear wheel positions.

ΔLPF% | e_0 = 50 mm | Bot Flange Imperfection | Shear						
hw \ bf	700	600	500	400	300	200
2500	0.07%	0.13%	0.19%	0.24%	0.43%	0.78%
3000	1.42%	2.23%	2.36%	1.60%	0.66%	1.65%
3510	1.01%	1.23%	1.47%	1.73%	2.31%	1.67%
4000	0.67%	0.80%	0.93%	1.03%	1.15%	1.46%
4500	0.39%	0.47%	0.54%	0.59%	0.65%	1.03%
5000	0.16%	0.19%	0.22%	0.24%	0.26%	1.05%

Table 5.14: ΔLPF comparison for geometric bottom flange mode imperfection amplitude $e_0 = 100$ mm with critical shear wheel positions.

ΔLPF% | e_0 = 100 mm | Bot Flange Imperfection | Shear						
hw \ bf	700	600	500	400	300	200
2500	-0.02%	0.45%	0.12%	0.37%	0.82%	1.47%
3000	0.33%	0.35%	0.38%	0.56%	0.37%	1.55%
3510	0.42%	0.49%	0.55%	0.60%	0.77%	1.16%
4000	0.33%	0.37%	0.37%	0.35%	0.37%	1.02%
4500	0.20%	0.22%	0.22%	0.19%	0.19%	0.55%
5000	0.07%	0.07%	0.06%	0.04%	0.01%	0.56%

Table 5.15: ΔLPF comparison for geometric bottom flange mode imperfection amplitude $e_0 = 200$ mm with critical shear wheel positions.

ΔLPF% | e_0 = 200 mm | Bot Flange Imperfection | Shear						
hw \ bf	700	600	500	400	300	200
2500	-2.03%	-0.34%	-0.06%	0.49%	1.47%	2.77%
3000	-1.73%	-2.68%	-3.32%	-3.02%	-0.70%	1.20%
3510	-0.72%	-1.00%	-1.37%	-1.99%	-2.48%	0.61%
4000	-0.36%	-0.54%	-0.77%	-1.07%	-1.30%	-0.02%
4500	-0.21%	-0.31%	-0.47%	-0.68%	-0.80%	-0.39%
5000	-0.15%	-0.23%	-0.33%	-0.46%	-0.57%	-0.89%

Table 5.16: ΔLPF comparison for geometric bottom flange mode imperfection amplitude $e_0 = 300$ mm with critical shear wheel positions.

ΔLPF% | e_0 = 300 mm | Bot Flange Imperfection | Shear						
hw \ bf	700	600	500	400	300	200
2500	-5.15%	-2.16%	-0.49%	0.42%	1.95%	3.99%
3000	-3.68%	-4.99%	-6.12%	-6.63%	-4.70%	-0.03%
3510	-1.91%	-2.58%	-3.53%	-4.68%	-5.68%	0.07%
4000	-1.06%	-1.46%	-1.99%	-2.60%	-3.15%	-1.35%
4500	-0.64%	-0.90%	-1.25%	-1.67%	-1.92%	-1.67%
5000	-0.40%	-0.57%	-0.80%	-1.09%	-1.29%	-2.48%

6

Discussion

This chapter discusses the results presented in Chapter 5 and aims to explain the physical behaviour observed in the parametric study. The influence of web height, load case, and bottom flange displacement on the ultimate capacity are examined in turn.

6.1 LPF gain with different web heights and bottom flange widths

As seen in the results, the web height influences the relative ΔLPF gain between the bracing configurations, though the overall magnitude remains modest with a maximum gain of approximately 6%. The largest gains occur for intermediate web heights in the range h_w = 3000–3510 mm, while both the smallest and largest web heights show comparatively smaller differences.

For the lowest web heights, the beam primarily fails in bending, where the cross section can no longer carry the applied moment. This is illustrated in Fig. 6.1, where yielding occurs in the bottom flange and the lower part of the web at midspan, with large vertical displacements. In this regime, the bottom flange restraint has little influence since the governing failure mode is not stability-driven.

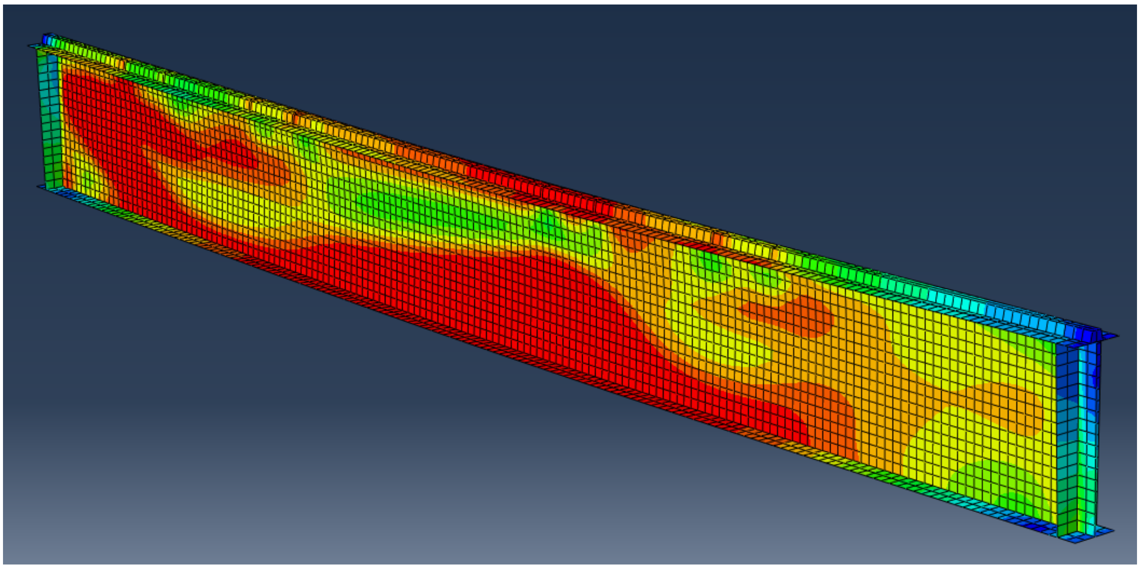

Figure 6.1: Von Mises stress distribution for $h_w = 2500$ mm and $b_{bf} = 700$ mm with both flanges restrained and wheel positions for critical moment, showing concentration at the lower part of the web and bottom flange indicating failure in bending.

For the largest web heights, the beam fails by local instability, as shown in Fig. 6.2, where yielding concentrates just below the top compression flange and the web buckles locally. The top flange tends to fold over itself in this mode, and since the web is very slender for these heights and it fails inbetween the flanges the bottom flange restraint have little to no affect on this behavior.

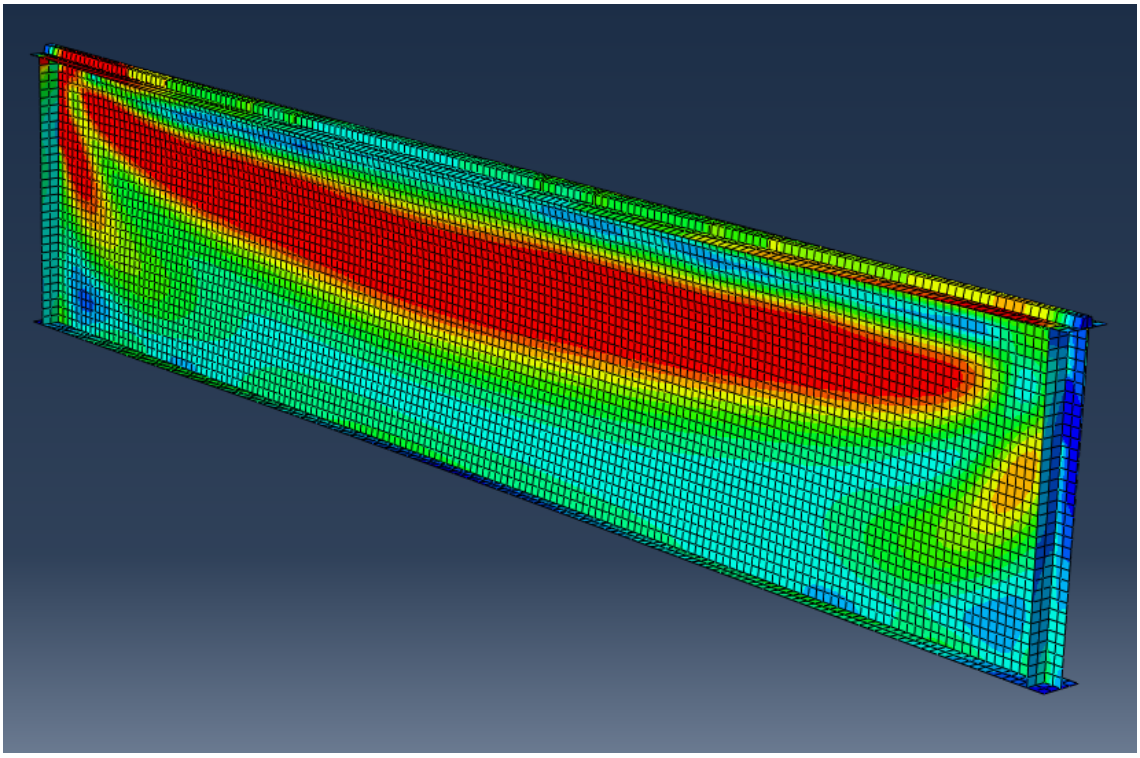

Figure 6.2: Von Mises stress distribution for $h_w = 5000$ mm and $b_{bf} = 700$ mm with both flanges restrained and wheel positions for critical moment, showing concentration below the compression flange indicating on local web buckling.

For the intermediate web heights, the governing failure mode is shear buckling, illustrated in Fig. 6.3 for the configuration with only the top flange braced and Fig. 6.4 for the configuration with both flanges braced, for $h_w = 3510$ mm, $b_{bf} = 400$ mm. Characteristic 45-degree yield lines form at the support region for both configurations, consistent with shear failure. With bottom flange bracing added, a larger portion of the web participates in carrying the forces, evidenced by a more distributed yielded zone across the full beam length compared to bracing only at the top flange. Without bottom flange restraint, the forces concentrate at the support earlier, limiting the effective web area and reducing the ultimate capacity.

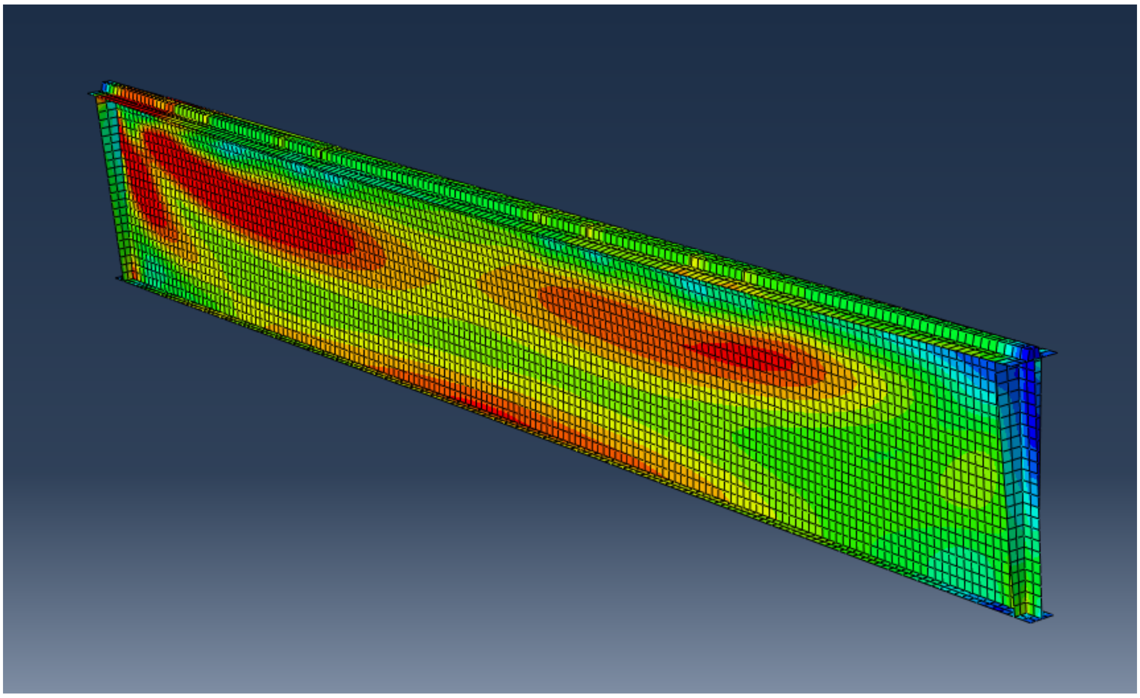

Figure 6.3: Von Mises stress distribution for $h_w = 3510$ mm, $b_{bf} = 400$ mm and with the top flange braced and wheel positions for critical moment.

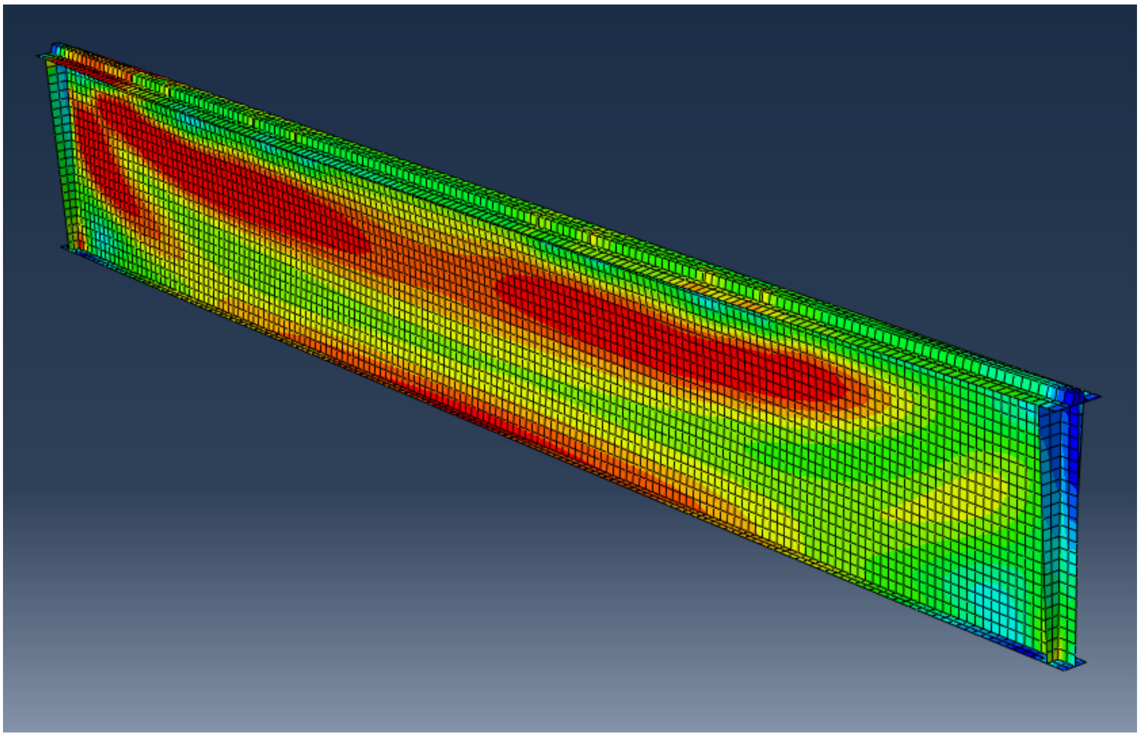

Figure 6.4: Von Mises stress distribution for $h_w = 3510$ mm, $b_{bf} = 400$ mm and with bracing on both flanges and wheel positions for critical moment.

6.2 LPF gain for different load cases

For the different load cases the largest ΔLPF gain is observed for the buckling mode imperfection with the cross section $h_w = 3000$ mm and $b_{bf} = 400$ mm at an imperfection amplitude of $e_0 = 25$ mm when subjected to the critical shear wheel positions. This can be explained by comparing with the case with $e_0 = 0$ mm shown in Fig. 6.5, where the behaviour is governed by bending and the bottom flange bracing has a limited impact. When the imperfection amplitude of $e_0 = 25$ mm is applied to the buckling mode, the failure mode shifts to shear failure and the bottom flange restraint allows the forces to be distributed more effectively across the web, shown in Fig. 6.6.

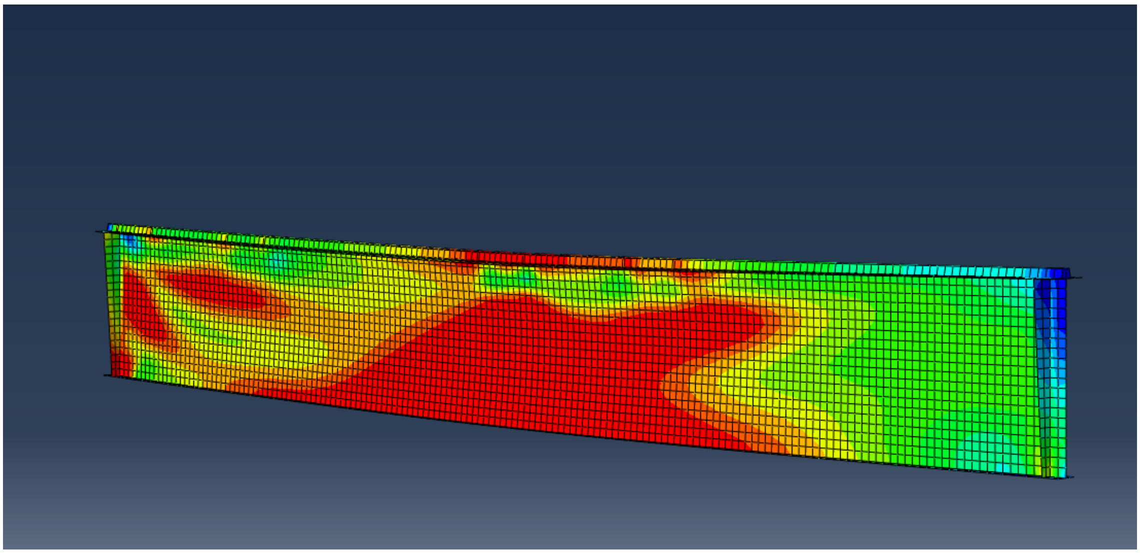

Figure 6.5: Von Mises stress distribution for $h_w = 3000$ mm, $b_{bf} = 400$ mm and e_0=0 mm with both flanges restrained and wheel positions for critical shear, showing concentration at the lower part of the web and bottom flange indicating failure in bending.

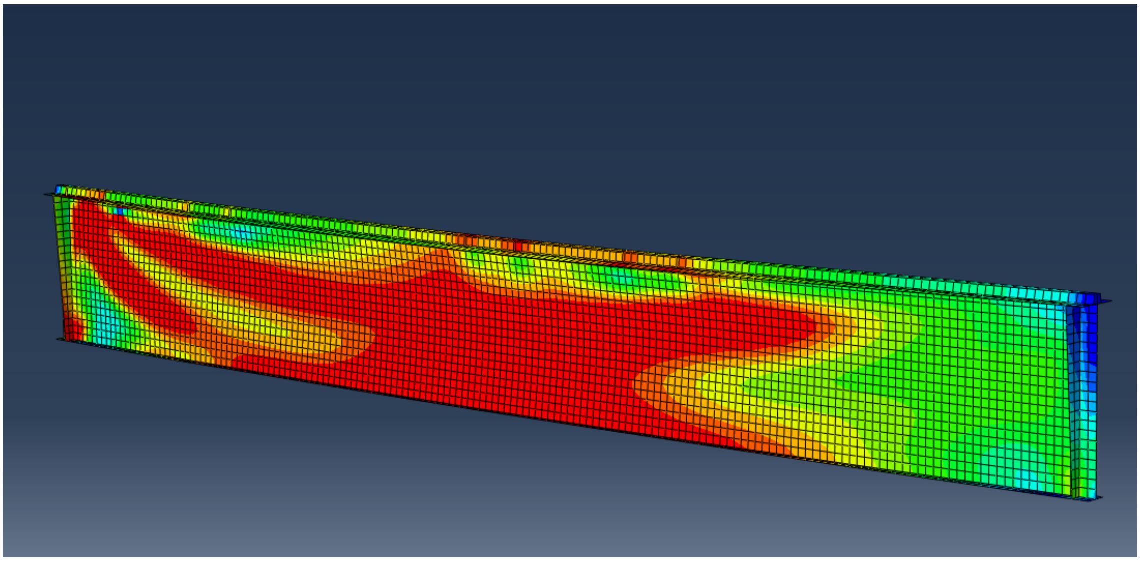

Figure 6.6: Von Mises stress distribution for h_w = 3000 mm, b_{bf} = 400 mm and e_0=25 mm with both flanges restrained and wheel positions for critical shear, showing concentration at the lower part and of 45-degree yield lines near left support indicating on shear buckling.

Overall, the critical moment wheel positions produce a more evenly distributed stress state, where for lower imperfection amplitudes the ΔLPF values are mostly positive and decrease with increasing amplitude. This can be attributed to the wheel loads being distributed over a larger portion of the beam length, which as discussed in Section 6.1, allows the bottom flange restraint to engage a greater part of the web. For the critical shear case, the wheel loads are concentrated near one support, making it more difficult to engage the full web and promoting localised shear failure rather than a distributed response. Localised yielding over the support is more prevalent for this case, affecting bottom flange widths up to 400 mm, which reduces the reliability of results for those configurations, an example is shown in Fig 6.7.

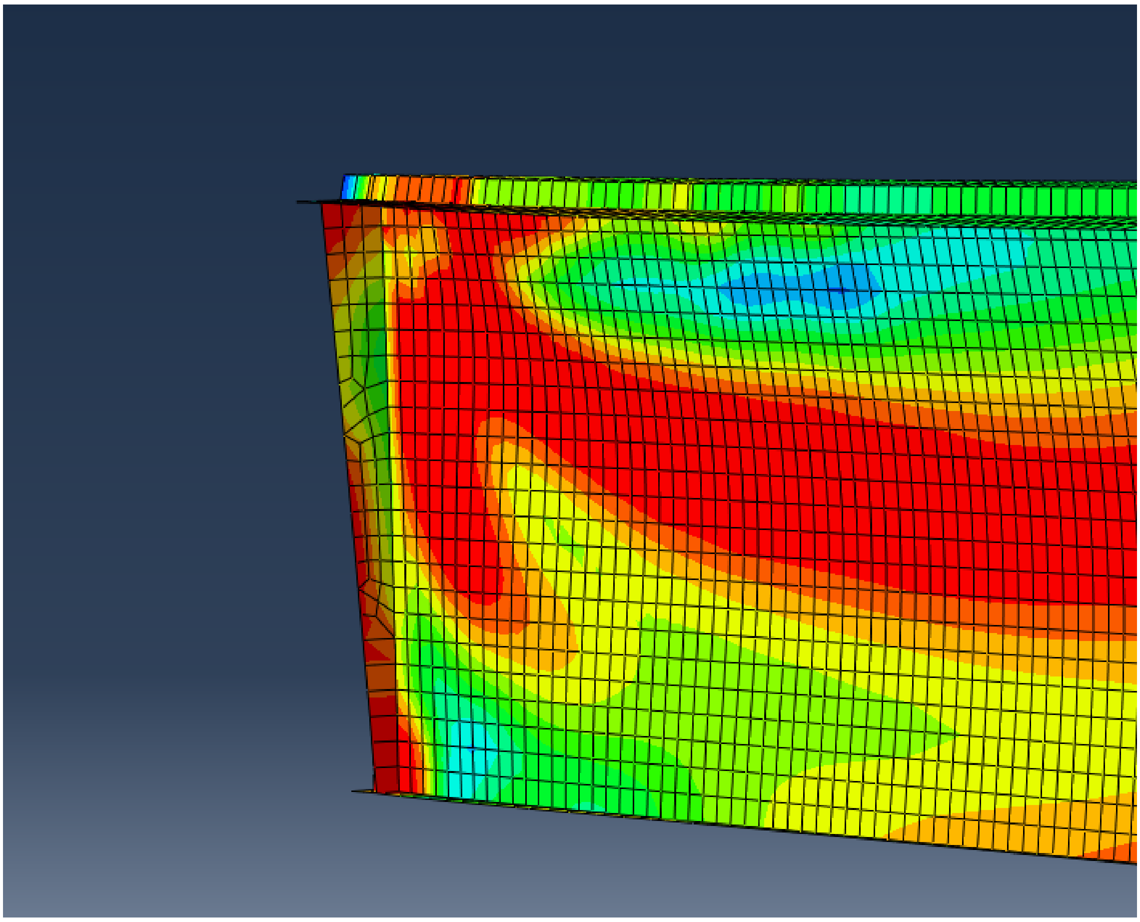

Figure 6.7: Von Mises stress distribution for $h_w = 3000$ mm and $b_{bf} = 300$ mm with both flanges restrained and wheel positions for critical shear, showing concentration of yielding over the support.

6.3 Displacement of the bottom flange

The lateral displacement of the bottom flange has been examined to understand how it influences the ultimate load capacity. Fig. 6.8 shows the lateral displacement U3 of the bottom flange against the LPF for both the unrestrained and restrained cases, for $h_w = 3510$ mm and $b_{bf} = 400$ mm across all imperfection amplitudes. The imperfection is applied in the negative U3 direction, meaning the bottom flange starts at its imperfection amplitude as a negative displacement and moves towards zero as the beam straightens.

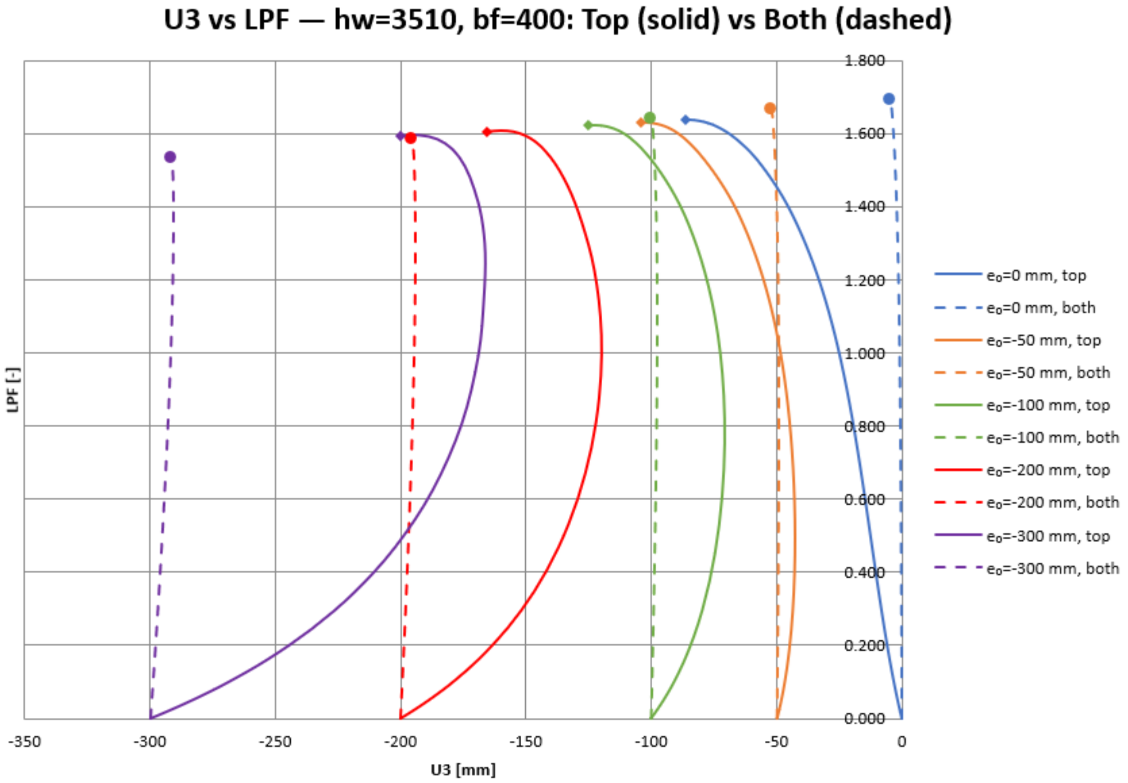

Figure 6.8: Displacement of the bottom flange for the restrained and unrestrained bot flange case width h_w = 3510 mm and b_{bf} = 400 mm, for the bottom flange imperfection case with maximum moment wheel positions.

For the restrained case, the bottom flange is effectively prevented from displacing laterally, reflected by the near-vertical lines in the diagram regardless of imperfection amplitude. For the unrestrained case, the behaviour depends strongly on the imperfection amplitude. For $e_0 = 0$, the bottom flange displaces monotonically in the negative direction as the load increases. For larger amplitudes such as $e_0 = 200$ mm and $e_0 = 300$ mm, a distinctly different behaviour is observed. The bottom flange initially moves towards zero as the load increases, reflecting the tendency of the beam to straighten itself when the bottom flange enters tension. Only when the load becomes very large, does the displacement reverse and move further in the negative direction before the beam fails.

This self-straightening behaviour is prevented in the restrained case, where the bracing locks the bottom flange in its initial imperfect position. For large imperfection amplitudes this restraint works against the natural load-carrying mechanism of the beam, explaining why the ΔLPF becomes negative - restraining the bottom flange at large imperfections inhibits the beam from redistributing forces optimally, reducing rather than improving the ultimate capacity. For the web buckling imperfection case, the behaviour is fundamentally different. Since the imperfection is applied to the web rather than directly to the bottom flange, all curves originate from U3 = 0 and they all deflect in the negative direction. The lateral displacement at failure increases with imperfection amplitude, from 84 mm to 107 mm, reflecting a greater tendency to lateral movement for larger imperfections as the load increases.

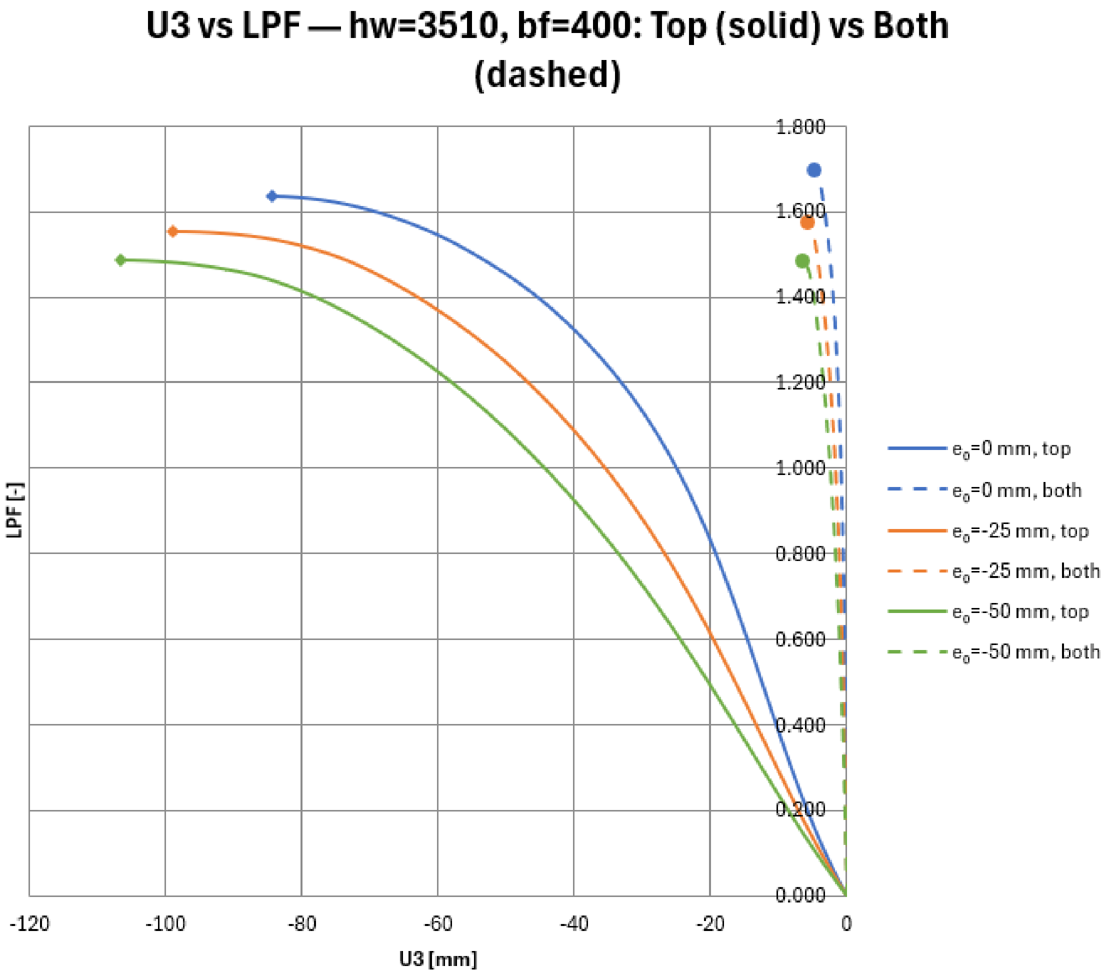

Figure 6.9: Displacement of the bottom flange for the restrained and unrestrained bot flange case width h_w = 3510 mm and b_{bf} = 400 mm, for the web buckling imperfection case with maximum moment wheel positions.

What can also be seen by examining the comparison between different widths shown in Fig. 6.10 is why, for larger imperfection amplitudes, the benefit of the bracing system diminishes more for narrower bottom flanges than for wider ones. Since b_{bf} = 700 mm is laterally stiffer, it self-straightens less under load compared to b_{bf} = 200 mm, meaning the penalty of restraining it and preventing that straightening at large imperfections is smaller. And for smaller imperfection amplitudes, the narrower flange displaces more laterally in the unrestrained case, meaning the bracing is comparatively more effective at limiting that displacement and improving capacity.

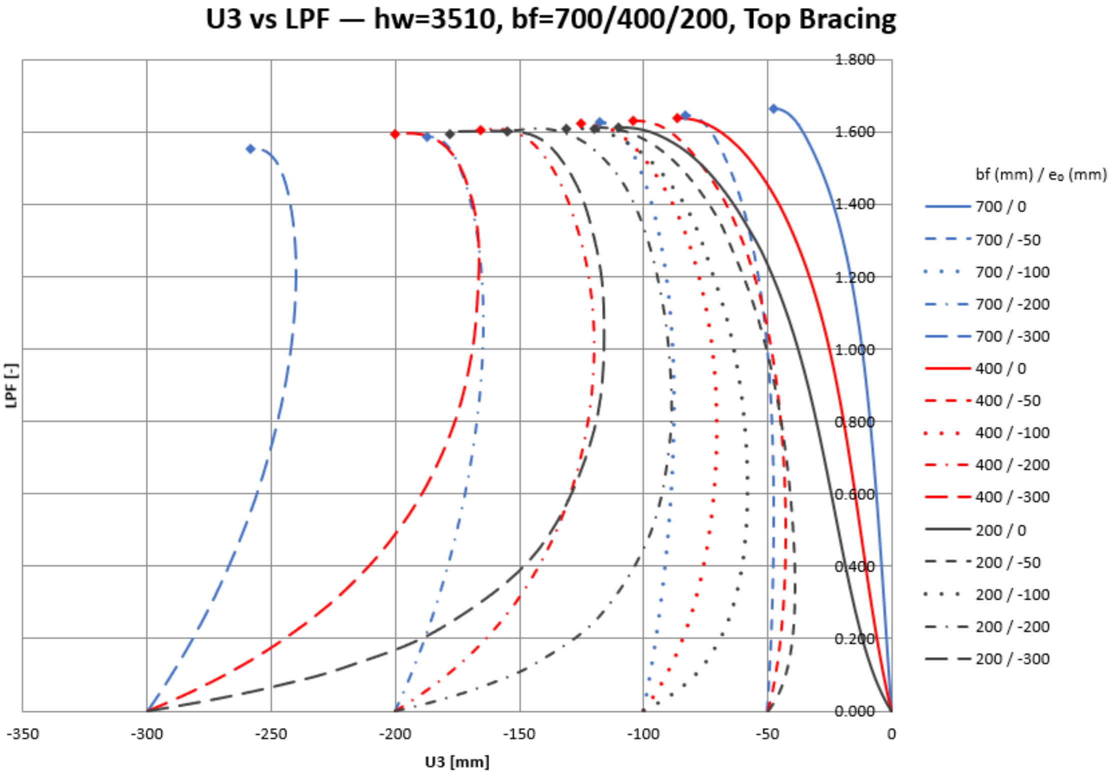

Figure 6.10: Displacement of the bottom flange for the restrained and unrestrained bot flange case with $h_w = 3510$ mm, $b_{bf} = 700$ mm, $b_{bf} = 400$ mm and $b_{bf} = 200$ mm for bottom flange imperfection case with maximum moment wheel positions.

6.4 LPF gain differences between imperfection amplitudes

For thebuckling mode imperfection results, a consistent pattern of decreasing ΔLPF with increasing imperfection amplitudes is observed. For the case of $h_w = 3000$ mm and $b_{bf} = 500$ mm subjected to the critical moment wheel positions, with an imperfection amplitude of $e_0 = 0$ mm has a ΔLPF of 4.16% while $e_0 = 50$ mm has a ΔLPF of 1.56%. For $e_0 = 0$ mm, the web starts geometrically perfect and lateral displacement of the bottom flange develops gradually during loading, resulting in a total lateral displacement of 70.96 mm at failure. For $e_0 = 50$ mm, the web is already deformed from the onset of loading, meaning that local web buckling is triggered earlier and the bottom flange restraint has less influence on the overall response before failure occurs.

Figures 6.11–6.12 illustrate the difference in stress distribution between the two imperfection amplitudes $e_0 = 0$ mm and $e_0 = 50$ mm, with both flanges restrained. For $e_0 = 0$ mm the LPF is 1.819, while for $e_0 = 50$ mm the LPF is 1.556. As seen in Fig. 6.11, the yielded zone is concentrated in the lower part of the web and in the bottom flange. In contrast, Fig. 6.12 shows a more uniformly distributed stress pattern across the full web height, indicating that the already existing imperfection promotes a more distributed web buckling failure mode, which is less sensitive to bottom flange restraint.

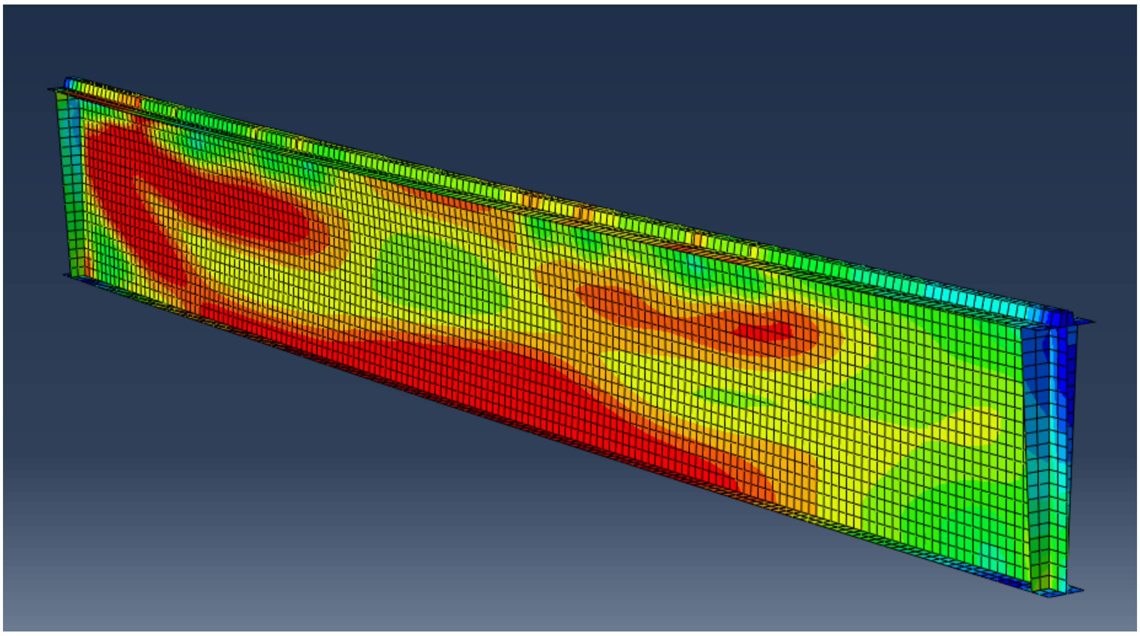

Figure 6.11: Von Mises stress distribution for h_w=3000 mm, b_{bf}=500 mm, e_0=0 mm under critical moment with both flanges restrained.

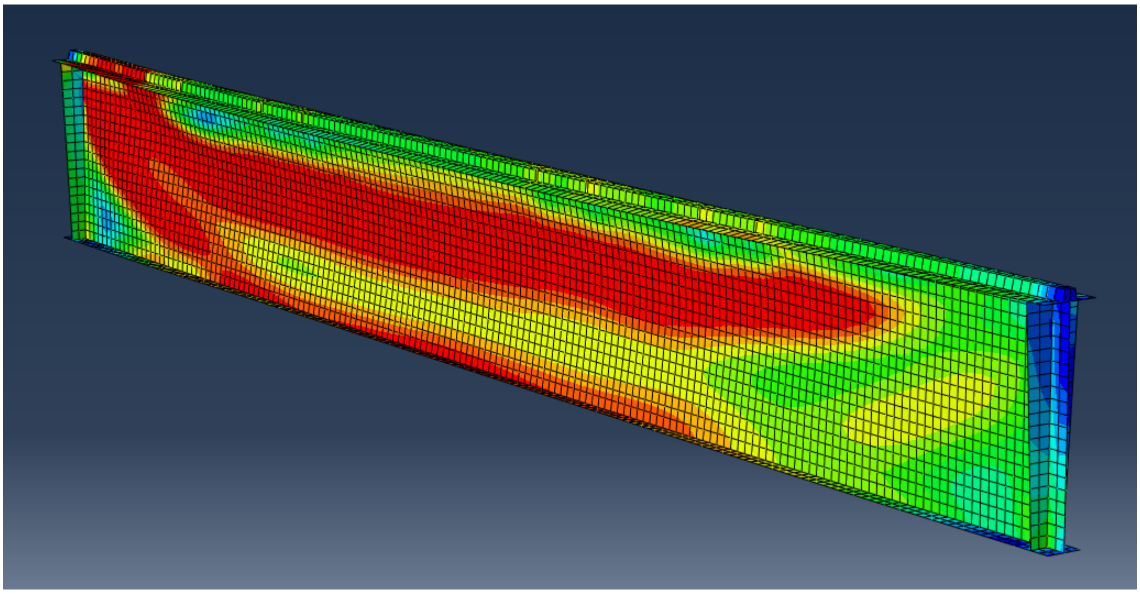

Figure 6.12: Von Mises stress distribution for h_w=3000 mm, b_{bf}=500 mm, e_0=50 mm under critical moment with both flanges restrained. Restraint of the bottom flange redistributes yielding more uniformly across the full web height.

For the geometric bottom flange imperfection the difference in the imperfection amplitudes are discussed in Section 6.3 where the pattern is clear that for increasing imperfection amplitudes the ΔLPF goes from having a positive effect to having a negative effect, with restraining the bottom flange out of plane and restraining the straightening movement for large imperfections leads to a negative effect. For the lower imperfection amplitudes, the bottom flange does not straighten but deflect out of plane. Meaning that restraining that out of plane deflection leads to a small increase in capacity.

This is most clearly explained for the geometry of h_w=3000 mm, b_{bf}=500 mm where the percent gain in ΔLPF goes from 4.16% for the imperfection e_0=0 mm and reduces to -5% for e_0=300 mm. For the case with e_0=0 mm a larger part of the web is mobilized compared to the unrestrained case, with LPF values of 1.82 and 1.75 for the both-flanges and top-only restrained cases respectively. When e_0=300 mm this decreases to 1.57 and 1.66 respectively, meaning the capacity of the restrained case reduces by about 13.7%. The explanation for this behaviour is discussed in Section 6.3, and the stress distributions are shown in Fig. 6.13–Fig. 6.16.

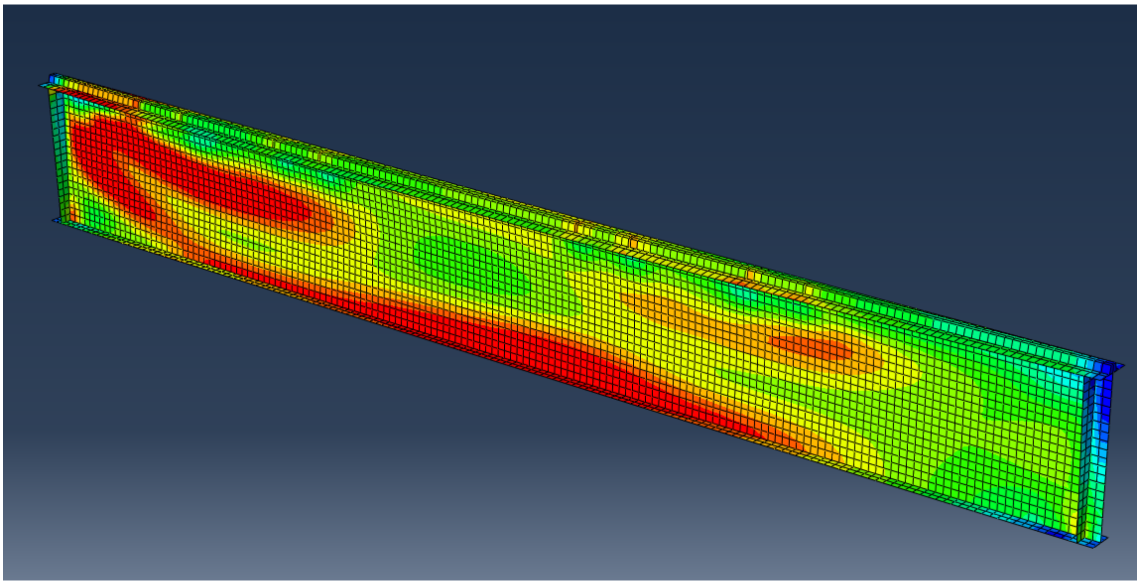

Figure 6.13: Von Mises stress distribution for h_w=3000 mm, b_{bf}=500 mm, e_0=0 mm under critical moment with top-flange restraint only for the geometric bottom flange imperfection case.

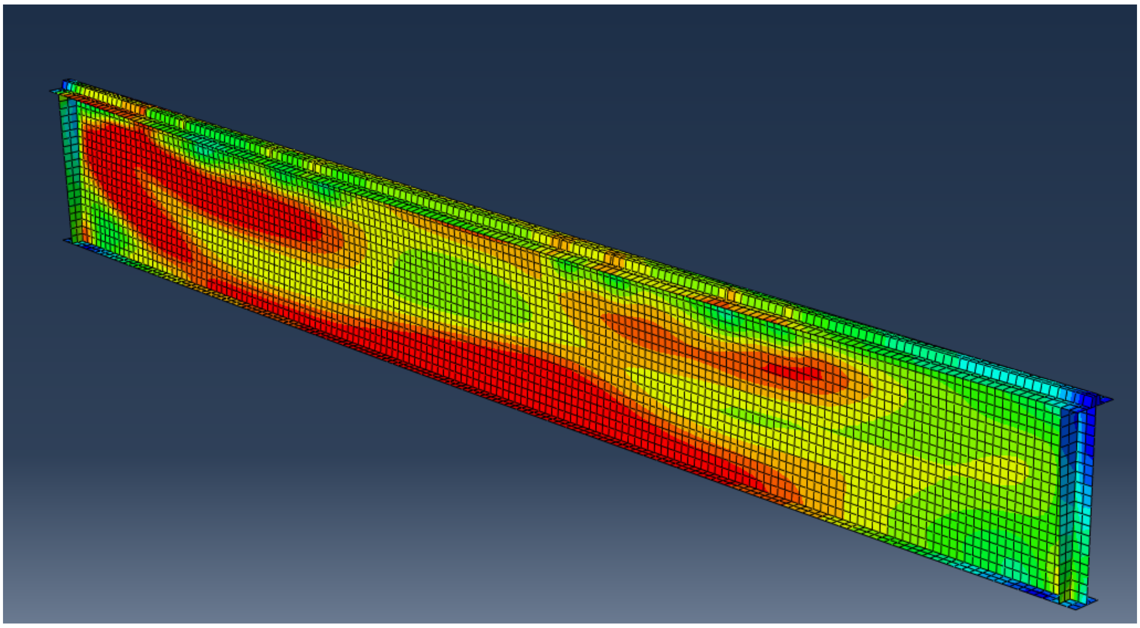

Figure 6.14: Von Mises stress distribution for h_w=3000 mm, b_{bf}=500 mm, e_0=0 mm under critical moment with both flanges restrained for the geometric bottom flange imperfection case.

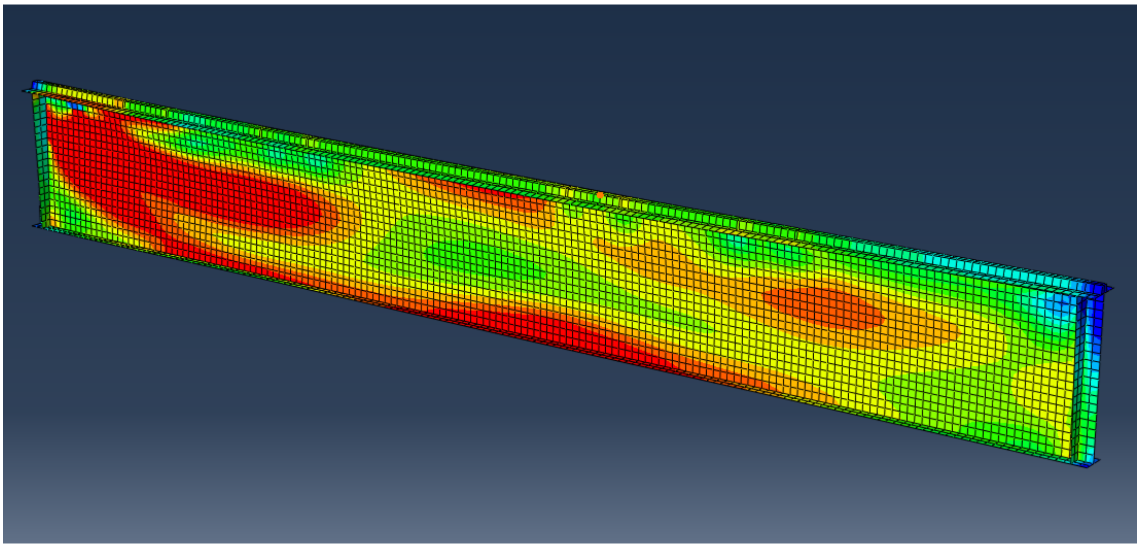

Figure 6.15: Von Mises stress distribution for h_w=3000 mm, b_{bf}=500 mm, e_0=300 mm under critical moment with top-flange restraint only for the geometric bottom flange imperfection case.

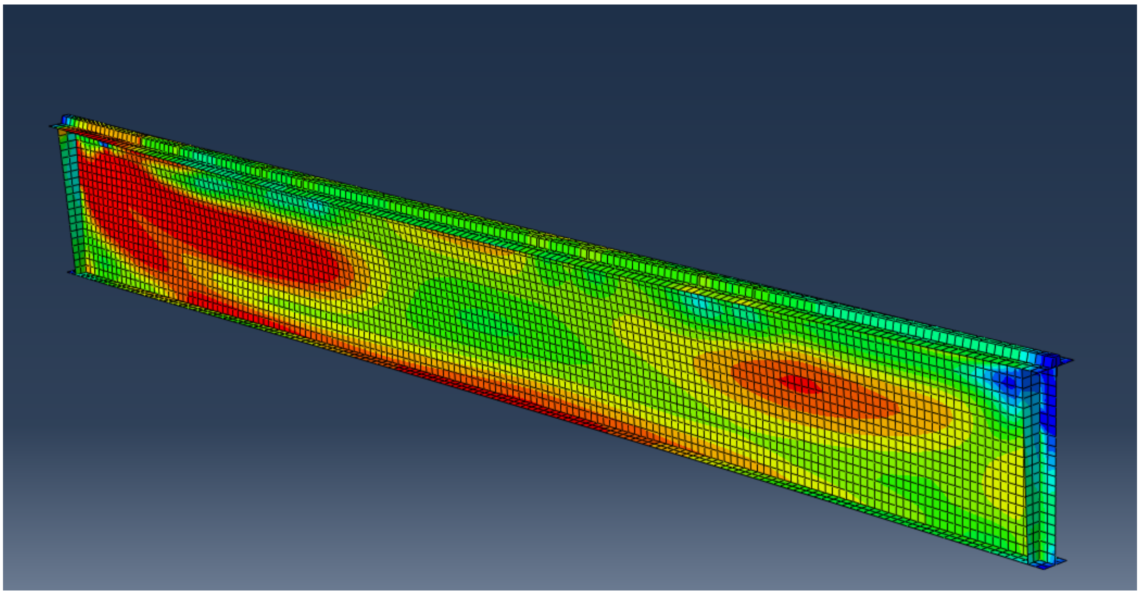

Figure 6.16: Von Mises stress distribution for h_w=3000 mm, b_{bf}=500 mm, e_0=300 mm under critical moment with both flanges restrained for the goemetric bottom flange imperfection case.

6.5 Comparison between FEM Results and American design practice

According to the provisions presented in Section 2.6, certain girder configurations are susceptible to web sidesway buckling. The capacity calculations for all parametric combinations are presented in Appendix B and summarised in Fig. 6.17. Dark green cells indicate combinations where the slenderness ratio exceeds 2.3 and the limit state does not apply. Light green cells indicate combinations where the ratio is below 2.3 but the nominal strength ϕR_n exceeds the maximum wheel load of 1626 kN, and the check is satisfied. Red cells indicate combinations where ϕR_n falls below the maximum wheel load and the check is not satisfied.

Web sidesway buckling: ϕRn vs. maximum wheel load (1626 kN)

hw \ bf	700	600	500	400	300	200
2500		4476	2998	2028	1408	1099
3000			6216	1920	1199	829
3510				3878	2235	696
4000				4082	2160	1173
4500					2176	1066
5000					2238	1004

Figure 6.17: Web sidesway buckling nominal strength ϕR_n [kN] for varying web height and bottom flange width.

From the figure it can be seen that all web heights with a bottom flange width of 200 mm fail the check, as do the two lowest web heights with a flange width of 300 mm. This suggests that narrow bottom flanges are particularly susceptible, as they offer less resistance to lateral displacement, while more stocky webs can more readily induce lateral displacement of a somewhat wider flange. From the parametric study results, a similar pattern can be observed, where the largest ΔLPF gains generally occur for the lower web heights and narrower bottom flange widths, at least for smaller imperfection amplitudes.

It should be noted, however, that the most narrow bottom flange widths investigated, particularly 200 mm, would likely not satisfy other design checks such as local buckling or minimum flange slenderness requirements. In practice, such dimensions would therefore rarely be used, which limits the practical relevance of the sidesway buckling check for those configurations.

6.6 Limitations and further developments

The springs are modelled as a continuous spring bed along the full length of the beam, which approximates the parabolic stiffness distribution of the physical truss well in a global sense. However, a real truss attaches to the flange only at discrete points corresponding to the vertical members, meaning that the flange is unrestrained between these attachment points. The continuous spring bed may therefore overestimate the lateral restraint provided to the bottom flange, and consequently the LPF gain attributed to bottom flange bracing could be slightly overestimated. Whether this effect is significant would require a more detailed model where the bracing is represented as discrete point supports at the actual vertical spacing, which is suggested as a topic for further study.

Only one load combination was studied in detail, corresponding to the maximum vertical wheel loads. A trial run with larger horizontal loads produced similar results, but other combinations - particularly those involving skewing forces or crane bridge acceleration - could potentially make the influence of bottom flange bracing more

pronounced. The skewing forces are concentrated at the extreme wheels of each end carriage, while the horizontal forces from bridge acceleration are more distributed, and it remains unclear which of these produces a larger effect on the lateral behaviour of the bottom flange. Investigating additional load combinations could clarify this and potentially identify cases where bottom flange bracing becomes more critical.
A consistent load case throughout the entire report, covering both the verification, bracing design and parametric study, could have increased the clarity and comparability of the results.

To strengthen the motivation for the study, more contact with professionals in the American steel industry could have been established to better understand the background to the removal of the bottom flange bracing requirement from the AISC mill building specification, including what tests or analyses formed the basis for that decision.

7
Conclusion

This thesis has investigated the structural behaviour of the bottom flange in large crane runway girders, with the aim of assessing whether dedicated bottom flange bracing should be considered a necessary design measure and whether equivalent guidance to American practice should be introduced in Eurocode.

The parametric study shows that adding bottom flange restraint produces a modest gain in ultimate load capacity, with the largest improvements observed for intermediate web heights and narrower bottom flange widths. For these geometries, the bottom flange restraint allows a more distributed stress state across the web, improving the overall resistance. However, the gains are generally small, with a maximum ΔLPF of approximately 5-6% across the configurations studied.

For larger geometric imperfections, the results show that restraining the bottom flange can have a negative effect on capacity. This is attributed to the self-straightening behaviour of the beam under load, where the bottom flange naturally tends to return towards its ideal geometry. Locking the imperfection in place through bracing prevents this and reduces the effective load-carrying capacity. The lateral displacement of the bottom flange was also examined. While displacements at ultimate load can exceed typical serviceability limits, the beam is designed to carry loads well below the ultimate capacity in practice, and the corresponding deflections under service loads would be significantly smaller.

It should be noted that the conclusions drawn are limited to the load cases and geometries investigated in this study. In practice, bottom flange bracing is already used for longer span crane girders, as seen in the project drawings forming the basis of this work, suggesting that experienced engineers consider it beneficial in certain configurations. Whether other load combinations, particularly those involving skewing forces or larger horizontal loads, would produce a more pronounced effect on bottom flange behaviour remains an open question and is suggested as a topic for future studies.

Based on the findings of this study, no strong case is found for introducing mandatory bottom flange bracing requirements in Eurocode for the geometries and load cases investigated. The capacity gain is modest, and for imperfect geometries the bracing may be counterproductive. A possible alternative would be to introduce deflection limits for the bottom flange as a serviceability check, though further research would be needed to establish appropriate limit values and is suggested for future studies.

Finally, the MATLAB-based bracing design script developed in this study could serve as a foundation for a more comprehensive design tool, where both the cross-sectional geometry and loading are taken as input and the appropriate bracing system is generated automatically. Further development and validation would be required, but such a tool could significantly simplify the design of bracing systems for crane runway girders in practice.

Bibliography

Ádány, S. and Schafer, B. (2004). BUCKLING MODE CLASSIFICATION OF MEMBERS WITH OPEN THIN-WALLED CROSS-SECTIONS. Technical report.

AISC (2022). Specification for Structural Steel Buildings Supersedes the Specification for Structural Steel Buildings. Technical report.

AISE (2003). Guide for the Design and Construction of Mill Buildings. Technical report, AISE.

AIST (2021). Guide for the Design and Construction of Mill Buildings. Technical report.

Al-Emrani, M. (2025). VSM191 Steel Structures. Technical report, Division of Structural Engineering at Chalmers, Gothenburg.

Al-Emrani, M. and Åkesson, B. (2013). STEEL STRUCTURES Course Literature-VSM 191. Technical report, Department of Civil and Environmental Engineering.

ANSYS, I. (2024). Eigenvalue Buckling Analysis.

ArcelorMittal (2024). ArcelorMittal A150 Rail.

Boverket (2011). Boverket mandatory provisions amending the board's
}mandatory provisions and general recommendations
}(2011:10) on the application of European design
}standards (Eurocodes), EKS.

Gagliardi, G. M., Kulkarni, M. D., and Marulo, F. (2025). Continuum and Discrete Analytical Methods for Vibration and Buckling Eigenvalues Shape Sensitivities. *Aerotecnica Missili & Spazio*, 104(4):259–275.

Goldman, C. (1990). Design of crane runway girders for top running and underrunning cranes and monorails. Technical report.

Hughes A F, Iles D C, and Malik A S (2011). Design of steel
}beams in torsion. Technical report, SCI.

Kalkan, I. and Buyukkaragoz, A. (2012). A numerical and analytical study on distortional buckling of doubly-symmetric steel I-beams. *Journal of Constructional Steel Research*, 70:289–297.

Modares, M., Mullen, R., Muhanna, R. L., and Zhang, H. (2004). Buckling Analysis of Structures with Uncertain Properties and Loads Using an Interval Finite Element Method. Technical report.

Naderian, H. R., Ronagh, H. R., and Azhari, M. (2014). Elastic distortional buckling of doubly symmetric steel I-section beams with slender webs. *Thin-Walled Structures*, 84:289–301.

Nyman, H. (2025). *Lateral-Torsional Buckling in Crane Runway Girders: A Comparative Study of Different Standards Hannes Nyman Degree Project in Structural Engineering and Bridges Second Cycle 30.0 Credits.* PhD thesis.

Roark, R. J., Young, W. C., Budynas, R. G., and Sadegh, A. M. (2012). *Roark's formulas for stress and strain.* McGraw-Hill.

Rossi, A., Ferreira, F. P. V., Martins, C. H., and Mesacasa Júnior, E. C. (2020). Assessment of lateral distortional buckling resistance in welded I-beams. *Journal of Constructional Steel Research*, 166.

Samanta, A. and Kumar, A. (2005). Distortional buckling in monosymmetric I-beams. *Thin-Walled Structures*, 44(1):51–56.

Sedlacek, G. and Schneider, R. (2000). Neue europäische Regelwerke für die Bemessung von Kranbahnträgern. Technical report.

SIS (2008a). Eurocode 3: Design of steel structures-Part 1-1: General rules and rules for buildings. Technical report.

SIS (2008b). Eurocode 3: Design of steel structures –
}Part 1-5: Plated structural elements. Technical report.

SIS (2008c). Eurocode 3: Design of steel structures –
}Part 1-9: Fatigue. Technical report.

SIS (2009). Eurocode 3: Design of steel structures –
}Part 6: Crane supporting structures. Technical report.

SIS (2010). Eurocode 1 – Actions on structures –
}Part 3: Actions induced by cranes and machinery. Technical report.

SIS (2022). Eurocode 3 – Design of steel structures –
}Part 1-1: General rules and rules for buildings (2022).

SIS (2024). Execution of steel structures and aluminium structures - Part 2: Technical requirements for steel structures. Technical report.

SIS (2025a). Eurocode 3 – Design of steel structures – Part 6: Crane supporting structures. Technical report.

SIS (2025b). Eurocode 3 — Design of steel structures — Part 1-14: Design assisted
}by finite element analysis.

Summers, P. B., Yura, J. A., and Ferguson, P. M. (1982). THE BEHAVIOR OF BEAMS SUBJECTED TO CONCENTRATED LOADS Sponsored by American Iron and Steel Institute. Technical report.

The Efficient Engineer (2024). Understanding the Area Moment of Inertia.

Zauchner, P., Kettler, M., and Unterweger, H. (2026). Assessing local stresses in crane runway girders considering the rail support. *Journal of Constructional Steel Research*, 239.

A
Appendix

A.1 Nonlinear material model

Carbon steel					
Eng stress	Eng strain	True stress = Nominal stress (1+Nominal strain)	True strain = ln(1+Nominal strain)	True Elastic strain = (True stress/E)	True Plastic strain = True strain- True Elastic strain
369.4417981	0.003121823	370.59513	0.00311696	0.001785011	0
375.4146451	0.019844409	382.8645267	0.019650075	0.001844108	0.017805967
418.0006311	0.027646142	429.556736	0.027270888	0.002069006	0.025201882
443.1493832	0.035134738	458.7193208	0.0345316	0.002209471	0.032322129
507.7778159	0.06991671	543.2799703	0.067580805	0.002616766	0.064964038
540.1177567	0.180995582	637.8766846	0.166357797	0.003072402	0.163285395
E=	207615	MPa			

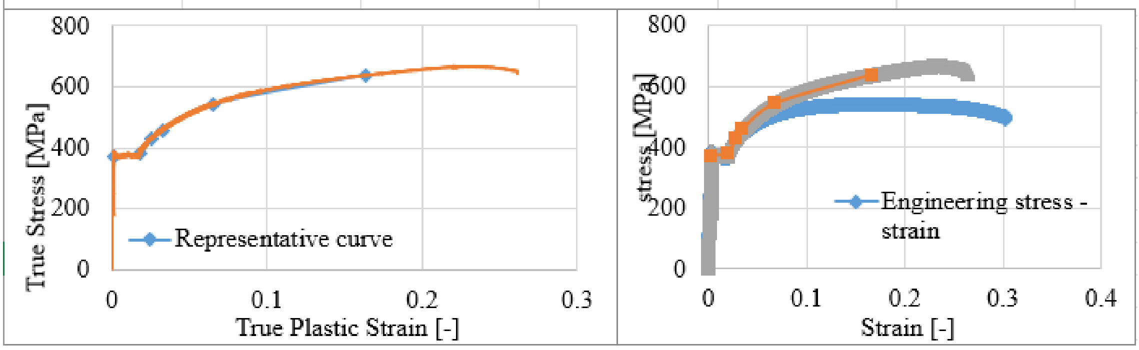

Figure A.1: Non linear data for carbon steel used in the FEM-model (Al-Emrani, 2025)

B

Mathcad calculations

B.1 Geometry and constants calculations

Loads from hoist load, crab, bridge

$l := 31\ m$ Bridge length

$craneload := 465000\ kg$ Weight of hoist load

$bridge := 565000\ kg$ Weight of beam

$crab := 205000\ kg$ Weight of crab

Design of cross section

$t_w := 30\ mm$

$h_w := 3420\ mm$

$t_{tf} := 100\ mm$

$b_{tf} := 800\ mm$

$t_{bf} := 80\ mm$

$b_{bf} := 700\ mm$

Rail data

$$\begin{bmatrix} h_r \\ b_r \end{bmatrix} := \text{A150} = \begin{bmatrix} 150 \\ 150 \end{bmatrix}\ mm$$

$e_r := \frac{b_r}{4} = 37.5\ mm$ (SS-EN 1991-3:2006, 2.5.2.1 (2))

Thickness for steel quality

$t := \max\left(t_w, t_{tf}, t_{bf}\right) = 100\ mm$

Total cross sectioal area

$A_{tot} := t_w \cdot h_w + t_{tf} \cdot b_{tf} + t_{bf} \cdot b_{bf} = 0.239\ m^2$

Centroid for cross section

$$z := \frac{t_{tf} \cdot b_{tf} \cdot \frac{t_{tf}}{2} + h_w \cdot t_w \cdot \left(t_{tf} + \frac{h_w}{2}\right) + t_{bf} \cdot b_{bf} \cdot \left(t_{tf} + h_w + \frac{t_{bf}}{2}\right)}{t_{tf} \cdot b_{tf} + h_w \cdot t_w + t_{bf} \cdot b_{bf}} = 1.631\ m$$

Moment of inertia in y and z

$$I_y := \frac{t_w \cdot h_w^3}{12} + \frac{b_{tf} \cdot t_{tf}^3}{12} + b_{tf} \cdot t_{tf} \cdot \left(z - \frac{t_{tf}}{2}\right)^2 + \frac{b_{bf} \cdot t_{bf}^3}{12} + b_{bf} \cdot t_{bf} \cdot \left(z - \left(t_{tf} + h_w + \frac{t_{bf}}{2}\right)\right)^2 = \left(5.084 \cdot 10^{11}\right)\ mm^4$$

$$I_z := \frac{h_w \cdot t_w^3}{12} + \frac{t_{tf} \cdot b_{tf}^3}{12} + \frac{t_{bf} \cdot b_{bf}^3}{12} = 0.007\ m^4$$

Shear centre

$$h_{tot} := h_w + t_{tf} + t_{bf} = 3.6\ m$$

Full height of cc

$$S := \frac{t_{bf} \cdot b_{bf}^3 \cdot h_{tot}}{t_{tf} \cdot b_{tf}^3 + t_{bf} \cdot b_{bf}^3} = 1.256\ m$$

From the top

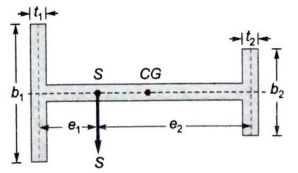

$$e_1 = \frac{t_2 b_2^3 h}{t_1 b_1^3 + t_2 b_2^3}\ ;\ e_2 = \frac{t_1 b_1^3 h}{t_1 b_1^3 + t_2 b_2^3}$$

Sectional modulus

Elastic sectional modulus

$$z_{top} := z = 1.631\ m$$

$$z_{bot} := \left(t_{tf} + h_w + t_{bf} - z\right) = 1.969\ m$$

$$M_{el} = W_{el} \cdot f_y$$

$$W_{el} = \frac{I}{h/2}$$

$$W_{el.y.top} := \frac{I_y}{z_{top}} = \left(3.118 \cdot 10^8\right)\ mm^3$$

$$W_{el.y.bot} := \frac{I_y}{z_{bot}} = \left(2.582 \cdot 10^8\right)\ mm^3$$

$$W_{el.y} := min\left(W_{el.y.top}, W_{el.y.bot}\right) = \left(2.582 \cdot 10^8\right)\ mm^3$$

$$y_{z.z} := \max\left(b_{tf}, b_{bf}\right) = 800\ mm$$

$$W_{el.z} := \frac{I_z}{\frac{y_{z.z}}{2}} = \left(1.64 \cdot 10^{7}\right)\ mm^{3}$$

Plastic sectional modulus

$$W_{pl.y} := t_{tf} \cdot b_{tf} \cdot \left(z - \frac{t_{tf}}{2}\right) + \frac{t_w \cdot {h_w}^{2}}{4} + t_{bf} \cdot b_{bf} \cdot \left(t_{tf} + h_w + \frac{t_{bf}}{2} - z\right) = \left(3.222 \cdot 10^{8}\right)\ mm^{3}$$

$$W_{pl.z} := \frac{t_{tf} \cdot {b_{tf}}^{2}}{4} + \frac{h_w \cdot {t_w}^{2}}{4} + \frac{t_{bf} \cdot {b_{bf}}^{2}}{4} = \left(2.657 \cdot 10^{7}\right)\ mm^{3}$$

$$M_{pl} = f_y\left[t_f \cdot b_f\left(t_f + h_w\right) + \frac{t_w h_w^2}{4}\right]$$

$$W_{pl} = \frac{M_{pl}}{f_y}$$

$$W_{pl} = t_f \cdot b_f\left(t_f + h_w\right) + \frac{t_w h_w^2}{4}$$

Warping constant

$$I_{tf.z} := \frac{t_{tf} \cdot {b_{tf}}^{3}}{12} = 0.004\ m^{4}$$

Moment of inertia of top flange around z-z

$$I_{bf.z} := \frac{t_{bf} \cdot {b_{bf}}^{3}}{12} = 0.002\ m^{4}$$

Moment of inertia of bot flange around z-z

$$h_m := h_w + \frac{t_{bf}}{2} + \frac{t_{tf}}{2} = \left(3.51 \cdot 10^{3}\right)\ mm$$

Height between centroids of flanges

$$I_W := \frac{I_{tf.z} \cdot I_{bf.z} \cdot {h_m}^{2}}{I_{tf.z} + I_{bf.z}} = \left(1.834 \cdot 10^{16}\right)\ mm^{6}$$

Warping constant

Torsional constant

$$I_T := \frac{h_w \cdot {t_w}^{3}}{3} + \frac{{t_{tf}}^{3} \cdot b_{tf}}{3} + \frac{{t_{bf}}^{3} \cdot b_{bf}}{3} = \left(4.169 \cdot 10^{8}\right)\ mm^{4}$$

Torsional constant

Steel properties

$E := 207.615\ GPa$ $\gamma_{M1} := 1$ $\gamma_{M2} := 1.25$

$\nu := 0.3$ Poissions ratio

$G := \dfrac{E}{2\ (1+\nu)} = 79.852\ GPa$ Shear modulus

$\rho := 7850\ \dfrac{kg}{m^3}$ Density steel

$Sq :=$ Steel quality: S355 $= 3$

Steel qualities according to EN 10025-2:2019 Table 6

S235

$$
\begin{aligned}
f_{y.235} := &\text{ if } (Sq = 1) \wedge (t \le 16\ mm) \\
&\quad\| 235 \\
&\text{else if } (Sq = 1) \wedge (16\ mm < t \le 40\ mm) \\
&\quad\| 225 \\
&\text{else if } (Sq = 1) \wedge (40\ mm < t \le 63\ mm) \\
&\quad\| 215 \\
&\text{else if } (Sq = 1) \wedge (63\ mm < t \le 80\ mm) \\
&\quad\| 215 \\
&\text{else if } (Sq = 1) \wedge (80\ mm < t \le 100\ mm) \\
&\quad\| 215 \\
&\text{else if } (Sq = 1) \wedge (100\ mm < t \le 150\ mm) \\
&\quad\| 195 \\
&\text{else if } (Sq = 1) \wedge (150\ mm < t \le 200\ mm) \\
&\quad\| 185 \\
&\text{else if } (Sq = 1) \wedge (200\ mm < t \le 250\ mm) \\
&\quad\| 175 \\
&\text{else if } (Sq = 1) \wedge (250\ mm < t \le 400\ mm) \\
&\quad\| 165 \\
&\text{else} \\
&\quad\| 0
\end{aligned}
\cdot MPa = 0\ MPa
$$

$$f_{u.235} := \begin{cases} 360 & \text{if } (Sq = 1) \wedge (t < 3\ mm) \\ 360 & \text{else if } (Sq = 1) \wedge (3\ mm < t \le 100\ mm) \\ 350 & \text{else if } (Sq = 1) \wedge (100\ mm < t \le 150\ mm) \\ 340 & \text{else if } (Sq = 1) \wedge (150\ mm < t \le 250\ mm) \\ 330 & \text{else if } (Sq = 1) \wedge (250\ mm < t \le 400\ mm) \\ 0 & \text{else} \end{cases} \cdot MPa = 0\ MPa$$

S275

$$f_{y.275} := \begin{cases} 275 & \text{if } (Sq = 2) \wedge (t \le 16\ mm) \\ 265 & \text{else if } (Sq = 2) \wedge (16\ mm < t \le 40\ mm) \\ 255 & \text{else if } (Sq = 2) \wedge (40\ mm < t \le 63\ mm) \\ 245 & \text{else if } (Sq = 2) \wedge (63\ mm < t \le 80\ mm) \\ 235 & \text{else if } (Sq = 2) \wedge (80\ mm < t \le 100\ mm) \\ 225 & \text{else if } (Sq = 2) \wedge (100\ mm < t \le 150\ mm) \\ 215 & \text{else if } (Sq = 2) \wedge (150\ mm < t \le 200\ mm) \\ 205 & \text{else if } (Sq = 2) \wedge (200\ mm < t \le 250\ mm) \\ 195 & \text{else if } (Sq = 2) \wedge (250\ mm < t \le 400\ mm) \\ 0 & \text{else} \end{cases} \cdot MPa = 0\ MPa$$

$$
f_{u.275} := \begin{cases} 430 & \text{if } (Sq=2)\wedge(t<3\ mm) \\ 410 & \text{else if } (Sq=2)\wedge(3\ mm<t\le 100\ mm) \\ 400 & \text{else if } (Sq=2)\wedge(100\ mm<t\le 150\ mm) \\ 380 & \text{else if } (Sq=2)\wedge(150\ mm<t\le 250\ mm) \\ 380 & \text{else if } (Sq=2)\wedge(250\ mm<t\le 400\ mm) \\ 0 & \text{else} \end{cases}
$$

$MPa = 0\ MPa$

S355

$$
f_{y.355} := \begin{cases} 355 & \text{if } (Sq=3)\wedge(t\le 16\ mm) \\ 345 & \text{else if } (Sq=3)\wedge(16\ mm<t\le 40\ mm) \\ 335 & \text{else if } (Sq=3)\wedge(40\ mm<t\le 63\ mm) \\ 325 & \text{else if } (Sq=3)\wedge(63\ mm<t\le 80\ mm) \\ 315 & \text{else if } (Sq=3)\wedge(80\ mm<t\le 100\ mm) \\ 295 & \text{else if } (Sq=3)\wedge(100\ mm<t\le 150\ mm) \\ 285 & \text{else if } (Sq=3)\wedge(150\ mm<t\le 200\ mm) \\ 275 & \text{else if } (Sq=3)\wedge(200\ mm<t\le 250\ mm) \\ 265 & \text{else if } (Sq=3)\wedge(250\ mm<t\le 400\ mm) \\ 0 & \text{else} \end{cases}
$$

$MPa = 315\ MPa$

$$f_{u.355} := \begin{cases} \text{if } (Sq=3) \land (t<3\ mm) & 510 \\ \text{else if } (Sq=3) \land (3\ mm<t\le 100\ mm) & 470 \\ \text{else if } (Sq=3) \land (100\ mm<t\le 150\ mm) & 450 \\ \text{else if } (Sq=3) \land (150\ mm<t\le 250\ mm) & 450 \\ \text{else if } (Sq=3) \land (250\ mm<t\le 400\ mm) & 450 \\ \text{else} & 0 \end{cases} \quad MPa = 470\ MPa$$

S460

$$f_{y.460} := \begin{cases} \text{if } (Sq=4) \land (t\le 16\ mm) & 460 \\ \text{else if } (Sq=4) \land (16\ mm<t\le 40\ mm) & 440 \\ \text{else if } (Sq=4) \land (40\ mm<t\le 63\ mm) & 420 \\ \text{else if } (Sq=4) \land (63\ mm<t\le 80\ mm) & 400 \\ \text{else if } (Sq=4) \land (80\ mm<t\le 100\ mm) & 390 \\ \text{else if } (Sq=4) \land (100\ mm<t\le 150\ mm) & 390 \\ \text{else if } (Sq=4) \land (150\ mm<t\le 200\ mm) & 0 \\ \text{else if } (Sq=4) \land (200\ mm<t\le 250\ mm) & 0 \\ \text{else if } (Sq=4) \land (250\ mm<t\le 400\ mm) & 0 \\ \text{else} & 0 \end{cases} \quad MPa = 0\ MPa$$

$$
f_{u.460} := \text{if } (Sq=4) \land (t<3\ mm) \\
\quad \| \ 0 \\
\text{else if } (Sq=4) \land (3\ mm<t \le 100\ mm) \\
\quad \| \ 550 \\
\text{else if } (Sq=4) \land (100\ mm<t \le 150\ mm) \\
\quad \| \ 530 \\
\text{else if } (Sq=4) \land (150\ mm<t \le 250\ mm) \\
\quad \| \ 0 \\
\text{else if } (Sq=4) \land (250\ mm<t \le 400\ mm) \\
\quad \| \ 0 \\
\text{else} \\
\quad \| \ 0
$$

$MPa = 0\ MPa$

S500

$$
f_{y.500} := \text{if } (Sq=5) \land (t \le 16\ mm) \\
\quad \| \ 500 \\
\text{else if } (Sq=5) \land (16\ mm<t \le 40\ mm) \\
\quad \| \ 480 \\
\text{else if } (Sq=5) \land (40\ mm<t \le 63\ mm) \\
\quad \| \ 460 \\
\text{else if } (Sq=5) \land (63\ mm<t \le 80\ mm) \\
\quad \| \ 450 \\
\text{else if } (Sq=5) \land (80\ mm<t \le 100\ mm) \\
\quad \| \ 450 \\
\text{else if } (Sq=5) \land (100\ mm<t \le 150\ mm) \\
\quad \| \ 450 \\
\text{else if } (Sq=5) \land (150\ mm<t \le 200\ mm) \\
\quad \| \ 0 \\
\text{else if } (Sq=5) \land (200\ mm<t \le 250\ mm) \\
\quad \| \ 0 \\
\text{else if } (Sq=5) \land (250\ mm<t \le 400\ mm) \\
\quad \| \ 0 \\
\text{else} \\
\quad \| \ 0
$$

$MPa = 0\ MPa$

$$f_{u.500} := \text{if } (Sq = 5) \wedge (t < 3\ mm) \quad \| \ 0 \quad \text{else if } (Sq = 5) \wedge (3\ mm < t \le 100\ mm) \quad \| \ 580 \quad \text{else if } (Sq = 5) \wedge (100\ mm < t \le 150\ mm) \quad \| \ 560 \quad \text{else if } (Sq = 5) \wedge (150\ mm < t \le 250\ mm) \quad \| \ 0 \quad \text{else if } (Sq = 5) \wedge (250\ mm < t \le 400\ mm) \quad \| \ 0 \quad \text{else} \quad \| \ 0$$

$$MPa = 0\ MPa$$

$$f_y := \max\left(f_{y.235}, f_{y.275}, f_{y.355}, f_{y.460}, f_{y.500}\right) = 315\ MPa$$

$$f_u := \max\left(f_{u.235}, f_{u.275}, f_{u.355}, f_{u.460}, f_{u.500}\right) = 470\ MPa$$

Steel yield strength $f_y = 315\ MPa$

Steel ultimate strength $f_u = 470\ MPa$

B.2 Dynamic factors, load combinations and loads

Dynamic factors **SS-EN 1991-3:2006 Table 2.4**

$\varphi_1 := 1.1$ upper value, lower value is 0.9

$HC :=$ Hoisting class: HC4 $= 4$ **SS-EN 1991-3:2006 Table 2.5**

$$\varphi_{2.min} := \begin{array}{l} \text{if } HC = 1 \\ \quad \| \; 1.05 \\ \text{else if } HC = 2 \\ \quad \| \; 1.1 \\ \text{else if } HC = 3 \\ \quad \| \; 1.15 \\ \text{else} \\ \quad \| \; 1.2 \end{array} \qquad \beta_2 := \begin{array}{l} \text{if } HC = 1 \\ \quad \| \; 0.17 \\ \text{else if } HC = 2 \\ \quad \| \; 0.34 \\ \text{else if } HC = 3 \\ \quad \| \; 0.51 \\ \text{else} \\ \quad \| \; 0.68 \end{array}$$

$v_h := 6 \dfrac{m}{60 \cdot s} \cdot \dfrac{s}{m} = 0.1$ in meters/second

$\varphi_2 := \varphi_{2.min} + \beta_2 \cdot v_h = 1.268$

$\Delta mass := 0 \; kg$ $mass := 200 \; kg$ Maximum if entire load is dropped

$\beta_3 :=$ Hoisting class: Rapid release $= 1$ **SS-EN 1991-3:2006 Table 2.4**

$\varphi_3 := \max\left(0, 1 - \dfrac{\Delta mass}{mass} \cdot (1 + \beta_3)\right) = 1$

$\varphi_4 := 1$ **SS-EN 1991-3:2006 Table 2.4**

$\varphi_5 :=$ Use: Forces change smootly $= 1.5$ **SS-EN 1991-3:2006 Table 2.6**

Test load

$\varphi_6 := \dfrac{(\varphi_2 + 1)}{2} = 1.134$ **SS-EN 1991-3:2006 2.10 (2.13)**

$$\varphi := \begin{bmatrix} \varphi_1 \\ \varphi_2 \\ \varphi_3 \\ \varphi_4 \\ \varphi_5 \end{bmatrix} = \begin{bmatrix} 1.1 \\ 1.268 \\ 1 \\ 1 \\ 1.5 \end{bmatrix}$$

ULS combination factors(EKS)

$\gamma_d :=$ Reliability Class: 3 $= 1$ **EKS, Article 14**

$comb :=$ Load combination: 6.10b.Point.Un/Un $= 7$ **EKS Table B-3**

$$\gamma_{d.ULS} := \begin{array}{l} \text{if } comb = 1 \\ \quad \gamma_d \cdot 1.35 \\ \text{else if } comb = 2 \\ \quad 1 \\ \text{else if } comb = 3 \\ \quad \gamma_d \cdot 0.89 \cdot 1.35 \\ \text{else if } comb = 4 \\ \quad 1 \\ \text{else if } comb = 5 \\ \quad \gamma_d \cdot 0.89 \cdot 1.35 \\ \text{else if } comb = 6 \\ \quad 1 \\ \text{else if } comb = 7 \\ \quad \gamma_d \cdot 1.35 \\ \text{else if } comb = 8 \\ \quad 1 \\ \text{else if } comb = 9 \\ \quad \gamma_d \cdot 1.35 \\ \text{else} \\ \quad 1 \end{array} = 1.35$$

$$\gamma_{var.ULS} := \begin{array}{l} \text{if } comb = 1 \\ \quad 0 \\ \text{else if } comb = 2 \\ \quad 0 \\ \text{else if } comb = 3 \\ \quad \gamma_d \cdot 1.5 \\ \text{else if } comb = 4 \\ \quad \gamma_d \cdot 1.5 \\ \text{else if } comb = 5 \\ \quad 0 \\ \text{else if } comb = 6 \\ \quad 0 \\ \text{else if } comb = 7 \\ \quad \gamma_d \cdot 1.5 \\ \text{else if } comb = 8 \\ \quad \gamma_d \cdot 1.5 \\ \text{else if } comb = 9 \\ \quad 0 \\ \text{else} \\ \quad 0 \end{array} = 1.5$$

Vertical and horizontal loads

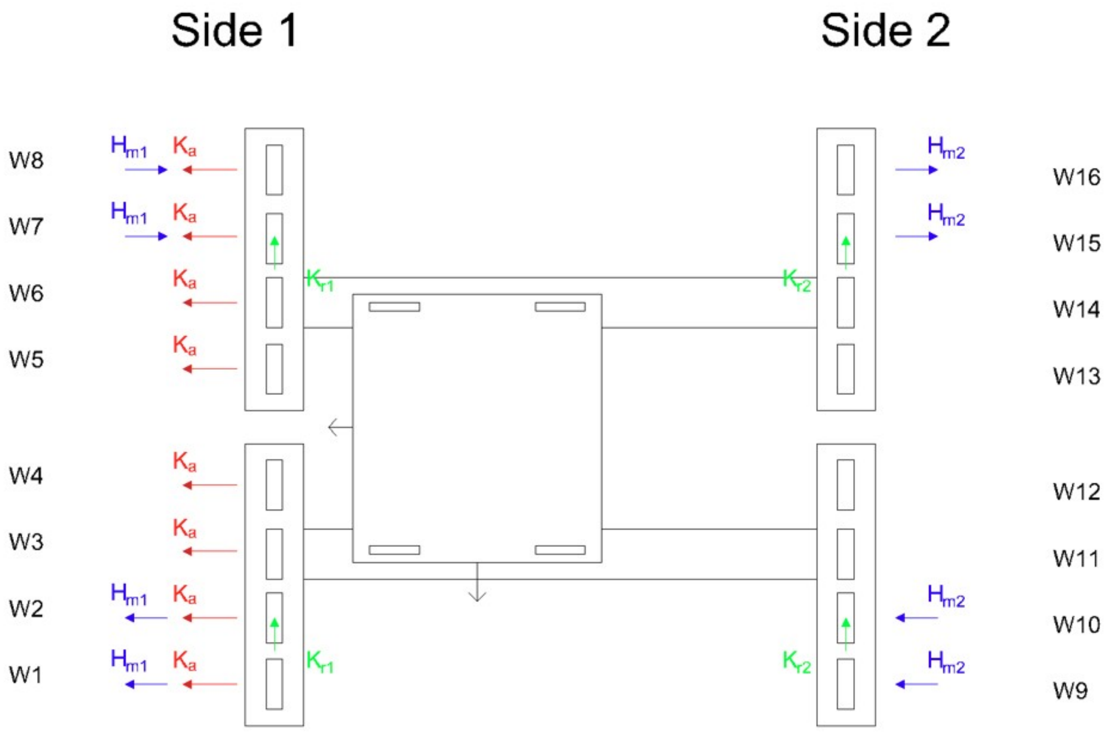

Skewing loads

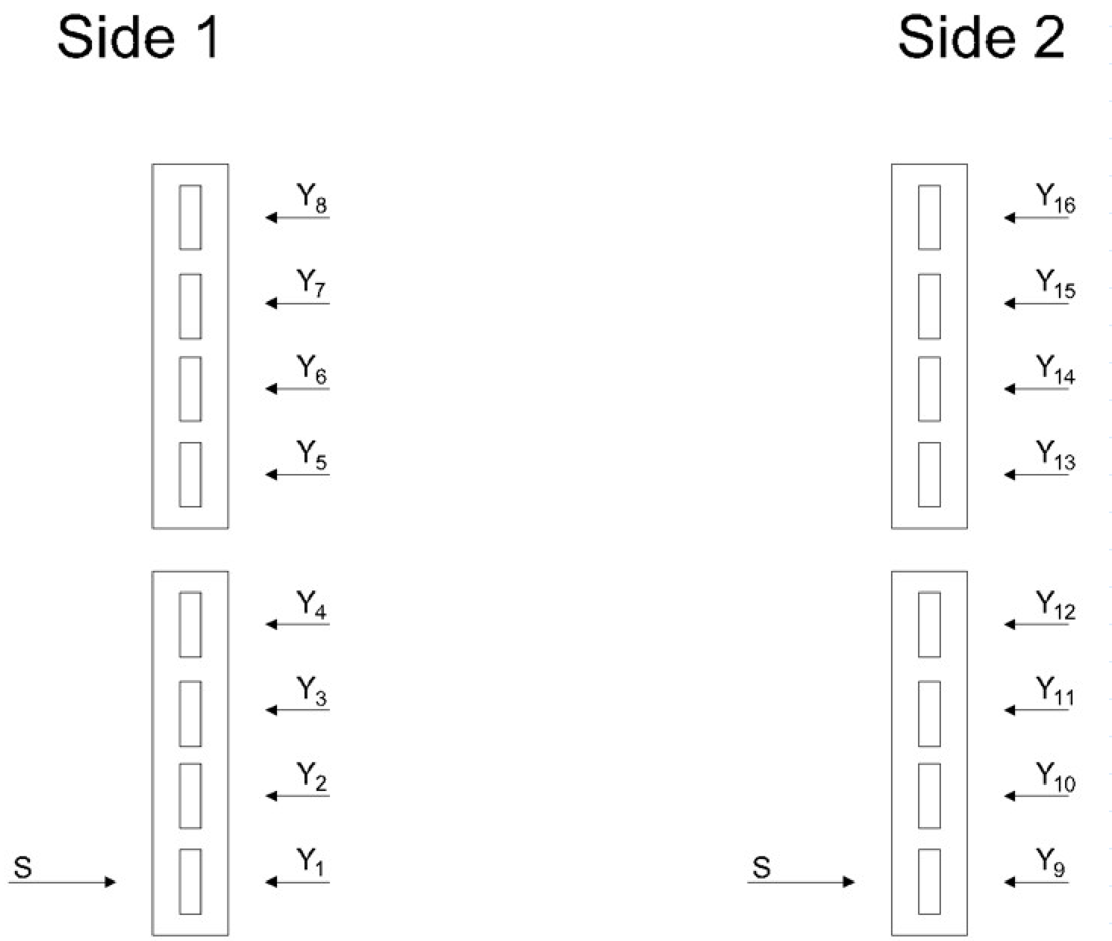

Characteristic loads

Vertical loads

$i := 0..7$ $\quad j :=$ Loadcase: 2

$$P_{wheel} := \begin{bmatrix} 86787 & 86787 & 94798 & 94798 & 95471 & 95471 & 90678 & 90678 \\ 92468 & 92468 & 101004 & 101004 & 100451 & 100451 & 95407 & 95407 \end{bmatrix} \, kg$$

Horizontal loads

$$H_m := \begin{bmatrix} 6602 & 6602 & 0 & 0 & 0 & 0 & -6602 & -6602 \\ 17977 & 17977 & 0 & 0 & 0 & 0 & -17977 & -17977 \end{bmatrix} \, kg$$

$$K_a := \begin{bmatrix} 3844 & 3844 & 3844 & 3844 & 3844 & 3844 & 3844 & 3844 \\ 0 & 0 & 0 & 0 & 0 & 0 & 0 & 0 \end{bmatrix} \, kg$$

$$K_r := \begin{bmatrix} 0 & 11735 & 0 & 0 & 0 & 0 & 11735 & 0 \\ 0 & 11735 & 0 & 0 & 0 & 0 & 11735 & 0 \end{bmatrix} \, kg$$

Skewing forces

$$S_k := \begin{bmatrix} 63438 & 0 & 0 & 0 & 0 & 0 & 0 & 0 \\ 63438 & 0 & 0 & 0 & 0 & 0 & 0 & 0 \end{bmatrix} \, kg$$

$$Y_k := \begin{bmatrix} 16523 & 14925 & 11561 & 9963 & 1637 & 39 & -3325 & -4924 \\ 6088 & 5481 & 4246 & 3659 & 601 & 14 & -1221 & -1808 \end{bmatrix} \, kg$$

Design loads

$$permloads := bridge + crab = \left(7.7 \cdot 10^5\right) \, kg$$

$$varloads := craneload = \left(4.65 \cdot 10^5\right) \, kg$$

$$R_{perm} := \frac{permloads}{varloads + permloads} = 0.623$$

$$R_{var} := 1 - R_{perm} = 0.377$$

Load combinations according to Table 2.2 SS-EN 1991-3:2006

Table 2.2 — Groups of loads and dynamic factors to be considered as one characteristic crane action

		Symbol	Section	Groups of loads									
				Ultimate Limit State							Test load	Accidental	
				1	2	3	4	5	6	7	8	9	10
1	Self-weight of crane	Q_c	2.6	φ_1	φ_1	1	φ_4	φ_4	φ_4	1	φ_1	1	1
2	Hoist load	Q_h	2.6	φ_2	φ_3	-	φ_4	φ_4	φ_4	$\eta^{1)}$	-	1	1
3	Acceleration of crane bridge	H_L, H_T	2.7	φ_5	φ_5	φ_5	φ_5	-	-	-	φ_5	-	-
4	Skewing of crane bridge	H_S	2.7	-	-	-	-	1	-	-	-	-	-
5	Acceleration or braking of crab or hoist block	H_{T3}	2.7	-	-	-	-	-	1	-	-	-	-
6	In-service wind	F_W^*	Annex A	1	1	1	1	1	-	-	1	-	-
7	Test load	Q_T	2.10	-	-	-	-	-	-	-	φ_6	-	-
8	Buffer force	H_B	2.11	-	-	-	-	-	-	-	-	φ_7	-
9	Tilting force	H_{TA}	2.11	-	-	-	-	-	-	-	-	-	1

NOTE: For out of service wind, see Annex A.

[1] η is the proportion of the hoist load that remains when the payload is removed, but is not included in the self-weight of the crane.

$$\varphi_5 := 1$$

$$\varphi = \begin{bmatrix} 1.1 \\ 1.268 \\ 1 \\ 1 \\ 1.5 \\ 1 \end{bmatrix}$$

Loads that are active for each case

$$loadMatrix := \begin{bmatrix} 1 & 1 & 1 & 0 & 0 \\ 1 & 1 & 1 & 0 & 0 \\ 1 & 0 & 1 & 0 & 0 \\ 1 & 1 & 1 & 0 & 0 \\ 1 & 1 & 0 & 1 & 0 \\ 1 & 1 & 0 & 0 & 1 \end{bmatrix}$$

Vertical load dynamic factor depending on case

$$phiMatrix := \begin{bmatrix} 0 & 1 \\ 0 & 2 \\ 5 & 5 \\ 3 & 3 \\ 3 & 3 \\ 3 & 3 \end{bmatrix}$$

Horizontal and skewing force dynamic factor depending on case

$$phiHMatrix := \begin{bmatrix} 4 & 5 & 5 \\ 4 & 5 & 5 \\ 4 & 5 & 5 \\ 4 & 5 & 5 \\ 4 & 5 & 5 \\ 4 & 5 & 5 \end{bmatrix}$$

Select ULS case

$ULS\_sel := 0$ Select uls case, 0 = ULS 1

Verification of dynamic factors

$\varphi_{perm} := \varphi_{phiMatrix_{ULS\_sel,0}} = 1.1$ $Perm_{on} := loadMatrix_{ULS\_sel,0} = 1$

$\varphi_{var} := \varphi_{phiMatrix_{ULS\_sel,1}} = 1.268$ $Var_{on} := loadMatrix_{ULS\_sel,1} = 1$

$\varphi_{Hm.Kr} := \varphi_{phiHMatrix_{ULS\_sel,0}} = 1.5$ $Hm.Kr_{on} := loadMatrix_{ULS\_sel,2} = 1$

$\varphi_{Ka} := \varphi_{phiHMatrix_{ULS\_sel,1}} = 1$ $Ka_{on} := loadMatrix_{ULS\_sel,4} = 0$

$\varphi_{Sk.Yk} := \varphi_{phiHMatrix_{ULS\_sel,2}} = 1$ $Sk.Yk_{on} := loadMatrix_{ULS\_sel,3} = 0$

Design Loads

Vertical loads

$$P_{wheel.d_i} := Perm_{on} \cdot \varphi_{perm} \cdot \gamma_{d.ULS} \cdot R_{perm} \cdot g \cdot P_{wheel_{j,i}} + Var_{on} \cdot \varphi_{var} \cdot \gamma_{var.ULS} \cdot R_{var} \cdot g \cdot P_{wheel_{j,i}} = \begin{bmatrix} 1.489 \\ 1.489 \\ 1.626 \\ 1.626 \\ 1.618 \\ 1.618 \\ 1.536 \\ 1.536 \end{bmatrix} MN$$

Horizontal design loads

$$H_{m.d_i} := Hm.Kr_{on} \cdot \varphi_{Hm.Kr} \cdot \gamma_{d.ULS} \cdot R_{perm} \cdot g \cdot H_{m_{j,i}} + Hm.Kr_{on} \cdot \varphi_{Hm.Kr} \cdot \gamma_{var.ULS} \cdot R_{var} \cdot g \cdot H_{m_{j,i}} = \begin{bmatrix} 371.931 \\ 371.931 \\ 0 \\ 0 \\ 0 \\ 0 \\ -371.931 \\ -371.931 \end{bmatrix} kN$$

$$K_{a.d_i} := Ka_{on} \cdot \varphi_{Ka} \cdot \gamma_{d.ULS} \cdot R_{perm} \cdot g \cdot K_{a_{j,i}} + Ka_{on} \cdot \varphi_{Ka} \cdot \gamma_{var.ULS} \cdot R_{var} \cdot g \cdot K_{a_{j,i}} = \begin{bmatrix} 0 \\ 0 \\ 0 \\ 0 \\ 0 \\ 0 \\ 0 \\ 0 \end{bmatrix} kN$$

$$K_{r.d_i} := Hm.Kr_{on} \cdot \varphi_{Hm.Kr} \cdot \gamma_{d.ULS} \cdot R_{perm} \cdot g \cdot K_{r_{j,i}} + Hm.Kr_{on} \cdot \varphi_{Hm.Kr} \cdot \gamma_{var.ULS} \cdot R_{var} \cdot g \cdot K_{r_{j,i}} = \begin{bmatrix} 0 \\ 242.788 \\ 0 \\ 0 \\ 0 \\ 0 \\ 242.788 \\ 0 \end{bmatrix} kN$$

Skewing design loads

$$S_{k.d_i} := Sk.Yk_{on} \cdot \varphi_{Sk.Yk} \cdot \gamma_{d.ULS} \cdot R_{perm} \cdot g \cdot S_{k_{j,i}} + Sk.Yk_{on} \cdot \varphi_{Sk.Yk} \cdot \gamma_{var.ULS} \cdot R_{var} \cdot g \cdot S_{k_{j,i}} = \begin{bmatrix} 0 \\ 0 \\ 0 \\ 0 \\ 0 \\ 0 \\ 0 \\ 0 \end{bmatrix} kN$$

$$Y_{k.d_i} := Sk.Yk_{on} \cdot \varphi_{Sk.Yk} \cdot \gamma_{d.ULS} \cdot R_{perm} \cdot g \cdot Y_{k_{j,i}} + Sk.Yk_{on} \cdot \varphi_{Sk.Yk} \cdot \gamma_{var.ULS} \cdot R_{var} \cdot g \cdot Y_{k_{j,i}} = \begin{bmatrix} 0 \\ 0 \\ 0 \\ 0 \\ 0 \\ 0 \\ 0 \\ 0 \end{bmatrix} kN$$

SLS loads, no partial factors or dynamic factors

$$P_{wheel.SLS_i} := g \cdot P_{wheel_{j,i}} = \begin{bmatrix} 906.801 \\ 906.801 \\ 990.511 \\ 990.511 \\ 985.088 \\ 985.088 \\ 935.623 \\ 935.623 \end{bmatrix} kN$$

$$H_{m.SLS_i} := g \cdot H_{m_{j,i}} = \begin{bmatrix} 176.294 \\ 176.294 \\ 0 \\ 0 \\ 0 \\ 0 \\ -176.294 \\ -176.294 \end{bmatrix} kN$$

$$K_{a.SLS_i} := g \cdot K_{a_{j,i}} = \begin{bmatrix} 0 \\ 0 \\ 0 \\ 0 \\ 0 \\ 0 \\ 0 \\ 0 \end{bmatrix} kN$$

$$K_{r.SLS_i} := g \cdot K_{r_{j,i}} = \begin{bmatrix} 0 \\ 115.081 \\ 0 \\ 0 \\ 0 \\ 0 \\ 115.081 \\ 0 \end{bmatrix} kN$$

$$S_{k.SLS_i} := g \cdot S_{k_{j,i}} = \begin{bmatrix} 622.114 \\ 0 \\ 0 \\ 0 \\ 0 \\ 0 \\ 0 \\ 0 \end{bmatrix} kN$$

$$Y_{k.SLS_i} := g \cdot Y_{k_{j,i}} = \begin{bmatrix} 59.703 \\ 53.75 \\ 41.639 \\ 35.883 \\ 5.894 \\ 0.137 \\ -11.974 \\ -17.73 \end{bmatrix} kN$$

INPUT FOR MATLAB

$$P_{wheel.d}=\begin{bmatrix}1.489\cdot10^3\\1.489\cdot10^3\\1.626\cdot10^3\\1.626\cdot10^3\\1.618\cdot10^3\\1.618\cdot10^3\\1.536\cdot10^3\\1.536\cdot10^3\end{bmatrix}\ kN \quad H_{m.d}=\begin{bmatrix}371.931\\371.931\\0\\0\\0\\0\\-371.931\\-371.931\end{bmatrix}\ kN \quad K_{a.d}=\begin{bmatrix}0\\0\\0\\0\\0\\0\\0\\0\end{bmatrix}\ kN$$

$$S_{k.d}=\begin{bmatrix}0\\0\\0\\0\\0\\0\\0\\0\end{bmatrix}\ kN \quad Y_{k.d}=\begin{bmatrix}0\\0\\0\\0\\0\\0\\0\\0\end{bmatrix}\ kN$$

$$P_{wheel.SLS}=\begin{bmatrix}906.801\\906.801\\990.511\\990.511\\985.088\\985.088\\935.623\\935.623\end{bmatrix}\ kN \quad H_{m.SLS}=\begin{bmatrix}176.294\\176.294\\0\\0\\0\\0\\-176.294\\-176.294\end{bmatrix}\ kN \quad K_{a.SLS}=\begin{bmatrix}0\\0\\0\\0\\0\\0\\0\\0\end{bmatrix}\ kN$$

$$S_{k.SLS}=\begin{bmatrix}622.114\\0\\0\\0\\0\\0\\0\\0\end{bmatrix}\ kN \quad Y_{k.SLS}=\begin{bmatrix}59.703\\53.75\\41.639\\35.883\\5.894\\0.137\\-11.974\\-17.73\end{bmatrix}\ kN$$

$A_{tot} = 0.239\ m^2$

$g_{rb.k} := 0.89 \cdot \gamma_d \cdot 1.35 \cdot \rho \cdot g \cdot A_{tot} = 22.069\ \frac{kN}{m}$

$L := 24\ m$ Span of crane girder

OUTPUT FROM MATLAB

$x_{pos} := [2.35\ \ 3.55\ \ 6.075\ \ 7.275\ \ 13.525\ \ 14.725\ \ 17.25\ \ 18.45]\ m$

$M_{y.Ed} := 43550.61\ kN \cdot m$ Maximum moment in y from matlab

$M_{z.H.Ed} := 1620.3\ kN \cdot m$ Maximum moment in z from matlab

$V_{Ed} := 8628.07\ kN$ From matlab

$V_{max.y} := 7346.99\ kN$ Maximum shear force with wheel positions for maximum moment

$M_{y.SLS} := 27143.24\ kN \cdot m$ Maximum SLS moment in y from matlab

$M_{z.SLS} := 1105.94\ kN \cdot m$ Maximum SLS moment in z from matlab

Moment in z from rotation and torque in the worst case (Design of Steel Beams in Torsion, Example 2)

$$a_c := \sqrt{\frac{E \cdot I_W}{G \cdot I_T}} = 10.695\ m$$

$$T_{r.max} := P_{wheel.d} \cdot e_r = \begin{bmatrix} 55.837 \\ 55.837 \\ 60.991 \\ 60.991 \\ 60.657 \\ 60.657 \\ 57.611 \\ 57.611 \end{bmatrix} kN \cdot m \qquad T_{r.SLS} := P_{wheel.SLS} \cdot e_r = \begin{bmatrix} 34.005 \\ 34.005 \\ 37.144 \\ 37.144 \\ 36.941 \\ 36.941 \\ 35.086 \\ 35.086 \end{bmatrix} kN \cdot m$$

$$e_z := z + h_r = 1.781\ m$$

$$T := T_{r.max} + \left(H_{m.d} + K_{a.d} - S_{k.d} + Y_{k.d}\right) \cdot e_z = \begin{bmatrix} 718.104 \\ 718.104 \\ 60.991 \\ 60.991 \\ 60.657 \\ 60.657 \\ -604.656 \\ -604.656 \end{bmatrix} kN \cdot m$$

$$T_{SLS} := T_{r.SLS} + \left(H_{m.SLS} + K_{a.SLS} - S_{k.SLS} + Y_{k.SLS}\right) \cdot e_z = \begin{bmatrix} -653.523 \\ 443.627 \\ 111.287 \\ 101.037 \\ 47.435 \\ 37.185 \\ -300.148 \\ -310.398 \end{bmatrix} kN \cdot m$$

$$\alpha := \frac{x_{pos}}{L} = \begin{bmatrix} 0.098 & 0.148 & 0.253 & 0.303 & 0.564 & 0.614 & 0.719 & 0.769 \end{bmatrix}$$

$x_{pos_{0,4}} = 13.525\ m$ Maximum position according to MATLAB

$$\alpha_5 := \frac{x_{pos_{0,4}}}{L} = 0.564$$

To the left of T5

$$\alpha_1 := \frac{x_{pos_{0,0}}}{L} = 0.098$$

$$\alpha_2 := \frac{x_{pos_{0,1}}}{L} = 0.148$$

$$\alpha_3 := \frac{x_{pos_{0,2}}}{L} = 0.253$$

$$\alpha_4 := \frac{x_{pos_{0,3}}}{L} = 0.303$$

To the right of T5

$$\alpha_6 := \frac{x_{pos_{0,5}}}{L} = 0.614$$

$$\alpha_7 := \frac{x_{pos_{0,6}}}{L} = 0.719$$

$$\alpha_8 := \frac{x_{pos_{0,7}}}{L} = 0.769$$

Rotation in the beam at T5

To the left of the point

T1

$\alpha_1 \cdot L = 2.35\ m$ < $x_{pos_{0,4}} = 13.525\ m$

$$\phi_1 := \frac{T_0 \cdot a_c}{G \cdot I_T} \cdot \left(\left(L - x_{pos_{0,4}}\right) \cdot \frac{\alpha_1}{a_c} + \frac{\sinh\left(\frac{\alpha_1 \cdot L}{a_c}\right)}{\tanh\left(\frac{L}{a_c}\right)} \cdot \sinh\left(\frac{x_{pos_{0,4}}}{a_c}\right) - \sinh\left(\frac{\alpha_1 \cdot L}{a_c}\right) \cdot \cosh\left(\frac{x_{pos_{0,4}}}{a_c}\right) \right) = 0.01$$

T2

$\alpha_2 \cdot L = 3.55\ m$ < $x_{pos_{0,4}} = 13.525\ m$

$$\phi_2 := \frac{T_1 \cdot a_c}{G \cdot I_T} \cdot \left(\left(L - x_{pos_{0,4}}\right) \cdot \frac{\alpha_2}{a_c} + \frac{\sinh\left(\frac{\alpha_2 \cdot L}{a_c}\right)}{\tanh\left(\frac{L}{a_c}\right)} \cdot \sinh\left(\frac{x_{pos_{0,4}}}{a_c}\right) - \sinh\left(\frac{\alpha_2 \cdot L}{a_c}\right) \cdot \cosh\left(\frac{x_{pos_{0,4}}}{a_c}\right) \right) = 0.014$$

$T3$

$\alpha_3 \cdot L = 6.075\ m$ $<$ $x_{pos_{0,4}} = 13.525\ m$

$$\phi_3 := \frac{T_2 \cdot a_c}{G \cdot I_T} \cdot \left(\left(L - x_{pos_{0,4}}\right) \cdot \frac{\alpha_3}{a_c} + \frac{\sinh\left(\frac{\alpha_3 \cdot L}{a_c}\right)}{\tanh\left(\frac{L}{a_c}\right)} \cdot \sinh\left(\frac{x_{pos_{0,4}}}{a_c}\right) - \sinh\left(\frac{\alpha_3 \cdot L}{a_c}\right) \cdot \cosh\left(\frac{x_{pos_{0,4}}}{a_c}\right) \right) = 0.002$$

$T4$

$\alpha_4 \cdot L = 7.275\ m$ $<$ $x_{pos_{0,4}} = 13.525\ m$

$$\phi_4 := \frac{T_3 \cdot a_c}{G \cdot I_T} \cdot \left(\left(L - x_{pos_{0,4}}\right) \cdot \frac{\alpha_4}{a_c} + \frac{\sinh\left(\frac{\alpha_4 \cdot L}{a_c}\right)}{\tanh\left(\frac{L}{a_c}\right)} \cdot \sinh\left(\frac{x_{pos_{0,4}}}{a_c}\right) - \sinh\left(\frac{\alpha_4 \cdot L}{a_c}\right) \cdot \cosh\left(\frac{x_{pos_{0,4}}}{a_c}\right) \right) = 0.002$$

$T5$

$\alpha_5 \cdot L = 13.525\ m$ $=$ $x_{pos_{0,4}} = 13.525\ m$

$$\phi_5 := \frac{T_4 \cdot a_c}{G \cdot I_T} \cdot \left(\left(L - x_{pos_{0,4}}\right) \cdot \frac{\alpha_5}{a_c} + \frac{\sinh\left(\frac{\alpha_5 \cdot L}{a_c}\right)}{\tanh\left(\frac{L}{a_c}\right)} \cdot \sinh\left(\frac{x_{pos_{0,4}}}{a_c}\right) - \sinh\left(\frac{\alpha_5 \cdot L}{a_c}\right) \cdot \cosh\left(\frac{x_{pos_{0,4}}}{a_c}\right) \right) = 0.003$$

T6

$\alpha_6 \cdot L = 14.725\ m$ > $x_{pos_{0,4}} = 13.525\ m$

$$\phi_6 := \frac{T_5 \cdot a_c}{G \cdot I_T} \cdot \left((1-\alpha_6) \cdot \frac{x_{pos_{0,4}}}{a_c} + \left(\frac{\sinh\left(\frac{\alpha_6 \cdot L}{a_c}\right)}{\tanh\left(\frac{L}{a_c}\right)} - \cosh\left(\frac{\alpha_6 \cdot L}{a_c}\right) \right) \cdot \sinh\left(\frac{x_{pos_{0,4}}}{a_c}\right) \right) = 0.003$$

T7

$\alpha_7 \cdot L = 17.25\ m$ > $x_{pos_{0,4}} = 13.525\ m$

$$\phi_7 := \frac{T_6 \cdot a_c}{G \cdot I_T} \cdot \left((1-\alpha_7) \cdot \frac{x_{pos_{0,4}}}{a_c} + \left(\frac{\sinh\left(\frac{\alpha_7 \cdot L}{a_c}\right)}{\tanh\left(\frac{L}{a_c}\right)} - \cosh\left(\frac{\alpha_7 \cdot L}{a_c}\right) \right) \cdot \sinh\left(\frac{x_{pos_{0,4}}}{a_c}\right) \right) = -0.023$$

T7

$\alpha_8 \cdot L = 18.45\ m$ > $x_{pos_{0,3}} = 7.275\ m$

$$\phi_8 := \frac{T_7 \cdot a_c}{G \cdot I_T} \cdot \left((1-\alpha_8) \cdot \frac{x_{pos_{0,4}}}{a_c} + \left(\frac{\sinh\left(\frac{\alpha_8 \cdot L}{a_c}\right)}{\tanh\left(\frac{L}{a_c}\right)} - \cosh\left(\frac{\alpha_8 \cdot L}{a_c}\right) \right) \cdot \sinh\left(\frac{x_{pos_{0,4}}}{a_c}\right) \right) = -0.02$$

$$\phi_{tot} := \phi_1 + \phi_2 + \phi_3 + \phi_4 + \phi_5 + \phi_6 + \phi_7 + \phi_8 = -0.009$$

$$M_{z.T.Ed} := \phi_{tot} \cdot M_{y.Ed} = -406.935\ kN \cdot m$$

Warping moment

T1

$\alpha_1 \cdot L = 2.35\ m$ < $x_{pos_{0,4}} = 13.525\ m$

$$\phi''_1 := \frac{T_0}{G \cdot I_T \cdot a_c} \cdot \left(\frac{\sinh\left(\frac{\alpha_1 \cdot L}{a_c}\right)}{\tanh\left(\frac{L}{a_c}\right)} \cdot \sinh\left(\frac{x_{pos_{0,4}}}{a_c}\right) - \sinh\left(\frac{\alpha_1 \cdot L}{a_c}\right) \cdot \cosh\left(\frac{x_{pos_{0,4}}}{a_c}\right) \right) = -1.096 \cdot 10^{-4}\ \frac{1}{m^2}$$

T2

$\alpha_2 \cdot L = 3.55\ m$ < $x_{pos_{0,3}} = 7.275\ m$

$$\phi''_2 := \frac{T_1}{G \cdot I_T \cdot a_c} \cdot \left(\frac{\sinh\left(\frac{\alpha_2 \cdot L}{a_c}\right)}{\tanh\left(\frac{L}{a_c}\right)} \cdot \sinh\left(\frac{x_{pos_{0,4}}}{a_c}\right) - \sinh\left(\frac{\alpha_2 \cdot L}{a_c}\right) \cdot \cosh\left(\frac{x_{pos_{0,4}}}{a_c}\right) \right) = -1.672 \cdot 10^{-4}\ \frac{1}{m^2}$$

T3

$\alpha_3 \cdot L = 6.075\ m$ < $x_{pos_{0,4}} = 13.525\ m$

$$\phi''_3 := \frac{T_2}{G \cdot I_T \cdot a_c} \cdot \left(\frac{\sinh\left(\frac{\alpha_3 \cdot L}{a_c}\right)}{\tanh\left(\frac{L}{a_c}\right)} \cdot \sinh\left(\frac{x_{pos_{0,4}}}{a_c}\right) - \sinh\left(\frac{\alpha_3 \cdot L}{a_c}\right) \cdot \cosh\left(\frac{x_{pos_{0,4}}}{a_c}\right) \right) = -2.517 \cdot 10^{-5}\ \frac{1}{m^2}$$

T4

$\alpha_4 \cdot L = 7.275\ m$ < $x_{pos_{0,4}} = 13.525\ m$

$$\phi''_4 := \frac{T_3}{G \cdot I_T \cdot a_c} \cdot \left(\frac{\sinh\left(\frac{\alpha_4 \cdot L}{a_c}\right)}{\tanh\left(\frac{L}{a_c}\right)} \cdot \sinh\left(\frac{x_{pos_{0,4}}}{a_c}\right) - \sinh\left(\frac{\alpha_4 \cdot L}{a_c}\right) \cdot \cosh\left(\frac{x_{pos_{0,4}}}{a_c}\right) \right) = -3.084 \cdot 10^{-5}\ \frac{1}{m^2}$$

T5

$\alpha_5 \cdot L = 13.525\ m$ = $x_{pos_{0,4}} = 13.525\ m$

$$\phi''_5 := \frac{T_4}{G \cdot I_T \cdot a_c} \cdot \left(\frac{\sinh\left(\frac{\alpha_5 \cdot L}{a_c}\right)}{\tanh\left(\frac{L}{a_c}\right)} \cdot \sinh\left(\frac{x_{pos_{0,4}}}{a_c}\right) - \sinh\left(\frac{\alpha_5 \cdot L}{a_c}\right) \cdot \cosh\left(\frac{x_{pos_{0,4}}}{a_c}\right) \right) = -6.81 \cdot 10^{-5}\ \frac{1}{m^2}$$

T6

$\alpha_6 \cdot L = 14.725\ m$ > $x_{pos_{0,4}} = 13.525\ m$

$$\phi''_6 := \frac{T_5}{G \cdot I_T \cdot a_c} \cdot \left(\left(\frac{\sinh\left(\frac{\alpha_6 \cdot L}{a_c}\right)}{\tanh\left(\frac{L}{a_c}\right)} - \cosh\left(\frac{\alpha_6 \cdot L}{a_c}\right) \right) \sinh\left(\frac{x_{pos_{0,4}}}{a_c}\right) \right) = -5.836 \cdot 10^{-5}\ \frac{1}{m^2}$$

T7

$\alpha_7 \cdot L = 17.25\ m \qquad > \qquad x_{pos_{0,4}} = 13.525\ m$

$$\phi''_7 := \frac{T_6}{G \cdot I_T \cdot a_c} \cdot \left(\left(\frac{\sinh\left(\frac{\alpha_7 \cdot L}{a_c}\right)}{\tanh\left(\frac{L}{a_c}\right)} - \cosh\left(\frac{\alpha_7 \cdot L}{a_c}\right) \right) \sinh\left(\frac{x_{pos_{0,4}}}{a_c}\right) \right) = \left(4 \cdot 10^{-4}\right) \frac{1}{m^2}$$

T8

$\alpha_8 \cdot L = 18.45\ m \qquad > \qquad x_{pos_{0,4}} = 13.525\ m$

$$\phi''_8 := \frac{T_7}{G \cdot I_T \cdot a_c} \cdot \left(\left(\frac{\sinh\left(\frac{\alpha_8 \cdot L}{a_c}\right)}{\tanh\left(\frac{L}{a_c}\right)} - \cosh\left(\frac{\alpha_8 \cdot L}{a_c}\right) \right) \sinh\left(\frac{x_{pos_{0,4}}}{a_c}\right) \right) = \left(3.22 \cdot 10^{-4}\right) \frac{1}{m^2}$$

$$\phi'' := \phi''_1 + \phi''_2 + \phi''_3 + \phi''_4 + \phi''_5 + \phi''_6 + \phi''_7 + \phi''_8 = \left(2.627 \cdot 10^{-4}\right) \frac{1}{m^2}$$

Warping moment

$I_{z.tf} := \frac{t_{tf} \cdot b_{tf}^{\ 3}}{12} \qquad I_{z.bf} := \frac{t_{bf} \cdot b_{bf}^{\ 3}}{12}$

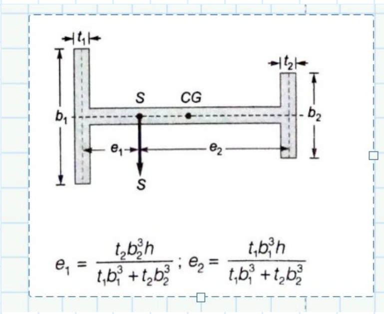

$$h_{cent} := h_w + \frac{t_{tf}}{2} + \frac{t_{bf}}{2} = 3.51\ m$$

$$e_1 := \frac{t_{bf} \cdot b_{bf}^{\ 3} \cdot h_{cent}}{t_{tf} \cdot b_{tf}^{\ 3} + t_{bf} \cdot b_{bf}^{\ 3}} = 1.225\ m$$

$$e_2 := \frac{t_{tf} \cdot b_{tf}^{\ 3} \cdot h_{cent}}{t_{bf} \cdot b_{bf}^{\ 3} + t_{tf} \cdot b_{tf}^{\ 3}} = 2.285\ m$$

$$M_{w.Ed.1} := E \cdot I_{z.tf} \cdot \phi'' \cdot e_1 = 285.031\ kN \cdot m$$

$$M_{w.Ed.2} := E \cdot I_{z.bf} \cdot \phi'' \cdot e_2 = 285.031\ kN \cdot m$$

$$M_{w.Ed} := \min\left(M_{w.Ed.1}, M_{w.Ed.2}\right) = 285.031\ kN \cdot m$$

SLS Calculations for deflections in z

Rotation in the beam at T5
To the left of the point

T1

$\alpha_1 \cdot L = 2.35\ m$ < $x_{pos_{0,4}} = 13.525\ m$

$$\phi_{1.SLS} := \frac{T_{SLS_0} \cdot a_c}{G \cdot I_T} \cdot \left(\left(L - x_{pos_{0,4}}\right) \cdot \frac{\alpha_1}{a_c} + \frac{\sinh\left(\frac{\alpha_1 \cdot L}{a_c}\right)}{\tanh\left(\frac{L}{a_c}\right)} \cdot \sinh\left(\frac{x_{pos_{0,4}}}{a_c}\right) - \sinh\left(\frac{\alpha_1 \cdot L}{a_c}\right) \cdot \cosh\left(\frac{x_{pos_{0,4}}}{a_c}\right) \right) = -0.009$$

T2

$\alpha_2 \cdot L = 3.55\ m$ < $x_{pos_{0,4}} = 13.525\ m$

$$\phi_{2.SLS} := \frac{T_{SLS_1} \cdot a_c}{G \cdot I_T} \cdot \left(\left(L - x_{pos_{0,4}}\right) \cdot \frac{\alpha_2}{a_c} + \frac{\sinh\left(\frac{\alpha_2 \cdot L}{a_c}\right)}{\tanh\left(\frac{L}{a_c}\right)} \cdot \sinh\left(\frac{x_{pos_{0,4}}}{a_c}\right) - \sinh\left(\frac{\alpha_2 \cdot L}{a_c}\right) \cdot \cosh\left(\frac{x_{pos_{0,4}}}{a_c}\right) \right) = 0.009$$

T3

$\alpha_3 \cdot L = 6.075\ m$ < $x_{pos_{0,4}} = 13.525\ m$

$$\phi_{3.SLS} := \frac{T_{SLS_2} \cdot a_c}{G \cdot I_T} \cdot \left(\left(L - x_{pos_{0,4}}\right) \cdot \frac{\alpha_3}{a_c} + \frac{\sinh\left(\frac{\alpha_3 \cdot L}{a_c}\right)}{\tanh\left(\frac{L}{a_c}\right)} \cdot \sinh\left(\frac{x_{pos_{0,4}}}{a_c}\right) - \sinh\left(\frac{\alpha_3 \cdot L}{a_c}\right) \cdot \cosh\left(\frac{x_{pos_{0,4}}}{a_c}\right) \right) = 0.004$$

T4

$\alpha_4 \cdot L = 7.275\ m$ < $x_{pos_{0,4}} = 13.525\ m$

$$\phi_{4.SLS} := \frac{T_{SLS_3} \cdot a_c}{G \cdot I_T} \cdot \left(\left(L - x_{pos_{0,4}}\right) \cdot \frac{\alpha_4}{a_c} + \frac{\sinh\left(\frac{\alpha_4 \cdot L}{a_c}\right)}{\tanh\left(\frac{L}{a_c}\right)} \cdot \sinh\left(\frac{x_{pos_{0,4}}}{a_c}\right) - \sinh\left(\frac{\alpha_4 \cdot L}{a_c}\right) \cdot \cosh\left(\frac{x_{pos_{0,4}}}{a_c}\right) \right) = 0.004$$

T5

$\alpha_5 \cdot L = 13.525\ m$ = $x_{pos_{0,4}} = 13.525\ m$

$$\phi_{5.SLS} := \frac{T_{SLS_4} \cdot a_c}{G \cdot I_T} \cdot \left(\left(L - x_{pos_{0,4}}\right) \cdot \frac{\alpha_5}{a_c} + \frac{\sinh\left(\frac{\alpha_5 \cdot L}{a_c}\right)}{\tanh\left(\frac{L}{a_c}\right)} \cdot \sinh\left(\frac{x_{pos_{0,4}}}{a_c}\right) - \sinh\left(\frac{\alpha_5 \cdot L}{a_c}\right) \cdot \cosh\left(\frac{x_{pos_{0,4}}}{a_c}\right) \right) = 0.002$$

T6

$\alpha_6 \cdot L = 14.725\ m$ > $x_{pos_{0,4}} = 13.525\ m$

$$\phi_{6.SLS} := \frac{T_{SLS_5} \cdot a_c}{G \cdot I_T} \cdot \left(\left(1 - \alpha_6\right) \cdot \frac{x_{pos_{0,4}}}{a_c} + \left(\frac{\sinh\left(\frac{\alpha_6 \cdot L}{a_c}\right)}{\tanh\left(\frac{L}{a_c}\right)} - \cosh\left(\frac{\alpha_6 \cdot L}{a_c}\right) \right) \cdot \sinh\left(\frac{x_{pos_{0,4}}}{a_c}\right) \right) = 0.002$$

T7

$\alpha_7 \cdot L = 17.25\ m$ > $x_{pos_{0,4}} = 13.525\ m$

$$\phi_{7.SLS} := \frac{T_{SLS_6} \cdot a_c}{G \cdot I_T} \cdot \left((1-\alpha_7) \cdot \frac{x_{pos_{0,4}}}{a_c} + \left(\frac{\sinh\left(\frac{\alpha_7 \cdot L}{a_c}\right)}{\tanh\left(\frac{L}{a_c}\right)} - \cosh\left(\frac{\alpha_7 \cdot L}{a_c}\right) \right) \cdot \sinh\left(\frac{x_{pos_{0,4}}}{a_c}\right) \right) = -0.012$$

T8

$\alpha_8 \cdot L = 18.45\ m$ > $x_{pos_{0,3}} = 7.275\ m$

$$\phi_{8.SLS} := \frac{T_{SLS_7} \cdot a_c}{G \cdot I_T} \cdot \left((1-\alpha_8) \cdot \frac{x_{pos_{0,4}}}{a_c} + \left(\frac{\sinh\left(\frac{\alpha_8 \cdot L}{a_c}\right)}{\tanh\left(\frac{L}{a_c}\right)} - \cosh\left(\frac{\alpha_8 \cdot L}{a_c}\right) \right) \cdot \sinh\left(\frac{x_{pos_{0,4}}}{a_c}\right) \right) = -0.01$$

$$\phi_{tot.SLS} := \phi_{1.SLS} + \phi_{2.SLS} + \phi_{3.SLS} + \phi_{4.SLS} + \phi_{5.SLS} + \phi_{6.SLS} + \phi_{7.SLS} + \phi_{8.SLS} = -0.01$$

$$M_{z.T.SLS} := \phi_{tot.SLS} \cdot M_{y.SLS} = -278.655\ kN \cdot m$$

B.3 Deflections and design of bracing system

Deflection condition

$$\delta_{limit} := \frac{L}{1000} = 24\ mm$$

Deflection using superposition method, deflection at position of Maximum moment

$$g_{rb.SLS} := 1 \cdot \rho \cdot g \cdot A_{tot} = 18.368\ \frac{kN}{m}$$

$$x_{pos} = \begin{bmatrix} 2.35 & 3.55 & 6.075 & 7.275 & 13.525 & 14.725 & 17.25 & 18.45 \end{bmatrix}\ m$$

$$a_{wheel} := x_{pos} = \begin{bmatrix} 2.35 & 3.55 & 6.075 & 7.275 & 13.525 & 14.725 & 17.25 & 18.45 \end{bmatrix}\ m$$

$$b_{wheel} := L - a_{wheel} = \begin{bmatrix} 21.65 & 20.45 & 17.925 & 16.725 & 10.475 & 9.275 & 6.75 & 5.55 \end{bmatrix}\ m$$

For a < L/2, 4 first

$$\delta_{w.1} := P_{wheel.SLS_0} \cdot \left(\frac{a_{wheel_{0,0}} \cdot L^2}{48\ E \cdot I_y} \cdot \left(3 - \frac{4 \cdot a_{wheel_{0,0}}^{\ 2}}{L^2} \right) \right) = 0.717\ mm$$

$$\delta_{w.2} := P_{wheel.SLS_1} \cdot \left(\frac{a_{wheel_{0,1}} \cdot L^2}{48\ E \cdot I_y} \cdot \left(3 - \frac{4 \cdot a_{wheel_{0,1}}^{\ 2}}{L^2} \right) \right) = 1.066\ mm$$

$$\delta_{w.3} := P_{wheel.SLS_2} \cdot \left(\frac{a_{wheel_{0,2}} \cdot L^2}{48\ E \cdot I_y} \cdot \left(3 - \frac{4 \cdot a_{wheel_{0,2}}^{\ 2}}{L^2} \right) \right) = 1.877\ mm$$

$$\delta_{w.4} := P_{wheel.SLS_3} \cdot \left(\frac{a_{wheel_{0,3}} \cdot L^2}{48\ E \cdot I_y} \cdot \left(3 - \frac{4 \cdot a_{wheel_{0,3}}^{\ 2}}{L^2} \right) \right) = 2.156\ mm$$

For a > L/2 4 last

$$\delta_{w.5} := P_{wheel.SLS_4} \cdot \left(\frac{b_{wheel_{0,4}} \cdot L^2}{48\ E \cdot I_y} \cdot \left(3 - \frac{4 \cdot b_{wheel_{0,4}}^{\ 2}}{L^2} \right) \right) = 2.625\ mm$$

$$\delta_{w.6} := P_{wheel.SLS_5} \cdot \left(\frac{b_{wheel_{0,5}} \cdot L^2}{48\ E \cdot I_y} \cdot \left(3 - \frac{4 \cdot b_{wheel_{0,5}}^{\ 2}}{L^2} \right) \right) = 2.496\ mm$$

$$\delta_{w.7} := P_{wheel.SLS_6} \cdot \left(\frac{b_{wheel_{0,6}} \cdot L^2}{48\ E \cdot I_y} \cdot \left(3 - \frac{4 \cdot b_{wheel_{0,6}}^{\ 2}}{L^2} \right) \right) = 1.927\ mm$$

$$\delta_{w.8} := P_{wheel.SLS_7} \cdot \left(\frac{b_{wheel_{0,7}} \cdot L^2}{48\ E \cdot I_y} \cdot \left(3 - \frac{4 \cdot b_{wheel_{0,7}}^{\ 2}}{L^2} \right) \right) = 1.645\ mm$$

$\delta_{tot.w} := \delta_{w.1} + \delta_{w.2} + \delta_{w.3} + \delta_{w.4} + \delta_{w.5} + \delta_{w.6} + \delta_{w.7} + \delta_{w.8} = 14.509\ mm$

Distributed load in mid span

$$\delta_{dist.mid} := \frac{g_{rb.SLS} \cdot 5 \cdot L^4}{384 \cdot E \cdot I_y} = 0.752\ mm$$

$\delta_{tot.mid} := \delta_{dist.mid} + \delta_{tot.w} = 15.261\ mm$

$Deflection.cap.y :=$ if $\delta_{tot.mid} < \delta_{limit}$
‖ "Deflection ok"
else
‖ "Deflection not ok"
= "Deflection ok"

Deflection in z direction

$M_{z.T.SLS} = -278.655\ kN \cdot m$

Moment from bending in y and angel of rot, assumed distributed

$$q_z := \frac{M_{z.T.SLS} \cdot 8}{L^2} = -3.87\ \frac{kN}{m}$$

$$w_{dist.z} := \frac{q_z \cdot 5 \cdot L^4}{384 \cdot E \cdot I_z} = -12.274\ mm$$

$$H_{SLS} := H_{m.SLS} + K_{a.SLS} - S_{k.SLS} + Y_{k.SLS} = \begin{bmatrix} -386.117 \\ 230.044 \\ 41.639 \\ 35.883 \\ 5.894 \\ 0.137 \\ -188.268 \\ -194.025 \end{bmatrix} kN$$

$$\delta_{wheel.z.1} := H_{SLS_0} \cdot \left(\frac{a_{wheel_{0,0}} \cdot L^2}{48\ E \cdot I_z} \cdot \left(3 - \frac{4 \cdot a_{wheel_{0,0}}{}^2}{L^2} \right) \right) = -23.674\ mm$$

$$\delta_{wheel.z.2} := H_{SLS_1} \cdot \left(\frac{a_{wheel_{0,1}} \cdot L^2}{48\ E \cdot I_z} \cdot \left(3 - \frac{4 \cdot a_{wheel_{0,1}}{}^2}{L^2} \right) \right) = 20.953\ mm$$

$$\delta_{wheel.z.3} := H_{SLS_2} \cdot \left(\frac{a_{wheel_{0,2}} \cdot L^2}{48\ E \cdot I_z} \cdot \left(3 - \frac{4 \cdot a_{wheel_{0,2}}{}^2}{L^2} \right) \right) = 6.114\ mm$$

$$\delta_{wheel.z.4} := H_{SLS_3} \cdot \left(\frac{a_{wheel_{0,3}} \cdot L^2}{48\ E \cdot I_z} \cdot \left(3 - \frac{4 \cdot a_{wheel_{0,3}}{}^2}{L^2} \right) \right) = 6.054\ mm$$

Wheel 7/8 negative

$$\delta_{wheel.z.5} := H_{SLS_4} \cdot \left(\frac{b_{wheel_{0,4}} \cdot L^2}{48\ E \cdot I_z} \cdot \left(3 - \frac{4 \cdot b_{wheel_{0,4}}{}^2}{L^2} \right) \right) = 1.217\ mm$$

$$\delta_{wheel.z.6} := H_{SLS_5} \cdot \left(\frac{b_{wheel_{0,5}} \cdot L^2}{48\ E \cdot I_z} \cdot \left(3 - \frac{4 \cdot b_{wheel_{0,5}}{}^2}{L^2} \right) \right) = 0.027\ mm$$

$$\delta_{wheel.z.7} := H_{SLS_6} \cdot \left(\frac{b_{wheel_{0,6}} \cdot L^2}{48\ E \cdot I_z} \cdot \left(3 - \frac{4 \cdot b_{wheel_{0,6}}{}^2}{L^2} \right) \right) = -30.043\ mm$$

$$\delta_{wheel.z.8} := H_{SLS_7} \cdot \left(\frac{b_{wheel_{0,7}} \cdot L^2}{48\ E \cdot I_z} \cdot \left(3 - \frac{4 \cdot b_{wheel_{0,7}}{}^2}{L^2} \right) \right) = -26.43\ mm$$

$$\delta_{w.z} := \delta_{wheel.z.1} + \delta_{wheel.z.2} + \delta_{wheel.z.3} + \delta_{wheel.z.4} + \delta_{wheel.z.5} + \delta_{wheel.z.6} + \delta_{wheel.z.7} + \delta_{wheel.z.8} = -45.782\ mm$$

$$\delta_{tot.z} := \left| \delta_{w.z} \right| + \left| w_{dist.z} \right| = 58.056\ mm$$

$$Deflection.cap.z := \text{if abs}\left(\delta_{tot.z}\right) < \delta_{limit} \ \| \ \text{“Deflection ok”} \ \text{else} \ \| \ \text{“Deflection not ok”} = \text{“Deflection not ok”}$$

Design of bracing system

Horizontal bracing system, SS-EN 1993-1-1:2022 7.3.5.1

$m_{brace} := 1$ numbers of members to be restrained

$$h_{mid.p} := \frac{t_{tf}}{2} + h_w + \frac{t_{bf}}{2} = \left(3.51 \cdot 10^3\right)\ mm$$

$$\alpha_m := \sqrt{0.5 \cdot \left(1 + \frac{1}{m_{brace}}\right)} = 1$$ **SS-EN 1993-1-1:2022 (7.13)**

$$e_0 := \frac{\alpha_m \cdot L}{500} = 48\ mm$$ **SS-EN 1993-1-1:2022 (7.13)**

$$N_{Ed} := \frac{M_{y.Ed}}{h_{mid.p}} = \left(1.241 \cdot 10^4\right)\ kN$$ **SS-EN 1993-1-1:2022 (7.15)**

$$\delta_q := \delta_{tot.z} = 58.056\ mm$$

$$q_{d.brace} := N_{Ed} \cdot 8 \cdot \frac{e_0 + \delta_q}{L^2} = 18.276\ \frac{kN}{m}$$ **SS-EN 1993-1-1:2022 (7.14)**

B.4 Model verifications

Model Verifications

$$g_{rb.model} := 1 \cdot \rho \cdot g \cdot A_{tot} = 18.368 \ \frac{kN}{m}$$

Reaction forces

Support 1

Name: RF_Left_Supp

	X	Y
1	0	520754
2	116.667	990435
3	233.333	1.2841E+06
4	350	2.0098E+06
5	466.667	1.2841E+06
6	583.333	990435
7	700	520754

Support 2

Name: RF_Right_Supp

	X	Y
1	0	383289
2	116.667	728680
3	233.333	947462
4	350	1.47453E+06
5	466.667	947462
6	583.333	728680
7	700	383289

$$RF_{abaqus} := \left(\begin{array}{l} 2 \cdot 520754 + 2 \cdot 990435 + 2 \cdot 1.2841 \cdot 10^{6} + 2.0098 \cdot 10^{6} \\ + 2 \cdot 383289 + 2 \cdot 728680 + 2 \cdot 947462 + 1.47453 \cdot 10^{6} \end{array}\right) N = 13.194 \ MN$$

$$RF_{tot} := \sum_{i=0}^{7} \left(P_{wheel.d_i}\right) + g_{rb.model} \cdot (L + 0.6 \ m) = 12.99 \ MN$$

$$DiffRF := 1 - \frac{RF_{abaqus}}{RF_{tot}} = -1.566\%$$

Deflection using superposition method,
deflection at position of Maximum moment

$$I_y = \left(5.084 \cdot 10^{11}\right) \ mm^4$$

$$P_{wheel.d} = \begin{bmatrix} 1.489 \\ 1.489 \\ 1.626 \\ 1.626 \\ 1.618 \\ 1.618 \\ 1.536 \\ 1.536 \end{bmatrix} MN$$

For a < L/2, 4 first

$$\delta_{w.1.model} := P_{wheel.d_0} \cdot \left(\frac{a_{wheel_{0,0}} \cdot L^2}{48\ E \cdot I_y} \cdot \left(3 - \frac{4 \cdot a_{wheel_{0,0}}^{\ 2}}{L^2} \right) \right) = 1.178\ mm$$

$$\delta_{w.2.model} := P_{wheel.d_1} \cdot \left(\frac{a_{wheel_{0,1}} \cdot L^2}{48\ E \cdot I_y} \cdot \left(3 - \frac{4 \cdot a_{wheel_{0,1}}^{\ 2}}{L^2} \right) \right) = 1.75\ mm$$

$$\delta_{w.3.model} := P_{wheel.d_2} \cdot \left(\frac{a_{wheel_{0,2}} \cdot L^2}{48\ E \cdot I_y} \cdot \left(3 - \frac{4 \cdot a_{wheel_{0,2}}^{\ 2}}{L^2} \right) \right) = 3.082\ mm$$

$$\delta_{w.4.model} := P_{wheel.d_3} \cdot \left(\frac{a_{wheel_{0,3}} \cdot L^2}{48\ E \cdot I_y} \cdot \left(3 - \frac{4 \cdot a_{wheel_{0,3}}^{\ 2}}{L^2} \right) \right) = 3.541\ mm$$

For a > L/2 4 last

$$\delta_{w.5.model} := P_{wheel.d_4} \cdot \left(\frac{b_{wheel_{0,4}} \cdot L^2}{48\ E \cdot I_y} \cdot \left(3 - \frac{4 \cdot b_{wheel_{0,4}}^{\ 2}}{L^2} \right) \right) = 4.311\ mm$$

$$\delta_{w.6.model} := P_{wheel.d_5} \cdot \left(\frac{b_{wheel_{0,5}} \cdot L^2}{48\ E \cdot I_y} \cdot \left(3 - \frac{4 \cdot b_{wheel_{0,5}}^{\ 2}}{L^2} \right) \right) = 4.098\ mm$$

$$\delta_{w.7.model} := P_{wheel.d_6} \cdot \left(\frac{b_{wheel_{0,6}} \cdot L^2}{48\ E \cdot I_y} \cdot \left(3 - \frac{4 \cdot b_{wheel_{0,6}}^{\ 2}}{L^2} \right) \right) = 3.164\ mm$$

$$\delta_{w.8.model} := P_{wheel.d_7} \cdot \left(\frac{b_{wheel_{0,7}} \cdot L^2}{48\ E \cdot I_y} \cdot \left(3 - \frac{4 \cdot b_{wheel_{0,7}}^{\ 2}}{L^2} \right) \right) = 2.701\ mm$$

$$\delta_{tot.w.model} := \delta_{w.1.model} + \delta_{w.2.model} + \delta_{w.3.model} + \delta_{w.4.model} + \delta_{w.5.model} + \delta_{w.6.model} + \delta_{w.7.model} + \delta_{w.8.model} = 23.824\ mm$$

$$\delta_{dist.mid.model} := \frac{g_{rb.model} \cdot 5 \cdot L^4}{384 \cdot E \cdot I_y} = 0.752\ mm$$

$$\delta_{tot.mid.model} := \delta_{dist.mid.model} + \delta_{tot.w.model} = 24.575\ mm$$

Name: U2_NoRail

	X	Y
1	0	-28.9207
2	116.64	-28.9157
3	233.281	-28.9126
4	349.921	-28.9115
5	466.562	-28.9126
6	583.202	-28.9157
7	699.843	-28.9207

$$\delta_{abaqus.norail} := \frac{\begin{array}{l}28.9207+28.9157+28.9126+28.9115 \\ +28.9126+28.9157+28.9207\end{array}}{7}\ mm = 28.916\ mm$$

$$Defdiff_{norail} := 1 - \frac{\delta_{tot.mid.model}}{\delta_{abaqus.norail}} = 15.01\%$$

Shear correction factor

$$A_w := h_w \cdot t_w = 0.103\ m^2$$

$$w_s := \frac{M_{y.Ed}}{G \cdot A_w} = 5.316\ mm$$

$$R_{corr} := \frac{w_s}{\delta_{tot.mid.model}} = 0.216$$

$$\delta_{tot.mid.model.corr} := \left(1 + R_{corr}\right) \cdot \delta_{tot.mid.model} = 29.891\ mm$$

$$Defdiff_{norail.corr} := 1 - \frac{\delta_{tot.mid.model.corr}}{\delta_{abaqus.norail}} = -3.374\%$$

Bending stresses, without rail

$$M_{y.Ed} = \left(4.355 \cdot 10^{4}\right)\ kN \cdot m$$

$$W_{el.y.bot} = \left(2.582 \cdot 10^{8}\right)\ mm^{3}$$

$$\sigma_{no.rail} := \frac{M_{y.Ed}}{W_{el.y.bot}} = 168.691\ MPa$$

Name: Stress_NoRail

	X	Y
1	0	151.793
2	116.64	151.832
3	233.281	151.94
4	349.921	152.009
5	466.562	151.94
6	583.202	151.832
7	699.843	151.793

Only use the elements in the flange

$$\sigma_{abaqus.norail} := \frac{151.793 + 151.832 + 151.94 + 152.009 + 151.94 + 151.832 + 151.793}{7}\ MPa = 151.877\ MPa$$

$$Stressdiff_{norail} := 1 - \frac{\sigma_{abaqus.norail}}{\sigma_{no.rail}} = 9.967\%$$

Bending stresses and delfection with trapezoidal rail

$b_{rail} := 220\ mm$ $t_{rail} := 150\ mm$ $h_{rail} := 150\ mm$

$$I_{y.rail} := \frac{h_{rail}^{3}}{36} \cdot \left(\frac{b_{rail}^{2} + b_{rail} \cdot t_{rail} + t_{rail}^{2}}{b_{rail} + t_{rail}} \right) = \left(2.633 \cdot 10^{7}\right)\ mm^{4}$$

$$A_{rail} := \frac{\left(b_{rail} + t_{rail}\right) \cdot h_{rail}}{2} = \left(2.775 \cdot 10^{4}\right)\ mm^{2}$$

$$y_{rail.bot} := \frac{h_{rail}}{3} \cdot \left(\frac{b_{rail} + 2 \cdot t_{rail}}{b_{rail} + t_{rail}} \right) = 70.27\ mm$$

$$y_{rail} := h_{rail} - y_{rail.bot} = 79.73\ mm$$

Calculate new centre of gravity etc

$$z_{rail} := \frac{A_{rail} \cdot y_{rail} + t_{tf} \cdot b_{tf} \cdot \left(h_{rail} + \frac{t_{tf}}{2} \right) + h_w \cdot t_w \cdot \left(h_{rail} + t_{tf} + \frac{h_w}{2} \right) + t_{bf} \cdot b_{bf} \cdot \left(h_{rail} + t_{tf} + h_w + \frac{t_{bf}}{2} \right)}{A_{rail} + t_{tf} \cdot b_{tf} + h_w \cdot t_w + t_{bf} \cdot b_{bf}} = \left(1.603 \cdot 10^{3}\right)\ mm$$

$$I_{y.rail.tot} := \frac{t_w \cdot h_w^{3}}{12} + \frac{b_{tf} \cdot t_{tf}^{3}}{12} + b_{tf} \cdot t_{tf} \cdot \left(z_{rail} - h_{rail} - \frac{t_{tf}}{2} \right)^{2} + \frac{b_{bf} \cdot t_{bf}^{3}}{12} + b_{bf} \cdot t_{bf} \cdot \left(z_{rail} - \left(h_{rail} + t_{tf} + h_w + \frac{t_{bf}}{2} \right) \right)^{2} + I_{y.rail} + A_{rail} \cdot \left(z_{rail} - y_{rail} \right)^{2} = \left(5.706 \cdot 10^{11}\right)\ mm^{4}$$

$$W_{el.rail.top} := \frac{I_{y.rail.tot}}{z_{rail}} = \left(3.559 \cdot 10^{8}\right)\ mm^{3}$$

$$W_{el.rail.bot} := \frac{I_{y.rail.tot}}{h_{rail} + t_{tf} + h_w + t_{bf} - z_{rail}} = \left(2.658 \cdot 10^{8}\right)\ mm^{3}$$

$$\sigma_{rail} := \frac{M_{y.Ed}}{W_{el.rail.bot}} = 163.829\ MPa$$

Name: Stress_Rail

	X	Y
1	0	149.064
2	174.961	149.144
3	349.923	149.225
4	524.884	149.144
5	699.846	149.064

$$\sigma_{abaqus.rail} := \frac{149.064 + 149.144 + 149.225 + 149.144 + 149.064}{5}\ MPa = 149.128\ MPa$$

$$Stressdiff_{rail} := 1 - \frac{\sigma_{abaqus.rail}}{\sigma_{rail}} = 8.973\%$$

Deflection

$$\delta_{w.1.model.r} := P_{wheel.d_0} \cdot \left(\frac{a_{wheel_{0,0}} \cdot L^2}{48\ E \cdot I_{y.rail.tot}} \cdot \left(3 - \frac{4 \cdot a_{wheel_{0,0}}{}^2}{L^2} \right) \right) = 1.05\ mm$$

$$\delta_{w.2.model.r} := P_{wheel.d_1} \cdot \left(\frac{a_{wheel_{0,1}} \cdot L^2}{48\ E \cdot I_{y.rail.tot}} \cdot \left(3 - \frac{4 \cdot a_{wheel_{0,1}}{}^2}{L^2} \right) \right) = 1.559\ mm$$

$$\delta_{w.3.model.r} := P_{wheel.d_2} \cdot \left(\frac{a_{wheel_{0,2}} \cdot L^2}{48\ E \cdot I_{y.rail.tot}} \cdot \left(3 - \frac{4 \cdot a_{wheel_{0,2}}{}^2}{L^2} \right) \right) = 2.746\ mm$$

$$\delta_{w.4.model.r} := P_{wheel.d_3} \cdot \left(\frac{a_{wheel_{0,3}} \cdot L^2}{48\ E \cdot I_{y.rail.tot}} \cdot \left(3 - \frac{4 \cdot a_{wheel_{0,3}}{}^2}{L^2} \right) \right) = 3.155\ mm$$

For a > L/2 4 last

$$\delta_{w.5.model.r} := P_{wheel.d_4} \cdot \left(\frac{b_{wheel_{0,4}} \cdot L^2}{48\ E \cdot I_{y.rail.tot}} \cdot \left(3 - \frac{4 \cdot b_{wheel_{0,4}}^{\ 2}}{L^2} \right) \right) = 3.841\ mm$$

$$\delta_{w.6.model.r} := P_{wheel.d_5} \cdot \left(\frac{b_{wheel_{0,5}} \cdot L^2}{48\ E \cdot I_{y.rail.tot}} \cdot \left(3 - \frac{4 \cdot b_{wheel_{0,5}}^{\ 2}}{L^2} \right) \right) = 3.651\ mm$$

$$\delta_{w.7.model.r} := P_{wheel.d_6} \cdot \left(\frac{b_{wheel_{0,6}} \cdot L^2}{48\ E \cdot I_{y.rail.tot}} \cdot \left(3 - \frac{4 \cdot b_{wheel_{0,6}}^{\ 2}}{L^2} \right) \right) = 2.819\ mm$$

$$\delta_{w.8.model.r} := P_{wheel.d_7} \cdot \left(\frac{b_{wheel_{0,7}} \cdot L^2}{48\ E \cdot I_{y.rail.tot}} \cdot \left(3 - \frac{4 \cdot b_{wheel_{0,7}}^{\ 2}}{L^2} \right) \right) = 2.406\ mm$$

$$\delta_{tot.w.model.r} := \delta_{w.1.model.r} + \delta_{w.2.model.r} + \delta_{w.3.model.r} + \delta_{w.4.model.r} + \delta_{w.5.model.r} + \delta_{w.6.model.r} + \delta_{w.7.model.r} + \delta_{w.8.model.r} = 21.227\ mm$$

$$g_{rb.model.rail} := g_{rb.model} + \rho \cdot g \cdot A_{rail} = 20.504\ \frac{kN}{m}$$

$$\delta_{dist.mid.model.r} := \frac{g_{rb.model.rail} \cdot 5 \cdot L^4}{384 \cdot E \cdot I_{y.rail.tot}} = 0.748\ mm$$

$$\delta_{tot.mid.model.rail} := \delta_{dist.mid.model.r} + \delta_{tot.w.model.r} = 21.975\ mm$$

Name: U2_Rail

	X	Y
1	0	-26.5819
2	174.961	-26.5756
3	349.923	-26.5733
4	524.884	-26.5756
5	699.846	-26.5819

$$\delta_{abaqus.rail} := \frac{26.5819 + 26.5756 + 26.5733 + 26.5756 + 26.5819}{5}\ mm = 26.578\ mm$$

$$Defdiff_{rail} := 1 - \frac{\delta_{tot.mid.model.rail}}{\delta_{abaqus.rail}} = 17.319\%$$

$$\delta_{tot.mid.model.rail.corr} := \left(1 + R_{corr}\right) \cdot \delta_{tot.mid.model.rail} = 26.728\ mm$$

$$Defdiff_{rail.corr} := 1 - \frac{\delta_{tot.mid.model.rail.corr}}{\delta_{abaqus.rail}} = -0.565\%$$

B.5 Web sidesway buckling checks

Web sidesway buckling accorind to Specification for Structural Steel Buildings

$$h_{w.mat} := \begin{bmatrix} 2500 & 2500 & 2500 & 2500 & 2500 & 2500 \\ 3000 & 3000 & 3000 & 3000 & 3000 & 3000 \\ 3420 & 3420 & 3420 & 3420 & 3420 & 3420 \\ 4000 & 4000 & 4000 & 4000 & 4000 & 4000 \\ 4500 & 4500 & 4500 & 4500 & 4500 & 4500 \\ 5000 & 5000 & 5000 & 5000 & 5000 & 5000 \end{bmatrix} mm$$

$$b_{bf.mat} := \begin{bmatrix} 700 & 600 & 500 & 400 & 300 & 200 \\ 700 & 600 & 500 & 400 & 300 & 200 \\ 700 & 600 & 500 & 400 & 300 & 200 \\ 700 & 600 & 500 & 400 & 300 & 200 \\ 700 & 600 & 500 & 400 & 300 & 200 \\ 700 & 600 & 500 & 400 & 300 & 200 \end{bmatrix} mm$$

$$num := t_{tf} \cdot b_{tf} \cdot \frac{t_{tf}}{2} + \overrightarrow{\left(t_{tf} + \frac{h_{w.mat}{}^{\langle 0 \rangle}}{2}\right) \cdot \left(t_w \cdot h_{w.mat}{}^{\langle 0 \rangle}\right)} \cdot \begin{bmatrix} 1 & 1 & 1 & 1 & 1 & 1 \end{bmatrix} \\ + \left(t_{tf} + h_{w.mat}{}^{\langle 0 \rangle} + \frac{t_{bf}}{2}\right) \cdot t_{bf} \cdot b_{bf.mat}{}^{\widehat{0}}$$

$$num = \begin{bmatrix} 0.253 & 0.232 & 0.211 & 0.19 & 0.169 & 0.147 \\ 0.324 & 0.299 & 0.274 & 0.248 & 0.223 & 0.198 \\ 0.389 & 0.361 & 0.332 & 0.304 & 0.275 & 0.247 \\ 0.488 & 0.455 & 0.422 & 0.388 & 0.355 & 0.322 \\ 0.581 & 0.544 & 0.507 & 0.47 & 0.433 & 0.395 \\ 0.682 & 0.641 & 0.6 & 0.558 & 0.517 & 0.476 \end{bmatrix} m^3$$

$$dem := t_{tf} \cdot b_{tf} + h_{w.mat} \cdot t_w + t_{bf} \cdot b_{bf.mat} = \begin{bmatrix} 0.211 & 0.203 & 0.195 & 0.187 & 0.179 & 0.171 \\ 0.226 & 0.218 & 0.21 & 0.202 & 0.194 & 0.186 \\ 0.239 & 0.231 & 0.223 & 0.215 & 0.207 & 0.199 \\ 0.256 & 0.248 & 0.24 & 0.232 & 0.224 & 0.216 \\ 0.271 & 0.263 & 0.255 & 0.247 & 0.239 & 0.231 \\ 0.286 & 0.278 & 0.27 & 0.262 & 0.254 & 0.246 \end{bmatrix} m^2$$

$$z_{top.mat} := \begin{array}{l} \text{for } k \in 0..5 \\ \quad \text{for } m \in 0..5 \\ \quad \quad z_{top.mat_{m,k}} \leftarrow \dfrac{num_{m,k}}{dem_{m,k}} \\ \quad z_{top.mat} \end{array} = \begin{bmatrix} 1.199 & 1.143 & 1.081 & 1.015 & 0.942 & 0.863 \\ 1.433 & 1.37 & 1.303 & 1.23 & 1.151 & 1.066 \\ 1.631 & 1.564 & 1.492 & 1.415 & 1.332 & 1.242 \\ 1.906 & 1.834 & 1.757 & 1.674 & 1.586 & 1.492 \\ 2.144 & 2.068 & 1.988 & 1.902 & 1.81 & 1.712 \\ 2.384 & 2.305 & 2.221 & 2.132 & 2.037 & 1.936 \end{bmatrix} m$$

$$z_{bot.mat} := h_{tot} - z_{top.mat} = \begin{bmatrix} 2.401 & 2.457 & 2.519 & 2.585 & 2.658 & 2.737 \\ 2.167 & 2.23 & 2.297 & 2.37 & 2.449 & 2.534 \\ 1.969 & 2.036 & 2.108 & 2.185 & 2.268 & 2.358 \\ 1.694 & 1.766 & 1.843 & 1.926 & 2.014 & 2.108 \\ 1.456 & 1.532 & 1.612 & 1.698 & 1.79 & 1.888 \\ 1.216 & 1.295 & 1.379 & 1.468 & 1.563 & 1.664 \end{bmatrix} m$$

$$I_{y.mat} := \overrightarrow{\frac{t_w \cdot h_{w.mat}^{\ 3}}{12}} + \frac{b_{tf} \cdot t_{tf}^{\ 3}}{12} + \overrightarrow{b_{tf} \cdot t_{tf} \cdot \left(z_{top.mat} - \frac{t_{tf}}{2}\right)^2} \\ + \frac{b_{bf.mat} \cdot t_{bf}^{\ 3}}{12} + \overrightarrow{b_{bf.mat} \cdot t_{bf} \cdot \left(z_{top.mat} - \left(t_{tf} + h_{w.mat} + \frac{t_{bf}}{2}\right)\right)^2}$$

$$I_{y.mat} = \begin{bmatrix} 2.611 \cdot 10^{11} & 2.423 \cdot 10^{11} & 2.214 \cdot 10^{11} & 1.981 \cdot 10^{11} & 1.72 \cdot 10^{11} & 1.425 \cdot 10^{11} \\ 3.838 \cdot 10^{11} & 3.574 \cdot 10^{11} & 3.282 \cdot 10^{11} & 2.957 \cdot 10^{11} & 2.595 \cdot 10^{11} & 2.19 \cdot 10^{11} \\ 5.084 \cdot 10^{11} & 4.747 \cdot 10^{11} & 4.375 \cdot 10^{11} & 3.964 \cdot 10^{11} & 3.507 \cdot 10^{11} & 2.997 \cdot 10^{11} \\ 7.151 \cdot 10^{11} & 6.699 \cdot 10^{11} & 6.203 \cdot 10^{11} & 5.657 \cdot 10^{11} & 5.054 \cdot 10^{11} & 4.386 \cdot 10^{11} \\ 9.276 \cdot 10^{11} & 8.712 \cdot 10^{11} & 8.097 \cdot 10^{11} & 7.421 \cdot 10^{11} & 6.679 \cdot 10^{11} & 5.861 \cdot 10^{11} \\ 1.174 \cdot 10^{12} & 1.105 \cdot 10^{12} & 1.03 \cdot 10^{12} & 9.488 \cdot 10^{11} & 8.595 \cdot 10^{11} & 7.614 \cdot 10^{11} \end{bmatrix} mm^4$$

$$S_x := \begin{array}{l} \text{for } k \in 0..5 \\ \quad \text{for } m \in 0..5 \\ \quad \quad S_{x_{m,k}} \leftarrow min\left(\dfrac{I_{y.mat_{m,k}}}{z_{top.mat_{m,k}}}, \dfrac{I_{y.mat_{m,k}}}{z_{bot.mat_{m,k}}}\right) \\ \quad S_x \end{array}$$

$$S_x = \begin{bmatrix} 1.088 \cdot 10^8 & 9.86 \cdot 10^7 & 8.791 \cdot 10^7 & 7.663 \cdot 10^7 & 6.471 \cdot 10^7 & 5.206 \cdot 10^7 \\ 1.771 \cdot 10^8 & 1.603 \cdot 10^8 & 1.429 \cdot 10^8 & 1.248 \cdot 10^8 & 1.06 \cdot 10^8 & 8.64 \cdot 10^7 \\ 2.582 \cdot 10^8 & 2.331 \cdot 10^8 & 2.075 \cdot 10^8 & 1.814 \cdot 10^8 & 1.546 \cdot 10^8 & 1.271 \cdot 10^8 \\ 3.753 \cdot 10^8 & 3.654 \cdot 10^8 & 3.365 \cdot 10^8 & 2.938 \cdot 10^8 & 2.51 \cdot 10^8 & 2.08 \cdot 10^8 \\ 4.326 \cdot 10^8 & 4.212 \cdot 10^8 & 4.073 \cdot 10^8 & 3.902 \cdot 10^8 & 3.69 \cdot 10^8 & 3.104 \cdot 10^8 \\ 4.923 \cdot 10^8 & 4.795 \cdot 10^8 & 4.64 \cdot 10^8 & 4.451 \cdot 10^8 & 4.22 \cdot 10^8 & 3.933 \cdot 10^8 \end{bmatrix} \mathit{mm}^3$$

$$M_y := S_x \cdot f_y = \begin{bmatrix} 34.258 & 31.059 & 27.691 & 24.139 & 20.382 & 16.398 \\ 55.786 & 50.487 & 45 & 39.306 & 33.386 & 27.217 \\ 81.323 & 73.43 & 65.374 & 57.138 & 48.701 & 40.04 \\ 118.213 & 115.091 & 106.003 & 92.548 & 79.068 & 65.535 \\ 136.268 & 132.688 & 128.314 & 122.928 & 116.236 & 97.783 \\ 155.086 & 151.047 & 146.162 & 140.216 & 132.921 & 123.884 \end{bmatrix} \mathit{MN} \cdot \mathit{m}$$

$$M_{y.Ed} = \left(4.355 \cdot 10^4\right) \mathit{kN} \cdot \mathit{m}$$

```
C_r := for k ∈ 0..5
         for m ∈ 0..5
           C_r[k,m] ← if M_y[k,m] > M_y.Ed
                          6.6·10^6 MPa
                      else
                          3.3·10^6 MPa
         C_r
```

$$C_r = \begin{bmatrix} 3.3 \cdot 10^6 & 3.3 \cdot 10^6 & 3.3 \cdot 10^6 & 3.3 \cdot 10^6 & 3.3 \cdot 10^6 & 3.3 \cdot 10^6 \\ 6.6 \cdot 10^6 & 6.6 \cdot 10^6 & 6.6 \cdot 10^6 & 3.3 \cdot 10^6 & 3.3 \cdot 10^6 & 3.3 \cdot 10^6 \\ 6.6 \cdot 10^6 & 6.6 \cdot 10^6 & 6.6 \cdot 10^6 & 6.6 \cdot 10^6 & 6.6 \cdot 10^6 & 3.3 \cdot 10^6 \\ 6.6 \cdot 10^6 & 6.6 \cdot 10^6 & 6.6 \cdot 10^6 & 6.6 \cdot 10^6 & 6.6 \cdot 10^6 & 6.6 \cdot 10^6 \\ 6.6 \cdot 10^6 & 6.6 \cdot 10^6 & 6.6 \cdot 10^6 & 6.6 \cdot 10^6 & 6.6 \cdot 10^6 & 6.6 \cdot 10^6 \\ 6.6 \cdot 10^6 & 6.6 \cdot 10^6 & 6.6 \cdot 10^6 & 6.6 \cdot 10^6 & 6.6 \cdot 10^6 & 6.6 \cdot 10^6 \end{bmatrix} \mathit{MPa}$$

$$L_b := L = 24\ \mathit{m}$$

Check ratio if limit state is applicable

$$Ratio := \text{for } k \in 0..5 \quad \text{for } m \in 0..5 \quad Ratio_{m,k} \leftarrow \frac{\left(\frac{h_{w.mat_{m,k}}}{t_w}\right)}{\left(\frac{L_b}{b_{bf.mat_{m,k}}}\right)} \quad Ratio$$

$$= \begin{bmatrix} 2.431 & 2.083 & 1.736 & 1.389 & 1.042 & 0.694 \\ 2.917 & 2.5 & 2.083 & 1.667 & 1.25 & 0.833 \\ 3.325 & 2.85 & 2.375 & 1.9 & 1.425 & 0.95 \\ 3.889 & 3.333 & 2.778 & 2.222 & 1.667 & 1.111 \\ 4.375 & 3.75 & 3.125 & 2.5 & 1.875 & 1.25 \\ 4.861 & 4.167 & 3.472 & 2.778 & 2.083 & 1.389 \end{bmatrix}$$

Check which combinations are safe or not, 0=safe, 1=unsafe

$$Unsafe := \text{for } k \in 0..5 \quad \text{for } m \in 0..5 \quad Unsafe_{m,k} \leftarrow \text{if } Ratio_{m,k} > 2.3 \; \| \; 0 \; \text{else} \; \| \; 1 \quad Unsafe$$

$$= \begin{bmatrix} 0 & 1 & 1 & 1 & 1 & 1 \\ 0 & 0 & 1 & 1 & 1 & 1 \\ 0 & 0 & 0 & 1 & 1 & 1 \\ 0 & 0 & 0 & 1 & 1 & 1 \\ 0 & 0 & 0 & 0 & 1 & 1 \\ 0 & 0 & 0 & 0 & 1 & 1 \end{bmatrix}$$

Compute nominal strength for unsafe case (ANSI/AISC 360-22, J10-6)

$$R_n := \text{for } k \in 0..5 \quad \text{for } m \in 0..5 \quad R_{n_{m,k}} \leftarrow \frac{Unsafe_{m,k} \cdot C_{r_{m,k}} \cdot t_w^{\,3} \cdot t_{bf}}{h_{w.mat_{m,k}}^{\;2}} \cdot \left(1 + 0.4 \cdot \left(\frac{\left(\frac{h_{w.mat_{m,k}}}{t_w}\right)}{\left(\frac{L_b}{b_{bf.mat_{m,k}}}\right)}\right)^3\right) \quad R_n$$

$$R_n = \begin{bmatrix} 0 & 5.265 \cdot 10^3 & 3.528 \cdot 10^3 & 2.363 \cdot 10^3 & 1.656 \cdot 10^3 & 1.293 \cdot 10^3 \\ 0 & 0 & 7.313 \cdot 10^3 & 2.259 \cdot 10^3 & 1.411 \cdot 10^3 & 975.333 \\ 0 & 0 & 0 & 4.563 \cdot 10^3 & 2.63 \cdot 10^3 & 818.418 \\ 0 & 0 & 0 & 4.802 \cdot 10^3 & 2.541 \cdot 10^3 & 1.38 \cdot 10^3 \\ 0 & 0 & 0 & 0 & 2.56 \cdot 10^3 & 1.254 \cdot 10^3 \\ 0 & 0 & 0 & 0 & 2.633 \cdot 10^3 & 1.181 \cdot 10^3 \end{bmatrix} kN$$

Maximum vertical load from load case 2

Vertical loads

$$P_{wheel.d_i} := Perm_{on} \cdot \varphi_{perm} \cdot \gamma_{d.ULS} \cdot R_{perm} \cdot g \cdot P_{wheel_{j,i}} + Var_{on} \cdot \varphi_{var} \cdot \gamma_{var.ULS} \cdot R_{var} \cdot g \cdot P_{wheel_{j,i}} = \begin{bmatrix} 1.489 \\ 1.489 \\ 1.626 \\ 1.626 \\ 1.618 \\ 1.618 \\ 1.536 \\ 1.536 \end{bmatrix} MN$$

$MaxP := 1.626\ MN$

Check nominal strength with safety factor

$\phi := 0.85$ **(LFRD)**

$$\phi \cdot R_n = \begin{bmatrix} 0 & 4.476 & 2.998 & 2.008 & 1.408 & 1.099 \\ 0 & 0 & 6.216 & 1.92 & 1.199 & 0.829 \\ 0 & 0 & 0 & 3.878 & 2.235 & 0.696 \\ 0 & 0 & 0 & 4.082 & 2.16 & 1.173 \\ 0 & 0 & 0 & 0 & 2.176 & 1.066 \\ 0 & 0 & 0 & 0 & 2.238 & 1.004 \end{bmatrix} MN$$

Find which cases have a unsafe load

$$UnsafeLoad := \begin{array}{l} \text{for } k \in 0..5 \\ \quad \text{for } m \in 0..5 \\ \quad\quad UnsafeLoad_{m,k} \leftarrow \text{if } \phi \cdot R_{n_{m,k}} > MaxP \\ \quad\quad\quad\quad 0 \\ \quad\quad\quad \text{also if } Unsafe_{m,k} = 0 \\ \quad\quad\quad\quad 0 \\ \quad\quad\quad \text{else} \\ \quad\quad\quad\quad 1 \\ \quad UnsafeLoad \end{array} = \begin{bmatrix} 0 & 0 & 0 & 0 & 1 & 1 \\ 0 & 0 & 0 & 0 & 1 & 1 \\ 0 & 0 & 0 & 0 & 0 & 1 \\ 0 & 0 & 0 & 0 & 0 & 1 \\ 0 & 0 & 0 & 0 & 0 & 1 \\ 0 & 0 & 0 & 0 & 0 & 1 \end{bmatrix}$$

Display the unsafe load for the unsafe cases

$$UnsafeR_n := \begin{array}{l} \text{for } k \in 0..5 \\ \quad \text{for } m \in 0..5 \\ \quad\quad UnsafeR_{n_{m,k}} \leftarrow UnsafeLoad_{m,k} \cdot \left(\phi \cdot R_n\right)_{m,k} \\ \quad UnsafeR_n \end{array} = \begin{bmatrix} 0 & 0 & 0 & 0 & 1.408 & 1.099 \\ 0 & 0 & 0 & 0 & 1.199 & 0.829 \\ 0 & 0 & 0 & 0 & 0 & 0.696 \\ 0 & 0 & 0 & 0 & 0 & 1.173 \\ 0 & 0 & 0 & 0 & 0 & 1.066 \\ 0 & 0 & 0 & 0 & 0 & 1.004 \end{bmatrix} MN$$

Unsafe for combination

All web heights with bottom flange width 200

Web height 2500,3000, with bottom flange width 300

C

Matlab Codes

C.1 Stiffness Calculation and Capacity Checks for Truss Bracing System

```
clc
clear all
close all

% --- INPUTS ---
L = 24.0;
H = 2;
target_w = 2;
E = 207.615e9;
fy = 355e6; % Yield strength in Pa
SF = 1.5;
N_Ed = 1.241e7; % Design compressive force taken from Mathcad (
    Appendix B)

% --- EUROCODE STABILIZATION LOAD ---
m_brace = 1;
alpha_m = sqrt(0.5 * (1 + (1 / m_brace)));
e0 = (alpha_m * L) / 500;
delta_q = 58.056e-3; % Deflection from SLS loads taken from Mathcad
     (Appendix B)
qd = N_Ed * 8 * ((e0 + delta_q) / L^2);

% --- DYNAMIC CALCULATIONS ---
n_bays = round(L / target_w);
w = L / n_bays;
L_diag = sqrt(w^2 + H^2);

% --- 1. COORDINATES ---
n_nodes = 2 * (n_bays + 1);
coords = zeros(n_nodes, 2);
for i = 1:(n_bays + 1)
    x = (i-1) * w;
    coords(i, :) = [x, 0];
    coords(i + n_bays + 1, :) = [x, H];
end

% --- 2. SECTION PROPERTIES ---
d_bar = 0.001;
P_cr = 0;
```

```
while P_cr < (SF * N_Ed/n_bays)
    d_bar = d_bar + 0.001;
    A_bar = (pi * d_bar^2) / 4;
    I_bar = (pi / 4) * (d_bar / 2)^4;
    P_cr = (pi^2 * E * I_bar) / (L_diag^2);
end

t_tf_brace = 10e-3; b_tf_brace = 200e-3;
t_bf_brace = 10e-3; b_bf_brace = 200e-3;
t_w_brace  = 10e-3; h_w_brace  = 500e-3;
Area_brace = (t_tf_brace * b_tf_brace) + (t_bf_brace * b_bf_brace)
   + (h_w_brace * t_w_brace);
Iz_brace = (t_tf_brace * b_tf_brace^3)/12 + (t_bf_brace *
   b_bf_brace^3)/12 + (h_w_brace * t_w_brace^3)/12;
Iy_brace = (t_tf_brace^3 * b_tf_brace)/12 + (t_bf_brace^3 *
   b_bf_brace)/12 + (h_w_brace^3 * t_w_brace)/12;

ep_beam  = [E, Area_brace, Iz_brace];
ep_bar   = [E, A_bar, I_bar];
% --- NEW: Ghost property for bottom chord connectivity only ---
% --- Test, having top flange of main beam as bottom chord
t_tf = 100e-3;
b_tf = 800e-3;
A_flange = t_tf*b_tf;
Iz_flange = (t_tf*b_tf^3)/12
ep_flange = [E, A_flange, Iz_flange];

% --- 3. ASSEMBLY ---
ndof = 3 * n_nodes;
K = zeros(ndof, ndof);
edof = [];
el_id = 1;
eq = [0 0];
d = @(n) [3*n-2, 3*n-1, 3*n];

for i = 1:n_bays
    bL = i; bR = i + 1; tL = i + n_bays + 1; tR = i + n_bays + 2;

    % A. Bottom Chord (GHOST - Connectivity only)
    ex = [coords(bL,1) coords(bR,1)]; ey = [coords(bL,2) coords(bR
   ,2)];
    edof(el_id,:) = [el_id, d(bL), d(bR)];
    Ke = beam2e(ex, ey, ep_flange, eq);
    K = assem(edof(el_id,:), K, Ke); el_id = el_id + 1;

    % B. Top Chord (REAL BEAM)
    ex = [coords(tL,1) coords(tR,1)]; ey = [coords(tL,2) coords(tR
   ,2)];
    edof(el_id,:) = [el_id, d(tL), d(tR)];
    Ke = beam2e(ex, ey, ep_beam, eq);
    K = assem(edof(el_id,:), K, Ke); el_id = el_id + 1;

    % C. Vertical (Bar)
    ex = [coords(bL,1) coords(tL,1)]; ey = [coords(bL,2) coords(tL
   ,2)];
    edof(el_id,:) = [el_id, d(bL), d(tL)];
```

```
    Ke = beam2e(ex, ey, ep_bar, eq);
    K = assem(edof(el_id,:), K, Ke); el_id = el_id + 1;

    % D. Diagonal 1 (Bar)
    ex = [coords(bL,1) coords(tR,1)]; ey = [coords(bL,2) coords(tR
   ,2)];
    edof(el_id,:) = [el_id, d(bL), d(tR)];
    Ke = beam2e(ex, ey, ep_bar, eq);
    K = assem(edof(el_id,:), K, Ke); el_id = el_id + 1;

    % E. Diagonal 2 (Bar)
    ex = [coords(tL,1) coords(bR,1)]; ey = [coords(tL,2) coords(bR
   ,2)];
    edof(el_id,:) = [el_id, d(tL), d(bR)];
    Ke = beam2e(ex, ey, ep_bar, eq);
    K = assem(edof(el_id,:), K, Ke); el_id = el_id + 1;
end

% Final Vertical
ex = [coords(n_bays+1,1) coords(2*n_bays+2,1)]; ey = [coords(n_bays
    +1,2) coords(2*n_bays+2,2)];
edof(el_id,:) = [el_id, d(n_bays+1), d(2*n_bays+2)];
Ke = beam2e(ex, ey, ep_bar, eq);
K = assem(edof(el_id,:), K, Ke);

% --- 4. BOUNDARY CONDITIONS ---
bc = [];
corners = [1, n_bays+1, n_bays+2, 2*(n_bays+1)];
for n = corners
    bc = [bc; (n*3-2), 0; (n*3-1), 0; (n*3), 0];
end

% --- 5. LOAD VECTOR ---
f = zeros(ndof, 1);
for i = 1:(n_bays + 1)
    dof_y = (i * 3) - 1;
    if i == 1 || i == n_bays + 1
        f(dof_y) = (qd * w / 2);
    else
        f(dof_y) = (qd * w);
    end
end

% --- 6. SOLVE & PLOT ---
fprintf('Condition Number: %e\n', condest(K));
a = solveq(K, f, bc);
ed = extract(edof, a);
delta_q_max = max(abs(a(2:3:end)));

figure; hold on;
mag = 100.0; % Adjusted magnification for potentially larger
    deflection
for e = 1:size(edof, 1)
    n1 = round((edof(e, 2) + 2) / 3);
    n2 = round((edof(e, 5) + 2) / 3);
    x_def = [coords(n1, 1) + ed(e, 1)*mag, coords(n2, 1) + ed(e, 4)
```

```
    *mag];
    y_def = [coords(n1, 2) + ed(e, 2)*mag, coords(n2, 2) + ed(e, 5)*mag];

    pos_in_bay = mod(e-1, 5) + 1;

    if pos_in_bay == 2 && e <= 5*n_bays
        h1 = plot(x_def, y_def, 'r-s', 'LineWidth', 1.5); % Top Chord Only
    elseif pos_in_bay == 1 && e <= 5*n_bays
        plot(x_def, y_def, 'k:', 'LineWidth', 0.5); % Ghost Bottom Chord
    else
        h2 = plot(x_def, y_def, 'b-', 'LineWidth', 1.0); % Webbing
    end
end


axis equal; grid on;
title(['Truss Only Stiffness (Mag = ', num2str(mag), 'x)']);
xlabel(['Max Deflection = ', num2str(delta_q_max*1000, '%.2f'), ' mm']);
% --- 7. BAY-BY-BAY STIFFNESS EXTRACTION (for Abaqus) ---

% --- 7. BAY-BY-BAY STIFFNESS EXTRACTION (4-Node Average) ---
ks_bay_vec = zeros(n_bays, 1);
ks_bay_elast_vec = zeros(n_bays, 1);

% Offset to reach the corresponding node on the Top Chord
offset = n_bays + 1;

fprintf('\n--- Bay-by-Bay Stiffness Extraction (4-Node Average) ---\n');
fprintf('%-8s | %-12s | %-15s | %-15s\n', 'Bay #', 'Def (mm)', 'ks (N/mm)', 'ks_elast (N/mm^2)');
fprintf('--------------------------------------------------------------------------\n');

for i = 1:n_bays
    % Node Indices for the 4 corners of the bay:
    idx_bot_L = i;
    idx_bot_R = i + 1;
    idx_top_L = i + offset;
    idx_top_R = i + 1 + offset;

    % Vertical Displacements (u_y is the 2nd DOF of every 3-DOF node)
    % DOF formula: 3 * node_index - 1
    u_y_bot_L = abs(a(3 * idx_bot_L - 1));
    u_y_bot_R = abs(a(3 * idx_bot_R - 1));
    u_y_top_L = abs(a(3 * idx_top_L - 1));
    u_y_top_R = abs(a(3 * idx_top_R - 1));

    % Average deflection of all 4 corners of the bay in meters
    delta_bay_avg = (u_y_bot_L + u_y_bot_R + u_y_top_L + u_y_top_R)
```

```
    / 4;

    if delta_bay_avg > 1e-9
        % 1. Total stiffness for the bay (N/mm)
        ks_bay_vec(i) = (qd * w / delta_bay_avg) / 1e3;

        % 2. Distributed stiffness (N/mm^2)
        ks_bay_elast_vec(i) = (qd / delta_bay_avg) / 1e6;
    else
        ks_bay_vec(i) = inf;
        ks_bay_elast_vec(i) = inf;
    end

    fprintf('Bay %-4d | %-12.4f | %-15.4f | %-15.6f\n', ...
            i, delta_bay_avg*1000, ks_bay_vec(i), ks_bay_elast_vec(
    i));
end
% This copies your 12 values directly to your Windows clipboard
clipboard('copy', sprintf('%.6f, ', ks_bay_elast_vec));


% --- GEOMETRY CHECK ---
theta_rad = atan(H / w);         % Angle in radians
theta_deg = rad2deg(theta_rad);  % Angle in degrees

fprintf('\n--- Geometry Check ---\n');
fprintf('Bay Width (w): %.2f m\n', w);
fprintf('Truss Height (H): %.2f m\n', H);
fprintf('Diagonal Length (L_diag): %.2f m\n', L_diag);
fprintf('Diagonal Angle: %.2f degrees\n', theta_deg);

if theta_deg < 30 || theta_deg > 60
    fprintf('Warning: Diagonal angle is outside the ideal 30-60
    degree range.\n');
end


% 2. Chord Axial Force from Global Moment
M_Ed_brace = (qd * L^2) / 8;
N_Ed_brace = SF * M_Ed_brace / H; % Axial force in the chord

% 3. Yielding Resistance (Strength)
N_Rd_brace = Area_brace * fy; %
UR_strength_brace = (N_Ed_brace / N_Rd_brace); %

% 4. Buckling Resistance (Euler)
I_local = min(Iy_brace,Iz_brace);

% Buckling length is the bay length (w or L_bay)
P_cr_brace = (pi^2 * E * I_local) / (w^2); %
UR_buckling_brace = N_Ed_brace / P_cr_brace; %

% 5. Yielding Resistance Bar (Strength)
N_Rd_bar = A_bar * fy; %
UR_strength_bar = ((SF * N_Ed / n_bays) / N_Rd_bar); %

```

```matlab

% --- Display Results ---
fprintf('\n--- System Capacity Checks ---\n');
fprintf('Number of bays (n_bays): %.2f st\n', n_bays);
fprintf('Max Chord Force (N_Ed): %.2f kN\n', N_Ed_brace / 1e3);
fprintf('Strength Utilization Brace:   %.2f %%\n',
    UR_strength_brace * 100);
fprintf('Buckling Utilization Brace:   %.2f %%\n',
    UR_buckling_brace * 100);
fprintf('Strength Utilization Bar:   %.2f %%\n', UR_strength_bar *
    100);

if UR_buckling_brace > 1.0 || UR_strength_brace > 1.0
    fprintf('WARNING: Bracing beam fails capacity checks!\n');
else
    fprintf('Bracing beam is safe.\n');
end
```

```
Condition Number: 3.383383e+18

--- Bay-by-Bay Stiffness Extraction (4-Node Average) ---
Bay #     | Def (mm)      | ks (N/mm)         | ks_elast (N/mm^2)
--------------------------------------------------------------------------
Bay 1     | 0.1760        | 208423.4788       | 104.211739
Bay 2     | 0.6522        | 56232.9980        | 28.116499
Bay 3     | 1.2749        | 28766.1134        | 14.383057
Bay 4     | 1.8727        | 19583.6864        | 9.791843
Bay 5     | 2.3313        | 15731.0612        | 7.865531
Bay 6     | 2.5788        | 14221.5490        | 7.110775
Bay 7     | 2.5788        | 14221.5490        | 7.110775
Bay 8     | 2.3313        | 15731.0612        | 7.865531
Bay 9     | 1.8727        | 19583.6864        | 9.791843
Bay 10    | 1.2749        | 28766.1134        | 14.383057
Bay 11    | 0.6522        | 56232.9980        | 28.116499
Bay 12    | 0.1760        | 208423.4788       | 104.211739

--- Geometry Check ---
Bay Width (w): 2.00 m
Truss Height (H): 2.00 m
Diagonal Length (L_diag): 2.83 m
Diagonal Angle: 45.00 degrees

--- System Capacity Checks ---
Number of bays (n_bays): 12.00 st
Max Chord Force (N_Ed): 990.20 kN
Strength Utilization Brace:   30.99 %
Buckling Utilization Brace:   14.45 %
Strength Utilization Bar:   49.52 %
Bracing beam is safe.
```

Figure C.1: Bracing truss stiffness extraction and capacity checks

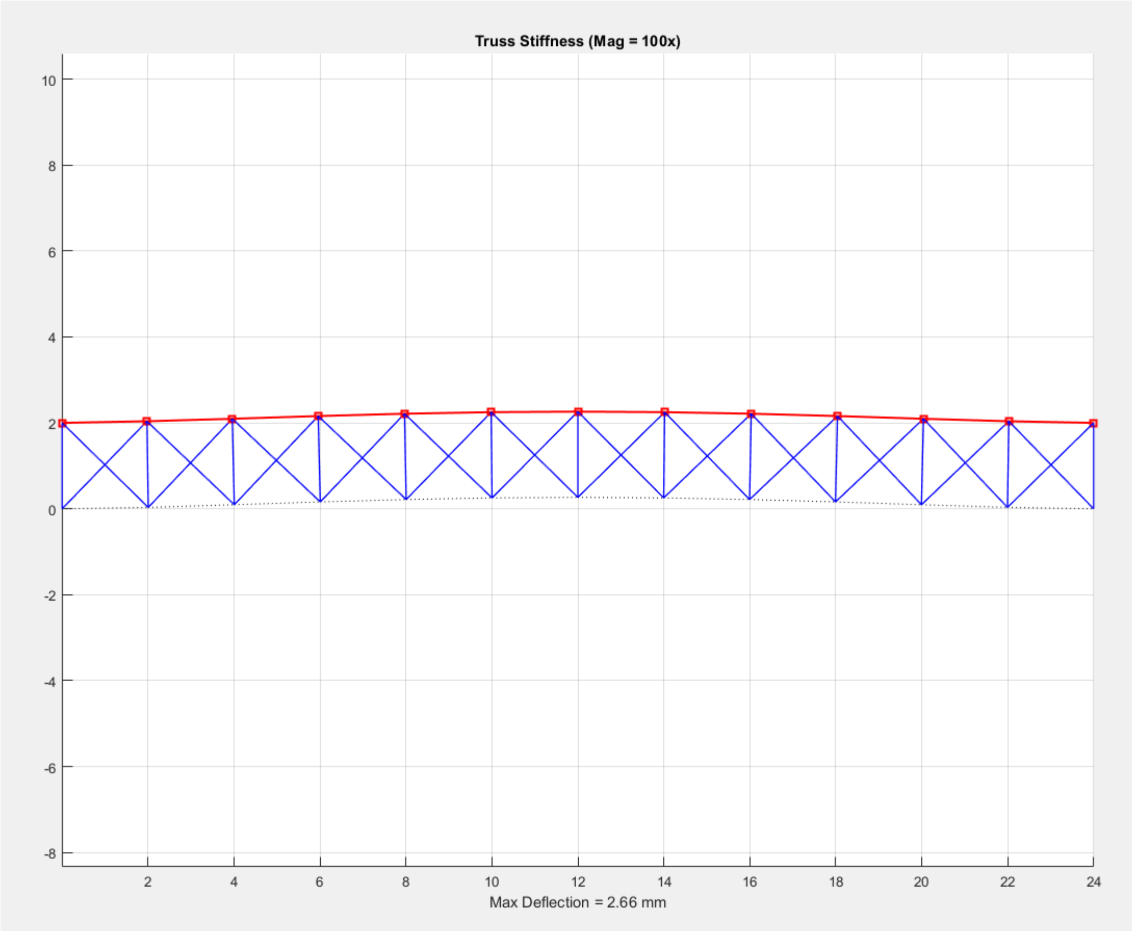

Figure C.2: Truss deflection and layout, deformation magnified 100× (actual max deflection = 2.66 mm)

C.2 Critical Wheel Positions and Maximum Load Effects in ULS and SLS

```
clc; clear all; close all;

%% 1. Selection Setting
target_row = 1;

%% 2. Geometry and Discretization
L = 24;
s = [0, 1.2, 3.725, 4.925, 11.175, 12.375, 14.9, 16.1];
Gcb = 22.402;
RA_q = Gcb * L / 2;
dx_step = 0.005;
x = 0:dx_step:L;
dx_move = 0.05;
x0_range = -max(s):dx_move:L;

%% 3. Load Definitions

ULS.P_mat = [1397, 1397, 1526, 1526, 1537, 1537, 1460, 1460;
             1489, 1489, 1626, 1626, 1618, 1618, 1536, 1536];

ULS.H_mat = [136.59, 136.59, 0, 0, 0, 0, -136.59, -136.59;
            371.931, 371.931, 0, 0, 0, 0, -371.931, -371.931];

ULS.K_mat = [0, 0, 0, 0, 0, 0, 0, 0;
             0, 0, 0, 0, 0, 0, 0, 0];

ULS.Kr_mat = [0, 242.788, 0, 0, 0, 0, 242.788, 0;
              0, 242.788, 0, 0, 0, 0, 242.788, 0];

ULS.Sk_mat = [0, 0, 0, 0, 0, 0, 0, 0;
              0, 0, 0, 0, 0, 0, 0, 0];

ULS.Yk_mat = [0, 0, 0, 0, 0, 0, 0, 0;
              0, 0, 0, 0, 0, 0, 0, 0];

% SLS loads
SLS.P_mat = [851.09, 851.09, 929.651, 929.651, 936.251, 936.251, 889.247, 889.247;
             906.801, 906.801, 990.511, 990.511, 985.088, 985.088, 935.623, 935.623];

SLS.H_mat = [64.744, 64.744, 0, 0, 0, 0, -64.744, -64.744;
             176.294, 176.294, 0, 0, 0, 0, -176.294, -176.294];

SLS.K_mat = [37.697, 37.697, 37.697, 37.697, 37.697, 37.697, 37.697, 37.697;
             0, 0, 0, 0, 0, 0, 0, 0];

SLS.Kr_mat = [0, 115.081, 0, 0, 0, 115.081, 0, 0;
              0, 115.081, 0, 0, 0, 115.081, 0, 0];

```

```
SLS.Sk_mat = [622.114, 0, 0, 0, 0, 0, 0, 0;
              622.114, 0, 0, 0, 0, 0, 0, 0];

SLS.Yk_mat = [162.035, 146.364, 113.375,  97.704, 16.053,  0.382,
    -32.607, -48.288;
               59.703,  53.750,  41.639,  35.883,  5.894,  0.137,
    -11.974, -17.730];

%% 4. Main Calculation Loop
LimitStates = {ULS, SLS};
StateNames = {'ULS (Design)', 'SLS (Service)'};

for ls = 1:length(LimitStates)
    current_state = LimitStates{ls};

    % --- Use target_row for ALL load vectors ---
    P  = current_state.P_mat(target_row, :);
    H  = current_state.H_mat(target_row, :);
    K  = current_state.K_mat(target_row, :);
    Kr = current_state.Kr_mat(target_row, :);
    Sk = current_state.Sk_mat(target_row, :);
    Yk = current_state.Yk_mat(target_row, :);

    Mmax_env  = -inf * ones(size(x));
    V_pos_env = -inf * ones(size(x));
    V_neg_env =  inf * ones(size(x));

    M_best_global  = -inf;
    x0_at_abs_maxM = 0;

    %% --- Step A: Calculation Loop ---
    for x0 = x0_range
        xw_all = x0 + s;
        idx = (xw_all >= 0) & (xw_all <= L);
        xw = xw_all(idx);
        Pw = P(idx);

        RA = sum(Pw .* (L - xw)) / L;
        V = (RA + RA_q) - Gcb*x;
        M = (RA + RA_q)*x - Gcb*x.^2/2;

        for i = 1:length(xw)
            V = V - Pw(i) * (x >= xw(i));
            M = M - Pw(i) * max(0, x - xw(i));
        end

        Mmax_env  = max(Mmax_env, M);
        V_pos_env = max(V_pos_env, V);
        V_neg_env = min(V_neg_env, V);

        [M_local_max, ~] = max(M);
        if M_local_max >= M_best_global
            M_best_global  = M_local_max;
            x0_at_abs_maxM = x0;
        end
    end
```

```
%% --- Step B: Extract Results for Max Moment Position ---
[M_abs, i_absM] = max(Mmax_env);
x_critM         = x(i_absM);
xw_at_Mmax      = x0_at_abs_maxM + s;

% Vertical reactions at supports
idx_vM       = (xw_at_Mmax >= 0) & (xw_at_Mmax <= L);
RA_at_Mcrit = sum(P(idx_vM) .* (L - xw_at_Mmax(idx_vM))) / L +
RA_q;
RB_at_Mcrit = sum(P(idx_vM) .* xw_at_Mmax(idx_vM))        / L +
RA_q;

% --- Mz from H + K ---
PH_total = H + K;
idx_h     = (xw_at_Mmax >= 0) & (xw_at_Mmax <= L);
xw_h      = xw_at_Mmax(idx_h);
PH_h      = PH_total(idx_h);

RA_H  = sum(PH_h .* (L - xw_h)) / L;
Mz_HK = RA_H * x;
for i = 1:length(xw_h)
    Mz_HK = Mz_HK - PH_h(i) * max(0, x - xw_h(i));
end

% --- Mz from Sk + Yk ---
% Sk enters with minus sign per EN 1993-6 combination formula
PSk_total = -Sk + Yk;
idx_sk     = (xw_at_Mmax >= 0) & (xw_at_Mmax <= L);
xw_sk      = xw_at_Mmax(idx_sk);
PSk_h      = PSk_total(idx_sk);

RA_Sk = sum(PSk_h .* (L - xw_sk)) / L;
Mz_Sk = RA_Sk * x;
for i = 1:length(xw_sk)
    Mz_Sk = Mz_Sk - PSk_h(i) * max(0, x - xw_sk(i));
end

% --- Total Mz ---
Mz_total = Mz_HK + Mz_Sk;

% --- Find peak Mz at its own critical section ---
[~, i_maxMz_HK]    = max(abs(Mz_HK));
[~, i_maxMz_Sk]    = max(abs(Mz_Sk));
[~, i_maxMz_total] = max(abs(Mz_total));

%% --- Step C: Display ---
global_max_ved = max(max(abs(V_pos_env)), max(abs(V_neg_env)));

fprintf('\n================ %s ================\n', StateNames{
ls});
fprintf('ABS MAX My:         %10.2f kNm (at x = %.3f m)\n',
M_abs, x_critM);
fprintf('GLOBAL PEAK Vy:     %10.2f kN\n', global_max_ved);
fprintf('----------------------------------------------\n');
fprintf('SHEAR AT SUPPORTS (for Max My truck pos):\n');
```

```
    fprintf('  At Left Support  (x=0):  %10.2f kN\n', RA_at_Mcrit);
    fprintf('  At Right Support (x=L):  %10.2f kN\n', RB_at_Mcrit);
    fprintf('----------------------------------------------\n');
    fprintf('Mz PEAK VALUES (at their own critical sections):\n');
    fprintf('  Mz from H+K:    %10.2f kNm (at x = %.3f m)\n', ...
            Mz_HK(i_maxMz_HK), x(i_maxMz_HK));
    fprintf('  Mz from Sk+Yk:  %10.2f kNm (at x = %.3f m)\n', ...
            Mz_Sk(i_maxMz_Sk), x(i_maxMz_Sk));
    fprintf('  Mz TOTAL peak:  %10.2f kNm (at x = %.3f m)\n', ...
            Mz_total(i_maxMz_total), x(i_maxMz_total));
    fprintf('  Mz at My crit (x=%.3f m): %10.2f kNm\n', ...
            x_critM, Mz_total(i_absM));
    fprintf('----------------------------------------------\n');
    fprintf('Wheel Positions at Max My [m]:\n');
    for w = 1:8
        status = ' (ON)';
        if (xw_at_Mmax(w) < 0 || xw_at_Mmax(w) > L)
            status = ' (OFF)';
        end
        fprintf('  Wheel %d: %10.3f m %s\n', w, xw_at_Mmax(w), status);
    end

    %% --- Step D: Plotting ---
    figure(1);
    subplot(2,1,1); hold on;
    plot(x, Mmax_env, 'LineWidth', 1.5, 'DisplayName', StateNames{ls});
    subplot(2,1,2); hold on;
    p_v = plot(x, V_pos_env, 'LineWidth', 1.5, 'DisplayName', StateNames{ls});
    plot(x, V_neg_env, 'LineWidth', 1.5, 'Color', get(p_v,'Color'), ...
         'HandleVisibility', 'off');

    figure(2); hold on;
    plot(x, Mz_HK,    '--', 'LineWidth', 1.2, 'DisplayName', [StateNames{ls} ' H+K']);
    plot(x, Mz_Sk,    ':',  'LineWidth', 1.2, 'DisplayName', [StateNames{ls} ' Sk+Yk']);
    plot(x, Mz_total, '-',  'LineWidth', 1.5, 'DisplayName', [StateNames{ls} ' Total']);
end

%% 5. Formatting
figure(1);
subplot(2,1,1); grid on; legend show; title('My Envelopes'); ylabel('kNm');
subplot(2,1,2); grid on; legend show; title('Vy Envelopes'); ylabel('kN'); xlabel('x [m]');
figure(2); grid on; legend show; yline(0,'k--','HandleVisibility','off');
title('Mz at Max My Position'); xlabel('x [m]'); ylabel('kNm');
```

```
================ ULS (Design) ================
ABS MAX My:              43550.61 kNm (at x = 13.525 m)
GLOBAL PEAK Vy:           8628.07 kN
----------------------------------------------
SHEAR AT SUPPORTS (for Max My truck pos):
  At Left Support  (x=0):      7346.99 kN
  At Right Support (x=L):      5728.65 kN
----------------------------------------------
Mz PEAK VALUES (at their own critical sections):
  Mz from H+K:        -2670.93 kNm (at x = 17.250 m)
  Mz from Sk+Yk:          0.00 kNm (at x = 0.000 m)
  Mz TOTAL peak:      -2670.93 kNm (at x = 17.250 m)
  Mz at My crit (x=13.525 m):    -1620.30 kNm
----------------------------------------------
Wheel Positions at Max My [m]:
  Wheel 1:       2.350 m   (ON)
  Wheel 2:       3.550 m   (ON)
  Wheel 3:       6.075 m   (ON)
  Wheel 4:       7.275 m   (ON)
  Wheel 5:      13.525 m   (ON)
  Wheel 6:      14.725 m   (ON)
  Wheel 7:      17.250 m   (ON)
  Wheel 8:      18.450 m   (ON)
```

Figure C.3: Peak moment and shear values in ULS with corresponding wheel positions

```
================= SLS (Service) =================
ABS MAX My:            27143.24 kNm (at x = 13.475 m)
GLOBAL PEAK Vy:         5359.82 kN
-------------------------------------------------
SHEAR AT SUPPORTS (for Max My truck pos):
  At Left Support  (x=0):     4595.61 kN
  At Right Support (x=L):     3578.08 kN
-------------------------------------------------
Mz PEAK VALUES (at their own critical sections):
  Mz from H+K:       -1276.96 kNm (at x = 17.200 m)
  Mz from Sk+Yk:      -945.82 kNm (at x = 2.300 m)
  Mz TOTAL peak:     -1552.06 kNm (at x = 17.200 m)
  Mz at My crit (x=13.475 m):   -1105.94 kNm
-------------------------------------------------
Wheel Positions at Max My [m]:
  Wheel 1:       2.300 m   (ON)
  Wheel 2:       3.500 m   (ON)
  Wheel 3:       6.025 m   (ON)
  Wheel 4:       7.225 m   (ON)
  Wheel 5:      13.475 m   (ON)
  Wheel 6:      14.675 m   (ON)
  Wheel 7:      17.200 m   (ON)
  Wheel 8:      18.400 m   (ON)
```

Figure C.4: Peak moment and shear values in SLS with corresponding wheel positions

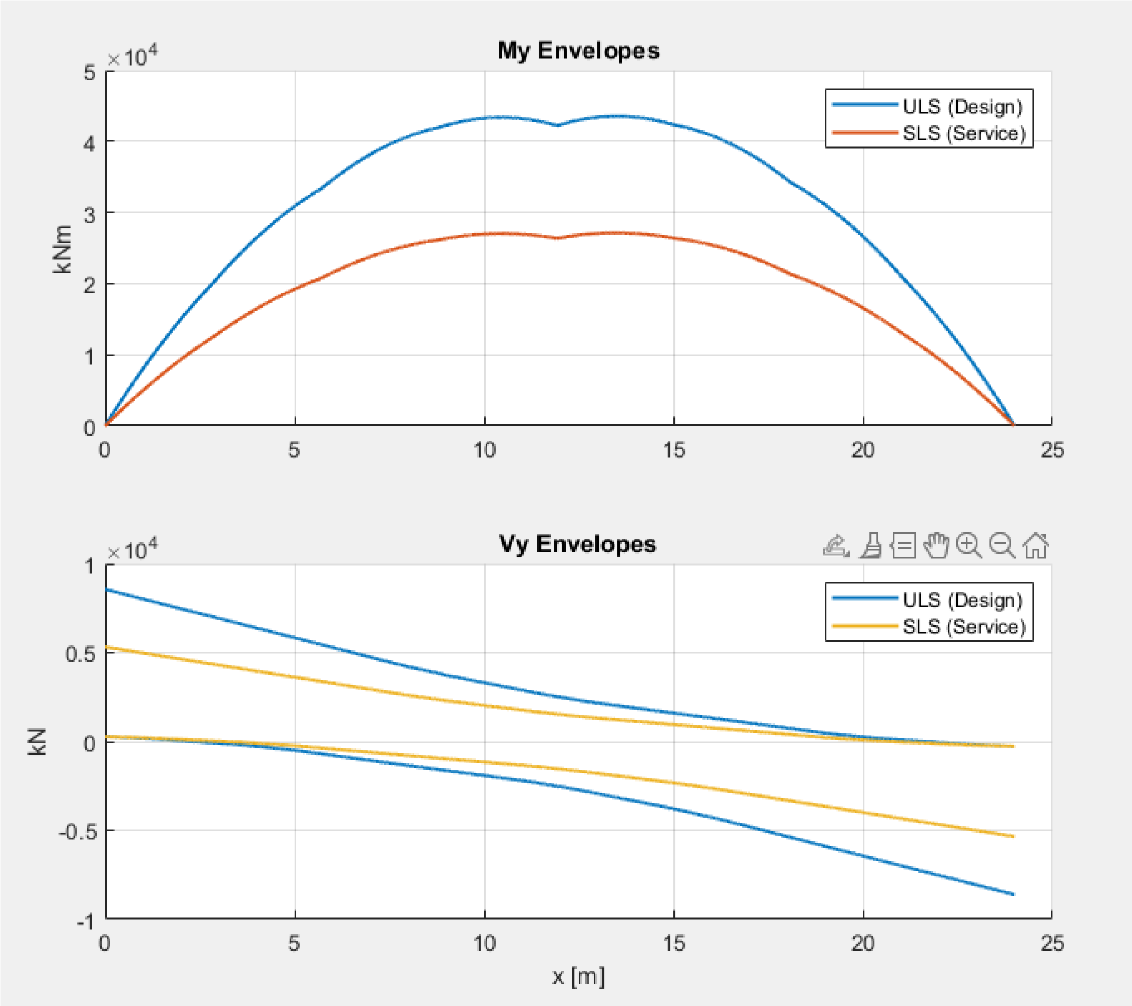

Figure C.5: Maximum moment and shear envelope as a function of wheel position

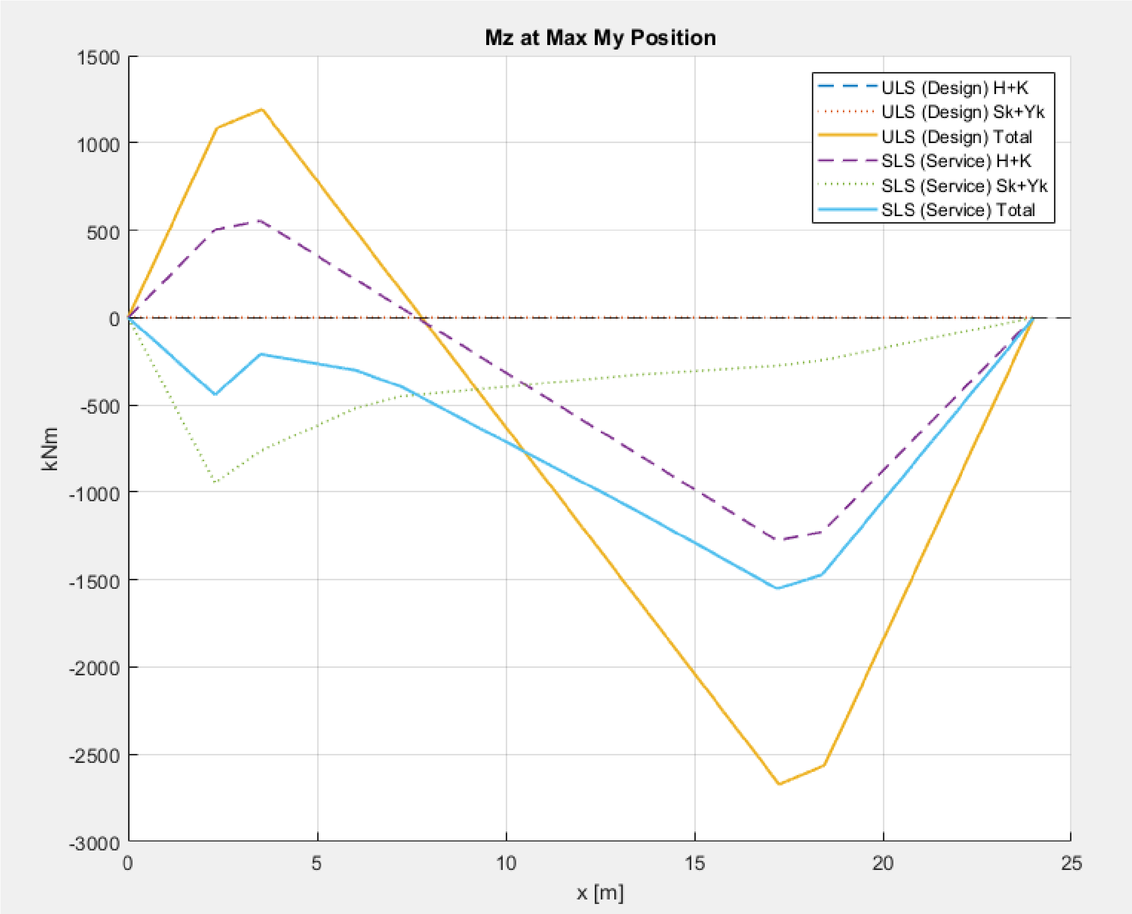

Figure C.6: Maximum moment about the z-axis M_z for the wheel position governing maximum M_y

D

Excel Worksheets

D.1 Web sidesway buckling comparison

Web sidesway buckling: ϕRn vs. maximum wheel load (1626 kN)						
hw \ bf	700	600	500	400	300	200
2500		4476	2998	2028	1408	1099
3000			6216	1920	1199	829
3510				3878	2235	696
4000				4082	2160	1173
4500					2176	1066
5000					2238	1004

Figure D.1: Web sidesway buckling nominal strength ϕR_n [kN] for varying web height and bottom flange width, according to AISC.

D.2 Imperfections

D.2.1 Web tolerances

No	Criterion	Parameter	Essential tolerances Permitted deviation Δ	Functional tolerances Permitted deviation Δ	
			Class 1 and 2	Class 1	Class 2
7	Plate curvature: 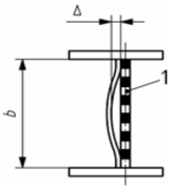	Deviation Δ over plate height b:	$\Delta = \pm b/200$ if $b/t \le 80$ $\Delta = \pm b^2/(16\,000\, t)$ if $80 < b/t \le 200$ $\Delta = \pm b/80$ if $b/t > 200$ but $\|\Delta\| \ge t$ (t = plate thickness)	$\Delta = \pm b/100$ but $\|\Delta\| \ge 5$ mm	$\Delta = \pm b/150$ but $\|\Delta\| \ge 3$ mm
8	Web distortion: 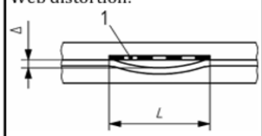	Deviation Δ on gauge length L equal to web height b (see (7)): NOTE For components that are tapered or have variable web height b the permitted deviation is related to the mean web height at the location of the gauge.	$\Delta = \pm b/100$ but $\|\Delta\| \ge t$ (t = plate thickness)	$\Delta = \pm b/100$ but $\|\Delta\| \ge 5$ mm	$\Delta = \pm b/150$ but $\|\Delta\| \ge 3$ mm

Thickness					
30		Plate curvature		Web distortion	
hw	b/t	Essential tolerances	Functional tolerances Class 1	Essential	Functional Class 1
5000	166.6667	52.08333	50	50	50
4500	150	42.1875	45	45	45
4000	133.3333	33.33333	40	40	40
3500	116.6667	25.52083	35	35	35
3000	100	18.75	30	30	30
2500	83.33333	13.02083	30	30	25

Figure D.2: Tolerances and imperfections for plate curvature

D.2.2 Squareness imperfection

			Essential tolerances Permitted deviation Δ	Functional tolerances Permitted deviation Δ	
			Class 1 and 2	Class 1	Class 2
6	Squareness at bearings: 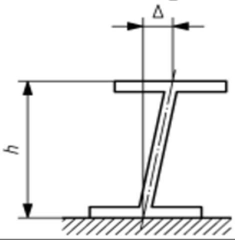	Verticality of web at supports, for components without bearing stiffeners:	$\Delta = \pm h/200$ but $\lvert\Delta\rvert \geq t_w$ (t_w = web thickness)	$\Delta = \pm h/300$ but $\lvert\Delta\rvert \geq 3$ mm	$\Delta = \pm h/500$ but $\lvert\Delta\rvert \geq 2$ mm

				Essential		Functional	
hw(abaqus)	ttf	tbf	h	delta		delta C1	delta C2
5000	100	80	5090	30		16.96667	10.18
4500	tw		4590	30		15.3	9.18
4000	30		4090	30		13.63333	8.18
3510			3600	30		12	7.2
3000			3090	30		10.3	6.18
2500			2590	30		8.633333	5.18

Figure D.3: Tolerances and imperfections for squareness at bearings

D.2.3 Flexural Buckling imperfection

(5) Equivalent geometric imperfections for use in geometrically and materially nonlinear analysis (GMNIA) of structural members for flexural buckling may be determined from Formula (5.15). The equivalent imperfection shape can be either a bow (half-sine wave) or buckling mode.

$$e_0 = \frac{\alpha L}{150} \quad \text{but } e_0 \geq \frac{L}{1\,000} \tag{5.15}$$

where

α the imperfection factor, taken from EN 1993-1-1 or EN 1993-1-4.

Table 6.1: Imperfection factors for buckling curves

Buckling curve	a_0	a	b	c	d
Imperfection factor α	0,13	0,21	0,34	0,49	0,76

Thickness	L				
30	24000				
alpha	a0	a	b	c	d
	0.13	0.21	0.34	0.49	0.76
e0	24	33.6	54.4	78.4	121.6

Table 5.6 — Equivalent geometric imperfections for cross-sections of plated structures

Component/type of imperfection	Shape	Magnitude
longitudinal stiffener with length a	bow	min (a/400, b/400)
panel or sub-panel with short span a or b	buckling shape	min (a/200, b/200)
stiffener or flange subject to twist	bow twist	1 / 50
outstand elements for cold-formed structures – local	buckling shape	b / 125
outstand elements for cold-formed structures – distortional	buckling shape	see Formula (5.17)

panel short span	
hw	panel
5000	25
4500	22.5
4000	20
3500	17.5
3000	15

Figure D.4: Equivalent geometric imperfection for flexural buckling and plated structures

D.2.4 Flexural Buckling imperfection

(6) Equivalent geometric imperfections for use in geometrically and materially nonlinear analysis (GMNIA) of structural members for lateral torsional buckling may be determined from Formula (5.16).

$$e_0 = \alpha \cdot L \cdot \beta_{LT} \quad \text{but} \quad e_0 \geq \frac{L}{1\,000} \qquad (5.16)$$

Table 5.5 — Equivalent geometric imperfections for structural members for lateral torsional buckling

Shape	β_{LT}	Illustration
bow	combination of 1/150 (half-sine wave) and 1/215 (full sine wave)	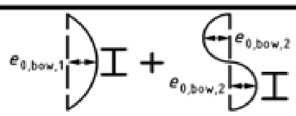
buckling shape	1/150	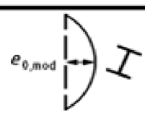

Beta(1/150)					
0.006667					
e0	20.8	33.6	54.4	78.4	121.6

Figure D.5: Equivalent geometric imperfection values for LTB

D.2.5 LTB imperfection

7.3.3.2 Lateral torsional buckling

(1) For a second order analysis taking account of lateral torsional buckling of a member in bending, the equivalent bow imperfection for flexural buckling about the weak axis of the cross-section $e_{0,\mathrm{LT}}$ may be determined according to Formula (7.11). In general, an additional torsional imperfection may be neglected.

$$e_{0,\mathrm{LT}} = \beta_{\mathrm{LT}} \frac{L}{\varepsilon} \tag{7.11}$$

where

L is the member length;

ε is the material parameter defined in 5.2.5(2);

β_{LT} is the reference relative bow imperfection for lateral torsional buckling according to Table 7.2.

Table 7.2 — Reference relative bow imperfection β_{LT} for lateral torsional buckling

Cross-section	Condition	Elastic cross-section verification	Plastic cross-section verification
rolled	$h/b \leq 2{,}0$	1/250	1/200
	$h/b > 2{,}0$	1/200	1/150
welded	$h/b \leq 2{,}0$	1/200	1/150
	$h/b > 2{,}0$	1/150	1/100

hw(abaqus	h/b	Belast	Bplast	eps	L	e0.elast	e0.plast
5000	7.142857	0.006667	0.01	0.813617	24000	196.6528	294.9793
4500	6.428571	0.006667	0.01			196.6528	294.9793
4000	5.714286	0.006667	0.01			196.6528	294.9793
3510	5.014286	0.006667	0.01			196.6528	294.9793
3000	4.285714	0.006667	0.01			196.6528	294.9793
2500	3.571429	0.006667	0.01			196.6528	294.9793

Figure D.6: Equivalent bow imperfection, elastic and plastic cross section verification

D.3 Convergence Study

Mesh size	U	Avg U	S11	Avg U	Beam elements	Rail elements	Total elements	Delta
400	-26.6255	-26.623	149.421	149.421	842	136	978	0.20%
	-26.6174		149.421					
	-26.6255		149.421					
350	-26.6179	-26.615	149.349	149.349	1020	152	1172	0.17%
	-26.6083		149.349					
	-26.6179		149.349					
300	-26.6086	-26.606	149.293	149.293	1360	178	1538	0.14%
	-26.6003		149.293					
	-26.6086		149.293					
250	-26.5978	-26.595	149.239	149.239	1820	214	2034	0.10%
	-26.5889		149.239					
	-26.5978		149.239					
200	-26.586	-26.582	149.091	149.156	3368	260	3628	0.05%
	-26.5797		149.172					
	-26.5774		149.253					
	-26.5797		149.172					
	-26.586		149.091					
150	-26.5819	-26.578	149.064	149.128	5268	344	5612	0.03%
	-26.5756		149.144					
	-26.5733		149.225					
	-26.5756		149.144					
	-26.5819		149.064					

Figure D.7: Convergence study, with mesh sizes 400-150

100	-26.5773	-26.572	148.998	149.091	13106	1008	14114	0.01%
	-26.5737		149.022					
	-26.571		149.085					
	-26.5693		149.183					
	-26.5687		149.241					
	-26.5693		149.183					
	-26.571		149.085					
	-26.5737		149.022					
	-26.5773		148.998					
50	-26.5739	-26.569	148.971	149.074	50176	5928	56104	0.00%
	-26.5717		148.98					
	-26.5699		149.004					
	-26.5683		149.039					
	-26.5671		149.085					
	-26.5661		149.142					
	-26.5656		149.211					
	-26.5653		149.248					
	-26.5656		149.211					
	-26.5661		149.142					
	-26.5671		149.085					
	-26.5683		149.039					
	-26.5699		149.004					
	-26.5717		148.98					
	-26.5739		148.971					

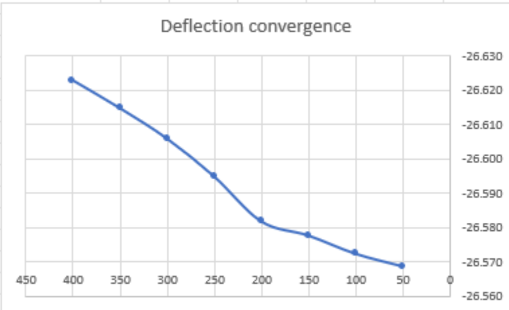

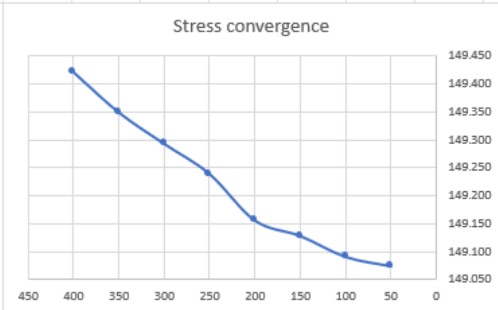

Figure D.8: Convergence study, with mesh sizes 100-50 and diagrams

D.4 Comparison table

D.4.1 Buckling job imperfection, maximum wheel positions moment

		$e_0 = 0$ mm						
hw	bf	Top LPF	Top U2 [mm]	Top U3 [mm]	Both LPF	Both U2 [mm]	Both U3 [mm]	ΔLPF%
2500	700	1.852857	-127.1814	-47.0291	1.907035	-150.8677	-3.0609	2.92
	600	1.794295	-208.1701	-55.1505	1.798937	-214.0615	-2.1532	0.26
	500	1.686615	-355.019	-61.3933	1.714865	-207.4404	-1.5034	1.67
	400	1.568306	-491.4089	-54.2923	1.5707	-499.272	-0.1932	0.15
	300	1.440128	-644.2997	-45.6848	1.439094	-643.2914	0.5064	-0.07
	200	1.302763	-859.3962	-13.8015	1.300291	-851.312	1.6293	-0.19
3000	700	1.793107	-65.9272	-45.1931	1.840793	-66.8086	-4.3157	2.66
	600	1.770821	-69.9016	-58.9442	1.833624	-71.665	-4.9055	3.55
	500	1.746578	-77.0652	-70.959	1.819287	-83.6633	-3.8665	4.16
	400	1.719387	-94.251	-75.6503	1.790239	-108.8408	-3.1759	4.12
	300	1.660475	-127.9756	-83.7863	1.713288	-164.2697	-2.1173	3.18
	200	1.572254	-284.0958	-80.2978	1.553453	-238.6002	-0.5385	-1.2
3510	700	1.66538	-42.5214	-46.8452	1.696253	-42.4411	-4.718	1.85
	600	1.655418	-44.8645	-58.0173	1.69426	-44.8286	-4.8359	2.35
	500	1.645382	-47.8161	-71.308	1.693425	-47.8082	-4.8682	2.92
	400	1.636064	-51.7615	-84.5102	1.693955	-51.6502	-4.8013	3.54
	300	1.609232	-56.3451	-104.9575	1.675878	-58.1396	-4.328	4.14
	200	1.610373	-70.7397	-106.8126	1.670829	-76.1341	-3.3152	3.75
4000	700	1.538098	-26.2999	-45.6673	1.554577	-25.5817	-4.4373	1.07
	600	1.53449	-28.0361	-58.2338	1.554991	-27.0788	-4.5921	1.34
	500	1.531847	-30.1852	-73.0883	1.55683	-29.0645	-4.6312	1.63
	400	1.531231	-33.0245	-87.487	1.56058	-31.528	-4.5508	1.92
	300	1.514127	-35.7892	-108.3062	1.546882	-33.8782	-4.4143	2.16
	200	1.523262	-41.554	-113.3416	1.555223	-39.8687	-3.9553	2.1
4500	700	1.459646	-14.6387	-43.0585	1.467688	-13.2576	-3.979	0.55
	600	1.458177	-16.016	-54.896	1.467819	-14.0806	-4.0916	0.66
	500	1.457444	-17.8284	-68.6885	1.468786	-15.3381	-4.0957	0.78
	400	1.458056	-19.9855	-83.2752	1.470964	-16.8371	-3.9925	0.89
	300	1.443877	-22.0692	-103.5661	1.458264	-18.2145	-3.8039	1
	200	1.449875	-25.6459	-108.0455	1.462919	-21.744	-3.3909	0.9
5000	700	1.425249	-8.132	-35.2393	1.427906			0.19
	600	1.424643	-9.0947	-45.2699	1.427906	-7.0236	-3.2187	0.23
	500	1.424369	-10.4137	-57.3378	1.428142	-7.5805	-3.2019	0.26
	400	1.424612	-11.9652	-70.6235	1.428829	-8.4418	-3.0785	0.3
	300	1.410025	-13.5194	-89.7397	1.414909	-9.0163	-2.8831	0.35
	200	1.411776	-15.5872	-95.7135	1.415669	-10.6903	-2.5676	0.28

Figure D.9: Comparison between the results from the buckling job imperfection for the critical wheel positions for maximum moment, with $e_0 = 0$ mm.

		e_0 = 25 mm						
hw	bf	Top LPF	Top U2 [mm]	Top U3 [mm]	Both LPF	Both U2 [mm]	Both U3 [mm]	ΔLPF%
2500	700	1.671111	-95.1413	-59.8186	1.706492	-99.2096	-4.0796	2.12
	600	1.638193	-112.7456	-65.4547	1.678323	-124.5354	-3.7149	2.45
	500	1.592551	-157.8941	-72.0969	1.622412	-192.5652	-2.9503	1.88
	400	1.507694	-331.8904	-75.8877	1.511641	-352.6759	-1.1575	0.26
	300	1.397591	-517.3555	-76.4181	1.387466	-248.6226	-1.0803	-0.72
	200	1.282804	-779.6591	-54.9522	1.253362	-668.2476	0.9775	-2.3
3000	700	1.653698	-61.5313	-54.7571	1.685974	-61.7955	-5.5942	1.95
	600	1.635412	-64.7385	-68.1502	1.674656	-64.7383	-5.7466	2.4
	500	1.617952	-69.8114	-86.3202	1.659806	-70.6387	-6.0545	2.59
	400	1.602448	-79.7947	-93.5238	1.635381	-83.162	-4.7445	2.06
	300	1.568347	-101.3916	-105.3373	1.584071	-105.8289	-3.9021	1
	200	1.530987	-184.4703	-105.3576	1.510076	-163.6635	-2.2494	-1.37
3510	700	1.560576	-38.0686	-52.2004	1.574151	-36.6599	-5.4813	0.87
	600	1.556128	-40.5488	-65.8608	1.571972	-38.8585	-5.6418	1.02
	500	1.553918	-43.7514	-80.7605	1.571494	-41.4659	-5.7821	1.13
	400	1.555086	-48.0392	-99.0518	1.573321	-45.2388	-5.6192	1.17
	300	1.541067	-52.7111	-122.0225	1.554222	-48.7271	-5.6284	0.85
	200	1.557133	-65.8823	-129.8478	1.562097	-62.3801	-4.5431	0.32
4000	700	1.471462	-22.08	-49.7057	1.480539	-20.5333	-4.8951	0.62
	600	1.470505	-24.0849	-62.7986	1.479881	-21.8019	-5.0687	0.64
	500	1.471388	-26.4503	-78.6386	1.48151	-23.4843	-5.1462	0.69
	400	1.475667	-29.6672	-93.3434	1.485007	-25.6053	-5.0967	0.63
	300	1.465241	-32.6567	-114.6062	1.471074	-27.6725	-4.9138	0.4
	200	1.482939	-38.3348	-121.5402	1.478732	-32.7943	-4.4059	-0.28
4500	700	1.423823	-11.8755	-43.739	1.428728	-10.0625	-4.0767	0.34
	600	1.424053	-13.3216	-55.7268	1.427929	-10.6596	-4.191	0.27
	500	1.425264	-15.2184	-69.7317	1.428766	-11.6054	-4.2149	0.25
	400	1.428203	-17.3751	-85.2136	1.430944	-12.8312	-4.1272	0.19
	300	1.41631	-19.57	-105.3413	1.417369	-13.7883	-3.9443	0.07
	200	1.425231	-22.9286	-110.5413	1.421569	-16.6013	-3.5514	-0.26
5000	700	1.405066	-6.4219	-34.3821	1.406448	-4.6738	-3.1177	0.1
	600	1.4057	-7.4348	-44.009	1.406175	-4.9891	-3.1651	0.03
	500	1.40686	-8.7028	-55.9306	1.406574	-5.3637	-3.1476	-0.02
	400	1.408838	-10.3155	-68.6166	1.407717	-5.9377	-3.0337	-0.08
	300	1.396024	-11.831	-87.2333	1.393378	-6.3112	-2.8369	-0.19
	200	1.399527	-13.7923	-92.6927	1.394401	-7.6078	-2.5358	-0.37

Figure D.10: Comparison between the results from the buckling job imperfection for the critical wheel positions for maximum moment, with $e_0 = 25$ mm.

		$e_0 = 50$ mm						
hw	bf	Top LPF	Top U2 [mm]	Top U3 [mm]	Both LPF	Both U2 [mm]	Both U3 [mm]	ΔLPF%
2500	700	1.567562	-89.2073	-63.3867	1.596686	-91.5624	-5.9433	1.86
	600	1.536107	-96.8317	-77.6682	1.570532	-103.6259	-4.7286	2.24
	500	1.500605	-118.9141	-84.7646	1.52996	-130.6551	-4.2956	1.96
	400	1.450292	-183.1544	-89.9896	1.457793	-202.7132	-3.2194	0.52
	300	1.358756	-397.1754	-96.7284	1.335838	-353.4391	-1.0769	-1.69
	200	1.26381	-705.1279	-89.618	1.212067	-518.9633	0.1629	-4.09
3000	700	1.561335	-58.1415	-61.759	1.584031	-57.4047	-6.5968	1.45
	600	1.545879	-61.5914	-78.6936	1.56998	-59.9064	-6.8086	1.56
	500	1.532388	-66.1781	-97.0969	1.556275	-63.6428	-7.2964	1.56
	400	1.522768	-73.4503	-110.6619	1.539286	-73.3484	-6.5823	1.08
	300	1.50017	-90.4605	-126.156	1.493368	-88.6351	-5.384	-0.45
	200	1.486504	-144.0632	-127.1288	1.438171	-124.321	-3.8322	-3.25
3510	700	1.481231	-33.8669	-57.5811	1.486146	-31.4228	-6.1343	0.33
	600	1.479247	-36.5571	-71.6308	1.483731	-33.2505	-6.3801	0.3
	500	1.480743	-39.8759	-89.0273	1.483029	-35.6132	-6.5249	0.15
	400	1.488767	-44.5051	-106.5625	1.484842	-38.9984	-6.4311	-0.26
	300	1.483821	-49.3282	-132.5011	1.465616	-41.7719	-6.3242	-1.23
	200	1.511744	-61.7429	-145.3764	1.473648	-50.6324	-5.5497	-2.52
4000	700	1.420165	-18.7898	-52.3081	1.424244	-16.4684	-5.208	0.29
	600	1.42081	-20.7151	-66.9654	1.423282	-17.4617	-5.4026	0.17
	500	1.423632	-23.3615	-82.972	1.425089	-18.947	-5.4869	0.1
	400	1.430422	-26.5073	-100.353	1.428624	-21.1321	-5.3929	-0.13
	300	1.423831	-29.7031	-121.7199	1.414282	-22.7623	-5.2133	-0.67
	200	1.44614	-35.3488	-129.6569	1.421194	-26.8945	-4.7517	-1.73
4500	700	1.392102	-9.6553	-43.9903	1.394827	-7.46	-4.1331	0.2
	600	1.393839	-11.049	-56.4138	1.393559	-7.835	-4.2488	-0.02
	500	1.396822	-12.8732	-71.357	1.394649	-8.4803	-4.2875	-0.16
	400	1.401835	-15.2127	-86.7992	1.397174	-9.6833	-4.1915	-0.33
	300	1.392075	-17.4498	-107.1936	1.382591	-10.1837	-4.0164	-0.68
	200	1.403025	-20.6101	-113.339	1.386536	-12.4247	-3.6451	-1.18
5000	700	1.385501	-4.9518	-33.6457	1.385436	-2.8718	-3.093	0
	600	1.387338	-5.9067	-43.2514	1.385101	-3.0234	-3.1326	-0.16
	500	1.389919	-7.2005	-54.9405	1.385728	-3.2554	-3.1053	-0.3
	400	1.393481	-8.7667	-67.7957	1.387355	-3.7558	-2.986	-0.44
	300	1.382296	-10.3485	-85.6224	1.373043	-3.8545	-2.7849	-0.67
	200	1.387115	-12.181	-90.9552	1.374257	-4.8936	-2.498	-0.93

Figure D.11: Comparison between the results from the buckling job imperfection for the critical wheel positions for maximum moment, with $e_0 = 50$ mm.

D.4.2 Buckling job imperfection, maximum wheel positions shear

		$e_0 = 0$ mm						
hw	bf	Top LPF	Top U2 [mm]	Top U3 [mm]	Both LPF	Both U2 [mm]	Both U3 [mm]	ΔLPF%
2500	700	2.149208	-213.8288	-36.4746	2.052586			-4.5
	600	1.932397	-312.2321	-42.6445	1.940049	-321.1827	-1.3124	0.4
	500	1.809872	-378.7398	-34.6234	1.813806	-384.0136	-0.2099	0.22
	400	1.680631	-477.7304	-22.0469	1.647668	-377.0426	0.3968	-1.96
	300	1.540453	-604.8198	-7.8872	1.540624	-607.3576	2.0772	0.01
	200	1.402891			1.391268	-796.5054	2.9836	-0.83
3000	700	2.085546	-68.7214	-41.7852	2.141395	-68.5074	-5.1778	2.68
	600	2.061183	-75.0121	-54.7622	2.147788	-81.7258	-4.5261	4.2
	500	2.039948	-93.871	-55.8149	2.1221	-110.3943	-3.0525	4.03
	400	1.986658	-134.9953	-57.9186	2.019908	-168.0436	-1.6031	1.67
	300	1.851495	-250.2778	-66.2777	1.883271	-200.4936	-0.3953	1.72
	200	1.679407	-292.3479	-64.2958	1.709971	-343.0999	0.372	1.82
3510	700	1.897679	-41.5966	-37.3513	1.926966	-41.1269	-4.4102	1.54
	600	1.889307	-44.1183	-46.1978	1.925878	-43.5798	-4.5502	1.94
	500	1.881367	-47.4658	-55.6302	1.926067	-46.8688	-4.5339	2.38
	400	1.874892	-52.3444	-67.7787	1.928203	-51.5248	-4.3867	2.84
	300	1.849818	-61.6223	-83.027	1.919991	-64.4613	-3.745	3.79
	200	1.626095	-69.0624	-65.7686	1.662682	-72.2263	-1.6996	2.25
4000	700	1.741546	-25.4511	-37.4901	1.758116	-24.6141	-4.1011	0.95
	600	1.738172	-27.2457	-47.0383	1.758644	-26.2032	-4.2006	1.18
	500	1.735897	-29.5118	-57.8865	1.760577	-28.3123	-4.1775	1.42
	400	1.735816	-32.6552	-67.2752	1.764366	-31.0408	-4.0201	1.64
	300	1.717821	-36.8557	-83.4958	1.750392	-35.3473	-3.7687	1.9
	200	1.563928	-46.943	-64.3297	1.595832	-48.2571	-2.0898	2.04
4500	700	1.65041	-14.3928	-37.2972	1.660434	-13.4784	-3.6353	0.61
	600	1.648071	-15.6842	-47.4713	1.660548	-14.3769	-3.7059	0.76
	500	1.626025	-19.6001	-48.6981	1.66141	-15.434	-3.6922	2.18
	400	1.646258	-19.6212	-70.6469	1.663231	-17.0851	-3.5225	1.03
	300	1.632836	-22.3205	-87.1108	1.651351	-19.2377	-3.257	1.13
	200	1.513739	-33.0555	-67.6138	1.538421	-32.8795	-2.0738	1.63
5000	700	1.608825	-8.1232	-32.3339	1.61309	-6.7827	-2.9784	0.27
	600	1.607591	-9.0379	-41.4239	1.612792	-7.3151	-2.9964	0.32
	500	1.606502	-10.2341	-52.419	1.612731	-7.9222	-2.9372	0.39
	400	1.605863	-11.7908	-64.167	1.613031	-8.9	-2.7593	0.45
	300	1.591844	-13.9477	-78.7544	1.600009	-10.0807	-2.4913	0.51
	200	1.467306	-22.8359	-68.6904	1.491078	-21.5665	-1.818	1.62

Figure D.12: Comparison between the results from the buckling job imperfection for the critical wheel positions for maximum shear, with $e_0 = 0$ mm.

		$e_0 = 25$ mm						
hw	bf	Top LPF	Top U2 [mm]	Top U3 [mm]	Both LPF	Both U2 [mm]	Both U3 [mm]	ΔLPF%
2500	700	1.966687	-125.4237	-47.549	1.935715	-119.4026	-0.4303	-1.57
	600	1.872911	-191.8673	-51.2704	1.901831			1.54
	500	1.741865	-294.7787	-54.9501	1.76251	-319.6279	-1.0363	1.19
	400	1.625604			1.603288			-1.37
	300	1.510701	-534.3721	-33.0383	1.501217	-514.7247	2.0006	-0.63
	200	1.376018	-740.3318	-13.8961	1.374116	-725.5345	3.0487	-0.14
3000	700	1.923636	-60.0415	-42.2594	1.948143	-59.8284	-5.1058	1.27
	600	1.894923	-64.2017	-54.4634	1.942181	-63.3416	-5.5506	2.49
	500	1.861432	-70.3803	-68.8026	1.943674	-74.3834	-5.3087	4.42
	400	1.807349	-86.3683	-74.9253	1.913623	-107.3517	-3.3511	5.88
	300	1.783389	-136.8447	-82.084	1.805583	-161.909	-1.3447	1.24
	200	1.665672	-278.0152	-87.5603	1.625507	-183.416	-0.1989	-2.41
3510	700	1.767173	-35.9611	-42.7483	1.791818	-35.3104	-4.7244	1.39
	600	1.75907	-38.3767	-53.0632	1.788393	-37.4894	-4.8346	1.67
	500	1.751356	-41.5314	-64.2278	1.785835	-39.9778	-4.9026	1.97
	400	1.744784	-45.7733	-78.7771	1.784082	-43.7509	-4.6984	2.25
	300	1.753331	-54.4062	-97.8218	1.765426	-49.1353	-4.4295	0.69
	200	1.617205	-68.0405	-84.709	1.641769	-65.1428	-2.7821	1.52
4000	700	1.663335	-21.2464	-41.8989	1.67707	-20.13	-4.3027	0.83
	600	1.659198	-22.9515	-52.9721	1.675972	-21.3259	-4.4099	1.01
	500	1.655766	-25.1143	-65.8921	1.675676	-23.1687	-4.3585	1.2
	400	1.654956	-28.0236	-78.886	1.676374	-25.276	-4.2023	1.29
	300	1.655466	-32.3014	-97.8364	1.662284	-28.0041	-3.9218	0.41
	200	1.552394	-46.0349	-84.3476	1.573801	-42.3003	-2.7557	1.38
4500	700	1.608219	-11.7365	-38.8081	1.616089	-10.3482	-3.6429	0.49
	600	1.606172	-12.9882	-49.4219	1.61538	-11.1002	-3.6823	0.57
	500	1.604845	-14.5244	-62.288	1.615157	-11.9754	-3.6333	0.64
	400	1.606057	-16.536	-75.9515	1.615678	-13.2643	-3.4479	0.6
	300	1.599387	-19.3353	-93.2789	1.60295	-14.6933	-3.1492	0.22
	200	1.500219	-30.5888	-77.1952	1.517732	-27.4686	-2.3226	1.17
5000	700	1.585897	-6.3891	-32.2483	1.588687	-4.81	-2.8787	0.18
	600	1.585154	-7.25	-41.3036	1.588374	-5.0987	-2.8789	0.2
	500	1.584921	-8.4017	-52.2102	1.588323	-5.543	-2.7906	0.21
	400	1.585804	-9.8554	-64.2091	1.588541	-6.1141	-2.5985	0.17
	300	1.57497	-11.8812	-79.7833	1.574401	-7.0446	-2.2997	-0.04
	200	1.454753	-20.848	-72.9798	1.474538	-17.487	-1.825	1.36

Figure D.13: Comparison between the results from the buckling job imperfection for the critical wheel positions for maximum shear, with $e_0 = 25$ mm.

		e_0 = 50 mm						
hw	bf	Top LPF	Top U2 [mm]	Top U3 [mm]	Both LPF	Both U2 [mm]	Both U3 [mm]	ΔLPF%
2500	700	1.784532	-53.3109	-43.158	1.828208	-103.3472	1.0746	2.45
	600	1.809518	-130.0037	-63.2065	1.825078	-139.84	0.5968	0.86
	500	1.701788	-190.6756	-63.8483	1.718458	-222.3932	-1.597	0.98
	400	1.586789	-331.4329	-71.196	1.565566			-1.34
	300	1.48657	-483.7873	-55.1051	1.468136			-1.24
	200	1.363293	-697.8422	-42.7389	1.360806	-690.3371	3.2421	-0.18
3000	700	1.784532	-53.3109	-43.158	1.79754	-52.5289	-5.6347	0.73
	600	1.760677	-56.7842	-54.1883	1.790887	-55.604	-5.7727	1.72
	500	1.73586	-61.7849	-72.448	1.782555	-59.7349	-5.8211	2.69
	400	1.707461	-72.6124	-100.6361	1.776529	-73.0629	-5.0362	4.05
	300	1.722244	-114.7915	-109.567	1.727895	-111.0043	-2.7747	0.33
	200	1.651014	-264.7496	-119.7507	1.63527	-214.2023	-0.1266	-0.95
3510	700	1.668392	-31.4281	-45.8814	1.688507	-30.2574	-4.9495	1.21
	600	1.661016	-33.7717	-56.9001	1.683952	-32.0111	-5.074	1.38
	500	1.653966	-36.5907	-71.3174	1.679631	-34.4189	-5.0291	1.55
	400	1.648663	-40.6057	-88.3198	1.675674	-37.2434	-4.8812	1.64
	300	1.680613	-49.5777	-112.1526	1.65793	-40.9705	-4.5507	-1.35
	200	1.611354	-67.1879	-100.596	1.615536	-56.5298	-3.67	0.26
4000	700	1.601453	-17.9322	-44.2088	1.612642	-16.2184	-4.3943	0.7
	600	1.597582	-19.5336	-56.2754	1.61055	-17.3462	-4.4482	0.81
	500	1.594853	-21.6027	-70.5425	1.608797	-18.6859	-4.3999	0.87
	400	1.59459	-24.2852	-86.7619	1.607669	-20.3626	-4.2111	0.82
	300	1.605617	-28.9376	-106.2159	1.594489	-22.1792	-3.8703	-0.69
	200	1.542963	-44.0182	-94.8986	1.550896	-35.684	-3.0944	0.51
4500	700	1.571462	-9.3329	-39.7798	1.577093	-7.7305	-3.5876	0.36
	600	1.569769	-10.5447	-50.666	1.576038	-8.1476	-3.6135	0.4
	500	1.568913	-12.0823	-63.8336	1.5754	-8.8315	-3.5295	0.41
	400	1.571147	-13.9398	-79.1693	1.575244	-9.6908	-3.3263	0.26
	300	1.568981	-16.9662	-96.2613	1.561655	-10.9264	-2.9756	-0.47
	200	1.48914	-28.6154	-85.7015	1.499881	-22.2679	-2.3807	0.72
5000	700	1.563473	-4.891	-31.7954	1.565346	-3.1257	-2.7588	0.12
	600	1.563174	-5.7205	-40.6604	1.564981	-3.2838	-2.7341	0.12
	500	1.563472	-6.8111	-51.5259	1.564876	-3.4574	-2.6242	0.09
	400	1.565402	-8.1907	-63.6745	1.565004	-3.8525	-2.4072	-0.03
	300	1.557125	-10.2058	-79.2181	1.549737	-4.3891	-2.0867	-0.47
	200	1.443476	-18.9641	-75.1434	1.460009	-14.2108	-1.7637	1.15

Figure D.14: Comparison between the results from the buckling job imperfection for the critical wheel positions for maximum shear, with $e_0 = 50$ mm

D.4.3 Moment bottom flange imperfection

		$e_0 = 0$ mm						
hw	bf	Top LPF	Top U2	Top U3	Both LPF	Both U2	Both U3	ΔLPF%
2500	700	1.852857	-127.1814	-47.0291	1.907035	-150.8677	-3.0609	2.92
	600	1.794295	-208.1701	-55.1505	1.843449			2.74
	500	1.686615	-355.019	-61.3933	1.715007			1.68
	400	1.568306	-491.4089	-54.2923	1.5707	-499.272	-0.1932	0.15
	300	1.440128	-644.2997	-45.6848	1.439094	-643.2914	0.5064	-0.07
	200	1.302763	-859.3962	-13.8015	1.300291	-851.312	1.6293	-0.19
3000	700	1.793107	-65.9272	-45.1931	1.840793	-66.8086	-4.3157	2.66
	600	1.770821	-69.9016	-58.9442	1.833624	-71.665	-4.9055	3.55
	500	1.746578	-77.0652	-70.959	1.819287	-83.6633	-3.8665	4.16
	400	1.719387	-94.251	-75.6503	1.790239	-108.8408	-3.1759	4.12
	300	1.660475	-127.9756	-83.7863	1.713288	-164.2697	-2.1173	3.18
	200	1.572254	-284.0958	-80.2978	1.586574	-316.812	-0.4456	0.91
3510	700	1.66538	-42.5214	-46.8452	1.696253	-42.4411	-4.718	1.85
	600	1.655418	-44.8645	-58.0173	1.69426	-44.8286	-4.8359	2.35
	500	1.645382	-47.8161	-71.308	1.693425	-47.8082	-4.8682	2.92
	400	1.636064	-51.7615	-84.5102	1.693955	-51.6502	-4.8013	3.54
	300	1.609232	-56.3451	-104.9575	1.675878	-58.1396	-4.328	4.14
	200	1.610373	-70.7397	-106.8126	1.670829	-76.1341	-3.3152	3.75
4000	700	1.538098	-26.2999	-45.6673	1.554577	-25.5817	-4.4373	1.07
	600	1.53449	-28.0361	-58.2338	1.554991	-27.0788	-4.5921	1.34
	500	1.531847	-30.1852	-73.0883	1.55683	-29.0645	-4.6312	1.63
	400	1.531231	-33.0245	-87.487	1.56058	-31.528	-4.5508	1.92
	300	1.514127	-35.7892	-108.3062	1.546882	-33.8782	-4.4143	2.16
	200	1.523262	-41.554	-113.3416	1.555223	-39.8687	-3.9553	2.1
4500	700	1.459646	-14.6387	-43.0585	1.467688	-13.2576	-3.979	0.55
	600	1.458177	-16.016	-54.896	1.467819	-14.0806	-4.0916	0.66
	500	1.457444	-17.8284	-68.6885	1.468786	-15.3381	-4.0957	0.78
	400	1.458056	-19.9855	-83.2752	1.470964	-16.8371	-3.9925	0.89
	300	1.443877	-22.0692	-103.5661	1.458264	-18.2145	-3.8039	1
	200	1.449875	-25.6459	-108.0455	1.462919	-21.744	-3.3909	0.9
5000	700	1.425249	-8.132	-35.2393	1.42797	-6.6144	-3.16	0.19
	600	1.424643	-9.0947	-45.2699	1.427906	-7.0236	-3.2187	0.23
	500	1.424369	-10.4137	-57.3378	1.428142	-7.5805	-3.2019	0.26
	400	1.424612	-11.9652	-70.6235	1.428829	-8.4418	-3.0785	0.3
	300	1.410025	-13.5194	-89.7397	1.414909	-9.0163	-2.8831	0.35
	200	1.411776	-15.5872	-95.7135	1.415669	-10.6903	-2.5676	0.28

Figure D.15: Comparison between the results from the bottom flange imperfection job for the critical wheel positions for maximum moment, with $e_0 = 0$ mm.

		e_0 = 50 mm						
hw	bf	Top LPF	Top U2	Top U3	Both LPF	Both U2	Both U3	ΔLPF%
2500	700	1.832217	-121.6403	-17.7006	1.861677	-130.5753	0.5441	1.61
	600	1.784995	-185.545	-20.6692	1.799635	-243.0753	0.7544	0.82
	500	1.680707	-343.8007	-28.6521	1.692435			0.7
	400	1.562675	-477.2819	-18.9726	1.566499	-488.0071	2.1288	0.24
	300	1.434376	-628.8542	-8.429	1.437803	-640.1086	2.7387	0.24
	200	1.297196	-837.0849	23.9984	1.302082			0.38
3000	700	1.766858	-65.2174	-24.4484	1.794531	-66.2443	-2.0121	1.57
	600	1.753044	-68.7662	-31.134	1.789916	-70.1907	-1.8619	2.1
	500	1.73439	-76.3198	-36.768	1.77823	-80.2391	-0.6671	2.53
	400	1.710716	-93.2201	-39.4427	1.755899	-101.712	-0.1849	2.64
	300	1.656809	-126.792	-45.1713	1.694136	-148.1503	0.5233	2.25
	200	1.569465	-280.8836	-40.4189	1.580346	-303.5284	2.0387	0.69
3510	700	1.645435	-42.9398	-32.2631	1.667549	-43.1915	-2.9546	1.34
	600	1.639134	-45.2442	-39.4064	1.666485	-45.603	-2.8719	1.67
	500	1.633639	-48.1163	-46.0794	1.666547	-48.6233	-2.6988	2.01
	400	1.629633	-51.8644	-52.6391	1.667865	-52.5212	-2.4071	2.35
	300	1.60739	-56.6087	-64.6601	1.651581	-58.4238	-1.6228	2.75
	200	1.610119	-71.2128	-66.4542	1.649699	-75.362	-0.486	2.46
4000	700	1.527837	-27.1098	-33.5317	1.539637	-26.7622	-3.1222	0.77
	600	1.526278	-28.8419	-41.5308	1.540736	-28.3533	-3.124	0.95
	500	1.525985	-30.9835	-50.5361	1.5433	-30.4405	-3.0066	1.13
	400	1.527871	-33.7003	-59.1171	1.547881	-33.045	-2.7739	1.31
	300	1.513645	-36.5081	-71.4037	1.535783	-35.8136	-2.3683	1.46
	200	1.524303	-42.2799	-72.4234	1.54522	-41.7663	-1.6521	1.37
4500	700	1.456032	-16.2919	-30.7964	1.461253	-15.4936	-2.839	0.36
	600	1.45549	-17.5185	-38.4521	1.4618	-16.3851	-2.8584	0.43
	500	1.455325	-19.2944	-46.1529	1.46321	-17.5672	-2.7904	0.54
	400	1.4575	-21.031	-55.3003	1.465899	-19.1433	-2.6036	0.58
	300	1.444894	-22.8307	-68.1927	1.454149	-20.6594	-2.2881	0.64
	200	1.45147	-26.3423	-67.8872	1.459492	-24.304	-1.6858	0.55
5000	700	1.42489	-10.2044	-23.9502	1.4268	-9.3042	-2.2166	0.13
	600	1.424628	-10.975	-30.1323	1.426883	-9.8257	-2.2108	0.16
	500	1.424764	-11.9718	-37.2707	1.427305	-10.4358	-2.1448	0.18
	400	1.425529	-13.1974	-44.3956	1.428163	-11.2552	-1.9871	0.18
	300	1.411934	-14.5332	-54.5527	1.414915	-12.0557	-1.7198	0.21
	200	1.413782	-16.3579	-55.8391	1.416142	-13.89	-1.2993	0.17

Figure D.16: Comparison between the results from the bottom flange imperfection job for the critical wheel positions for maximum moment, with $e_0 = 50$ mm.

		e_0 = 100 mm						
hw	**bf**	**Top LPF**	**Top U2**	**Top U3**	**Both LPF**	**Both U2**	**Both U3**	**ΔLPF%**
2500	700	1.810369	-117.0101	14.142	1.81414	-117.5612	4.1008	0.21
	600	1.772357	-169.7578	12.6706	1.779365	-177.1799	4.1066	0.4
	500	1.675022	-329.5021	6.1465	1.680456	-345.1663	4.0908	0.32
	400	1.557699	-463.7003	16.5009	1.561966	-474.8195	4.4635	0.27
	300	1.429115	-612.7639	29.3497	1.436331	-635.1678	4.9476	0.5
	200	1.292131	-815.8757	62.4359	1.303873	-862.2643	6.1095	0.91
3000	700	1.737355	-65.6187	-6.5641	1.747792	-66.0744	0.1944	0.6
	600	1.731477	-69.1831	-7.1586	1.744246	-69.8456	0.6287	0.74
	500	1.721397	-76.7064	-2.7676	1.735991	-77.998	2.3432	0.85
	400	1.700883	-92.7501	-0.5502	1.717355	-95.471	2.8923	0.97
	300	1.652518	-125.9087	-4.8489	1.668609	-133.3008	3.3455	0.97
	200	1.566848	-276.9586	1.2831	1.572153	-287.9661	4.4934	0.34
3510	700	1.625778	-44.0797	-16.6191	1.638083	-44.3971	-1.2778	0.76
	600	1.623006	-46.4232	-19.4624	1.637831	-46.8124	-1.0057	0.91
	500	1.621573	-49.3593	-21.0598	1.638483	-49.8517	-0.6349	1.04
	400	1.622247	-53.1793	-22.4291	1.640365	-53.7939	-0.1399	1.12
	300	1.605653	-57.9928	-25.4395	1.626159	-59.2012	1.1192	1.28
	200	1.609227	-72.5004	-24.2417	1.62694	-74.9895	2.329	1.1
4000	700	1.518608	-28.8763	-19.6297	1.525644	-28.7357	-1.765	0.46
	600	1.51895	-30.571	-23.1526	1.52729	-30.4126	-1.6155	0.55
	500	1.520954	-32.5733	-27.4136	1.530464	-32.4658	-1.385	0.63
	400	1.525246	-35.2433	-30.2504	1.535591	-35.1864	-0.991	0.68
	300	1.513687	-38.0737	-35.2422	1.524869	-37.9891	-0.4032	0.74
	200	1.525652	-44.0096	-30.907	1.535116	-44.0578	0.6262	0.62
4500	700	1.453075	-18.4991	-18.2968	1.456177	-18.1605	-1.7187	0.21
	600	1.453484	-19.5915	-21.8945	1.457071	-19.1927	-1.627	0.25
	500	1.454877	-21.0203	-25.1271	1.458862	-20.4343	-1.4695	0.27
	400	1.457882	-22.7251	-27.6748	1.461962	-22.0865	-1.1943	0.28
	300	1.446663	-24.5012	-32.0392	1.450964	-23.5997	-0.775	0.3
	200	1.453545	-27.7529	-28.6095	1.457045	-27.3493	0.0231	0.24
5000	700	1.424974	-12.6612	-12.773	1.425948	-12.2741	-1.3037	0.07
	600	1.425166	-13.2738	-15.2481	1.426188	-12.7916	-1.2476	0.07
	500	1.425821	-14.11	-17.1696	1.426794	-13.48	-1.1237	0.07
	400	1.427116	-15.1261	-17.9424	1.427939	-14.4018	-0.9124	0.06
	300	1.414486	-16.1486	-20.0973	1.415429	-15.274	-0.575	0.07
	200	1.416425	-18.1864	-14.2803	1.417088	-17.3198	-0.0382	0.05

Figure D.17: Comparison between the results from the bottom flange imperfection job for the critical wheel positions for maximum moment, with $e_0 = 100$ mm.

		e_0 = 200 mm						
hw	bf	Top LPF	Top U2	Top U3	Both LPF	Both U2	Both U3	ΔLPF%
2500	700	1.759863	-113.8232	70.9335	1.717478	-102.7501	10.6278	-2.41
	600	1.736208	-147.8364	80.1401	1.696989	-129.5445	10.9594	-2.26
	500	1.66263	-298.5962	76.7445	1.64689	-243.5616	10.1787	-0.95
	400	1.550076	-438.8526	87.3799	1.549586	-419.9292	9.4016	-0.03
	300	1.419799	-585.422	105.3043	1.431834	-611.8914	9.3363	0.85
	200	1.283519	-776.45	140.847	1.30786	-871.0674	10.4827	1.9
3000	700	1.678962	-68.846	29.6034	1.658607	-67.2633	4.1574	-1.21
	600	1.685773	-74.4101	41.6118	1.655769	-70.5663	5.1322	-1.78
	500	1.69099	-81.6065	62.016	1.651418	-76.1531	7.539	-2.34
	400	1.679907	-95.3551	73.8855	1.639963	-88.3506	8.8419	-2.38
	300	1.644063	-127.3301	72.0983	1.608311	-114.0823	9.1387	-2.17
	200	1.562161	-269.8822	81.6973	1.551239	-222.4792	9.8088	-0.7
3510	700	1.58752	-48.4056	13.8906	1.580403	-47.9761	1.8713	-0.45
	600	1.591852	-51.0787	20.3635	1.581411	-50.3587	2.5088	-0.66
	500	1.598256	-54.4687	28.2506	1.583286	-53.3995	3.2715	-0.94
	400	1.607879	-58.968	39.8881	1.586221	-57.3777	4.1843	-1.35
	300	1.60171	-64.3685	53.7144	1.575472	-62.2111	6.3503	-1.64
	200	1.608135	-78.021	60.4676	1.579615	-75.4565	8.0345	-1.77
4000	700	1.501962	-33.9758	7.4352	1.499469	-33.7343	0.8304	-0.17
	600	1.506166	-35.7749	12.1968	1.50209	-35.4256	1.2259	-0.27
	500	1.512526	-38.1096	20.1003	1.506185	-37.542	1.7129	-0.42
	400	1.521647	-41.0406	30.1964	1.511945	-40.3194	2.3871	-0.64
	300	1.51582	-43.9615	37.0682	1.503481	-43.4071	3.4704	-0.81
	200	1.531037	-50.3661	51.4653	1.514645	-49.5777	5.0739	-1.07
4500	700	1.448961	-24.3568	6.7519	1.447362	-24.178	0.4056	-0.11
	600	1.451508	-25.4433	11.3148	1.448923	-25.2604	0.6902	-0.18
	500	1.455457	-26.819	18.5165	1.451478	-26.5512	1.0069	-0.27
	400	1.461148	-28.6526	29.7823	1.455434	-28.3353	1.4917	-0.39
	300	1.452318	-30.1212	38.8098	1.445886	-30.1759	2.2018	-0.44
	200	1.459823	-34.3996	57.9126	1.453315	-34.2229	3.4345	-0.45
5000	700	1.426419	-18.6883	8.8829	1.425033	-18.6309	0.4302	-0.1
	600	1.427774	-19.3153	14.26	1.425691	-19.2527	0.6118	-0.15
	500	1.42986	-20.1017	22.9925	1.426807	-20.0298	0.8426	-0.21
	400	1.432665	-21.0374	35.4909	1.428491	-21.0576	1.1605	-0.29
	300	1.422261	-21.869	50.8778	1.417348	-22.2029	1.6993	-0.35
	200	1.423365	-23.5732	65.1019	1.420031	-24.6619	2.497	-0.23

Figure D.18: Comparison between the results from the bottom flange imperfection job for the critical wheel positions for maximum moment, with $e_0 = 200$ mm.

		$e_0 = 300$ mm						
hw	bf	Top LPF	Top U2	Top U3	Both LPF	Both U2	Both U3	ΔLPF%
2500	700	1.703779	-120.8921	118.3619	1.62479	-97.8239	14.1183	-4.64
	600	1.696043	-141.8615	141.7983	1.609129	-112.048	17.5226	-5.12
	500	1.65388	-235.0609	149.8821	1.583632	-148.2508	17.0057	-4.25
	400	1.54538	-419.3642	156.4088	1.519517	-324.9369	14.989	-1.67
	300	1.41272	-559.3271	182.0997	1.420137	-546.2833	14.1227	0.53
	200	1.27679	-741.33	220.849	1.311424	-871.1128	14.8051	2.71
3000	700	1.626388	-76.398	66.4776	1.658607	-67.2633	4.1574	1.98
	600	1.641735	-83.6367	90.8423	1.575621	-73.2389	9.0534	-4.03
	500	1.655097	-91.8763	117.2849	1.572271	-77.7569	11.6123	-5
	400	1.652912	-103.4213	136.0978	1.564678	-86.3505	14.4391	-5.34
	300	1.63417	-132.1635	148.301	1.541276	-103.3336	15.2028	-5.68
	200	1.5616	-261.8685	167.429	1.514234	-159.6384	15.8053	-3.03
3510	700	1.551206	-55.2884	43.2777	1.527498	-52.747	4.7779	-1.53
	600	1.561801	-58.8277	56.8757	1.529457	-55.0359	5.7721	-2.07
	500	1.577205	-63.3915	78.2045	1.532032	-57.9972	6.9281	-2.86
	400	1.595492	-68.9452	107.5796	1.535227	-61.9065	8.2696	-3.78
	300	1.596311	-75.449	121.1447	1.526476	-67.0642	10.8125	-4.37
	200	1.59989	-87.9102	127.4672	1.532164	-77.9028	13.6633	-4.23
4000	700	1.486356	-41.2831	33.9719	1.47405	-39.6719	3.2423	-0.83
	600	1.494404	-43.5922	46.7539	1.477207	-41.4091	3.8566	-1.15
	500	1.505484	-46.5122	67.0329	1.481574	-43.6434	4.5725	-1.59
	400	1.519927	-49.9923	87.1328	1.487724	-46.5252	5.5077	-2.12
	300	1.520389	-53.8445	115.6079	1.481216	-49.8506	7.0116	-2.58
	200	1.536348	-60.8786	139.7401	1.492936	-56.0628	9.3714	-2.83
4500	700	1.44592	-31.8234	30.5177	1.438827	-30.8126	2.3482	-0.49
	600	1.451062	-33.3009	42.7197	1.441079	-31.9087	2.8029	-0.69
	500	1.458179	-35.1581	61.4001	1.444323	-33.3221	3.3387	-0.95
	400	1.466813	-37.3011	84.3081	1.449036	-35.1854	4.0319	-1.21
	300	1.462165	-39.7342	116.4824	1.440986	-37.3285	5.1005	-1.45
	200	1.469935	-44.1373	142.5362	1.449448	-41.6262	6.7024	-1.39
5000	700	1.429435	-26.0844	29.1869	1.425213	-25.3579	1.9724	-0.3
	600	1.432251	-27.0438	42.0238	1.426319	-26.0402	2.2917	-0.41
	500	1.436082	-28.2107	62.2767	1.427932	-26.9277	2.6662	-0.57
	400	1.441251	-29.5767	89.2879	1.430189	-28.0883	3.1456	-0.77
	300	1.433676	-30.7156	123.7818	1.420127	-29.4393	3.848	-0.95
	200	1.434566	-32.6229	147.6331	1.423558	-32.3133	5.0178	-0.77

Figure D.19: Comparison between the results from the bottom flange imperfection job for the critical wheel positions for maximum moment, with $e_0 = 300$ mm.

D.4.4 Shear bottom flange imperfection

		$e_0 = 0$ mm						
hw	bf	Top LPF	Top U2	Top U3	Both LPF	Both U2	Both U3	ΔLPF%
2500	700	2.050132	-214.9704	-36.6699	2.052586	-209.3429	-1.7887	0.12
	600	1.932397	-312.2321	-42.6445	1.940049	-321.1827	-1.3124	0.4
	500	1.809872	-378.7398	-34.6234	1.813806	-384.0136	-0.2099	0.22
	400	1.680631	-477.7304	-22.0469	1.677215			-0.2
	300	1.540453	-604.8198	-7.8872	1.540624	-607.3576	2.0772	0.01
	200	1.389533			1.391268	-796.5054	2.9836	0.12
3000	700	2.085546	-68.7214	-41.7852	2.141395	-68.5074	-5.1778	2.68
	600	2.061183	-75.0121	-54.7622	2.147788	-81.7258	-4.5261	4.2
	500	2.039948	-93.871	-55.8149	2.1221	-110.3943	-3.0525	4.03
	400	1.986658	-134.9953	-57.9186	2.019908	-168.0436	-1.6031	1.67
	300	1.851495	-250.2778	-66.2777	1.871			1.05
	200	1.679407	-292.3479	-64.2958	1.709971	-343.0999	0.372	1.82
3510	700	1.897679	-41.5966	-37.3513	1.926966	-41.1269	-4.4102	1.54
	600	1.889307	-44.1183	-46.1978	1.925878	-43.5798	-4.5502	1.94
	500	1.881367	-47.4658	-55.6302	1.926067	-46.8688	-4.5339	2.38
	400	1.874892	-52.3444	-67.7787	1.928203	-51.5248	-4.3867	2.84
	300	1.849818	-61.6223	-83.027	1.919991	-64.4613	-3.745	3.79
	200	1.626095	-69.0624	-65.7686	1.662682	-72.2263	-1.6996	2.25
4000	700	1.741546	-25.4511	-37.4901	1.758116	-24.6141	-4.1011	0.95
	600	1.738172	-27.2457	-47.0383	1.758644	-26.2032	-4.2006	1.18
	500	1.735897	-29.5118	-57.8865	1.760577	-28.3123	-4.1775	1.42
	400	1.735816	-32.6552	-67.2752	1.764366	-31.0408	-4.0201	1.64
	300	1.717821	-36.8557	-83.4958	1.750392	-35.3473	-3.7687	1.9
	200	1.563928	-46.943	-64.3297	1.595832	-48.2571	-2.0898	2.04
4500	700	1.65041	-14.3928	-37.2972	1.660434	-13.4784	-3.6353	0.61
	600	1.648071	-15.6842	-47.4713	1.660548	-14.3769	-3.7059	0.76
	500	1.646397	-17.4228	-58.9571	1.66141	-15.434	-3.6922	0.91
	400	1.646258	-19.6212	-70.6469	1.663231	-17.0851	-3.5225	1.03
	300	1.632836	-22.3205	-87.1108	1.651351	-19.2377	-3.257	1.13
	200	1.513739	-33.0555	-67.6138	1.538421	-32.8795	-2.0738	1.63
5000	700	1.608825	-8.1232	-32.3339	1.61309	-6.7827	-2.9784	0.27
	600	1.607591	-9.0379	-41.4239	1.612792	-7.3151	-2.9964	0.32
	500	1.606502	-10.2341	-52.419	1.612731	-7.9222	-2.9372	0.39
	400	1.605863	-11.7908	-64.167	1.613031	-8.9	-2.7593	0.45
	300	1.591844	-13.9477	-78.7544	1.600009	-10.0807	-2.4913	0.51
	200	1.467306	-22.8359	-68.6904	1.491078	-21.5665	-1.818	1.62

Figure D.20: Comparison between the results from the bottom flange imperfection job for the critical wheel positions for maximum shear, with $e_0 = 0$ mm.

		$e_0 = 50$ mm						
hw	bf	Top LPF	Top U2	Top U3	Both LPF	Both U2	Both U3	ΔLPF%
2500	700	2.047758	-209.4099	-9.4	2.049143	-203.2725	1.175	0.07
	600	1.928238			1.930816	-311.4044	1.2402	0.13
	500	1.804171	-371.295	-3.5529	1.807553	-376.1273	2.2821	0.19
	400	1.674708	-466.2868	10.9014	1.678698	-471.7473	3.2716	0.24
	300	1.534307	-588.5556	27.0483	1.540891	-607.9341	4.2651	0.43
	200	1.383988	-768.3246	57.6394	1.394825	-813.5549	5.1903	0.78
3000	700	2.052619	-67.4488	-18.2097	2.081857	-67.9758	-1.9853	1.42
	600	2.03628	-73.7796	-24.1919	2.081652	-76.9338	-1.3642	2.23
	500	2.020295	-91.3449	-20.3068	2.067919	-99.0992	-0.0684	2.36
	400	1.975999	-129.5891	-19.4505	2.007519	-152.3971	0.9339	1.6
	300	1.847387	-245.112	-26.6406	1.859517	-264.2538	1.8578	0.66
	200	1.678729	-292.6555	-23.9396	1.706368			1.65
3510	700	1.874334	-42.1183	-22.4838	1.893206	-42.0487	-2.6205	1.01
	600	1.870175	-44.6678	-26.7134	1.893267	-44.5817	-2.5618	1.23
	500	1.867002	-47.881	-31.4254	1.894538	-47.9256	-2.3402	1.47
	400	1.865338	-52.4844	-34.5061	1.897642	-52.5481	-1.9729	1.73
	300	1.846169	-62.0171	-45.0483	1.888818	-64.0087	-0.9873	2.31
	200	1.626285	-69.4981	-24.6798	1.653402	-72.4885	1.0876	1.67
4000	700	1.727853	-26.3519	-25.2304	1.73937	-25.8516	-2.7436	0.67
	600	1.726754	-28.1916	-30.0814	1.740549	-27.5401	-2.6855	0.8
	500	1.727166	-30.4184	-35.2968	1.743198	-29.6124	-2.5408	0.93
	400	1.730145	-33.3754	-39.2289	1.747914	-32.6317	-2.1943	1.03
	300	1.715839	-37.554	-47.4235	1.735562	-37.0125	-1.7301	1.15
	200	1.563655	-47.7196	-25.9476	1.586533	-49.1609	0.1313	1.46
4500	700	1.643131	-15.7368	-26.2328	1.649521	-15.1296	-2.5483	0.39
	600	1.642273	-16.9931	-32.0113	1.649946	-16.09	-2.5168	0.47
	500	1.642285	-18.5258	-38.3705	1.651173	-17.3496	-2.3892	0.54
	400	1.643917	-20.5506	-43.7211	1.653571	-19.0938	-2.1348	0.59
	300	1.63262	-23.1653	-51.3686	1.64317	-21.3501	-1.753	0.65
	200	1.513523	-33.4959	-27.065	1.529182	-34.424	-0.3232	1.03
5000	700	1.605958	-10.0131	-21.3305	1.608531	-9.2608	-2.0242	0.16
	600	1.60537	-10.7715	-26.5497	1.608447	-9.7721	-1.9891	0.19
	500	1.605108	-11.7606	-32.2966	1.608651	-10.5243	-1.8666	0.22
	400	1.605431	-13.0244	-37.9014	1.609249	-11.497	-1.6559	0.24
	300	1.592855	-14.8779	-43.9255	1.597052	-12.8858	-1.321	0.26
	200	1.466608	-23.4367	-28.6044	1.482072	-23.4438	-0.4506	1.05

Figure D.21: Comparison between the results from the bottom flange imperfection job for the critical wheel positions for maximum shear, with $e_0 = 50$ mm.

		e_0 = 100 mm						
hw	bf	Top LPF	Top U2	Top U3	Both LPF	Both U2	Both U3	ΔLPF%
2500	700	2.045813	-204.6777	18.0137	2.045317	-209.0448	3.9589	-0.02
	600	1.920541	-296.8994	15.9862	1.929105			0.45
	500	1.799039	-364.2413	27.6507	1.801188	-369.2038	4.7418	0.12
	400	1.669452	-455.8118	44.0712	1.675604	-467.815	5.545	0.37
	300	1.528722	-576.0364	62.6186	1.541211	-607.0839	6.4206	0.82
	200	1.378561	-745.4446	93.2186	1.398834	-827.0983	7.2616	1.47
3000	700	2.014732	-67.7451	1.6345	2.021415	-67.8483	0.3711	0.33
	600	2.010571	-73.8942	6.4725	2.017634	-73.8599	1.6033	0.35
	500	2.001239	-90.284	13.6484	2.008872	-91.1781	2.8375	0.38
	400	1.963513	-125.0872	18.7947	1.974496	-130.1488	3.6424	0.56
	300	1.843619	-240.2837	12.7148	1.850491	-253.3968	4.2714	0.37
	200	1.677573	-292.4389	17.1235	1.703527			1.55
3510	700	1.851333	-43.3371	-7.616	1.859095	-43.31	-0.917	0.42
	600	1.85117	-45.9963	-7.0825	1.860226	-45.9132	-0.67	0.49
	500	1.852349	-49.3266	-6.0978	1.862493	-49.2999	-0.2491	0.55
	400	1.855222	-53.8107	-5.3326	1.86628	-53.9109	0.3212	0.6
	300	1.842459	-63.4358	-3.5298	1.856676	-64.0698	1.7701	0.77
	200	1.62432	-71.1443	14.6482	1.643197	-72.5853	3.9057	1.16
4000	700	1.714818	-27.9877	-12.0694	1.720449	-27.7719	-1.3658	0.33
	600	1.716031	-29.7705	-12.8332	1.722319	-29.4388	-1.1913	0.37
	500	1.719239	-31.9598	-12.9501	1.725675	-31.6226	-0.8912	0.37
	400	1.725173	-35.016	-10.0414	1.731211	-34.6107	-0.4263	0.35
	300	1.714415	-39.2762	-9.9756	1.720683	-39.0318	0.2619	0.37
	200	1.56071	-48.8303	16.0985	1.576664	-50.4864	2.3392	1.02
4500	700	1.637245	-17.9989	-13.4592	1.640485	-17.6269	-1.4273	0.2
	600	1.637639	-19.0817	-15.3759	1.641211	-18.6327	-1.3025	0.22
	500	1.639197	-20.494	-16.3788	1.642821	-19.9488	-1.0827	0.22
	400	1.642582	-22.3886	-15.3896	1.645753	-21.7664	-0.7412	0.19
	300	1.633163	-24.7281	-16.4486	1.636275	-24.242	-0.2123	0.19
	200	1.511559	-34.9983	13.0426	1.519808	-35.5477	1.4566	0.55
5000	700	1.603907	-12.4219	-10.1017	1.604987	-12.131	-1.0925	0.07
	600	1.603983	-13.0602	-11.477	1.605116	-12.6672	-1.0052	0.07
	500	1.604516	-13.8824	-12.1135	1.605528	-13.4332	-0.8307	0.06
	400	1.605808	-15.0031	-10.9119	1.606442	-14.4499	-0.5804	0.04
	300	1.594626	-16.5427	-9.1984	1.594859	-15.8881	-0.1812	0.01
	200	1.464445	-24.8063	12.68	1.472612	-25.3169	0.9428	0.56

Figure D.22: Comparison between the results from the bottom flange imperfection job for the critical wheel positions for maximum shear, with $e_0 = 100$ mm.

		e_0 = 200 mm						
hw	bf	Top LPF	Top U2	Top U3	Both LPF	Both U2	Both U3	ΔLPF%
2500	700	2.041239	-182.2595	77.6116	1.999747	-139.8951	10.8001	-2.03
	600	1.911411	-283.4962	76.0709	1.904844	-279.205	9.3222	-0.34
	500	1.790767	-352.8734	90.2172	1.789675	-352.8445	9.731	-0.06
	400	1.66131	-438.3874	110.7412	1.669438	-450.0904	10.0967	0.49
	300	1.519596	-548.4666	134.2849	1.541997	-603.5732	10.7143	1.47
	200	1.369642	-705.0498	166.5818	1.407566	-851.7146	11.2228	2.77
3000	700	1.942861	-71.7258	40.473	1.909254	-68.4189	4.5459	-1.73
	600	1.955418	-78.8878	62.1375	1.903023	-72.4909	6.2458	-2.68
	500	1.959983	-91.5803	81.6218	1.894847	-82.2292	8.5969	-3.32
	400	1.938563	-121.4357	91.1224	1.880067	-104.4519	9.2919	-3.02
	300	1.840268	-217.0696	100.2116	1.827368	-177.203	9.723	-0.7
	200	1.676098	-294.3893	97.6543	1.696224			1.2
3510	700	1.805918	-47.9532	23.3753	1.79285	-46.9688	2.4148	-0.72
	600	1.813097	-50.9147	31.0911	1.795035	-49.6477	3.0384	-1
	500	1.822649	-54.7033	43.5638	1.797593	-53	3.8728	-1.37
	400	1.836533	-60.149	59.6521	1.799934	-57.5256	4.7838	-1.99
	300	1.834695	-69.4552	78.3309	1.789132	-65.3369	7.163	-2.48
	200	1.61335	-75.6316	101.3575	1.623152	-75.3237	9.4573	0.61
4000	700	1.69071	-33.1695	15.1081	1.684586	-32.7086	1.2915	-0.36
	600	1.69658	-35.0129	21.9857	1.687484	-34.4459	1.7171	-0.54
	500	1.705217	-37.5151	33.3885	1.69201	-36.6916	2.2877	-0.77
	400	1.717135	-40.8104	48.8673	1.698841	-39.7435	3.0402	-1.07
	300	1.7137	-45.1338	61.5274	1.691382	-44.1139	4.1553	-1.3
	200	1.556346	-54.9149	95.5126	1.556104	-53.504	6.7206	-0.02
4500	700	1.627131	-23.7958	11.3176	1.623733	-23.6188	0.7669	-0.21
	600	1.630371	-24.9571	18.0039	1.625265	-24.6745	1.0551	-0.31
	500	1.635472	-26.4406	28.237	1.62778	-26.0454	1.4464	-0.47
	400	1.642885	-28.4128	42.796	1.631788	-27.9395	1.9633	-0.68
	300	1.637296	-30.8272	58.4209	1.624187	-30.5239	2.7544	-0.8
	200	1.507077	-41.0396	92.2429	1.501207	-39.4018	4.9499	-0.39
5000	700	1.600877	-18.4666	12.1047	1.598468	-18.3962	0.6505	-0.15
	600	1.602635	-19.1302	18.9979	1.599006	-19.0395	0.8635	-0.23
	500	1.605342	-19.961	29.6438	1.600009	-19.8685	1.1534	-0.33
	400	1.609102	-20.976	43.5086	1.601716	-21.0631	1.56	-0.46
	300	1.600915	-22.2825	62.0077	1.591866	-22.7053	2.1305	-0.57
	200	1.46373	-30.396	93.5314	1.450707	-29.7152	3.7287	-0.89

Figure D.23: Comparison between the results from the bottom flange imperfection job for the critical wheel positions for maximum shear, with $e_0 = 200$ mm.

		$e_0 = 300$ mm							
hw	bf	ΔLPF%	Top LPF	Top U2	Top U3	Both LPF	Both U2	Both U3	ΔLPF%
2500	700	-2.03	1.99365	-148.3277	141.1536	1.890913	-112.6086	16.8381	-5.15
	600	-0.34	1.907805	-256.9718	142.5759	1.866653	-157.7338	17.2661	-2.16
	500	-0.06	1.785796	-346.725	152.9464	1.777051	-330.4584	14.8052	-0.49
	400	0.49	1.656173	-426.3817	177.5701	1.663113	-433.243	14.7156	0.42
	300	1.47	1.513058	-526.7261	206.3959	1.542554	-595.2012	15.0213	1.95
	200	2.77	1.363069	-676.5776	243.2395	1.417498	-874.8788	15.062	3.99
3000	700	-1.73	1.875123	-79.605	81.4237	1.806156	-70.2241	8.2213	-3.68
	600	-2.68	1.894632	-88.1912	110.2297	1.800081	-73.8977	10.0298	-4.99
	500	-3.32	1.909963	-98.9013	146.8331	1.793081	-79.7347	13.5152	-6.12
	400	-3.02	1.908804	-122.4286	165.3509	1.782239	-93.4719	14.9574	-6.63
	300	-0.7	1.842683	-208.9537	175.9567	1.756008	-126.8771	15.4703	-4.7
	200	1.2	1.674438	-296.4688	178.8703	1.673901	-292.8595	14.998	-0.03
3510	700	-0.72	1.760918	-54.9634	53.0875	1.727254	-51.4879	5.4462	-1.91
	600	-1	1.77473	-58.8034	70.8395	1.728907	-54.2424	6.3459	-2.58
	500	-1.37	1.794597	-64.0153	98.855	1.73118	-57.3414	7.5983	-3.53
	400	-1.99	1.817963	-70.6179	129.9529	1.732934	-61.7452	8.9394	-4.68
	300	-2.48	1.827588	-80.4474	155.5577	1.723717	-68.5111	12.0651	-5.68
	200	0.61	1.603139	-84.834	186.1149	1.604289	-78.0324	15.0258	0.07
4000	700	-0.36	1.668329	-40.5359	41.7	1.650631	-38.5228	3.7665	-1.06
	600	-0.54	1.678883	-43.0376	58.361	1.654353	-40.3464	4.4189	-1.46
	500	-0.77	1.693373	-46.1003	79.9364	1.65969	-42.6116	5.3164	-1.99
	400	-1.07	1.711644	-50.0079	108.5403	1.66721	-45.7491	6.2889	-2.6
	300	-1.3	1.715899	-55.1236	138.4406	1.661866	-50.0611	7.9169	-3.15
	200	-0.02	1.558191	-65.4784	173.8161	1.537122	-58.0933	10.9579	-1.35
4500	700	-0.21	1.618697	-31.3382	35.3358	1.608343	-30.1458	2.7483	-0.64
	600	-0.31	1.625282	-32.9131	50.5097	1.610608	-31.2735	3.2442	-0.9
	500	-0.47	1.634371	-34.8226	70.8757	1.61394	-32.7424	3.8204	-1.25
	400	-0.68	1.646458	-37.2191	98.8273	1.618959	-34.7328	4.6006	-1.67
	300	-0.8	1.644451	-40.424	135.9791	1.612913	-37.522	5.6989	-1.92
	200	-0.39	1.507619	-49.9801	176.4477	1.482375	-43.7392	8.3978	-1.67
5000	700	-0.15	1.599443	-25.8977	32.6917	1.593079	-25.0791	2.2625	-0.4
	600	-0.23	1.603274	-26.8739	47.6603	1.594185	-25.788	2.6189	-0.57
	500	-0.33	1.608697	-28.1047	68.7378	1.595854	-26.7261	3.0303	-0.8
	400	-0.46	1.615824	-29.5746	98.2214	1.598289	-28.0163	3.5392	-1.09
	300	-0.57	1.610686	-31.3883	139.066	1.58994	-29.8347	4.3116	-1.29
	200	-0.89	1.463479	-39.1768	176.2636	1.427202	-34.5273	6.4915	-2.48

Figure D.24: Comparison between the results from the bottom flange imperfection job for the critical wheel positions for maximum shear, with $e_0 = 300$ mm.

DEPARTMENT OF STRUCTURAL ENGINEERING AND BUILDING TECHNOLOGY
CHALMERS UNIVERSITY OF TECHNOLOGY
Gothenburg, Sweden
www.chalmers.se

CHALMERS
UNIVERSITY OF TECHNOLOGY